Hyperspectral/ Multispectral imaging technology: Application for pomegranate fruit internal quality evaluation and bruise detection

By

Emmanuel Ekene Okere

Thesis presented in partial fulfilment of the requirements for the degree of Doctorate of Philosophy in Engineering in the Faculty of Engineering at Stellenbosch University

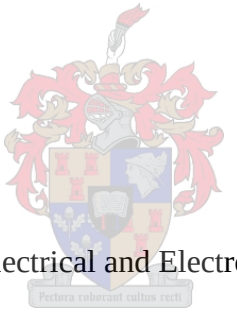

Department of Electrical and Electronic Engineering

Stellenbosch University

Private Bag X1, 7602 Matieland, South Africa

Supervisors:

Dr. Alemayehu Ambau Tsige, Prof. Umezuruike Linus Opara, Prof. Willem Jacobus Perold

March 2023

DECLARATION

By submitting this dissertation electronically, I declare that the work contained therein is my own, original work, that I am the sole author thereof (save to the extent explicitly otherwise stated), that reproduction and publication thereof by Stellenbosch University will not infringe any third-party rights and that I have not previously in its entirety or in part submitted it for any qualification.

March 2023

ABSTRACT

In recent years, consumer demand for fruit and vegetables are increasing due to a shift towards healthier and more sustainable diets. However, fruits and vegetables are highly perishable that providing the market with high-quality but affordable price is challenging. Also, fruit and vegetable diseases, due to fungal pathogens, are major causes of economic loss in agribusiness. There are multiple sources of contamination during preharvest and harvest–postharvest stages of production and particularly for pomegranate fruit. Pomegranate (*Punica granatum* L.) is undeniably one of the most ancient deciduous fruits in the world with growing increase in its demand due to its nutritional and health benefits. These quality issues have necessitated rapid and efficient quality and freshness monitoring and analysis tool in the postharvest. In the fruit and vegetable industries, quality inspections are mainly manual and mechanical, laborious, time-consuming, costly, and subjective. Hyperspectral imaging (HSI) has emerged as a powerful non-destructive inspection technique in the agricultural, biosecurity diagnostic and food domain recently. HSI is a non-invasive/ non-destructive technique that integrates spectroscopy as well imaging to form one system. This combined feature makes it a powerful tool for fruit\food quality assessment and defect detection, maturity indexing and physicochemical attributes in horticultural products. Therefore, the main objective of this study is to assess the application of hyperspectral/multispectral imaging for predicting the major quality attributes in fresh pomegranate fruit as well detect the presence of bruise or internal defect using artificial neural networks (ANNs).

Section I (Chapter 1, 2 & 3) provides background information, discussing the general aim and objectives (General introduction) of the thesis study. It further provides a comprehensive review on recent applications of hyperspectral imaging technology for preharvest and postharvest analysis for biosecurity diagnostics in the fruit industry (Chapter 2) and narrowed down to applications on pomegranate fruit (Chapter 3). It explores hyperspectral imaging architecture, its equipment, image acquisition and data processing. This information is useful for those in the growers/ processing industries and food safety and quality control stakeholders and provides a review of literature on previous work done on different non-invasive techniques for evaluating different processed horticultural products over the last ten years.

In Section II (Chapter 4, 5 and 6), hyperspectral imaging technique was investigated to evaluate maturity quality attributes which includes TSS, TA, pH, and colour components (a*, b*, L*, chrome and hue) of intact pomegranate fruit. The ANN prediction models for quality parameters performed well, with correlation coefficients from 0.421 to 0.951. three neural fitting algorithms were compared for prediction performance, LMG algorithm yielded better

results for four of the 9 quality attributes accessed. BR gave the best prediction statistics for TA (R^2=0.852, MSE=0.024), and b* (R^2=0.951, MSE=3.923). The VNIR spectral was applied to build model using 6 effective wavelengths. This research study has demonstrated that hyperspectral imaging technique in combination with artificial neural network has the potential to predict maturity quality attributes of pomegranate fruit.

Further in section II, two spectral ranges of VNIR and SWIR were deployed in the hyperspectral imaging technique to detect the presence of early bruise development of "Wonderful" pomegranate fruit, as well as classify bruit based on different levels of bruise severity. Scanned images were explored, and spectral data extracted for two surface area of interest (ROI and WF). ANN classification model showed model to be able to detect bruise immediately after occurrence to an accuracy of 90%. Both methods of data extraction are good enough to detect the early bruise damage which is invisible to the naked eye. The results confirm hyperspectral imaging technique combined with machine learning methods (ANN) to be an effective technique for early bruise detection. For bruise severity study, both SWIR and VNIR data yielded highly accurate classification results ranging from 80% - 96.7%. The overall average classification accuracy achieved was 93.3% for model to distinguish fruits dropped at 100cm and 90% for fruit dropped at 60cm height for the VNIR camera.

Section III (Chapter 7) presents a general discussion on the results and key findings of the different chapters of the thesis. It integrates the results from previous chapters. It highlights the important practical contribution of this thesis towards successful non-destructive evaluation of intact pomegranate fruit.

LIST OF PUBLICATIONS AND SUBMITTED MANUSCIPTS FROM THIS THESIS

Published articles

1. Okere, E.E., Ambaw, A., Perold, W.J., Opara, U.L. Non-destructive detection of bruises in pomegranate fruit by Vis-NIR and SWIR hyperspectral imaging. *Acta Hortic*. 1349, 381 – 388, 2022. doi:10.17660/ActaHortic.2022.1349.52.

2. Okere, E.E., Arendse, E., Ambaw, A, Perold, W.J., Opara, U.L. Pomegranate quality evaluation using non-destructive approaches: a review. *Agriculture* 2022, 12, 2034. https://doi.org/10.3390/ agriculture12122034.

Submitted article

1. Okere, E.E., Ambaw, A.; Perold, W.J.; Opara, U.L. Hyperspectral imaging technology: A novel method for agricultural and biosecurity diagnostics – a review. Submitted to *Biosystems Engineering.*

2. Okere, E.E., Ambaw, A.; Perold, W.J.; Opara, U.L. Non-destructive assay of internal quality of pomegranate fruit by Vis-NIR hyperspectral imaging. Prepared to be submitted to *Agriculture*.

3. Okere, E.E.; Ambaw, A.; Perold, W.J.; Opara, U.L. Early bruises detection on pomegranate (*Punica granatum* L.), using hyperspectral imaging coupled with artificial neutral network algorithm. Prepared to be submitted to *Frontiers in Food Science and Technology*.

LIST OF CONFERENCE PRESENTATIONS

1. Okere, E.E., Ambaw, A., Perold, W.J., Opara, U.L. 2022. Non-destructive detection of bruises in pomegranate fruit by Vis-NIR and SWIR hyperspectral imaging. Presented at the **Vth International Symposium on Pomegranate & Minor Mediterranean Fruits**, Stellenbosch, South Africa, 14th – 18th February 2022 (Oral).

2. Okere, E.E., Ambaw, A.., Perold, W.J., Opara, U.L. 2022. Detection and classification of bruise severity on pomegranate fruit using hyperspectral imaging technique. Presented at the **Consortium for Innovation in Post-harvest Loss & Food Waste Reduction, Annual Consortium meeting 2022**, Kwame Mkrumah University of Science and Technology, KNUST, Kumasi, Ghana. 6th – 10th June 2022. (Oral).

3. Okere, E.E., Ambaw, A., Perold, W.J., Opara, U.L. 2022. Hyperspectral imaging technology: An alternative method for agricultural and biosecurity diagnostics. To be presented at the **2nd Global Conference on Agriculture 2022**, Berlin, Germany, 9th – 11th December 2022. (Oral).

ACKNOWLEDGEMENTS

Firstly, this work is based on the research supported wholly / in part by the National Research Foundation of South Africa (Grant Numbers: 64813). The opinions, findings and conclusions or recommendations expressed are those of the author(s) alone, and the NRF accepts no liability whatsoever in this regard.

Furthermore, my sincere and profound gratitude and appreciation goes to my supervisor, Prof Willem Jacobus Perold for all his fatherly advice and encouragement throughout the project. You are always willing to help me under tight notice and schedules. I greatly appreciate your support and kindness towards me.

I want to specially thank Prof Umezuruike Linus Opara, whose thorough inputs and feedback had been immense, and insightful throughout this academic journey, especially during the Postharvest Discussion Forum (PDF). I am greatly honoured to have learnt under your supervision. Thank you very much for all your support and feedback on my work. Your inputs were highly valuable and are acknowledged.

To Dr Alemayehu Ambau Tsige, written words cannot thank you enough for your tireless effort on making sure I finish this research work. I appreciate every input, correction, meeting, advice and push geared towards my success. I must admit, you are the best mentor anyone could ever wish for.

Special thanks to Prof Olaniyi Amos Fawole, Dr Arendse Ebrahiema for all the inputs and suggestions in the course of this work. I greatly acknowledge and appreciate you sirs.

I would also like to thank Nazneen Ebrahim for her administrative duties and technical support throughout the course of this research work. I received immense assistance from the then laboratory assistant Mr Page Pierre, you were an amazing company and help in this academic journey.

The conducive working environment at the postgraduate office at SARChI Postharvest Technology Research Laboratory was made possible by my colleagues at the office. You guys were lovely and warm towards me from the start. Thank you for shared space and jokes and for all the encouragement and input all along this project.

Last but not the least is my family back home. Special thanks to my parents, my dad, Mr Raymond and mum, Mrs Lydia Okere, and my siblings Amarachi, Ogadinma, Jeremiah, Joseph and Chinaza, for staying strong with me during this period.

Finally, I would like to mention a few names that saw to my daily survival, To my brothers in farther land, Ikechukwu Opara, Samuel Ndukuba and Ndubuisi Madufor, Ndewo nu, and to the women dear to my heart; Mpho Molapo, Buhle Maphosa, Vuyiswa Dlamini and Deborah

Abobade, and to the gents: Mr Paul Adebayo, Mr George Teke, Mr Amika Usongo. Thank you all.

NOMENCLATURE

1^{st}: First Derivative

2^{nd}: Second Derivative

cm^{-1}: per centimetre

nm: Nanometre

a*: Redness

ATR-FT/MIR: Attenuated Total Reflectance-Fourier Transform/Mid-Infrared Spectroscopy

b*: Yellowness

BPNN: Back Propagation Neural Network

BR: Band Ratio

BRA: Bayesian Regularization Algorithms

C*: Chroma

CA: Classification Accuracy

Corr: Correlation Coefficient

CV: Coefficient of Variation

DA; Discriminant Analysis

DAFB: Days after full bloom

FNN: Fully-connected Neural Network

GAE: Gallic Acid Equivalents

h°: Hue Angle

HEA: Hierarchical Evolutionary Algorithm

HSI: Hyperspectral imaging

IR: Infrared

k-NN: K-Nearest Neighbour

L*: Lightness

LV: Latent Variables

LDA: Linear Discriminant Analysis

LLE: Locally Linear Embedding

LMBA: Levenberg-Marquardt backpropagation algorithm

LS-SVM: Least Squares Support Vector Machine

Max: Maximum

Min: Minimum

MLP: Multilayer perceptron

MSC: Multiplicative Scattering Correction

MSE: Mean Square Error

NIRS: Near-Infrared Spectroscopy

NMR: Nuclear Magnetic Resonance

PCA: Principal Component Analysis

PLS: Partial Least Squares

PLS-DA: Partial Least Squares Discriminant Analyses

PLSR: Partial Least Squares Regression

R^2: Coefficient of Determination

RMSEC: Root Mean Square Error of Calibration

RMSECV: Root Mean Square Error of Cross-Validation

RMSEP: Root Mean Square Error of Prediction

RPD: Ratio of Prediction to Deviation

RSD: Relative Standard Deviation

SAE: Stacked Auto-Encoders

SCGBA: Scaled Conjugate Gradient Backpropagation Algorithm

SD: Standard Deviation

SIMCA: Soft Independent Modelling of Class Analogies

SLOG: Simple Logistic

SMO: Sequential Minimal Optimization

SNV: Standard Normal Variate

SPA: successive projections algorithm

SVM: Support Vector Machine

TA: Titratable Acidity

TAC: Total Anthocyanin Content

TSS: Total Soluble Solid

TSS/TA: Total Soluble Solid/ Total Acid

TVC: Total Viable Count

QDA: Quadratic Discriminant Analysis

WF: Whole Fruit

WFS: Whole Fruit Surface

Y&M: Yeast and Mold count

Table of Contents

SECTION I

GENERAL INTRODUCTION AND LITERATURE REVIEW

CHAPTER 1

General introduction

1.1. Background

Pomegranate (*Punica granatum L.*), an ancient deciduous fruit of Middle Eastern origin is an emerging crop in South Africa [1]. The pomegranate is one of the most important fruits of the world which is consumed both as fresh and in processed form such as juice, jams, etc. In the past decades, the demand for pomegranate fruit has been increasing due to its nutritional and health benefits [2–4]. This global awareness has resulted in considerable increase in commercial farming of pomegranate fruit [5]. Fruit inspection and sorting is the core towards achieving premium quality produce for fresh consumption and to gain high-return [6] Therefore, together with the recent attention for food quality and safety, technologies for estimating the fresh quality of pomegranate fruit are being sought [7].

At present, fruit are sorted manually or automatically based on their appearance only. However, the aril quality attributes are very important for eating satisfaction. In addition, since the pomegranate is a non-climacteric fruit, to achieve good quality, it is essential to harvest at the optimum stage of ripening [8]. Fast and effective non-destructive methods for fruit maturity estimation is crucial to establishing maturity of fruit for harvest. Currently, many objective criteria for judging maturity of pomegranate have been used, for example, firmness, total soluble solids, titratable acidity, and determination of total anthocyanins. However, standard methods for these quality measurements are mostly destructive, slow, and prone to operational error.

Near-infrared spectroscopy (NIRS) and machine vision systems (MVS) were the most successful technologies in the past few decades for the automatic quality inspection of fruits and vegetables [9]. However, due to the inability of NIRS system to evaluate spatial features of an object and incapability of MVS to capture internal quality attributes, automatic quality inspection and defect detection in the fruit and vegitable industry are still challenging [9–13].

Hyperspectral imaging has emerged as a powerful nondestructive inspection technology in the agricultural, biosecurity diagnostic and food domain recently. This technique is based on a two-dimensional (2-D) spatial matrix of vectors, each of which represents a spectrum ranging from Visible (VIS) to near infrared (NIR) wavelength to form a three-dimensional (3-D) image dataset, known as hypercube. This technology integrates spectroscopy and imaging to acquire both spectral and spatial information simultaneously. This combined features makes it a powerful tool for fruit\food quality assessment and defect detection, maturity indexing and physicochemical attributes in horticultural products [9, 13–15].

Hyperspectral technique is however limited by several factors, which includes the speed of image acquisition and image data processing. To overcome this problem, studies in recent years have been focused on determining a few most effective wavebands by using hyperspectral imaging, then implementing it in a multispectral imaging configuration (MSI). Different machine learning algorithms have been developed to also improve on the analysis of hyperspectral imaging data and model performance in recent times [16].

Therefore, the main objective of this study is to assess the application of hyperspectral/multispectral imaging for predicting the major quality attributes in fresh pomegranate fruit and comparing the performance of prediction models obtained using Artificial neural networks (ANNs). Some ANN based machine leaning algorithms are ongoing and will require more research attention in the coming years.

1.2. Problem statement

The fresh pomegranate fruit quality inspection depends on the appearance (size, shape, color, gloss, and freedom from defects and decay) and the eating qualities and nutritive values of the arils. Standard methods of fruit internal quality measurement techniques are mostly destructive, slow, costly and labor intensive.

Recently, hyperspectral imaging techniques have gained huge attention in fruit industry for quality evaluation and efficient grading [13, 17, 18]. Based on findings demonstrated on other fruit, this study aims to investigate the technique for pomegranate fruit. Successful application would provide non-destructive inspection of external and internal fruit quality including decay and the total soluble solid (TSS), total acidity (TA), and pH of arils in pomegranate using this technique. However, the complex image acquisition and image data processing requirements of hyperspectral imaging technique are the problems that need critical investigation. In addition, the thick rind of pomegranate fruit may increase the challenge even further.

Handling and processing the high-volume data produced by hyperspectral sensors become problematic to store, transfer, process, and make sense. Making its use cumbersome and yet to

be optimized. Hence, requiring detailed analysis and optimization to achieve effective data reduction and wavelength selection techniques for fast online application.

1.3. Significance of research

1.3.1. Aims and objectives

The aim of this project is to develop optimum hyperspectral/multispectral imaging technique and prediction models to non-destructively quantify the major quality attributes of pomegranate fruit. The specific objectives are to:

(1) Determine optimal wavelength range, data pre-processing method and multivariate analysis technique for non-destructive measurement and prediction of pomegranate fruit quality attributes and maturity classification.

(2) Investigate the feasibility of hyperspectral imaging for early detection of bruise presence in pomegranate fruit.

(3) Investigate the feasibility of hyperspectral imaging to detect bruise severity on pomegranate fruit.

1.4. Motivation

Traditional approaches to quality assessment of fruit and vegetables are expensive, time-consuming, laborious and often demand expert handlers to deal with specialised laboratory experiments. Furthermore, there is a growing (both locally and globally) demand for consistent supply of safe, nutritious and traceable products by consumers [19]. With the United Nations (UN) declaration of food security as part of its sustainable development goal, agribusiness has shifted from subjective, destructive testing to objective, non-destructive testing [19, 20].

Hyperspectral imaging, as a hybrid system with the added advantage of spectroscopy and imaging provides potential advantage over other imaging techniques and spectroscopy technique [9]. Its adaptive nature for inline or online application also makes it an efficient non-invasive inspection technology able to provide information about external and internal quality attributes of fruit and horticultural products.

Several studies have investigated the application of non-destructive measurement techniques to assess the internal and external quality attributes of pomegranate whole fruit [21–23] and arils [24]. These studies showed varying level of successes in its application with some quality parameters showing high accuracy and others showing not so good model performance. Hyperspectral/multispectral have been successfully applied for different fruit/food quality

evaluation [18, 25–27]. These studies have yielded good and improved predictions models with high accuracy. However, to our knowledge, no comprehensive study on the feasibility of hyperspectral imaging technique for a quality attributes assessment, disease detection, fruit grading and safety inspection for pomegranate fruit has been conducted. This knowledge-gap has motivated and necessitated this PhD research project.

1.5. Thesis structure

This thesis is structured into three sections each addressing a specific research theme. It is structured as follows:

- Section I: provides background information, discussing the general aim and objectives (Chapter 1) of the thesis study and provides a review of literature on previous work done on different application of hyperspectral imaging techniques for evaluating quality concerns on different fruit and horticultural produces over the last ten years (Chapter 2), while application of different non-destructive quality evaluation techniques over the years on pomegranate fruit was reviewed in (Chapter 3).
- Section II: evaluates methodology, results and discussion of the application of hyperspectral imaging techniques for the measuring of physicochemical and phytochemical quality attributes of pomegranate fruit (Chapter 4), and bruise damage severity detection and development in pomegranate fruit (Chapter 5 and Chapter 6).
- Section III (Chapter 7): presents a summary and a general discussion from the previous chapters. It highlights the important practical contribution of this thesis towards successful application of hyperspectral imaging for quality evaluation of pomegranate fruit (Chapter 4, 5 & 6) and finally provides concluding remarks and future research prospects.

CHAPTER 2

Hyperspectral imaging technology: A novel method for agricultural and biosecurity diagnostics – a review

Abstract

Hyperspectral imaging (HSI) was originally developed for remote sensing. It has recently emerged as a novel analytical tool for non-destructive food analysis. Recent advances in computer technology have led to the development of imaging systems capable of identifying quality problems rapidly on the processing line, with the minimum of human intervention. Over the years, quality, and safety assessments of fresh and processed horticultural products have become increasingly important with issues such as global food security, and with the advent of a global pandemic. This paper provides a comprehensive review on recent applications of hyperspectral imaging technology for preharvest and postharvest analysis for biosecurity diagnostics. It explores hyperspectral imaging architecture, its equipment, image acquisition and data processing. This information is useful for those in the fruit processing industries, food safety, and quality control stakeholders.

2.1. Introduction

In recent years, consumer demand for fruit and vegetables has been increasing due to a shift towards healthier and more sustainable diets [28]. However, fruit and vegetables are highly perishable such that providing the market with high-quality but affordable price is challenging. This necessitates rapid and efficient quality and freshness monitoring and analysis tool in the postharvest. In the fruit and vegetable industries, quality inspections are mainly manual and mechanical, laborious, time-consuming, costly, and subjective [28, 29]. The current lack of objective indices for defining “freshness” of fruits or vegetables limits the capacity to control product quality, leading to food loss and waste [30]. Consumers’

attention to fruit or vegetable quality has not been limited to external attributes, such as shape, size, colour, texture, and various defects, but further extends to internal attributes, including the sugar content, firmness, soluble solids content (SSC) and nutritional contents [27, 31].

For instance, due to inappropriate and excessive external forces, agricultural products like fruit and vegetables can be bruised during postharvest handling and distribution causing external and internal defects [32]. Bruise is the most common defect of products like apples and pears [33]. Furthermore, the symptoms of this damage may not be visible immediately but after a certain period, making the sorting and grading process challenging [34, 35]. Some pre-harvest practices, the genetic predisposition of crops, harvesting methods, and postharvest storage conditions also play an important role in determining the overall quality of fruits and vegetables [36]. Hence, there is strong interest to improve objective quality control of fruits, vegetables, and crops.

Also, fruit and vegetable diseases, due to fungal pathogens, are major causes of economic loss in agribusiness [37–39]. There are multiple sources of contamination during preharvest and harvest–postharvest stages of production. Conventionally, diseases diagnostics approaches are manual and based on visual assessments. Infections not always show up in a test at the early stage to the human eyes. Accordingly, manual method of diagnosis is generally inaccurate. The polymerase chain reaction (PCR), enzyme linked immune sorbent assay (ELISA), fluorescence in situ hybridization and biomarker-based detection technology are mostly destructive, involves use of chemicals and trained expert for conducting and evaluating the tests [40, 41].

For most non-climacteric fruit, quality control requires knowledge of the optimum maturity stage for harvesting [2]. Many objective maturity indices are used, for example, firmness, total soluble solids, titratable acidity, and determination of total anthocyanins. However, the standard methods for these quality indices are destructive, slow, and not suitable for an on-line grading system. Access to quality and safe fresh and processed agro food is one of the greatest causes of public anxiety [42]. Fresh-cut-produce-associated foodborne outbreaks are a major public health concern worldwide. Recent foodborne outbreak statistics showed that there is an increasing trend in fresh-cut produce-linked outbreaks mostly associated with Salmonella and Escherichia coli O157:H7 as the causative agents [43, 44]. This poises an urgent need for food safety and security, and to the improvement of effectiveness and efficient non-destructive testing and diagnostic methods for fast and affordable quality assessment methods [7, 45].

To this end, non-destructive testing and diagnostic methods have made remarkable progress in the last few decades. Among many, near-infrared spectroscopy (NIRS) has been widely used in agricultural operations. NIRS uses the near-infrared (NIR) light covering the wavelength range of about 750–2500 nm. The light is incident on the food product in the form of diffuse reflectance, transmittance or interactance, and the acquired spectra are then quantitatively related to the chemical and physical properties of the product to determine crop parameters such as water content, sugar content, and other indicators of ripeness, as well as measuring chlorophyll fluorescence to determine the need for nitrogen-based fertilizers in the preharvest, or to look for bruising not visible to the human eye [34]. However, NIRS is point measurement and is inadequate for evaluating the spatial features of the object being detected [9, 10, 12].

Subsequent innovative technologies focus on imitating the visually human testing methods using computer vision (CV) that enables a computing device to inspect, evaluate and identify still or moving images [46]. The vision system uses software to identify pre-programmed features. The system can be used to trigger a variety of set “actions” based on the findings and forms a machine vision system (MVS) [37]. Conventional MVS uses broadband visible (VIS, 400–700 nm) light in monochromatic or colour mode, and it simulates human vision to perform automatic quality inspection of fruits and vegetables [9]. The problem of conventional MVS is that it is not suitable for assessing internal quality attributes, whether chemical or physical, and it also is not very effective for defect detection, due to the lack of sufficient spectral information [47].

Advanced machine vision system incorporates spectral and spatial imaging to acquire both spectral and spatial information simultaneously. Notably, the hyperspectral imaging (HSI) is the technology that have been steadily growing in utility over the past few decades. However, the cost and complexity of HSI system limits its application in the fruit and vegetable quality control. Fast computers, sensitive detectors, and large data storage capacities are needed to implement HSI technique. Significantly large data storage capacity is required to store the massive, multidimensional datasets.

Several researchers have reviewed the potential of HSI, many of these reviews have focused on the analytical technology aspect [48], sensors or hardware of the technique [49], machine learning methods [50, 51], applications [52] with some specific to applications on particular food substances [53, 54], sensory attributes [15] and to other fields like in medicine [55], geography [56], remote sensing [57, 58], archaeology [59, 60], and forensic [61]. However, issues in the application of HSI as diagnostic tool for biosecurity in the agricultural

field is not sufficiently addressed. And this review seeks to fill that knowledge gap. In this review, we will report on the recent advances that specifically focus on disease detection using multispectral and hyperspectral imaging technology.

2.2 Fundamentals of machine vision system

Machine vision system (MVS) refers to the use of computer vision in an industrial or practical application or process where it is necessary to execute a certain function or outcome based on the image analysis done by the vision system [9]. Hence, MVS performs automatic image capturing, evaluation and processing in a broad field of applications including automatic inspection, process control, and robotic guidance [62]. A common output from MVS is a pass/fail decision [63]. MVS usually includes sample-holding platform, lighting, a camera or other imager, a processor, software, and output devices [10, 64]. The imaging camera receives light from the object surface and converts it into electrical signals using a charge-coupled device (CCD). Conventional MVS uses different collections of imaging methods that use broadband visible (Vis, 400–700 nm) light in monochromatic or color mode and it simulates human vision to perform inspection tasks. The success of an application for the inspection of fruits or vegetables depends on the quality of the images that are acquired, which largely depends on two factors: the camera and the illumination. The quality of the camera mostly relies on advances in technology. The illumination depends on the application and the geometry of the sample to be inspected. Conventional MVS has been successfully applied in agri-food sector for quality inspection, sorting, and grading of horticultural and food products [49, 65]. Table 2.1 highlights notable applications of conventional MVS in the fruit and vegetable sector. Color and fruit size were used by Liming and Yanchao, [66] to develop a lab-scale automated grading system for strawberry. The developed grading system successfully classified the sizes with an error of less than 5%. The accuracy of color and shape classifications were 89% and 90%, respectively, with an average grading rate of one fruit per 3s. Similarly, López-García et al. [67] developed a CVS that can detect skin defects in citrus fruit. One of the shortcomings of conventional MVS is the difficulty in assessing internal quality attributes due to the lack of sufficient spectral information [47, 68]. Study have shown that spatial information, alone, is insufficient to obtain comprehensive quality information, especially for diagnostic application [69].

MSI and HSI techniques are recently advancing techniques to acquire the spatial distribution of physical and chemical quantities for objective fruit quality analysis [6, 70]. The MSI and HSI are similar in techniques. The main difference is the number of bands and

how narrow the bands are. Multispectral imagery generally refers to 3 to 10 bands [10, 44]. A hyperspectral image could have hundreds or thousands of bands. Typically, an RGB color image falls under the multispectral imagery system since captures three separate images at selected ranges of the visible spectrum representing blue, red and green tones. With a higher level of spectral detail, HSI gives better capability to see the unseen. However, the acquisition, processing and analysis of hyperspectral data is considerably challenging [44]. The comparative difference of conventional machine vision (CMVS), spectroscopy, multispectral imaging (MSI) and hyperspectral imaging (HSI) is summarized on Table 2.2.

Table 2.1 Applications of conventional machine vision systems

Fruit	Application	Data analysis	Accuracy	References
Apple	Surface defect	ROI Number counting, RVM	95,63%	[71]
Citrus	Skin defect	PCA, BER	-	[67]
Table grape	Grading		92% - 100%	[72]
Pineapple	Maturity	Modified basic sequential, Fuzzy logic, Binary ellipse mask, Texture analysis	85 – 100%	[73–76]
Pomegranate	Grading, disease detection	2DLDA, FLDA, F2DLDA, FF2DLDA, ANN, ANFIS, RSM	79.7 – 98%	[65, 77, 78].
Strawberry	Grading	k-means, horizontal diameter	-	[66]

Watermelon	Ripeness	ANN	73.33%	[79]

Table 2.2. Comparison of conventional machine vision (CMVS), spectroscopy, multispectral imaging (MSI) and hyperspectral imaging (HSI).

Feature	CMVS	Spectroscopy	HSI	MSI
Detect small sized sample	YES	NO	YES	YES
Flexibility of spectral extraction	NO	NO	YES	YES
Generation of quality attributes distribution	NO	NO	YES	Limited
Multi-constituent information	NO	YES	YES	Limited
Spectral information	NO	YES	YES	YES
Spatial information	YES	NO	YES	YES

2.3. Hyperspectral imaging – principles and instrumentation

2.3.1. Fundamentals of HSI

Hyperspectral imaging, known also as chemical or spectroscopic imaging, is an emerging technique that integrates conventional imaging and spectroscopy to simultaneously collect spatial and spectral information from an object [80, 81]. HSI is often referred to as imaging spectroscopy, literally translates as imaging "seeing'', hyperspectral – "many bands". This is because hyperspectral imaging techniques is designed to overcome the limits of spectroscopic techniques and vision techniques[6, 82], The fundamentals of HSI is hinged on the principle of electromagnetic spectrum and optical behaviour of surfaces when irradiated by light [82]. This technique is a powerful non-destructive tool in addressing quality and safety issues of fruit and vegetables [83, 84]. It collects images in reflectance and transmittance mode with a sensor to define fine wavelength intervals [19, 85]. This resulting reflected or transmitted light (photons) contains information about the absorbers near the surface of the target material [82]. The key difference between other imaging system and HSI is that hyperspectral devices give image output of continuous spectrum for each pixel [85].

A typical HSI system generally consists of 4 parts (Figure 2.1): (1) an imaging unit, (2) an illuminating source, (3) a sample stage, and (4) a computer with corresponding control software (Figure 2.1). The imaging unit is the core unit and is usually consists of a standard zoom lens, a specific spectrograph in conjunction with a charge-coupled device (CCD) or

complementary metal-oxide-semiconductor (CMOS) camera [86]. The light source produces light to illuminate the target [58]. The light source is also the optical probe that detects physical structure and chemical components of targets. The purpose of a spectrograph is to disperse the captured light into a continuous spectral range. To achieve this purpose, most of the spectrographs in HSI systems include optical devices, such as prism, diffraction grating, and electronically controlled liquid crystal tuneable filters or acousto-optic tuneable filter [68].

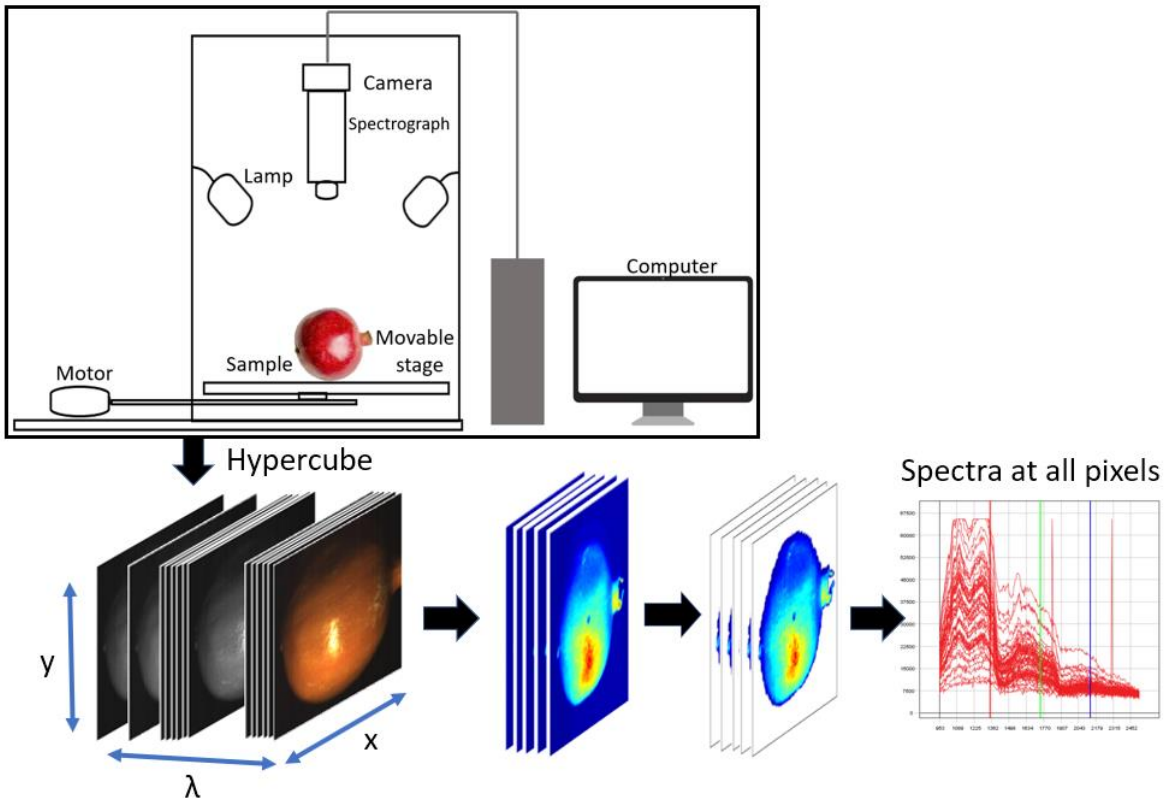

Figure 2.1: Schematics illustrating the configuration of a hyperspectral system.

2.3.2. Image acquisition modes

There are four hyperspectral image acquisition modes or methods, each with its own advantages and disadvantages (Figure 2.2) [49, 58], these are: the point scanning (also known as the whiskbroom method), line scanning (also known as push broom method), area scanning or plane scanning and the single shot or snapshot (Figure 2.2). The merits and demerits of the four image acquisition modes are summarised in Table 2.3

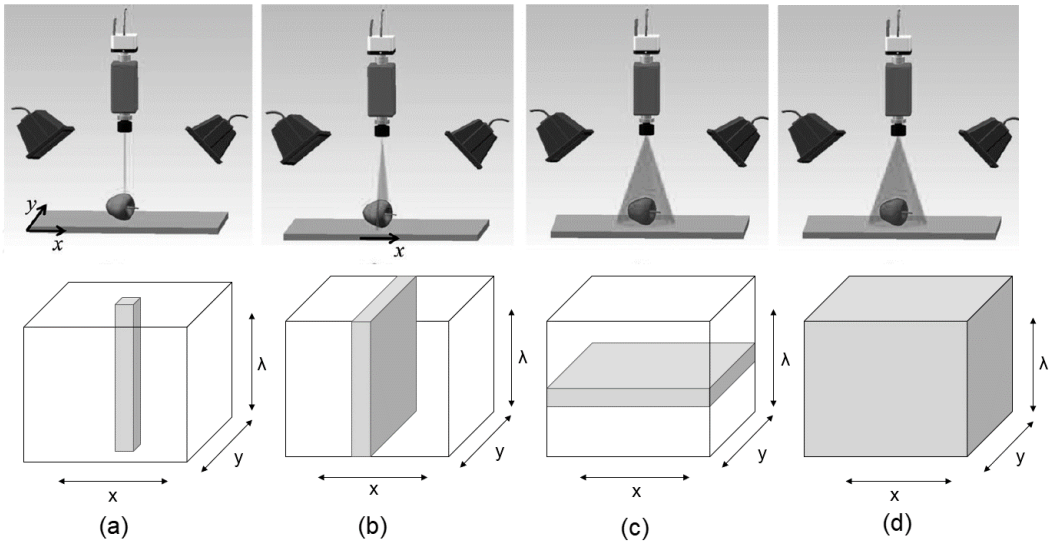

Figure 2.2: The four primary hyperspectral acquisition modes. Point scanning or whiskbroom (a); line scanning or push broom (b); area or plane scanning (c); and single shot or snapshot (d). Where x and y represent the spatial dimensions and λ is the wavelength.

Table 2.3 Comparison of the basic image acquisition modes

Mode	**Scanning**	**Advantages**	**Disadvantages**	**Application area**
PS	One spatial coordinate at a time.	Highest level of spectral resolution.	Very time consuming. Requires repositioning for repeatability of results.	Microscopic imaging.
LS	Row of pixels scans over an area.	Only a single axis of spatial movement.	Controlling time of exposures is critical.	Well suited for conveyor belt systems in the production line.
AS	Images the entire 2D area at once.	Does not require translation of the sensor.	Is not capable of detecting moving target on a production line	Is suitable for applications where sample movement is not required.
SS	Acquires all the spatial and spectral data at once.	Fastest speed	Lower spatial resolution and narrow spectral ranges.	Appears to be the preferred future of HSI implementation,

PS is point scanning mode, LS is line scanning, AS is area scanning and SS is single shot scanning.

2.3.3. Specimen sensing modes

Figure 3 illustrates the three commonly used sensing modes in the hyperspectral imaging – reflectance, transmittance and interactance. In reflectance mode (Figure 3a), the light source and the detector are mounted at the same side of the sample. In transmittance mode (Figure 3b), the light source is positioned opposite to the detector, while in interactance mode (Figure 3c) the light source and detector are positioned parallel to each other on the same side of the sample in such a way that light due to specular reflection cannot directly enter the detector.

The penetration of light into fruit tissue decreases exponentially with the depth. Hence, selection of the specimen sensing modes must consider this phenomenon [51]. External quality features such as size, shape, colour, surface texture and surface defects are typically detected using reflectance mode [6, 15]. Reflectance mode is the most used setup in hyperspectral imaging [87]. In transmittance mode, the detector which is in the opposite side of the light source captures the transmitted light through the sample which carries more valuable internal information. However, transmittance has a low signal level from light attenuation and is affected by the thickness of sample but is often very weak [88]. In interactance mode, both light source and the detector are in the same side of sample and parallel to each other. The interactance mode is a combination of reflectance and transmittance where both light source and the detector are in the same side of sample and parallel to each other. Interactance mode can detect deeper information into the sample compared to reflectance and reduces the influence of thickness, which is a practical advantage over transmittance [10, 12, 52, 64].

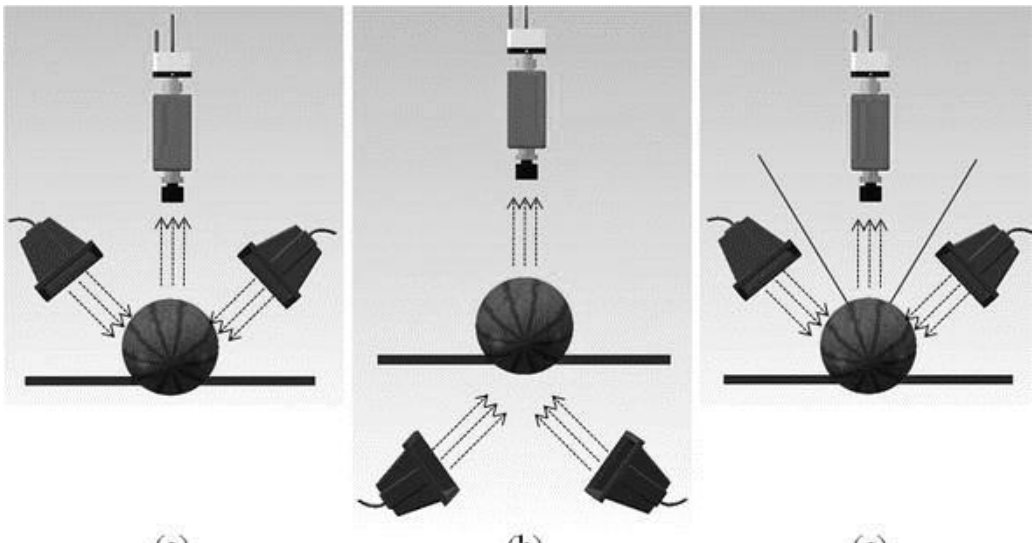

Figure 2.3. The three specimen sensing modes generate a hyperspectral image. (a) The reflectance mode. (b) The transmittance mode. (c) The interactance mode. Adapted from Li et al. [89].

2.3.4. Spectral preprocessing and calibration

Preprocessing of spectroscopic reflectance data is a necessary step to correct light–distance differences in the acquired image data to improve the modelling and analysis of the classification problem [90, 91]. Different preprocessing approaches are applied on the raw hyperspectral data. The preprocessing aims to limit or completely eliminate undesired effects during image acquisition, including light scattering, the morphology of sample surface, size of particles, surface roughness, and instrumental noise [85, 92]. Raw data usually undergo histogram equalization, filtering, transformation and baseline shifts corrections. Several authors have demonstrated increased accuracy of classification models following preprocessing [93, 94]. Some of the frequently applied preprocessing methods in literature includes Savitzky-Golay smoothing method, the first and second derivative (to eliminates the additive baseline and linear baseline), standard normal variate (SNV) (to remove the multiplicative interferences due to particle size of the sample), mean-centered (MC), multiplicative scatter correction (to reduce the scatter in the spectra) (MSC)[91, 95, 96].

HSI systems are generally an assembly of various optical and electronical components. Such systems necessitate adjustment of systematic defects or undesirable sensor characteristics before performing reliable data analysis [62]. Hence, wavelength calibration is crucial in the initial instrumentation stage when a hyperspectral imager is employed for analysis. Re-calibration of the instrument is also necessary after some physical changes in the instrument, such as when sensor maintenance, upgrading or repairing has been performed [62]. The goal of calibration is to improve comparability of such data [44]. Wavelength calibration is assigning a discrete wavelength to the hyperspectral image band. A light source that produces spectral lines at fixed wavelengths, regression programs, and (optional) integrating sphere, or standard white reflectance surface such as spectralon surface are required to calibrate the system. HSI system records raw images in radiance. Quality of imaged produced is usually very sensitive to the sensors employed for image capturing [62].

To minimize the impact of the uneven intensity distribution of the light source and dark current in the charge coupled device (CCD) detector on the hyperspectral images, image correction is usually performed using known true spectral information. Eqn. (1) provides the formula for the image correction.

$$\rho_{xy}(\lambda) = \rho_{ref}(\lambda)\frac{R_{xy}(\lambda)-R_{dark}(\lambda)}{R_{ref}(\lambda)-R_{dark}(\lambda)} \quad (2.1)$$

where $\rho_{ref(\lambda)}$ is the reflectivity of the 50% grey calibration plate (Zenith Polymer® Reflectance standard; SphereOptics GmbH, Germany); $R_{xy(\lambda)}$ is the original uncorrected hyperspectral image; $R_{ref(\lambda)}$ the image of the calibration board and $R_{dark(\lambda)}$ is the completed black image collected after turning off the light source and $\rho_{xy(\lambda)}$ the spectra of the corrected image. One specialized software that enables this operation is the Breeze software.

Calibration of a HSI system involves a set up made up as follows; a light source, regression programs and a reference surface (usually optional). Figure 2.4 illustrates the calibration set up made up of a pencil lamp from Oriel and the emission peaks for a mercury–argon (Hg–Ar) lamp. The effect of dark current which happens due to thermal effects requires that images be corrected after its acquisition [97]. This is because the detectors of the camera usually generate the dark current signal and they are added to the signal produced [97]. Calibration then enables the separation of the sample reflectance from the system response [98].

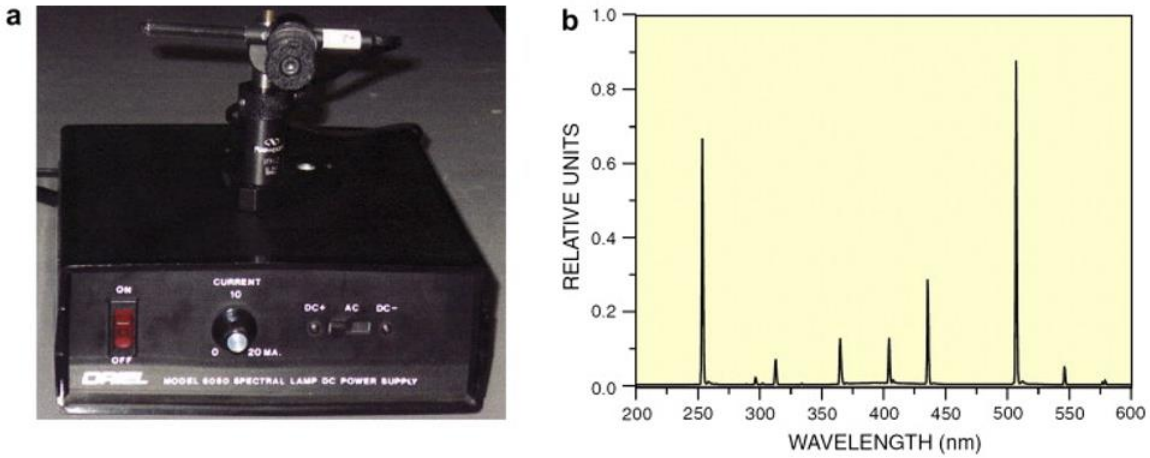

Figure 2.4: Wavelength calibration: (a) calibration pencil light (Hg–Ar, Oriel Model 6035) with power supply; (b) output spectrum of 6035 Hg-Ar Lamp, run at 18 mA, measured with MS257 ™ 1/4 m Monochromator with 50 μm slits [62].

2.3.5. Feature extraction of hyperspectral images

Typically, HSI images contains millions of data point [85]. Effective approach for data analysis, data mining, and pattern classification is crucial to extract the desired information, such as defects, from images. Multivariate analysis is used to decompose massive quantity of features into useful information and establish simple and easier understandable relationship between hyperspectral imaging data and the quality attributes of tested samples [52, 97]. One of the very effective ways for dimensional reduction in hyperspectral image analysis is the PCA method [99]. It enables contextualizing the obtained data by finding the dominant spectral data from the captured image. It follows the steps of; reflectance

calibration, data reduction and noise/stage background removal. PCA analysis usually aids in deciding the number of principal components needed by using the singular value decomposition (SVD) method for extracting principal components.

Ideally, two PCs provide the percentage of variance preservation in suitable for analysis [99]. The 1st component of the PCA model explains the majority of the variation in the initial sample and used to remove background pixels and interferences that are generally not useful for the numerical analysis [99]. For most applications, such as fruit bruise detection, disease detection or even maturity estimation of sample, a smaller area of interest on the PCA images can be obtained on the scanned fruit using thresholding algorithm to get a region of interest (ROI), with size ranging from 50 to 2500 pixels. This further reduction of the entire obtained image data into a computed average ROI of the reflectance spectra as shown in Figure 2.5a, reduces the data size and dimensionality. This process significantly reduces the complexity and improves the accuracy of the classification model. ROI can be manually selected depending on the application [100], or using the threshold segmentation method [101], the shape can be rectangular[14, 95], or circular [102]. It is often entirely difficult to obtain a complete filtered out bruised area of a sample, further analysis of the different regions using trained supervised algorithms can be utilized to achieve high-precision classification model [103].

Many general and specific purpose software have been developed to visualize and process large image data as that obtained from HS imaging. Table 2.4 summarizes some of the notable HS image processing and data analysis software. In the fresh fruit quality analysis and food processing related studies, the Hyperspectral Image Processing-MATLAB, ENVI and Evince are the frequently used tools. Particularly for image acquisition purposes, the Breeze is prominently used [86, 104, 105]. Other notable image acquisition software include spectral cube [106, 107], Spectra SENS [108], VideometerLab2 [109], Spectral imaging system HySpex [110], and LabVIEW [71, 111]. They are specialized for hyperspectral image

data acquisition and for controlling the entire acquisition set up of the hyperspectral imaging system.

Figure 2.5. An illustration of selecting a region of interest on apple fruit in the bruised area (B) and non-bruised area (S) to constitute the data, (X) is the area between the bruised area and non-bruised area (2.5a), adapted from [103]. Illustration of a binary confusion matrix

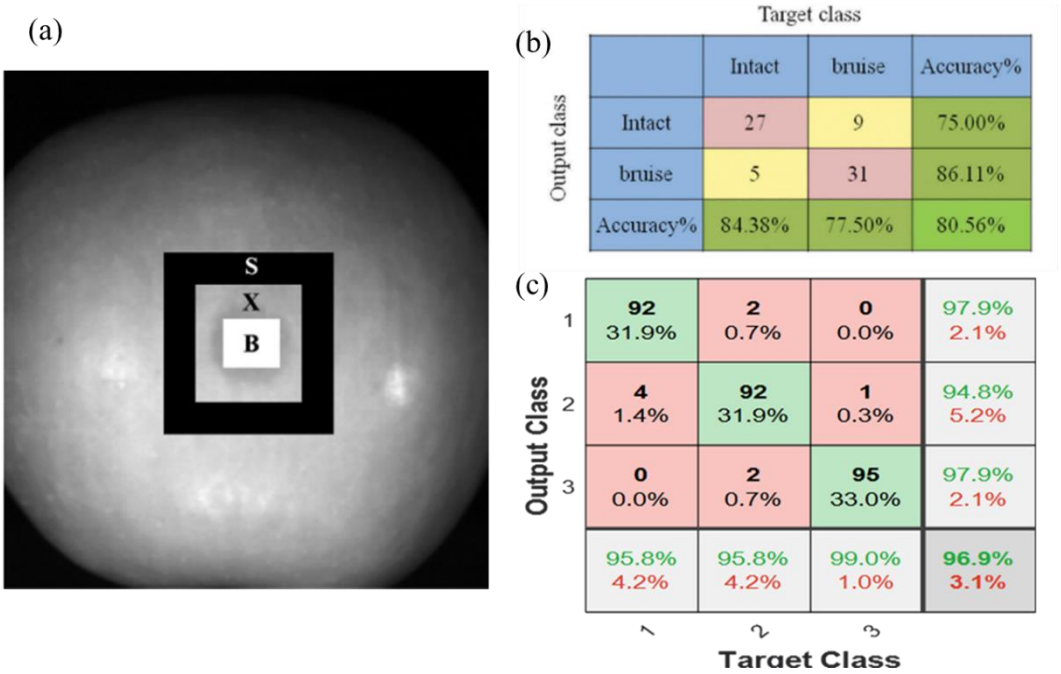

(2.5b) adapted from [95], and a multiple class confusion matrices (2.5c) of the backpropagation neural network model for pomegranate bruise detection.

There have been studies showing how advances in machine learning algorithms have improved calibration and prediction models [112–114]. The different machine learning algorithms and their comparative benefits have been reviewed by several authors [50, 115]. Some of the more recent evolution in the field of machine learning includes deep neural networks (DNNs) which includes convolution deep neural networks (CNN), very deep neutral networks (VDNNs) [112], and deep belief network [116].

Table 2.4. Summary of some of the notable HS image/spectral data processing software

Software	Description	References
ASFit	Windows-based for analysis of chromophoric dissolved organic matter (CDOM) Ultraviolet-visible (UV/Vis) spectra. ASFit can also be used to study trace metals complexation with Dissolved organic matter (DOM) based on differential spectra.	[117, 118]
EnMAP-Box	Python plugin for QGIS. Process and visualise hyperspectral remote sensing data. Environmental Mapping and Analysis Program Agricultural Applications (Agri-tools) of the EnMAP-Box include: - Plant water retrieval (PWR) - Vegetation vitality tools (VIs, Analyse Spectral Integral, Red Edge Inflection Point) - Physically based and hybrid inversion tools	[119–121]
HyTools	Is a python library for processing airborne and spaceborne imaging spectroscopy data.	[122, 123]
Hyperspectral Image Processing - MATLAB	Image Processing Toolbox™ Hyperspectral Imaging Library provides MATLAB® functions and tools for hyperspectral image processing and visualization.	[17, 108, 124]
SCIATRAN	Is a comprehensive software package which is designed to model radiative transfer processes in the terrestrial atmosphere and ocean in the spectral range from the ultraviolet to the thermal infrared (0.18–40 μm).	[125, 126]

Environment for Visualizing Images (ENVI)	Is a software application used to process and analyse geospatial imagery. It bundles together several scientific algorithms for image processing a lot of which are contained in automated, wizard-based approach that walks users through complex tasks	[25, 71, 107]
EPINA Image Lab	Is a Microsoft Windows-based multisensor imaging tool for processing and analyzing hyperspectral images	[127]
Trimble eCognition	Trimble eCognition enables you to accelerate and automate the interpretation of your geospatial data products by allowing you to design your own feature	[128, 129]
EVINCE	Is a software for multivariate data analysis and multivariate image analysis. Its key functionality includes analysis and explore large amounts of data (>1 000 000 data points), data Reduction, information extraction and data visualization	[109, 110]
BREEZE	Is a software that enables end users collect and analyse hyper- and multi-spectral images, and then develop and models to solve real-time complex problems	[104]
Waikato Environment for Knowledge Analysis (Weka)	Is a multipurpose GUI software that contains several collections of visualization tools and algorithms for data analysis and predictive modelling. It supports several standard data mining tasks, more specifically, data pre-processing, clustering, classification, regression, visualization, and feature selection.	[39, 101, 130–132]
The Unscrambler X	Is a multivariate data analysis software that integrates Design-Expert to deliver advanced data visualization solution. Some of its features includes data analysis, regression and	[39, 133, 134]

	classification methods, predictive modelling, design of experiments and descriptive statistics	
PLS Toolbox	Is one of the most extensively used software for multivariate and machine learning analysis and for chemometric applications, it is incorporated within the MATLAB® computational environment but also available as a standalone product (Solo). Some of its key features includes data exploration and pattern recognition, classifications, linear and non-linear regression, etc	[111, 135, 136]
OPUS	Is another leading multivariate software for measurement, processing, and evaluation of IR, NIR and Raman Spectra.	[137–139]
SIMCA	Is a popular advanced data analytics software for multivariate analysis. It adopts a data-intensive analytical approaches such as the use of spectroscopy and multi-omics “big data” and efficiently analyses and visualizes these data from batch processes in real-time for monitoring, prediction, and control purposes	[137, 140]

2.3.6 Performance criteria and accuracy metrics

Prediction models are typically evaluated by use of metrics such as the root mean squared error of calibration (RMSEC), cross validation (RMSECV) or prediction (RMSEP) and the coefficient of determination (R^2) [97]. In general, a good model consists of high R^2c, R^2p, and RPD values, and low RMSEC and RMSEP values as well as a small difference between them [141]. Typical values of R^2 should range between 0.90 and 0.82 as this are considered good models. whereas the values of RPD less than 1.5 and that higher than 3 are regarded as unsatisfactory and acceptable results, respectively [51, 142, 143].

For most quantitative application of HSI, especially for disease and defects detection, the classification accuracy is used to determine the accuracy of the classification model [37]. The confusion matrix table (Figure 2.5b and 2.5c) shows how the classifier performs in terms of correctly classified samples, wrongly classified samples, and the average overall accuracy. For most binary applications, where the classification problem is that of distinguishing between two samples groups, bruised and unbruised, or diseased and healthy samples, they are referred to as binary (two-class) problem. In a two-class problem, four (4) possible outcomes exist [100]. First is the true positive (TP), this is when a sample is positive and the classifier recognizes it as positive, then the false negative (FN), this is the instance where a positive sample is misjudged and classified as negative, when a negative sample is classified as negative, it is counted as a true negative (TN), and finally the instance where negative sample is wrongly classified as positive, it is regarded as a false positive (FP)[100, 144]. Typical accuracies values range between 85 – 100% [39, 145]. A comprehensive summary of performance metrics has been covered by Tripathi and Maktedar, [37].

Another performance index for evaluation classifiers is the ROC area under curve value (AUC). The ROC curve is a graphical plot of the true-positive rate vs. false-positive rate for a binary classifier. It represents a general measure of classifier performance that is invariant to the classifier discrimination threshold and the class distribution [146, 147]. Its values range between 0–1. With maximum accuracy at 1 and minimum at 0. A random guess separation involves an AUC value of 0.5 [101].

Other widespread parameters use in literature includes f-measure (sometimes together with precision and recall), Kappa statistic and the time spent for. classification [148]..

2.4. Preharvest applications of hyperspectral imaging technology in remote sensing

Hyperspectral imaging as a technique for quality or system monitoring originated with the airborne imaging spectrometer (AIS) [6]. Over the year, HSI has been shown to provide promising solution for a large- scale disease monitoring under field conditions [149]. During pre-harvest stage, disease causing pathogens tend to result in either loss of leaves and/or shoot area or changes in a leaf color due to a reduction in photosynthetic activity. These changes result in differences in spectral responses in the visible/near-infrared (Vis/NIR) regions of the Electromagnetic spectrum. However, existing on-farm detection or control strategies are cost intensive and increases the likelihood of ground water contamination (environmentally) and pesticide residues in agriculture products [150].

Precision agriculture involves the use of airborne/satellite devices for remote sensing applications. This is normally used at farmland scales due to its low spatial resolution and high operating cost and complexity. Unmanned aerial vehicle (UAV) remote sensing has been successfully used in many precision agriculture applications for preharvest quality detection and diagnostics.

During production, remote sensing is used in aspects such as pre-season planning, field preparation, planting, in-season monitoring, spraying for pest control, harvest, and post-harvest [151]. It provides a diagnostic tool for early detection of disease infestation in farm, orchards and serve to alert farmers on potential problems before they spread widely [151]. Since its first use in 1972, Remote sensing has witnessed increased application during the last two decades. This is due to technological advancement in global positioning systems (GPS), machinery, hardware and software, cloud computing, and internet of things (IoT) with hyperspectral and multispectral imaging sensors peaking on the application. Data collection for preharvest application of hyperspectral imaging technology is usually collected in various platform which includes handheld, aircraft, and satellite device [129]. There has also been development for unmanned ground vehicle (UGV) in recent time [152].

2.4.1. Remote sensing diagonostic application of hyperspectral and multispectral imaging technology

The non-destructive pre-harvest spatial yield variability was estimated for carrots using proximal hyperspectral and satellite multispectral data [153]. In their study, above ground biomass (AGB), canopy reflectance measurements and corresponding yield measures were collected from 414 sample sites in 24 fields in Western Australia (WA), Queensland (Qld) and Tasmania (Tas), Australia.

For disease detection, Vanegas et al. [154], applied airborne RGB, multi and hyperspectral imagery at two different vineyards with multiple grapevine varieties for the detection of phylloxera infestation. The authors used a multispectral MicaSense RedEdge camera to capture five discrete spectral bands: 475nm (blue), 560nm (green), 668nm (red), 840nm (red edge), 717nm (NIR). They developed a digital model of the vineyard to create a vigor assessment and compare it with an expert visual assessment Results showed that both assessment correlate to a good level, signaling that the developed method is a good approach for generating vigor assessments in vineyards.

In another study, Abdulridha et al. [155] detected the presence of citrus canker in sugar belle (immature) fruit using a UAV mounted with a hyperspectral imaging sensor. The same imaging system mounted on a UAV was used to detect citrus canker on tree canopies in the orchard. This technique successfully distinguished the late-stage canker-infected fruit with 92% classification accuracy. The UAV-based technique achieved 100% classification accuracy for identifying healthy and canker-infected trees. Other studies on preharvest application have been on maturity stages for blueberry [156], disease indices for ‘Flavescence Dorée’ Grapevine disease identification [157], salinity level on date palm fruit [158], wheat disease detection [159]. A comprehensive review of the different applications of hyperspectral imaging for preharvest purposes using remote sensing approach has been given by Panda et al., [129].

2.4.2. Challenges of preharvest application of hyperspectral imaging for disease diagnosis

RS systems provide robust and accurate database on the spectral behavior of agricultural crops [160]. Such information has found application in many areas such as quality monitoring, disease and growth detection, irrigation and crop yield monitoring and farm management. Despite the commercial availability and increased use of HSI mounted on RS systems for biosecurity diagnosis, it is still not readily available to those in the agribusiness as most of the harvesters are not equipped with them [160].

The type of sensor used in RS application also plays an important role in determining its efficiency. In a study on carrot root yield, the accuracy of two sensors (proximal hyperspectral and satellite multispectral sensors) were explored [153]. Results showed that vegetation indices derived from hyperspectral sensors produced poorer yield correlation coefficients ($R^2 < 0.1$) than similar measures from the multispectral sensors ($R^2 < 0.57$, $p < 0.05$), making multispectral sensors better alternative to be deployed for such investigations.

2.5. Postharvest applications of hyperspectral imaging technology

2.5.1. Infections and disease diagnostics for fresh agricultural produce

Starting from harvesting, fruits are highly susceptible to pathogen invasion, pests, and microbial contaminations and fruit safety are crucial throughout the supply chain. Removing fruits and vegetables with serious defects early can prevent the infection of the whole batch. Conventionally, fruits and vegetables are inspected with respect to color, texture, size, and shape by conventional machine vision system in the commercial sorting machines. However, sorting by defects is still a challenging task due to the high variance of defect types and existence of stem/calyx concavities. Some defects may have similar color and texture as sound peel, such as bruises, rottenness, or chilling injury. Therefore, recent trends in automated sorting are aimed to detect defects based on color, texture, and spectral reflectance by using HSI and MSI systems [52, 81].

Illumination of samples during imaging is critical for data acquisition using HSI technique. Different researchers have applied different light intensity depending on the fruit and the

condition of sample during the acquisition process. Two 50 W halogen lamps adjusted at angle of 45° were used to illuminate the camera's field of view to study disease diagnostics in apple fruit [68]. Munera et al. [134], used 12 halogen spotlights of 37 W each and eight 20W halogen lamps powered by 12V supply source placed in two opposite frames positioned at an angle of 45° to the persimmon fruit sample. In the case of apple fruit, eight 20W halogen lamps placed in two opposite frames positioned at an angle of 45° towards the conveyor belt surface was applied [39]. The reason for these different settings and configuration could be attributed to the difference in texture and peel of the various fruits.

Exposure time for sample scanning varies, for kiwifruit it was 10ms [161], 15ms for strawberry [136], 20ms for pear [162], 30ms for kiwifruit [163].

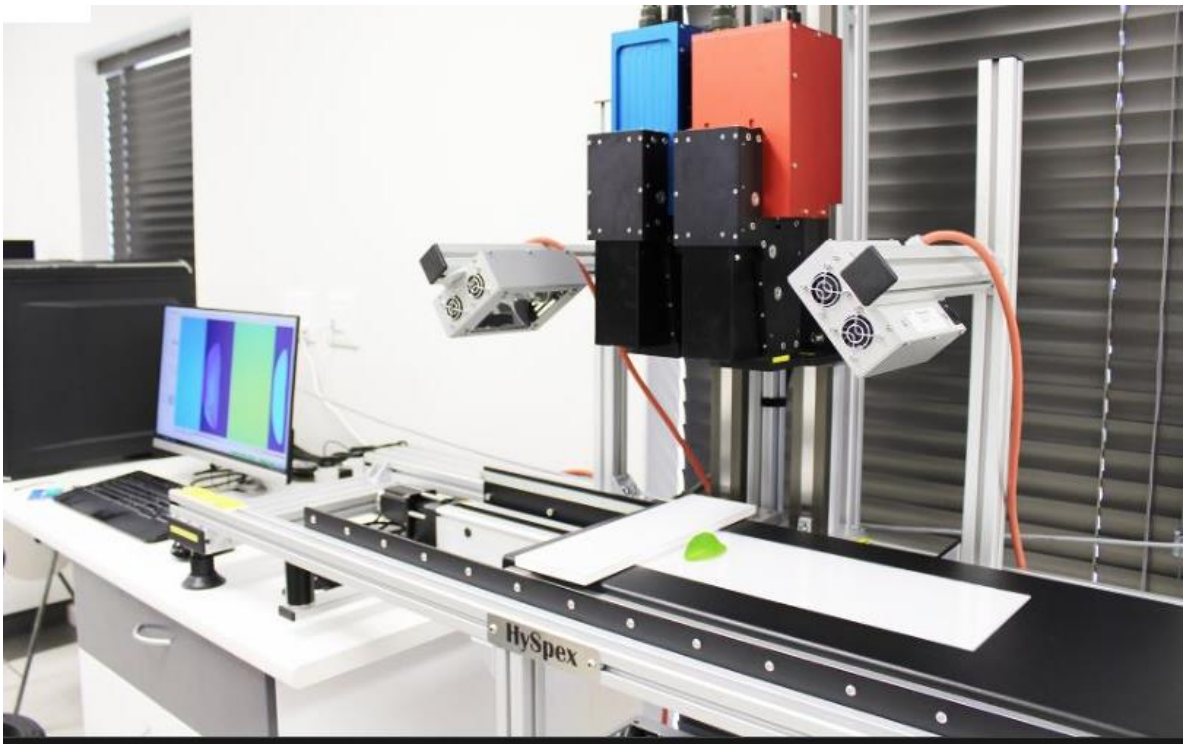

Figure 2.6: Image of hyperspectral image acquisition set up at the Central Analytical Facility (CAF) laboratory, Department of Food Science, Stellenbosch University, South Africa. The cameras were mounted above a translation stage which has speed regulation. A 30 cm focal length lens with a field of view of 9.470 cm (SWIR) and 9.733 cm (VNIR) was used. The illumination source for each camera consisted of two halogen lamps (12V/150W) placed in two opposite frames positioned at an angle of 45° and 30 cm above the translation stage.

2.5.2. Ground truth data acquisition

The accuracy of a model depends on the accuracy of the reference or ground truth measurement. Sample condition before scanning need to be grouped and identifiable as diseased or not infected [39, 146], bruised or not bruised [104, 164, 165]. The number of samples and the grouping for diagnostic application using hyperspectral imaging is also key to a successful experiment. Most studies usually have samples grouped into diseased(inoculated) and control. In a study to detect early decay in citrus, [166], using a total of 210 fruits grouped their sample between 80 sound fruits and 130 infected fruits with spores of *Penicillium digitatum* fungi. Classification model was built using 140 (60 sound samples and 80 infected samples) which were selected randomly as training set to develop the algorithm, whereas the remaining 70 samples (20 sound samples and 50 infected samples) as test set to evaluate the performance of algorithm. Their result indicates a high classification accuracy of 98.6%.

In another application on citrus, a total of 240 fruits were studied: 60 sound fruit were used as control while 60 inoculated with spores of *Penicillium digitatum* and 60 inoculated with spores of *Penicillium digitatum* [145]. Similar pattern of sample grouping and control method was adopted for mandarin study [167]. Other studies on strawberries where 1800 fruit were inoculated with fungal infection and 900 healthy fruit were used as control [39]. It would be observed that the ratio of inoculated and control subgroup for most diagnostic application is in range of 60:30 with more samples inoculated compared to the control group.

Diseases and infections are some of the greatest causes of losses in postharvest. Fungal infections generate great economic losses to the fruit and agricultural industry [168]. For non-destructive detection and discrimination, samples must be handled in such a manner that accurate ground truth data is captured. Considering the non-destructive nature of technique. It means that samples must be artificially inoculated in other to obtain a diseased set of samples. Samples are also conditioned and grouped for discriminant analysis purposes. Disease pathogens such as bacteria, fungus and viruses can be cultured in laboratories and

used for experimental study. This is the case in many HSI applications for disease detection, as it ensures the validity of the ground truth data to be employed for the study.

The inoculant or pathogen to be used on a fruit sample is usually dependent on the specific application. For example, gray mold, caused by *Botrytis cinerea* Pers., is the most economically important postharvest disease of pomegranate. This is also the case for strawberries [38, 101]. Other fungi causing fruit rot worldwide include *Aspergillus niger, Penicillium spp., Alternaria spp., Nematospora spp., Coniella granati* and *Pestalotiopsis versicolor*[5, 169].

In the citrus industry, decay caused by fungi is among the main cause of decay during post-harvest phase and handling of the fruit. The fungus *Penicillium* sp., has been identified to lead to the most postharvest loses in citrus packinghouses [145, 146]. Inoculants are usually chosen based on susceptibility to the sample under consideration. For most fungal disease detection study, the fungi are usually grown on potato dextrose agar (PDA) at 24 °C and 85% relative humidity for 7 days prior to inoculation experiments [38].

The method of inoculation is another area that defers for different fruit due to the fruit physical structure. Fruit with delicate structure and soft tissues or scale are very susceptible to tissue damage and infections caused by a wide range of phytopathogenic fungi, bacteria, and viruses [38]. Such fruit are usually inoculated by artificial immersion [39]. Li et al. [166] applied the inoculant by injection using syringe with steel needle. To inoculate Spinach leaves, the bacteria pathogen *E. coli* was infected by dipping in suspension [170]. In another study on citrus, sample inoculation was performed using a suspension of spores [145]. Pathogen with a concentration of 106 spores/ml for both fungi, which is sufficient to cause infestation in laboratory conditions.

Literature shows that most inoculation are based on a dissolution of spores in suspension with a concentration of 106 spores/ml. This concentration is usually used to produce rottenness and have been recommended for numerous applications for sample conditioning during non-destructive analysis and diagnostics of fruit and vegetables [39, 145, 171]. Spectral data of the different samples inoculated with different concentrations of inoculant was acquired under the same conditions for all the samples and monitored for fungal growth. The authors found that the different species showed increasing spectral signal as the fungus grew and were able to detect the presence of fungal contaminants on the maize after 48 h from inoculation and incubation.

HSI have found huge applications in the field of agriculture for diagnostic purposes. Different studies have shown varying range of classification success in applying this non-destructive technique for detection of infections and diseases in fruits, vegetable, and some agricultural products. Strawberries (*Fragaria sp.*) was diagnosed for fungal infection [39]. In their study, reflectance spectra of fruit were acquired during four days after inoculation and discrimination models was built using the backpropagation neural network (BNN) model. The prediction accuracy of distinguishing between inoculated and control fruit was higher than 97%. This study showed the effectiveness of HSI to successfully be used as diagnostic tool for early detection of fungal disease on strawberries.

The presence green mould and blue mould was investigated on mandarin using a Hyperspectral LCTF-based system [167]. Neural Networks was used to segment the hyperspectral images and a classifier based on decision trees achieved a very high accuracy of around 93%. This result indicates the effectiveness of this technique for non-destructive diagnostic application. Similar study was carried out by [146]. Three different approach was analysed, and result ranged between 87.5 – 95.5%. The third approach using the set of four input features yielded the highest classification performance (Figure 2.7).

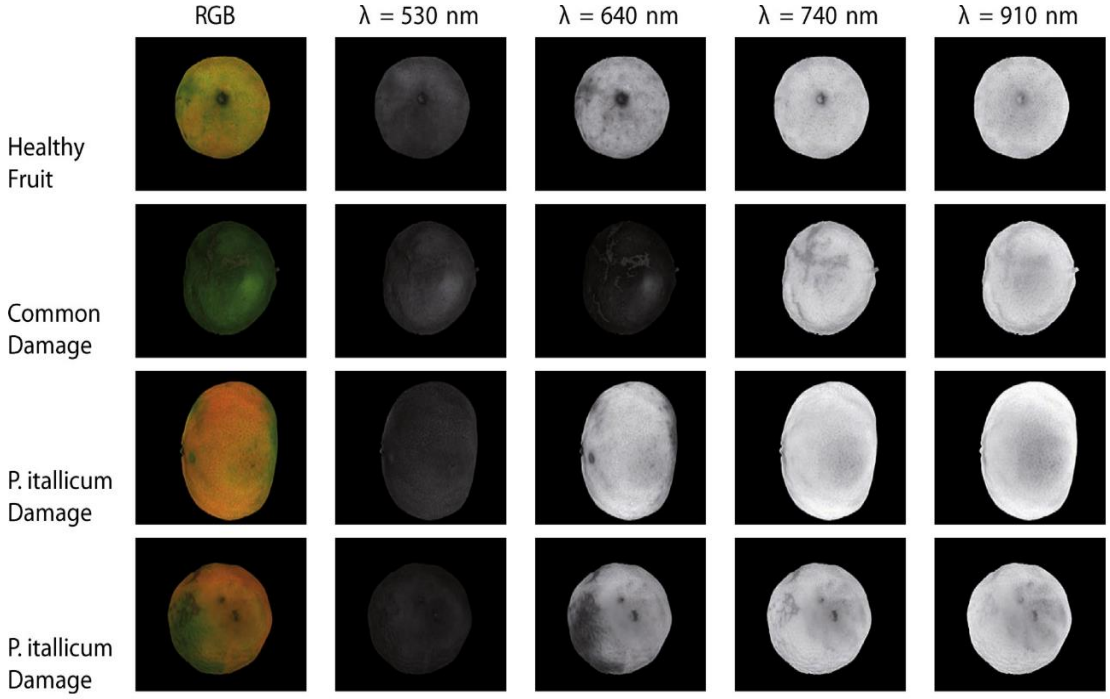

Figure 2.7: Hyperspectral (RGB and monochromatic) images (530 nm, 640 nm, 740 nm and 910 nm) acquired by hyperspectral computer vision system of sound mandarins and fruit affected by thrips/wind scars, *P. digitatum* and *P. italicum*. Adapted from [167].

Table 2.5 gives a summary of the application of HSI for diagnostic testing on selected horticultural produce.

Table 2.5. Overview of diagnostic applications of multispectral and hyperspectral imaging for disease and infection detection of fresh produce.

Produce	Detection	Sample size	Inoculant	Inoculation method	Classification accuracy	References
Apple	Rottenness	120 - 220	Penicillium	Inoculated with liquid suspension culture of Penicillium spores	97% - 99%	[71, 172]
Citrus	Decay, Black spot	-	PD		91% - 100%	[166, 173–175]
Mandarin	Decay	240	PD; PI	Performed using suspension of spores	82.92 – 97.18%	[145, 146, 167]
Peach	Fungal contamination		PD, PI		98.3% - 98.6%	[176]
Spinach leave	Decay		E. coli	Dipping in suspension		[170]
Strawberry	Fungal infection	2700	BC; CA	Immersion	97 – 99%	[39, 177]
Tomato	Virus infection				86 – 95%	[178, 179]

E. coli, *Escherichia coli*; PD, *Penicillium digitatum*; PI, *Penicillium italicum*; BC, *Botrytis cinerea*; CA, *Colletotrichum acutatum*; LCTF, Liquid crystal tunable filters

2.5.3. Other HSI applications in food safety and biosecurity

2.5.3.1. External damage and defect detection of agricultural produce

Table 2.5 summarizes application of hyperspectral imaging on different fruits for quality attributes and external defects detection. HSI have been deployed for the evaluation of apple quality with accuracies ranging from 80.4% to 99% in defect detection application and $R^2 \geq$ 0.8577 for most qualitative analysis. For banana, MLR and PLSR based models were used with accuracies ranging between 0.53 to 0.97 in R^2 and 1.95 to 5.92 in RMSEP [17], 175, 176]. Lee et al. [102] applied hyperspectral imaging beyond the NIR range of 950–1650 nm to detect bruise damage underneath pear fruit skin. The result demonstrated that the best threshold waveband ratio detected bruises with the accuracy of 92%. Other attributes of pear for which HSI have been applied for its evaluation include firmness, soluble solid content, variety identification and physical damage. Other fruit studied showed similar trend in terms of their model accuracies and data analysis used (Table 2.6). These studies indicated the feasibility of hyperspectral imaging technique to detect external and internal disorder.

Table 2.6: Overview of applications of multispectral and hyperspectral imaging for external defects and damages assessment of selected horticultural fruit.

Produce	Quality attribute	Data analysis	Model accuracy	References
Apple	Bruise, defect, firmness, mealiness, contamination	PLS-DA, PCA, MNF, SIMCA, LDA, SVM, BR, LLE, HEA, PLSR, iPLS-DA, SLOG, SMO, ESD, kNN,	CA range between 80.4% - 99%; $R^2 \geq 0.8577$.	[71, 99–101, 103, 104, 133, 182–186]
Banana	Moisture, firmness, colour	MLR, PLSR	R^2 range between 0.53 - 0.97; RMSEP ranged btw 1.95 - 5.92.	[17, 180, 181]
Blueberry	SSC, firmness, mechanical damage	PLSR, PLS-DA, SVM, FCN	R^2 = 0.79 – 0.87; CA range between 76.7% - 92.5%.	[131, 147, 164, 187, 188]
Citrus	Decay, canker,	MLP, BR, PCA	CA range between 87.46% - 96.5%;	[174, 175, 189, 190]
Cucumber	Defect	PLS-DA	CA range between 79.8%–100%	[191, 192]
Grape seed	Maturity	PCA, DA, PLSR	$R^2 \geq 0.95$	[20, 193]
Jujube	Defects	PCA, SVM, SIMCA	CA range between 93.3% - 100%;	[194–197]

Kiwifruit	Ripeness, firmness, SSC, Bruise detection, sugar content,	PLS, PLS-DA, GA, VIP, RBF-SVM, SPA,	R^2 = 0.76 – 0.98; CA range between 93% - 97%.	[124, 161, 163, 198, 199]
Limes	TSS, TA, maturity	PLSR	R^2 range between 0.69 - 0.83; RMSEP ranged btw 0.049% - 0.288%.	[200]
Loquat	Defects	CARS, PLS-DA, CARS-PLS-DA	CA range between 92.3% - 100%	[201, 202]
Mango	Mechanical damage, infestation	k-NN, NBC, ELM, DT, LDA	67.46% – 100%	[149, 203, 204]
Peaches	Bruise, firmness, chilling injury	PCA, PLSR, LS-SVM, PLS-DA, ANN, SVM	CA range between 85.37% - 100%; R^2 range between 0.50 - 0.75	[25, 205]
Pear	Bruise, firmness, SSC, varieties, physical damage	SVM; RF, PLS-DA, PCA, SAE-FNN, FNN, SPA-PLS, PLS, PCA, CARS, CARS-PLS	CA range between 92 - 100%; R^2 range between 0.78 - 0.99; RPD range between 3.05 – 3.68	[162, 165, 206–209]
Persimmon	Ripeness, firmness	LDA, SIMCA, LSSVM, QDA	CA range between 62.5 – 95.3%; R^2 = 0.91; RMSEP = 4.34	[134, 210, 211]
Pomegranate	pH, TSS, TA, grading,	PLS, MLR, ANFIS, RSM, ANN, PLS-DA, SIMCA, PCA	$R^2 \geq 0.88$, RPD $\geq$ 5.01 , MSE = 0,.202	[18, 212, 213]

			95%	
Plum	SSC, firmness, colour	PLSR	$R^2 \geq 0.8$	[214]
Strawberry	Bruise, fungal infection	LDA, ND, ANN	84.6 – 99.9%	[27, 39, 101, 177]
Tomato	Defect, contamination	PCA, BR	CA ≥ 99%	[215–219]

Abbreviations: R^2, Coefficient of Determination; PCA, Principal Component Analysis, BR; Band Ratio, SVM, Support Vector Machine; PLS-DA, Partial Least Squares Discriminant Analyses; SIMCA, Soft Independent Modelling of Class Analogies; LDA, Linear Discriminant Analysis; MLP, Multilayer perceptron; MSE, Mean Square Error; CA, Classification accuracy; LLE, Locally Linear Embedding; GA, Genetic Algorithm; VIP, Variable Importance in Projection; DA, Discriminant Analysis; PLSR, Partial Least Squares Regression; MLR, Multi-Linear Regression; RBF-SVM, Structural Risk Minimisation Support Vector Machine; LS-SVM, Least Squares Support Vector Machine; HEA, Hierarchical Evolutionary Algorithm; SLOG, Simple Logistic; SMO, Sequential Minimal Optimization; FCN, Fully Convolutional Networks SAE, Stacked Auto-Encoders; FNN, Fully-Connected Neural Network; SPA, Successive Projections Algorithm; k-NN, K-Nearest Neighbour; QDA, Quadratic Discriminant Analysis

2.5.3.2. Adulterants and varietal detection

HSI has found application as a check for adulterant in powdery and dried as well as to detect the origin or variety verification for agricultural processed products. In a similar study, Shrestha et al. [220] applied two different classifiers to discriminate different cultivars of tomato seed. The authors achieved an accuracy range of 94 - 100 %. SVM–DA proved to perform better than PLS–DA in their study. Similar results was achieved in a different study on tomato seeds [221]. Xiong et al. [222] used HSI to analyze the presence of polyphenols in tea and reported a coefficient of determination $R^2 = 0.915$. Other applications of HSI have been reported on spinach seed [223] watermelon seed [224], vegetable oil [225, 226], and for determination of storage duration of buhha tea [222].

Another area of emerging importance of multispectral/ hyperspectral imaging is in adulteration /fraud detection of homogenous food products. Food materials like herbs and spices are usually crushed or ground and are susceptible to adulteration at any stage of their long and complex supply chain. In addition, some group of adulterants can be really damaging to human health when consumed [227]. In a study to diagnose food fraud in black pepper, Orrillo et al. [228] investigated the potential of near infrared hyperspectral imaging (NIR-HSI) combined with multivariate analysis to identify black pepper adulterated with papaya seeds, a common adulterant. Their finding showed that classification models PCA and SIMCA achieved 100% accuracy for berry samples and sensitivity was higher than 90% for ground samples. In a similar study, certified raw materials (*Sceletium tortuosum* and *Cyclopia genistoides*) and herbal tea blends were adulterated, and hyperspectral data were acquired for discriminate analysis [229]. A partial least squares-discriminant analysis (PLS-DA) model with predictive ability of 95.8% was developed. Their results confirm that HSI is a reliable diagnostic visual tool for the quality assessment of herbal tea blends. Table 2.7 summarizes the application of hyperspectral imaging technique for quality diagnostic of processed products. Further studies on the nondestructive quality attributes of various processed horticultural products (dried, powder and oil products) have been extensively reviewed [19, 142].

Table 2.7: Overview of biosecurity applications of multispectral and hyperspectral imaging on selected processed horticultural products.

Produce	**Detection**	**Wavelength range (nm)**	**Chemometric analysis**	**References**
Black pepper	Adulteration	900 – 1710	PCA, SIMCA	[228]
Buhha tea	Storage duration		PLS-DA	[222]
Pistachio nuts	Adulteration	2703 - 50000	PLSR	[230]
Spinach seed	Seed viability	395 – 970	PLS-DA	[223]
Tea blend	Adulteration		PLS-DA	[229]
Tomatoes	Variety identification	375 – 970	nCDA, PCA, PLS-DA	[220, 221]

PCA, Principal Component Analysis; PLS-DA, Partial Least Square Discriminant Analysis; PLSR, Partial Least Squares Regression; nCDA, Normalized Canonical Discriminant Analysis, SIMCA, Soft Independent Method of Class Analogy.

2.6. Challenges in evaluating fruit quality by HSI

2.6.1. Physical and biological variability

Apart from the inherent problems related to the acquisition, processing, and analysis of the massive hyperspectral image data there are also challenges arising from the physical and biological variability of fruit on the application of HSI [69]. Whole surface detection, discrimination between defects and stems/calyxes, unobvious defect detection, robustness of the feature recognition algorithms, as well as rapid multispectral imaging system development. Like every other non-destructive technique, HSI require highly accurate reference measurements or ground truth in the case of preharvest application.

Image acquisition for most application requires that imaged samples are manually arranged to expose defect to the camera [216]. This is challenging as it cannot be replicable in an idea sorting line for practical application. Research must be geared towards fully automating image acquisition protocol to mimic practical applications in packhouses. It has been highlighted the different factors that influence the performance of calibration and prediction models of HSI imaging technique. Large representative samples size with variability in terms of cultivar difference, growing conditions and seasonality should be incorporated in the development of accurate and robust classification and calibration models. Accurate selection of image acquisition mode, wavelength range, and optimal data pre-processing technique can effectively be optimized to achieve higher model accuracy.

Inoculation of sample for diagnostic application must be cultured, incubated and temperature controlled. It is recommended that the right concentration is achieved as well as the spore count or CFU/ml. Classifiers greatly influence the performance of model, and with evolving data analysis and development, improved classification algorithm is being adopted for qualitative and quantitative analysis.

2.6.2. Dimensionality of hyperspectral images

Hyperspectral images with their spatial and spectral dimensions are usually large sets of information. To this end, data storage and analysis capabilities are frequent limitations of using hyperspectral data. Hence, image data size and dimensionality reduction process are very important in processing HS images. By implementing dimensionality reduction, redundant information can be eliminated. This process considerably simplifies the subsequent processes of classification model development. PLS, PCA and ANN methods frequently used to perform dimensionality reduction [6, 99, 206]. In this context, several dimensionality reduction methods have been proposed [6, 231]. Li et al. 2011 [14] applied PCA based dimensionality reduction

technique for bruise detection on oranges. The authors selected the most discriminant wavelengths in the range 400–1000 nm and achieved better detection accuracy at six wavelengths (630, 691, 769, 786, 810 and 875 nm). Similarly, Wang et al. 2012 [232] applied the same technique for sour skin damage detection on onions.

2.6.3. Insufficient training samples

Number of samples for training is crucial for artificial neural network-based classification problem [233, 234]. Insufficient training samples have been a significant bottleneck for supervised HSI classification. This problem considerably hinders the practical application of HSI system. Using insufficient training sets can significantly cause overfitting [235], while collecting sufficient HS image datasets remains costly and time-consuming [236]. Wambugu et al. (2021) [234] summarized and discussed several training sample generation methods including data augmentation: transformation-based (translation, flipping, rotation) mixture-based, or the addition of noise and synthetic data generation (synthesizer network using generative adversarial networks (GANs)). Augmentation implements realistic transformation to increase the diversity of the training set. Figure 2.8 depicts additional images generated by image rotation (top row) and noise injection (bottom row) implemented for fruit category identification problem [237].

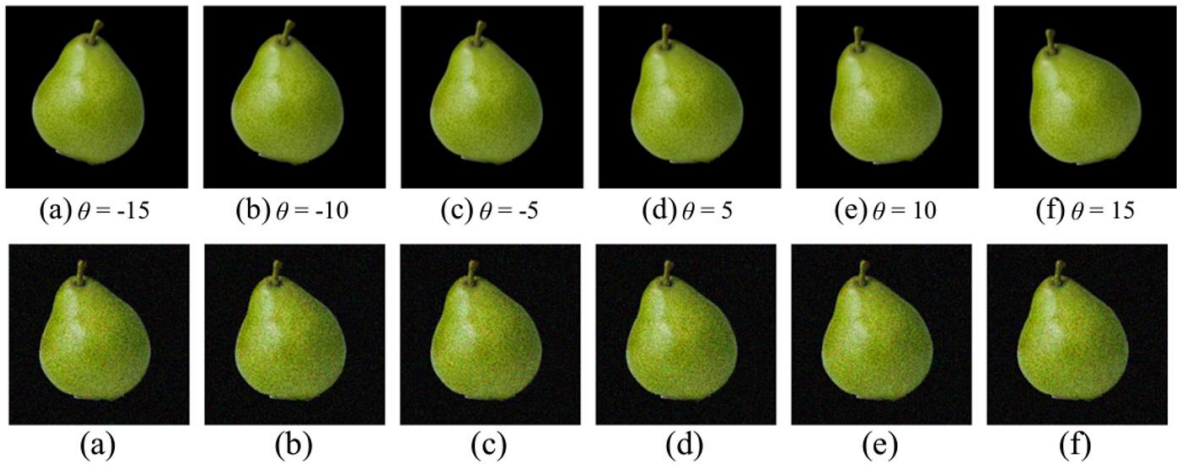

Figure 2.8: Augmentation based new image generation. Generated images by image rotation (top row) and generated images by noise injection (bottom row). Adopted from Zhang et al. (2019) [237].

Synthetic image is partly or completely artificially generated following methods such as compositing, styled transformation, and foreground and background augmentation, and have successfully been applied on images [37]. To address the problem of data shortage, Bird et al. [238] applied synthetic data generation using Conditional Generative Adversarial Network on

the training data for 2000 epochs, and it learns to generate relatively realistic images (PBP) to increase the number of training samples (Figure 2.9).

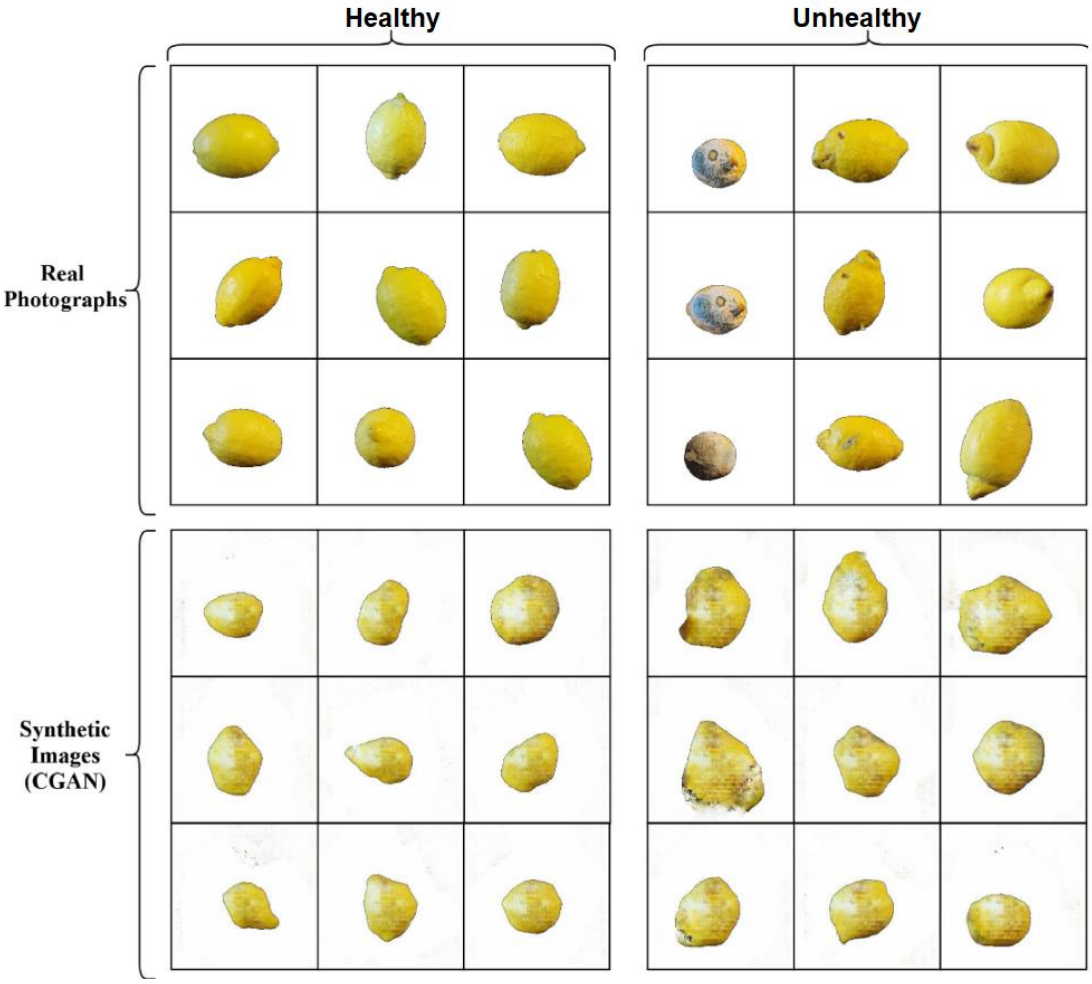

Figure 2.9: Examples of both real photographs and Conditional GAN outputs (Epoch 2000) for the two classes of healthy and unhealthy lemons [238].

2.7. Conclusion and future perspectives

The application and of hyperspectral imaging technique as a diagnostic tool for food inspection and biosecurity have been summarised. Various studies have shown varying range of application with high accuracy. The combined feature of imaging and spectroscopy enables the collection of massive spectral information for every pixel which provides the chemical constituents of samples and a chance to refine the data and perform critical analysis adequately [94].

HSI and MSI as a diagnostic technique for disease and biosecurity monitoring in agri-food products, research have demonstrated the potential for non-destructive, rapid, and online inspection of fruit qualities. Inspection of maturity or ripeness stage, evaluation of physicochemical attributes (firmness, TSS, TA, and varietal and geographical discrimination),

and detection of physical defects and contaminants in fruits are scientifically examined by many researchers. Also, the application of HSI and MSI in the quality analysis of processed agricultural products like dried seed samples and processed oil products have been reported. For real-time online monitoring implementation of hyperspectral imaging technique, high data

CHAPTER 3

Pomegranate quality evaluation using non-destructive approaches: A review

Abstract

Pomegranate (*Punica granatum L.*) is one of the healthful and popular fruit in the world. The increasing demand for pomegranate has resulted from it being processed into different food products and food supplement. Researchers over the years are garnering interest in exploring non-destructive techniques as an alternative approach for quality assessment of harvest from on farm point to retail level. The approach of non-destructive techniques is more efficient, inexpensive, faster and yield more accurate results. The aim of this study is to critically review recent and previous development in the application of non-destructive techniques in quality evaluation of pomegranate fruit. Future trend and challenges of using non-destructive techniques for quality evaluation are highlighted in this review paper. Some of the highlighted techniques include computer vision, imaging-based approaches, spectroscopy-based approaches electronic nose and hyperspectral imaging technique. Our findings shows that most of the applications are focused on grading of pomegranate fruit using machine visions systems and electronic nose. The measurement of total soluble solids (TSS), titratable acidity (TA) and pH as well as other phytochemical quality attributes have also been reported. Value added products of pomegranate fruit such as fresh-cut and dried arils, pomegranate juice, pomegranate seed oil has been non-destructively investigated for their numerous quality attributes. This information is expected to be useful not only for those in the growers/ processing industries but also for other agro-food commodities.

3.1. Introduction

For most fruit and vegetables, the features that distinctly indicate quality are four attributes: colour (appearance), flavour (taste, smell and aroma), texture and nutritional value [65, 239, 240]. In general, fruit freshness comprises of its colour, firmness and surface features (glossiness and shrivelling) [240]. These attributes affects consumer acceptance, consumption and usage of fruits and vegetables as well as their products [241]. In the last few decades, the improvement in society's standard of living has led to a significant increase in fruit consumption [51]. Some of the mostly consumed fruits includes apple, orange, kiwifruit, peach, grape, strawberry, grape, jujube, banana, mango, pomegranate among others.

Fruit quality control, inspection and sorting are essential to ensure adequate quality and safety for fresh consumption and to earn high-return on investment [6, 242, 243]. High quality product is still of utmost importance, especially for export market [244]. Pomegranate fruit is consumed globally both as fresh and in processed form such as dried arils, juice, seed oil, etc. (Figure 3.1). It is a fruit-bearing spherically shaped deciduous shrub or small tree [245]. It is composed of an internal edible portions called arils, and each aril contains a seed which is surrounded by a translucent sac containing juice [1, 169], and an outer hard thick covering called the peel [245]. In the past decades, the demand for pomegranate fruit has been increasing due to its nutritional and health benefits [2–4]. This global awareness has resulted in considerable increase in commercial farming of pomegranate fruit [5, 246]. Recently, pomegranate fruit value-added produce have included its peels utilization as animal feed [247, 248], as well as rich antioxidant, metabolomic peel extract [249, 250].

Recent attention in food quality and safety have resulted in in industry taking greater responsibility in finding alternative technological approaches for estimating the fresh quality of pomegranate fruit and its value-added produces [18, 212, 251]. Grading is one of the activities done in the industry to distinguish fruit quality. It is usually done based on weight, size and external rind appearances [252]. At present, pomegranate fruit are sorted based on external appearance only due to the thick rind [241, 244]. However, the arils which are delicate can be damaged during handling and assuring their quality is crucial [212]. On the other hand, pomegranate fruit sorting should be simple and reliable [241, 244]. Hence, fast and effective non-destructive methods have become an urgent need for quality detection.

Non-destructive/non-invasive approaches are recent advances in the evaluation and detection of the quality of horticultural fruit and its products [21, 50, 142, 253, 254]. Non-destructive

testing (NDT) provides quantitative and qualitative fruit quality data without destruction of the sample [255]. Compared to traditional quality analysis methods, NDT allows analysis of intact fresh fruit without cut opening or destroying the fruit making it best suited for online inspection.

Some of the widely used NDT techniques include: visible–infrared spectroscopy, Raman spectroscopy, nuclear magnetic resonance spectroscopy, X-ray CT and spectral imaging [19]. These techniques have been investigated for their potential as analytical tools for the quality evaluation of different food samples. Near-infrared spectroscopy (NIRS) and machine vision systems (MVS) were the most successful technologies in the past few decades for the automatic quality inspection of fruits and vegetables [241]. Spectral imaging which involves hyperspectral and multispectral imaging is a hybrid system that utilizes imaging and spectral data for fruit quality analysis [18, 212].

There are several published reviews that focuses on non-destructive quality measurement of fruits such as mangos [255], citrus [91] and watermelon [256]. Particularly for pomegranate fruit, several authors have written extensively on postharvest quality attributes and benefits of pomegranate and its products [4, 169, 257, 258]. To the best of our knowledge, no review has been published focusing on non-destructive assessment of pomegranate fruit despite several application of non-destructive assessment technologies for quality assessment of pomegranate fruit. Therefore, the objective of this review is to evaluate recent technological advancements and applications of various non-destructive methods for the measurement and prediction of external and internal quality attributes of pomegranate fruit and its products.

3.2. Quality attributes of pomegranate fruit

The term “quality” can connote the subjective perception of different explicit parameters, which can be analysed from different viewpoints [259]. In general, fruit quality is defined by four major attributes: colour and appearance, flavour (taste and aroma), texture and nutritional value [65, 260]. Pomegranate fruit maturity is perceived by its colour, firmness and surface features (glossiness and shrivelling) [240]. These attributes inform consumer acceptance, consumption and usage of these fruit as well as its products [241]. Quality assessment of pomegranate fruit is a combination of appearance, taste, aroma, and textural properties. Consumers judge initial quality based on external properties such as fruit mass, shape, and skin appearance (colour, free of cracks, sun scalds, and bruises). Their repeated purchase is based on organoleptic properties related to internal attributes these include total soluble solids (TSS),

titratable acidity (TA), and flavour (sugar/acid ratio) and phenolic content [2]. Fruit external features such as sunburn, cracks, and splits, and other mechanical damages such as bruises are also indices used to measure fruit quality and marketability by industry and packhouse operator [261, 262]. This section provides a brief overview on the quality attributes used for evaluating pomegranate fruit and its products.

3.2.1. External quality attributes of pomegranate fruit

Fruit physical properties and condition (aril volume and juice content) play key role in its commercialization (marketability, processing, and profitability of the fruit). This is because these attributes influence the quality of processed products from the fruit and influence consumer behaviours on the consumption of fruits [2, 5]. Colour is one of the most important quality attribute as it determines whether a fruit is considered fresh or not [32]. To this end, colour is one of the most widely measured product quality attributes in postharvest handling and food processing industries. The colour of pomegranate fruit is derived from its natural pigments. It changes over time as the fruit goes through maturation and ripening. Colour of pomegranate fruit is measured using colorimeter or Mansell colour charts. For the colorimeter, colour measurement is based on the CIE L*, a*, b* values. The L*, a*, and b* and C* defines the colour space on which human colour perception is based [263]. In defining these attributes, Pathare et al. [32]described L* value to represent lightness, a* value represents redness (+a*) or greenness (-a*), and b* value represents yellowness (+b*) or blueness (-b*). Another index derived from colour include glossiness. Study shows loss of gloss to be undesired and fruits with matt peel are being rejected by consumers [242, 243]. Consumer preference is towards fruit with deep red, glossy, smooth and slightly shiny surface appearance [264]. Typical values for colour attributes for pomegranate fruit at harvest maturity and its products are presented in Table 3.1.

Textural properties help to indicate how pomegranate fruit should be handled [265]. Furthermore, texture of pomegranate informs how the fruit response to physiological or pathological changes during maturation, ripening or storage [266]. Textural properties which include firmness, hardness and toughness of kernel are indicators to fruit resistance to bruise damage. Firmer pomegranate fruit and arils are reported to have low membrane lipid catabolism and stable shelf life and are thus less likely to be bruised during postharvest handling [265, 267]. Typical firmness of pomegranate grown in South Africa varies between 312.05 N and 390.60 N for whole fruit firmness, 75.53 – 83.76 N (fresh aril) and 220.50 – 253.98N (dried aril) Table 3.1.

Table 3.1: Summary of typical quality indicator values for intact pomegranate fruit and products

Quality Attributes	Cultivar	Intact Fruit	Typical Values				References
			Fresh Aril	Dried Aril	Seed Oil	Juice	
Weight (g)	Bhagwa, Ruby	250.0–509.8					[268, 269]
Shape index	Bhagwa, Ruby	0.91–1.10					[269]
Volume (cm^3)		220–300					[269]
Sphericity		1.02–1.08					[269]
Aril yield (%)		46.76–58.82					[269]
CIE colour coordinates (L*)	Omani, Bhagwa, Ruby	44.15–46.51	25.00–30.88	20.54–33.62			[4, 245, 268, 269]
(a*)		40.33–43.13	16.06–23.07	12.26–24.44		3.37–4.73	
(b*)		–	6.63–7.77			0.15–0.52	
(C*)		48.35–53.39	15.75–17.82	12.84–29.83		3.38–4.77	
(h°)		30.61–33.07	23.85–25.81	12.00–27.10		3.12–3.30	
Moisture (%)	Omani, Bhagwa, Ruby		66.00–75.58				
Total soluble solids (%)	Ruby, Wonderful		28.9	17.5–22.2		50.1–77.3	[268, 270]

TSS (°Brix)			13.70–15.21	1.14–3.15		5.8–14.27	
TA (%CA)						3.29–3.93	
pH	Bhagwa, Ruby, Wonderful		3.60–3.87				[4, 268]
Anthocyanins (mg/100 g)	Wonderful		9.73				[268]
TPC (mg/100 g)				7.03 ± 0.19			
TSS/TA							[268]
PV (meqO^2/kg)	Wonderful, Herskawitz, Acco				0.04–0.35		[271]
RI					1.5215–1.5218		
AV				43.39–125.26	2.00–14.22		
TOTOX				105.9	2.53–14.30		
TCC (mg β-carotene/100 g)	Wonderful, Herskawitz, Acco				19.25–22.26		[272]
TPC (mg GAE/g)					1.91–3.45		[270, 272]
YI (25 °C)			75.53–83.76		65.47–91.52		
Firmness (N)	Shavel, Bhagwa, Ruby	101.33–154.63	67.44–99.20				[46,47]

AV = Anisidine value, TOTOX = Total oxidation value, RI = Refractive, PV = Peroxide value, TPC = Total phenolic content, TCC; Total carotenoids content, GAE = Gallic acid equivalence, YI; Yellowness index, L*; Lightness, a*; Redness, b*; Yellowness, C*; Chroma, h°; Hue.

3.2.2. Internal quality attributes of pomegranate fruit

Internal quality attributes of pomegranate fruit include the physico-chemical, vitamin C content, and antimicrobial properties [4]. These quality attributes range in value depending on different factors [273]. Some of the significant amounts of bioactive compounds that constitute internal quality attributes of pomegranate fruit includes phenolic acids, flavonoids, and tannins. Internal fruit attributes indicate whether fruits can be processed or consumed fresh. Indicators like total soluble solids (TSS) and titratable acidity (TA) of a fruit are frequently used. For instance, a high TSS and a low TA of a fruit means it can be consumed whilst fresh. Moreover, the ratio of TSS to TA of a fruit defines its maturity index (MI) [169, 269].

3.2.3. Quality attributes of pomegranate products

Minimally processed pomegranate arils are the ready to eat and serves as an excellent dietary source [246]. The appearance of fresh arils varies from white to deep red depending upon the variety [246]. Fresh pomegranate arils have a short shelf-life of between 5 and 8 days [270]. Therefore, to extend the shelf-life pomegranate arils are often processed into dried arils (Figure 3.1).

Dried pomegranate arils are products of pomegranate fruit and often referred to as ‘anardana’ [274, 275]. They are prepared by pre-treating fresh pomegranate arils to a constant temperature of 60 ± 2°C [274, 276] until they reach a moisture content of between 9.33 and 15.73% [277]. The dehydrated arils have a sugar content between 13.7- 15.1°Brix and an acidic content ranging between (0.24 - 0.38%). Table 1 shows different parameters used to evaluate the quality attributes for dried pomegranate arils. One area of quality lapse is the processing of immature and unripe fruits in the production of anadama which usually result in dried arils with poor colour and quality. Typically, dried aril is prepared with matured fruit [278]. Effect of processing technique on dried aril have been investigated [270]. In this study, the authors compared hot-air and freeze-drying method to process dried aril. They recommended freeze-

drying which lowered degradation for parameters such as colour, total phenolic content, and total anthocyanin content.

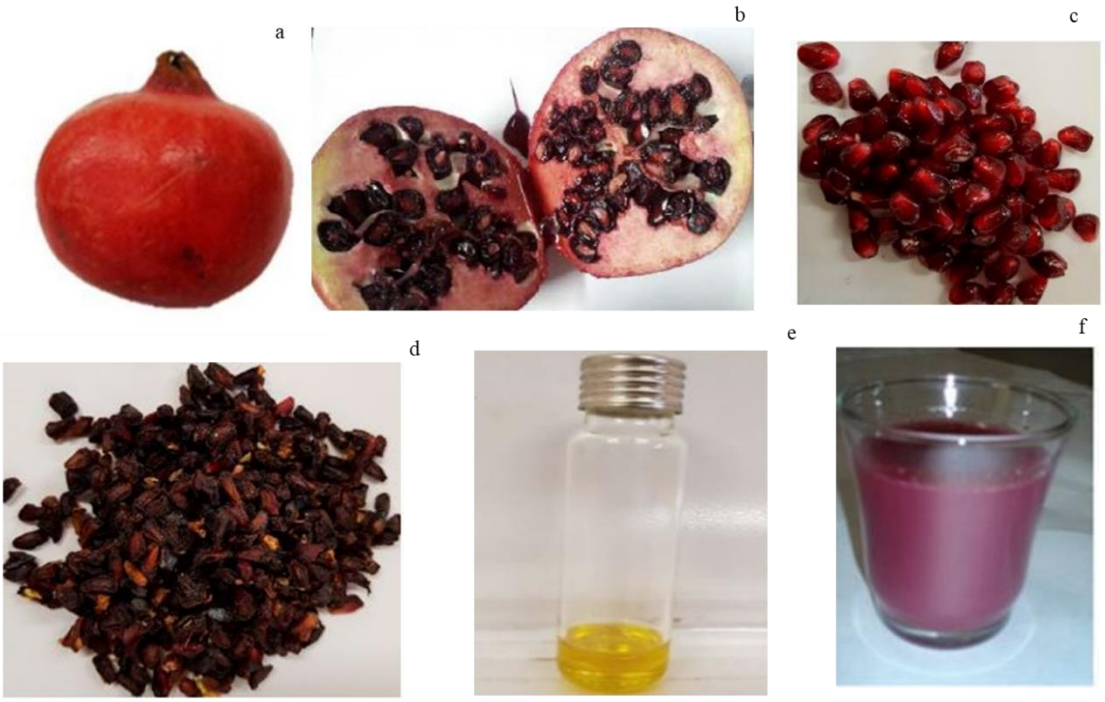

Figure 3.1: Pomegranate whole fruit and its different products (a): Whole fruit (b) fresh cut fruit (c) fresh aril, (d) dried aril, (e) seed oil; (f) juice.

Pomegranate seed oil comprises 12–20% of total seed weight [279]. The seed oil comprises of more than 80% conjugated octadecatrienoic fatty acids, with high content of punicic acid (9-cis, 11-trans, 13-cis, 18:3). The fatty acids comprises over 95% of the oil, of which 99% is triacylglycerols [280]. Seed oil can yield oil and ranging from 13.70 to 18.55% depending on the extraction method, solvent used and seed pre-treatment [271, 281]. Pomegranate seed oil is esteemed for its refractive index, yellowness Index, peroxide value, total carotenoids content and total phenolic content [279, 281]. Literature suggests that seed oil quality varies with respect to cultivar, fruit growing region and seed oil processing techniques [281, 282]. Kaseke et al. [281] reported ‘Acco’ to yield higher pomegranate seed oil (16.09%), followed by ‘Herskawitz’ (15.13%) and ‘wonderful’ cultivar (14.68%). The authors noted a significant improvement in oil yield (17% - 23%) after blanching dried seeds at 95 C for 3 min.

Pomegranate juice is another value-added by product of pomegranate fruit. Juice yield varies between 67.75 to 74.05 (mL per 100 g arils) depending on the cultivar, maturity stage and growing location [283, 284]. The juice contains 85.4% water, 10.6% total sugars, 1.4% pectin, 0.2-1.0% polyphenols [1, 280]. These quality indexes differ from one fruit to another and this

discrepancy may be due to differences in juice extraction methods, pomegranate cultivar and fruit maturity[283–285].

3.3. Non-destructive methods for quality evaluation of intact pomegranate fruit

3.3.1. Infrared (IR) Spectroscopy

Infrared technology employs the principle of interactions between matter that contains molecular bonds with the electromagnetic radiation in the near and mid-infrared range. NIR and MIR spectroscopy cover an electromagnetic range of 12500–4000 cm^{-1} or 800–2500 nm (NIR) and 4000–400 cm^{-1} or 2500–25000 nm (MIR), respectively [12, 21]. In recent years, the application of near infrared spectroscopy (NIRS) in agricultural product have been growing in terms of instrumentation and spectra analysis techniques to measure SSC, fruit firmness, pH, and TA of fruits [253, 286, 287].

3.3.1.1. Application on intact fruit

Pomegranate fruit quality attributes have been assessed non-destructively using the NIRS by several researchers. Attributes like TSS, TA and pH are most frequently correlated with NIRS measurements and predicted with high accuracy [11, 24]. Arendse et al. [11] compared two NIRS acquisition modes to evaluate both external and internal quality of intact pomegranate fruit. This study evaluated external attributes to include fruit weight, firmness, and colour components (a*, Chroma, hue angle), and internal attributes such as TSS, pH, TA, sugar to acid ratio (TSS: TA), BrimA, total phenolics, total anthocyanin and vitamin C. The authors reported good prediction statistics for both acquisition methods namely, emission head and integrating sphere. Emission head acquisition method was observed to yield best prediction for 9 quality attributes of the 13 analysed.

Khodabakhshian et al. [288] estimated maturity and several quality parameters of “Ashraf” variety of pomegranate fruit. Attributes include TSS, TA and pH were assessed during four distinct maturity stages and model was developed using partial least squares regression. The authors applied several pre-processing methods and obtained R^2 values for prediction ranging from 0.73 – 9.2. Their result showed model performance to improve with pre-processing of data. Best performing model was obtained when a combination of SNV, median filter, D1 and mean centre was applied.

For whole pomegranate fruit, Arendse et al. [289] developed models for several colour components (a*, C*, h°). The authors reported prediction statistics for a* (R^2 = 0.90 and RPD = 3.34), C* (R^2 = 0.83 and RPD = 2.43) and h° (R^2 = 0.83 and RPD = 2.50). Another

physiological disorder prevalent in pomegranate fruit is the presence of husk scald [289]. In a study to defect biochemical markers associated with the development of husk scald, Arendse et al. [289] applied Fourier transform near infrared reflectance spectroscopy to technique evaluate biochemical markers associated with the development of husk scald. The authors qualitatively discriminate between healthy and scalded fruit by classifying fruit into three categories, namely, healthy, moderate scald and severe scald. Using orthogonal partial least squares discriminant analysis (OPLS-DA), they achieved a classification accuracy of 100% healthy, 92.6% moderate scald and 93% severe scald showing high prediction model.

3.3.1.2. For internal quality parameters

Infrared spectroscopy is one of the mostly used non-destructive techniques for pomegranate quality assessment. It has found application in quality inspection, variety, and specie discrimination and even as quality control over disease infections. Particularly for pomegranate fruit, it has been implemented coupled with chemometric analysis for varying fruit quality indices [11, 24], all showing different degree of accuracies. (Table 6.2). Some of the parameters being measured includes total soluble solids, pH, titratable acidity, BrimA, aril hue, total phenolic concentration, total anthocyanin concentration, vitamin C concentration, aril firmness and aril colour components.

To evaluate pest infestation of pomegranate fruit by carob moth larvae, also known as "*Ectomyelois ceratoniae*" Jamshidi et al. [290], utilised visible/near-infrared (Vis/NIR) spectroscopy as an optical non-destructive technique in combination with supervised and unsupervised pattern recognition methods to detect the presence of carob moth larvae in pomegranate fruit. PCA and PCA-DA model were developed by authors with the best PCA-DA model achieving prediction accuracy of 90.6%. This study shows the feasibility of Vis/NIR spectroscopy for rapid screening of pomegranate fruit infested by carob moth. In a similar study, SIMCA and PLS-DA was used to discriminate carob moth infestation [23]. The authors achieved a prediction accuracy ranging from 86 – 90%). These results showed the potential of IR spectroscopy as a fast and efficient technique for internal quality evaluation.

Maturity index was investigated using the attributes TSS, TA and pH for pomegranate fruit [18]. In this study, the authors applied different pre-processing methods for the development of PLS calibration and prediction models for the different quality parameters. Results showed that the prediction of TSS (R^2 = 0.92, RMSEP = 0.23º Brix, RPD = 6.38) gave the best model and was developed when Standard Normal Variate (SNV), median filter, and first derivative were used as pre-processing. Similar pre-processing combination also yielded the best model for TA (R^2 = 0.93, RMSEP = 0.26, RPD = 5.31). The prediction of pH was best when SNV,

median filter and second order derivative was used as pre-processing technique with (R^2 = 0.85, RMSEP = 0.064, and RPD = 4.94). This study shows that the application of different pre-processing techniques effects the performance of the developed models and further studies should focus on the application of several spectral pre-processing to non-destructively predict maturity of pomegranate fruit. In a similar study, reflectance and transmission modes spectral data were acquired in the range of 400 – 1100 nm to determine TSS, TA and pH of pomegranate fruit [291]. The authors found both spectral acquisition mode feasible for non-destructive application on pomegranate fruit with the reflectance mode providing better accuracy for measurement of TSS, pH and firmness. Table 3.2 summaries application of NIRS for quality different quality evaluation.

3.3.1.3. Application on processed products

Increasing demand for pomegranate fruit has necessitated the processing of the intact fruit into different value-added products. Some of these products include fresh and dried aril [24, 270], seed oil [271] pomegranate juice [292]. The use of IR spectroscopy has also been extended for non-invasive evaluation of these different processed products. It can been applied as a quality control measure for the authentication of pomegranate juice concentrate [293]. The authors investigated the adulteration of pomegranate juice concentrate (PJC) with grape juice concentrate (GJC). By applying partial least square (PLS) regression of the spectra, the authors obtained high accuracy in prediction of the GJC adulterant concentration in PJC with a correlation coefficient, R^2 of 0.975. Further analysis of PJC to predict % titratable acidity and total solids yielded model with high R^2 values of 0.9114 and 0.9916, respectively.

Table 3.2: Summary of applications of Vis/NIR spectroscopy for intact pomegranate quality analysis

Quality attributes	Prediction Statistics	Data analysis	References
TSS	R^2 = 0.960, RMSEP = 0.092 °Brix	PLS, PCA	[288]
TA	R^2 = 0.920, RMSEP = 0.19%		
pH	R^2 = 0.920, RMSEP = 0.089		
TSS	R^2 = 0.920, RMSEP = 0.23 °Brix	PLS, PCA	[18]
TA	R^2 = 0.930, RMSEP = 0.26%		
pH	R^2 = 0.800, RMSEP = 0.064		
TSS	R^2 = 0.781, RMSEP = 0.28%	PLS, PCA	[292]
TA	R^2 = 0.768, RMSEP = 0.13%		
pH	R^2 = 0.849, RMSEP = 0.06		
TAC	R^2 = 0.626, RMSEP = 0.09 g /l		
TPC	R^2 = 0.889, RMSEP = 0.11 g /l		
Brim A	R^2 = 0.762, RMSEP = 0.39		
TSS/TA	R^2 = 0.868, RMSEP = 0.74		
Hue angle	R^2 = 0.466, RMSEP = 1.67		
Vitamin C	R^2 = 0.762, RMSEP = 0.09 g/l		
Chroma	R^2 = 0.830, RMSEP = 2.15		

a* Firmness (N) Hue Fruit Weight	R^2 = 0.909, RMSEP = 1.61 R^2 = 0.830, RMSEP = 7.45 R^2 = 0.839, RMSEP = 1.67 R^2 = 0.621, RMSEP = 0.013		
TSS Firmness (N) pH	R^2 = 0.940, RMSEP = 0.21 °Brix R^2 = 0.940, RMSEP = 0.68 R^2 = 0.860, RMSEP = 0.069	PLS, PCA	[291]
Ectomyelois ceratoniae infestation	CA = 97.9%	PCA-DA	[290]
Presence of husk scald	CA ≥ 92.6%	OPLS-DA	[289]
Carob moth infestation	CA ≥ 86%	PLS-DA	[23]

TA; Titrable acidity, TAC; Total anthocyanins content, TPC; Total phenolic content, TSS; Total soluble solid, PCA; Principal component analysis, PLS; Partial least squares, CA; Classification accuracy, PLS-DA; Partial least squares- Discriminant analysis

In another study, Boggia et al. [294] developed a screening method based on ultraviolet and visible (UV-Vis) regions spectroscopy combined with multivariate analysis to assess addition of water and other filler juice to pomegranate juice. In this study, 14 pomegranate juices (PG), 27 grape juices, 11 apple juices (AP) and seven mix fruit juices containing pomegranate juice were analysed and their absorption spectra in the range 190–1100 nm were obtained using an Agilent 8453 spectro-photometer with a 1 nm resolution. Spectral data from their study showed clear lines between profile of different juice samples (Figure 3.2). The authors found that the first two PCs yielded 96.8% of total variance which explains a satisfactory separation among the different juice categories. The spectral region around 250–300 nm had the greatest importance (loading value) on PC 1. All the juices containing pomegranate indicated high absorptions in this region, except for apple juices which showed weak absorptions.

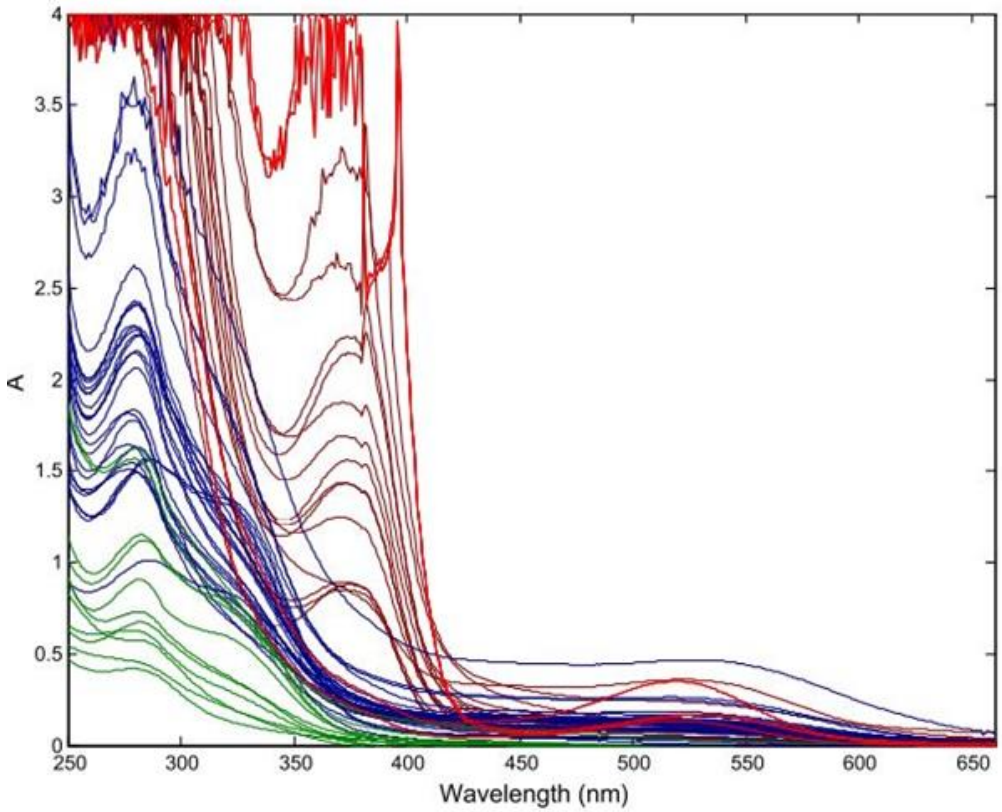

Figure 3.2. Spectral profile of different fruit juice samples analysed using a UV–VIS spectroscopy-based method. Red lines for authentic lab prepared pomegranate juices (PA), ginger lines for commercial pomegranate juices, blue line for commercial grape juices and green lines for commercial apple juices. Adopted from Boggia et al. [294]. A is for absorbance.

A comparative study to analyse the performance of mid and near infrared spectrometers for evaluating juice quality was conducted by Arendse et al. [292]. Several quality attributes including phytochemical, and antioxidant were evaluated with all showing varying degree of success. The authors observed that spectral acquisition modes (WineScan, MPA and the Alpha-P instruments) impacted on the performance of the prediction models for different attributes of

the juice with the instruments in the mid infrared region (WineScan and the Alpha-P instruments) outperforming the multipurpose analyser (MPA) instrument in the near infrared region.

Pomegranate seed oil have also been investigated for its many quality attributes using IR spectroscopy technique [295]. Fourier transform near-infrared (FT-NIR) and mid-infrared (FT-MIR) spectroscopy was employed to predict the quality attributes of pomegranate seed oil. The authors used partial least squares regression to construct prediction models. Their study reported good prediction model for total carotenoid content (TCC) $R^2 = 0.8045$, peroxide value (PV) $R^2 = 0.620$ and refractive index (RI) $R^2 = 0.8092$. Similar success was recorded for application on dried pomegranate aril [245]. These results demonstrated the potential of infrared spectroscopy combined with chemometric analysis to be used as a useful technique for rapid screening of pomegranate oil quality attributes.

In a study comparing three spectroscopic techniques, UV–visible spectroscopy (200 – 800 nm) Mid-infrared spectroscopy (4000 – 650 cm^{-1}) and Fluorescence spectroscopy (300 – 800 nm), pomegranate see oil was evaluated for free fatty acid values and fatty acid profiles [296]. The authors also discriminated the adulteration of cold pressed pomegranate oil with sunflower oil and observed that Mid-IR range provided the best results regarding in discriminating the mixing of cold pressed PSO with sunflower oil.

For the assessing of microbial quality of minimally processed pomegranate aril, Adiani et al. [297] acquired FTIR data pre-processed in three different ways viz; raw FTIR spectrum, first derivative for FTIR spectrum and peak integrated data of FTIR spectrum to develop prediction model. The authors analysed for total viable count (TVC) and yeast and mold count (Y&M). and obtained R^2 values of 0.909 for raw FTIR spectral data, 0.619 for FTIR first derivative data and 0.830 for Peak integrated data. Results showed that PLS-R models performed best for predicting microbial quality when FTIR first derivative data was used while ANN showed better model performance when applied on raw FTIR spectral data during model development. When spectral data pre-processed with peak integrated data was used, developed models showed poor performance for prediction in both ANN and PLS-R.

Arendse et al. [24] applied FT-NIR to develop calibration model for freshly extracted pomegranate aril. In this study, the authors acquired NIR data over two spectral equipment MPA FT-NIR spectrometer and MATRIX-F FT-NIR spectrometer (Bruker Optics, Ettlingen, Germany) of wavelength range of 800 - 2500 nm. Quality attributes assessed includes total soluble solids, titratable acidity, pH, BrimA, aril firmness, total phenolic concentration, total anthocyanin concentration and vitamin C concentration and several colour attributes with

model showing accurate predictions of 8 quality parameters. Recently, similar study has been carried out on fresh pomegranate aril [288], dried pomegranate [245]. The authors in these studies reported accurate prediction models for different quality attributes of fresh and dried arils. Table 3.3 provides a summary of the different application for evaluation of different products of pomegranate fruit. NIR spectroscopy is the most frequently used technique and is commercially available [21]. Though the NIRS is popular, sand somewhat preferred by experts, some of its limitation includes high operational cost, impracticality for in-line application and technical issues [21].

3.3.2. Raman Spectroscopy

Raman spectroscopy is another non-destructive technique used for the quality analysis of fruits and vegetables [298]. This technique, named after an Indian physicist, Sir Chandrasekhara Venkata Raman (1888 – 1970), was developed based on the phenomena of inelastic scattering of light. The technique is based on the fact that inelastic collision occurs between an incident photon and a molecule of the sample when samples are irradiated [299]. The concept and principle of Raman and its theoretical basis have been discussed in detail by many researchers. Raman Spectroscopy has several advantages in food analysis than other techniques [253, 298, 300].

Table 3.3: Summary of applications of Vis/NIR spectroscopy for processed pomegranate product quality analysis

Products	Quality attributes	Prediction Statistics	Data analysis	References
Fresh aril	TSS	R^2 = 0.875, RMSEP = 0.30%	PLS, PCA	[24]
	TA	R^2 = 0.855, RMSEP = 0.10%		
	pH	R^2 = 0.851, RMSEP = 0.10		
	TAC	R^2 = 0.705, RMSEP = 0.13 g /l		
	TPC	R^2 = 0.864, RMSEP = 0.11 g /l		
	Brim A	R^2 = 0.834, RMSEP = 0.43		
	Firmness	R^2 = 0.684, RMSEP = 6.71 N		
	TSS/TA	R^2 = 0.822, RMSEP = 1.03		
	Hue angle	R^2 = 0.885, RMSEP = 4.19		
	Vitamin C	R^2 = 0.848, RMSEP = 0.09 g/l		
	Chroma	R^2 = 0.783, RMSEP = 2.31		
	a*	R^2 = 0.735, RMSEP = 1.67		
Minimally processed aril	TVC	R^2 = 0.909, SEP = 0.914	ANN	[297]
	T&M	R^2 = 0.929, SEP = 0.777	PLS-R	
Dried aril	TA	R^2 = 0.850, RMSEP = 0.041	PLS, SVM	[245]
	TSS/TA	R^2 = 0.756, RMSEP = 1.951		
	pH	R^2 = 0.863, RMSEP = 0.131		
	a*	R^2 = 0.720, RMSEP = 1.815		

	Chroma	R^2 = 0.703, RMSEP = 1.986		
PJ	TSS TA pH TAC TPC Brim A TSS/TA Hue angle Vitamin C Chroma a*	R^2 = 0.923, RMSEP = 0.31% R^2 = 0.862, RMSEP = 0.11% R^2 = 0.670, RMSEP = 0.17 R^2 = 0.663, RMSEP = 0.19 g /l R^2 = 0.591, RMSEP = 0.18 g /l R^2 = 0.906, RMSEP = 0.40 R^2 = 0.768, RMSEP = 1.00 R^2 = 0.466, RMSEP = 1.67 R^2 = 0.709, RMSEP = 0.11 g/l R^2 = 0.832, RMSEP = 3.81 R^2 = 0.816, RMSEP = 3.78	PLS, PCA	[292]
Aril	TSS TA pH	R^2=0.92, RMSEP=0.23º Brix R^2 = 0.93, RMSEP = 0.26% R^2 = 0.85, RMSEP=0.064	PLS	[18]
PJ	Adulteration TA TSS	R^2 = 0.975 R^2 = 0.911 R^2 = 0.991	PCA, PLS	[293]
PSO	TCC PV	R^2 = 0.8045 R^2 = 0.620	PLSR	[245]

	RI	$R^2 = 0.8092$		
PSO	Adulteration detection	CA ≥ 88%	OPLS-DA	[296]

PV; Peroxide value, PSO; Pomegranate seed oil, PJ; Pomegranate juice, OPLS-DA; Orthogonal partial least square-discriminant analysis, PLS-R; partial Least square regression, ANN; Artificial neural networks, RI; Refractive index, TA; Titratable acidity, TCC; Total carotenoid content, TVC; Total viable count, Y&M; Yeast and mold count.

It has also frequently applied in fresh fruit and vegetable quality analysis [255, 301]. Khodabakhshian [291] applied modified polynomial, self-modelling mixture analysis (SMA) and spectral information divergence (SID) pre-processing techniques, combined with PLS regression, to develop tannin content prediction models. Prediction accuracy of models predicting tannin content in the three parts of pomegranate fruit: rind, aril and white spongy tissue have R^2 value of 0.960, 0.925 and 0.922, respectively.

More recently, a pattern recognition-based Raman spectroscopy technique was investigated for non-destructive quality assessment of pomegranates [302]. The authors used both supervised and unsupervised pattern recognition methods and distinguished different maturity stages of pomegranate "Ashraf variety". The partial least squares discriminant analysis (PLS-DA) and soft independent modelling of class analogy (SIMCA) were compared, showing prediction accuracies of 95% and 82%, respectively. The authors further considered two stages of maturity ("immature" and "mature"). The SIMCA based on PCA modelling was able to completely categorize the samples in two classes: immature or mature, with classification accuracy of 100%. Figure 3.3a provides image of inner pomegranate fruit at different maturity stages. Spectral profile of Raman shift for the different development stages have also been shown in Fig. 3.3b. Three Raman spectral peaks (650, 1357 and 1590 cm^{-1}), were identified to be those similar to pure tannin. SID values were indicative of the different maturity stages, the authors observed decreasing SID values from stage 1 to stage 4 of pomegranate fruit maturity.

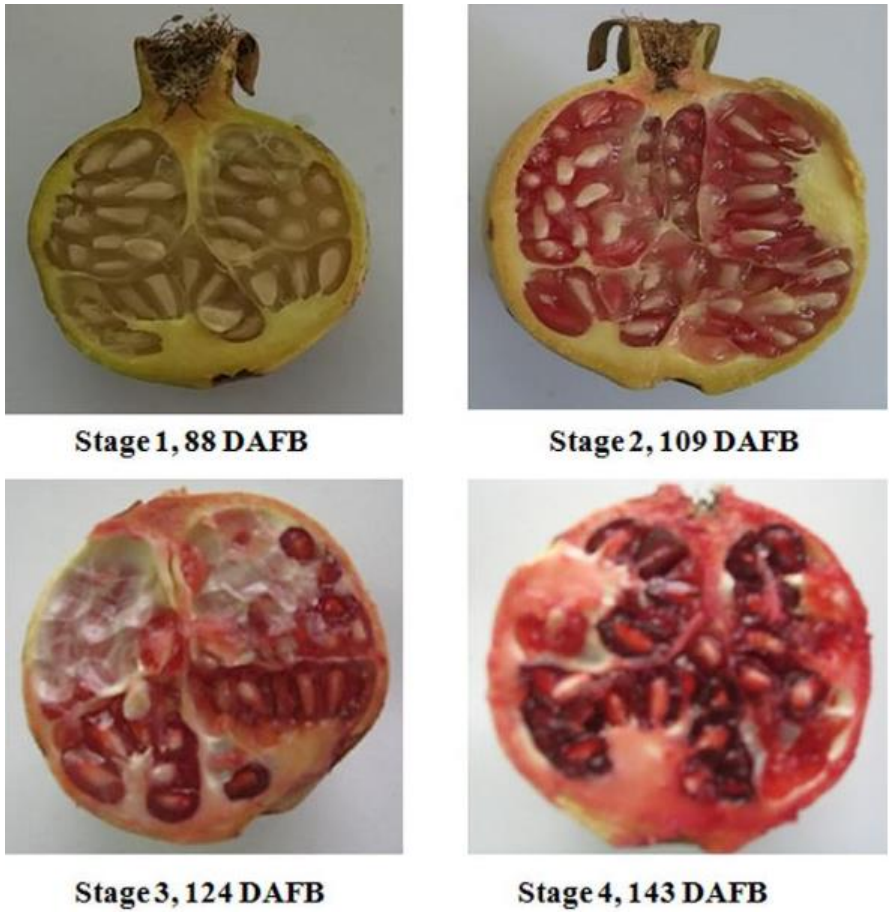

Figure 3.3a: Fruit samples and arils of pomegranate (Ashraf cultivar) at different maturity stages: Immature stage; 88 days after full bloom (DAFB); half-ripe stage, 109 DAFB; half-ripe stage, 124 DAFB; and full- ripe stage, 143 DAFB. Adapted from [302]

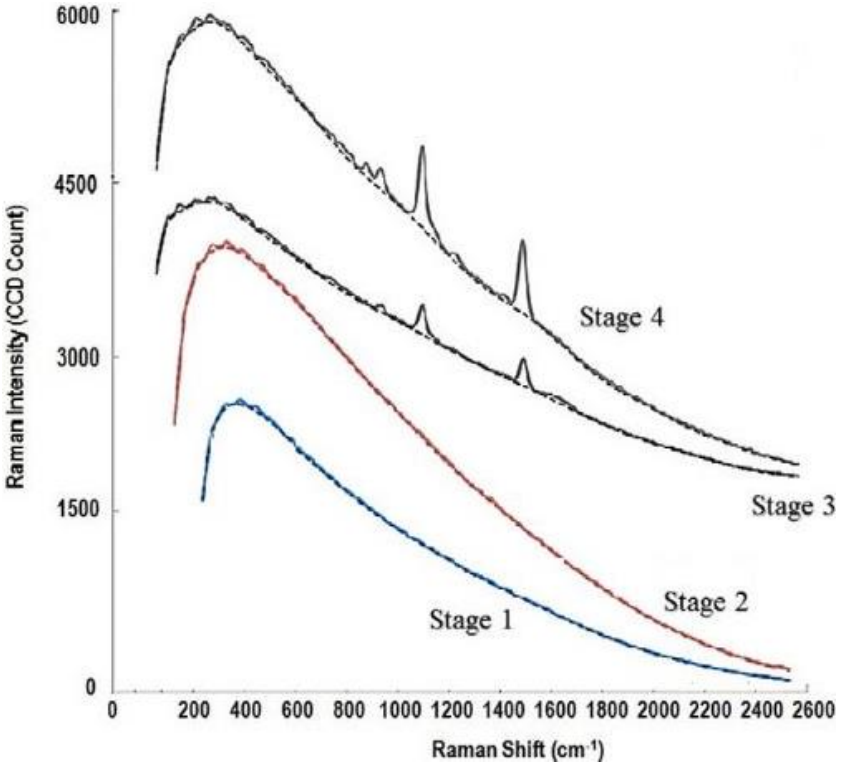

Figure 3.3b: A Raman spectra profile of four different maturity stages of intact pomegranate fruit at different maturity stages. Stage 1 (88), stage 2 (109), stage 3 (124), and stage 4 (143) DAFB. Adopted from [302].

3.4. Imaging-based non-destructive techniques for evaluating pomegranate quality

3.4.1. Machine vision systems (MVS)

Machine vision has been extensively used in agriculture over the last few decades [303]. Part of the reasons for this is the advances in the arena of digital imaging and data processing techniques that encourage intelligent control methods. In the agricultural industry, quality evaluation based on visual appearance such as colour attributes are subjective. Hence, machine vision systems play an important role in the field of automated preharvest and postharvest applications. Machine vision is widely applied for sorting and grading of agricultural, horticultural and food products [252, 303]. Evolving technologies in machine learning, big data acquisition, big data processing, internet of things and analytics have ushered the concept of industry 4.0 [304]. Machine vision in combination with machine learning have been applied to address different quality control problems in the field of agriculture [37] and the pomegranate industry [144, 252].

3.4.1.1 Application on intact fruit

Fashi et al. [213] applied machine vision technique to measure the pH of pomegranate fruit of Qom cultivar. In their study, images of 200 fruit were acquired and analysed using three different image processing algorithms. In total, the authors investigated 10 different colour channels of which the image corresponding to six of these channels are shown in Figure 3.4. Fourteen selected inputs were fed into the model along with the values for pomegranate pH, as model was developed for sensitivity analysis. Result showed the Adaptive Neuro-Fuzzy Inference System (ANFIS) and ANN based models achieved a regression coefficient (R^2) value greater than 0.980 while response surface methodology (RSM) based model achieved an R^2 value of 0.754.

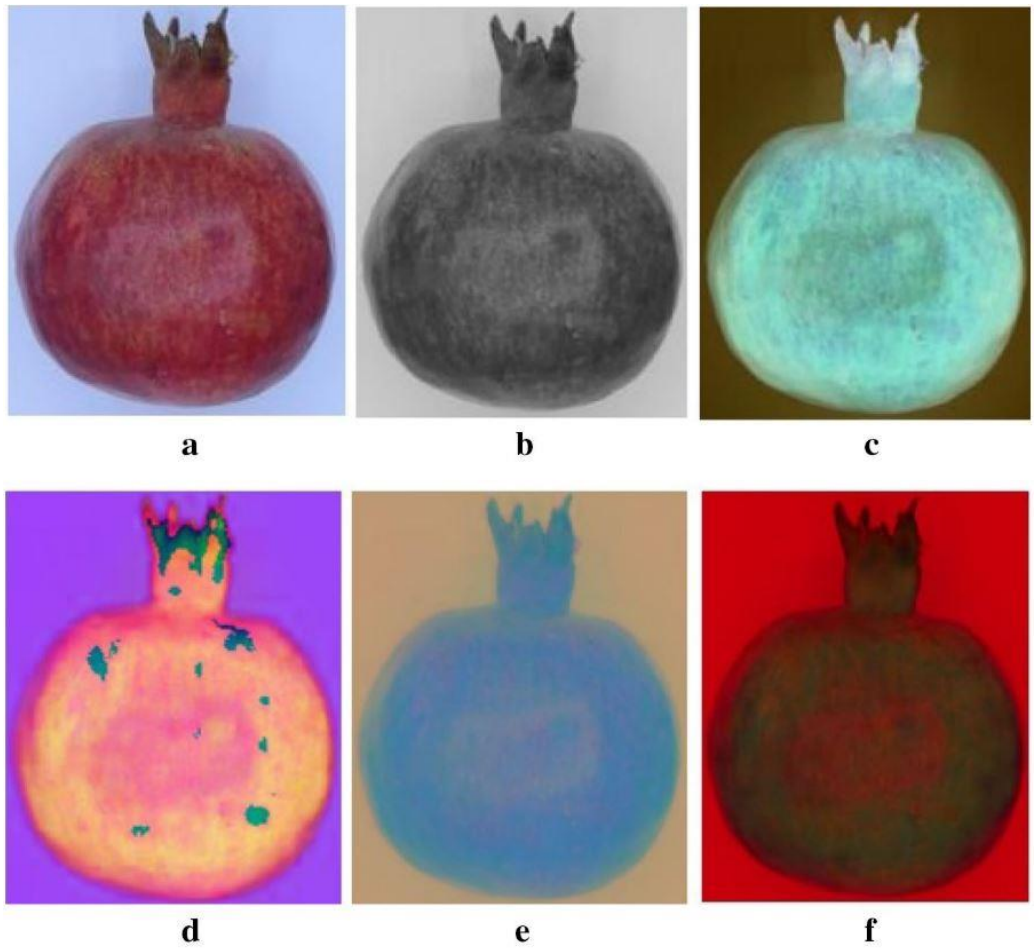

Figure 3.4: Different colour images of pomegranate fruit using machine vision systems for quality grading. The colour channels are described as (3a): RGB, (3b): Gray scale, (3c): CMY, (3d): HSV, (3e): YCbCr and (3f): YUV. Adapted from [315].

Different two-dimensional linear discriminant analysis approaches were explored for machines vision technique in pomegranate fruit grading [77]. In this study, four different linear discriminant analysis methods were compared: traditional two-dimensional linear discriminant analysis (2DLDA), fractional two-dimensional linear discriminant analysis (FLDA), fuzzy two-dimensional linear discriminant analysis (F2DLDA), and fractional fuzzy two-dimensional linear discriminant analysis (FF2DLDA). The authors used a digital camera (EOS 550D, Canon Inc., Japan) to capture high-quality pomegranates images of size 3456×2304 pixels and a resolution of 0.03 mm/ pixel. They found that of the four algorithms investigated, the FF2DLDA gave the best classification accuracy (97%) for grading pomegranate colour. This study confirmed the importance of image data analysis techniques on model prediction efficiency and accuracy.

Similar result was reported by Kumar et al. [144] in development of ANN based classification model for pomegranate fruit sorting application. The authors used spatial domain features and

wavelet features techniques for image features extraction. The results showed the superior classification performance of wavelet features (91.3%) compared to spatial domain features (77.46%). Their study revealed good accuracy thereby showing the potential of machine vision systems in grading and sorting of pomegranate fruit non-destructively. In another study, images of 1800 pomegranates were acquired using a closed metal compartment and a total of 134 features were extracted and used to train ANN based classification model in pomegranate fruit grading application [252]. The authors implemented image segmentation and histogram equalization followed by wavelet denoising steps for pre-processing of the image data. The study reported a classification accuracy of 97.83%.

3.4.1.2. Application on processed products

MVS have been also used in the evaluation of pomegranate arils quality analysis. For instance, Blasco. [305] established a prototype capable of correctly separating arils travelling at a speed of 1m s^{-1} and which were separated by a distance of at least 20 mm. This system accurately discriminated aril membranes from the arils. However, the system required human intervention to differentiate between the different categories of the arils. Blasco et al. [306] further investigated the feasibility of two different image segmentation methods for automatic sorting of pomegranate (*Punica granatum*) arils. One of the methods uses a threshold on the R/G ratio and the other takes a more complex approach based on Bayesian-Linear Discriminant Analysis (LDA) in the RGB space. Both methods offered an average classification accuracy of 90%. The authors were able to successfully implement a prototype system for inspecting and sorting of arils which could handle a maximum throughput of 75 kg/h.

In a different study, Fashi et al. [78] classified pomegranate arils into three categories according to three different indexes of healthiness, redness, and size) using MVS. Four features were extracted and used to train, test and validate adaptive neuro fuzzy inference system (ANFIS), response surface methodology (RSM) and artificial neural network (ANN) models. The authors found the ANN model performing best (with 98% of classification accuracy) for grading pomegranate aril based on colour and aril size. Results for the other two models showed classification accuracy of 95.5% (ANFIS) and 75.5% (RSM). Table 3.4 provides a summary on the application of MVS for quality assessment of pomegranate fruit and arils.

Machine intelligence, which helps to eliminate the bias of subjective manual sorting, is of tremendous impact on pomegranate fruit quality analysis [65]. Grading is one quality category that is performed based on weight, size and external rind appearance. Studies have shown that disease, pests, and infestation can also be detected using MVS [65] though quite a difficult task

considering the variation of disease or defect type and how they manifest on fruit [303]. Using appropriate image pre-processing and colour space conversion, region of interest segmentation and analysis of flaws, diseases and defects can be accurately detected.

Machine vision system for quality inspection is made up of four basic components: acquisition, segmentation, feature extraction and classification [303] Camera quality for image capturing and data storage has witnessed huge improvement in recent time. Recently, interest is growing in the direction of multiple sensing techniques [307]. A typical image processing flow chart for defect detection has been proposed by Pandey et al. [65] (Figure 3.5). The technique identified three infection severity classes: worst (infection covered over 75% of the surface), average (30 – 75%) and good (less than 30%). MVS has also found application for on-tree counting of pomegranate fruit [308–310].

The downside of the digital image system for food quality application is its limitation in capturing or detecting internal defects or internal quality [241]. To this end, in most packhouses, pomegranate product classification is not based on internal quality [241]. This has necessitated the need to finding other effective technique for internal quality assessment for pomegranate fruit [11, 212].

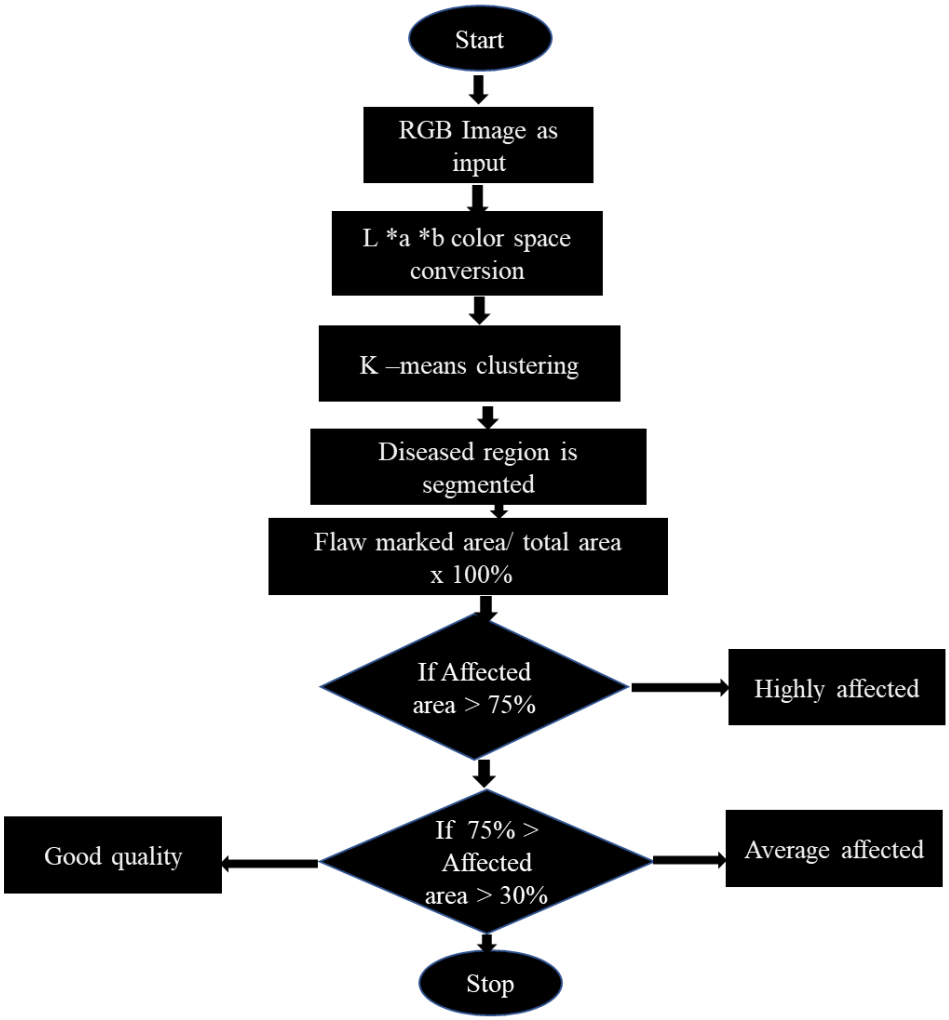

Figure 3.5: Flow chart of disease detection algorithm using colour space conversion method

Table 3.4. Summary of application of different non-destructive assessment for pomegranate quality attributes

Technique	Application	Data analysis	Accuracy	References
X-ray	Volume estimation	STA		[311]
MVS	Grading	2DLDA, FLDA, F2DLDA, FF2DLDA	97%	[77]
MVS	Grading	ANN	97.83%	[252]
MVS	Grading	ANN	77.46 - 91.3%	[144]
NMR	Black heart	PLS-DA	92%	[312]
E-nose system	Fungal disease	LDA, BPNN, and SVM	100%	[313]
MVS	Disease	-	79.73%	[65]
Raman Spectroscopy	Tannin changes	PLS	$R^2 = 0.9603$	[291]
MVS	Aril color and size	ANN, ANFIS, RSM	75.5 – 98%	[78]
E-nose	Fruit ripening	PCA, LDA	95.2%.	[314]

Table 3.4 Continued

Technique	Application	Data analysis	Accuracy	References
MVS	pH	ANFIS, RSM, ANN	R^2 = 0.984, MSE = 0,.202	[213]
Raman	Maturity indexing	PLS-DA, SIMCA and PCA	95%	[302]
X-Ray	Disease detection	-	t value = 0.469 with a 95% los	[315]
MVS	Industrial grading of fresh aril	LDA, threshold on the R/G ratio	83.3 – 100%	[306]
MVS	Preharvest yield estimation	adaptive threshold algorithm	ER = 9,1%	[308]
MVS	on tree fruit recognition	RGB, HSV and YCC colour space analysis	100%	[309]
MVS	Yield estimation	CHT, K-Means Clustering	R^2 = 0.7652	[310]
MSV	Physicochemical attributes	PCA, PLS-R		[212]
HSI	Maturity indexing	PLS-DA	95.0%,	[212]
MSI	TSS, TA and pH	PLS, MLR	$R^2 \geq 0.88$, RPD ≥ 5.01	[18]

CHT; Circular Hough Transform, ER; Error rate, LOS; level of significance, MSI; Multispectral imaging, PLS, MLR; Multiple linear regression, TSS; Total soluble solids; TA; Titratable acidity,

3.4.2. Nuclear magnetic resonance (NMR) and magnetic resonance imaging (MRI)

The basic principle of NMR spectroscopy is developed on the scientific fact that most elements have at least one isotope and therefore are magnetic. It was first successfully applied for measurement by Bloch and Purcell for which they were jointly awarded the Nobel prize in Physics in 1952 [316, 317]. For example, ^{1}H, ^{13}C, ^{31}P have a magnetic moment and can absorb resonance energy when placed in a strong magnetic field [318]. Several studies have shown that NMR and MRI can be used to measure and quantify several physical and chemical properties of pomegranate fruit [244, 312].

In a study using MRI, Khoshroo et al. [244] successfully classified pomegranate (cv. 'Malas-e-Torsh') fruits into semi-ripe, ripe and over-ripe classes and detected internal defects. The authors applied Gray level Co-occurrence Matrix (GLCM) and Pixel Run-Length Matrix (PRLM) features. Classification and internal defect identification accuracies were higher with GLCM features. Interestingly, combining 7 GLCM and 4 PRLM features resulted a classification accuracy of 98.33 % and the lowest type I and II errors confirming the potential of MRI as a powerful tool in pomegranate fruit quality analysis.

In order to determine the presence of black heart disease on pomegranate fruit, Zhang & McCarthy, [312] applied proton NMR relaxometry to investigate the water T_2 relaxation distribution in infected and healthy pomegranate fruit and to obtain information that indicates tissue damage. Partial least square discriminant analysis (PLS-DA) of the MR image provides a model with 92% accuracy in detecting the presence of black heart in pomegranate fruit. This study also highlighted that the significant change in T_2 relaxation distribution in arils after infection which indicate that T_2 relaxation time is a good indicator of black heart in pomegranate. In another study, Zhang et al. [312] measured TSS, TA and pH of pomegranate fruit based on partial least square (PLS) analysis of acquired MR images of the fruit. This approach correlates the destructively obtained reference data with corresponding MR imaging. The MR image based PLS predictive model achieved R^2 values of 0.54, 0.6, and 0.63 for TA, pH and TSS levels, respectively.

3.4.2. X-ray computed tomography

X-ray computed tomography (CT) is a non-destructive technique that reconstructs 2-dimentional images into 3-dimentional models for quantification and characterisation of horticultural produce. CT offers considerable advantages over other imaging techniques since it provides a large field of view [19, 319, 320]. This ensures whole sample surface to be scanned without preparation [321, 322]. X-rays CT is mostly applied in two ways in the food industry: for inspection of foreign bodies in food products for quality control and secondly to irradiate

food (a process that destroys bacteria). One distinct feature of the X-ray CT is that it measures variation in material density of the sample. This is based on the attenuation of X-ray that depends on the density of the irradiated object [319, 320].

The application of X-ray CT for characterization and quantification of pomegranate is summarized in Table 3.5. In a study that quantified the various parts of the fruit, Magwaza & Opara [7], employed X-ray CT imaging technique. This technique assesses and quantifies the distribution of edible (arils) and non-edible (albedo) parts of the fruit non-destructively. The authors developed linear regression models with high accuracy (R^2 values of 0.83 and 0.89, respectively, to predict volumes of albedo (external skin plus internal soft tissue) and arils). Another study employed soft X-ray technique for non-destructive quality analysis of pomegranate fruit [315]. The authors analysed the acquired images using the image processing toolbox - MATLAB (Figure 3.6) and were able to measure the exact area of defects based.

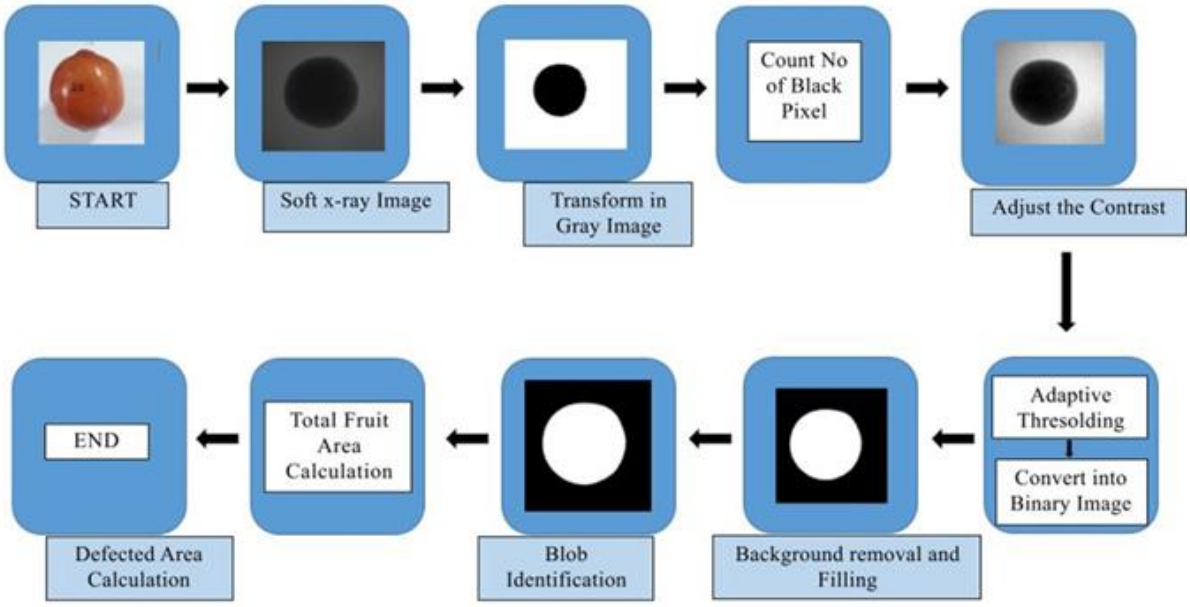

Figure 3.6: The Image processing and the defect identification algorithm flowchart for soft X-Ray application in detection of defect in pomegranate fruit. Adapted from [315].

In a similar study, Arendse et al. [323] investigated sample of twenty-three pomegranate fruit by X-ray CT technique. Sizes of physical attributes including length, diameter and peel thickness were estimated. Their result showed that average fruit length, diameter, radius and peel thickness were 76.67±2.93 mm, 86.82±3.34 mm, 44.19±2.93 mm and 4.67±0.60 mm, respectively. A plot of reference measurement against X-ray CT values shows R^2 values for the volume of peel, arils, kernels, juice content, air space and single aril of 0.97, 0.84, 0.90, 0.87, 0.82, and 0.80, respectively.

Also, the juice content, volume of the peel and density of intact pomegranate fruit were estimated using X-ray CT technique [324, 325]. In fact, the application of X-ray CT is diverse in the food industry (Schoeman et al., 2016), for identification and quantification of internal structures of fruit [7, 311, 325], and to detect bruise damage [326].

3.4.3. Hyperspectral and multispectral imaging

Multispectral imaging (MSI) and hyperspectral imaging (HIS) techniques are recently advancing techniques to acquire the spatial distribution of physical and chemical quantities for objective fruit quality analysis [6, 327]. The MSI and HSI are similar in techniques. The main difference is the number of bands and how narrow the bands are. Multispectral imagery generally refers to 3 to 10 bands [20] and hyperspectral image could have hundreds or thousands of bands. Having a higher level of spectral detail, HSI gives better capability to see the unseen. However, the acquisition, processing and analysis of hyperspectral data is considerably challenging [44]. The comparative difference of conventional machine vision (CMVS), near-infrared spectroscopy (NIRS), multispectral imaging (MSI) and hyperspectral imaging (HSI) is summarized on Table 3.4.

Table 3.5 Comparison of conventional machine vision (CMVS), near-infrared spectroscopy (NIRS), multispectral imaging (MSI) and hyperspectral imaging (HSI)

Feature	CMVS	Spectroscopy	HSI	MSI
Detect small sized sample	YES	NO	YES	YES
Flexibility of spectral extraction	NO	NO	YES	YES
Generation of quality attributes distribution	NO	NO	YES	Limited
Multi-constituent information	NO	YES	YES	Limited
Spectral information	NO	YES	YES	YES
Spatial information	YES	NO	YES	YES

Typical HSI system usually consists of a detector, illumination source, spectrograph, and a power supply unit [328]. A set up of image acquisition and the subsequent image processing workflow is shown in Figure 3.7.

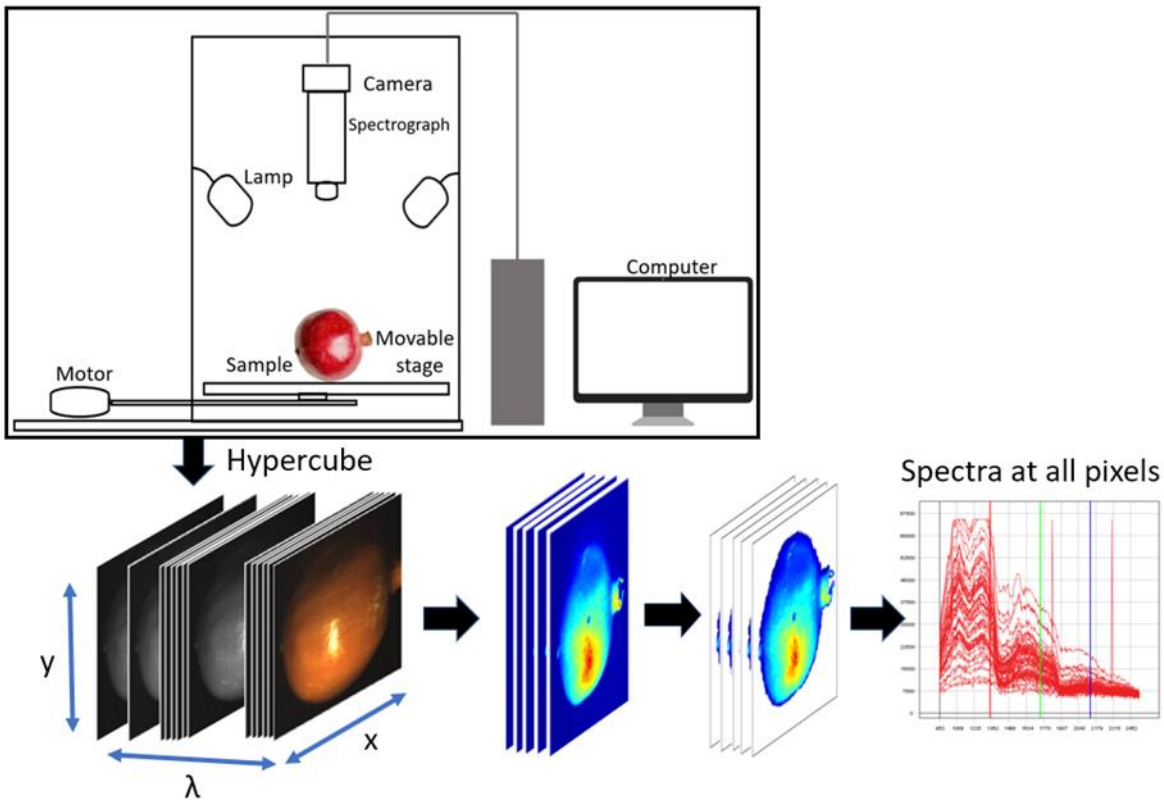

Figure 3.7: Schematics illustrating the configuration of a hyperspectral system.

Several authors have reviewed the application of HSI/MSI for food quality evaluation [20, 253, 329, 330]. The use of HSI and MSI for non-destructive assessment of pomegranate fruit quality is quite limited in literature as compared to Vis/NIRS. Khodabakhshian et al. [18] applied the MSI within the wavelength range of 200 - 1100 nm for online quality assessment of pomegranate fruit. The authors developed regression models using both partial least square (PLS) and multiple linear regression (MLR) methods for TSS, TA and pH of pomegranate fruit. The performances of the developed MLR based prediction model was for TSS (R^2 = 0.97, RMSEP = 0.22°Brix, RPD = 5.77), pH (R^2 = 0.94, RMSEP = 0.038, RPD = 4.98) and TA (R^2 = 0.92, RMSEP = 0.26, RPD = 5.22). Munera et al. [212] compared the capability of both machine vision techniques and hyperspectral imaging to predict the physicochemical properties and maturity stages of 'Mollar de Elche' pomegranate fruit (intact and fresh-cut aril). The authors applied PLS regression to develop models for discriminating different maturity stages. They reported classification accuracy of 95% for intact fruit and 100% for aril with HSI system and 84.3% for intact fruit and 85.7% for aril with MVS. These findings demonstrated the superior performance of HSI system compared to MVS.

3.5. Electronic-nose (e-nose)

The electronic nose (e-nose) is another non-destructive technique that have been applied for quality analysis of fruit. The e-nose is designed to simulate the human sense (smell) in identifying and realizing the complex aromas of fruits by employing a chemical sensors array [314]. Typical e-nose set up comprises of data acquisition, an array of metal oxide semiconductor (MOS) sensors, gas sensors and a power supply unit. Figure 3.8 illustrates the setup of a typical e-nose system.

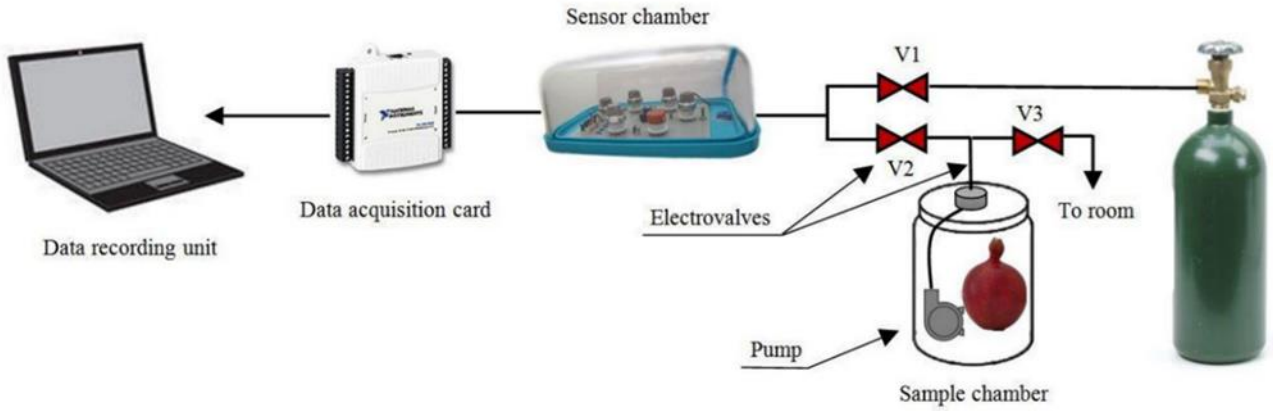

Fig. 3.8: Illustration of a typical data acquisition set up for an e-nose system application. Adapted from [314].

In a research study, Sanaeifar et al. [314] applied a low-cost e-nose system based on six MOS sensors for non-destructive recognition of different pomegranate varieties viz; “Ferdows”, “Rabab” and “Saveh”. The authors applied principal component analysis (PCA) and linear discriminant analysis (LDA) techniques and achieved a classification accuracy of 95.2%. E-nose has also been applied for the detection of diseases [313]. The authors compared three different data analysis methods: LDA, back propagation neural network (BPNN) and support vector machine (SVM). Their result showed BPNN to have the highest accuracy of 100% in the detection of 0, 25, 50, 75, and 100% infected fruit.

3.6. Challenges of non-destructive measurement for pomegranate fruit

The different Non-destructive testing (NDT) approach for quality assessment of pomegranate fruit are characterised by different challenges. One area of challenge with the application of NIRS, which is the widely used approach for quality evaluation, is its acquisition set up. Several studies demonstrated the importance of mode of acquisition of spectral data on the accuracy of predictive models [331].

MVS technique carries great potential as a fruit quality inspection tool, however, it is limited in its inability to detect internal defects and internal qualities [241]. It is ineffective for inline

packhouse operations as it tends to miss internal defects. MVS is effective for grading (which is mostly based on size, weight, and colour). Also, spectral data have shown to better perform over image (spatial) data for analysis on pomegranate fruit [212]. Also, illumination has crucial role in determining the effectiveness of imaging techniques. An adaptive threshold value is proposed during image processing analysis to counter the influence of illumination. There is also the case of cross polarisation during image acquisition of fruit sample. Researchers have been able to reduce this effect by placing polarising filters as shields in front of the lamps as well as camera lenses [77]. This approach helps to minimize the problem of bright spots and specular reflection when imaging pomegranate fruit.

X-ray CT system usually requires high voltages to generate two-dimensional (2D) radioscopic fruit images. Typical voltage requirement ranges from 100kV to 45 kV voltage [315, 326]. Such lengthy exposure time as well as the effect of radiation has sparked some health concerns regarding the use of X-ray CT [324]. Another major challenge with the X-ray CT technique is the acquisition time. Arendse et al. [325] reported a total scanning time of one hour for each sample showing the very slow image acquisition characteristics of this technique. This problem renders this technique undesirable for automated and online grading applications. Future improvement in computing time and image acquisition would greatly improve the X-ray system as a real-time/inline quality evaluation technique.

Very limited research investigation of electronic nose exhibited the possibility for the accessing pomegranate fruit quality have been implemented and further studies should be aimed at utilizing the capability of the e-nose technique for other quality attributes evaluation.

Hyperspectral images with their spatial and spectral dimensions are usually large sets of information. To this end, data storage and analysis capabilities are frequent limitations of using hyperspectral data. Hence, image data size and dimensionality reduction are very important in HS image applications. By implementing dimensionality reduction, redundant information can be eliminated. This process considerably simplifies the subsequent processes of classification model development. PLS, PCA and ANN methods frequently used to perform dimensionality reduction [6, 99, 206].

3.7. Conclusion and prospects

This review has reported the application of different non-destructive techniques for the evaluation of intact pomegranate fruit and its products. The application of infrared spectroscopy has shown to predict the internal quality attributes such as soluble solid content, acidity, its ratio, and vitamin C content. well as firmness. External attributes such as the presence of husk scald, carob moth larvae infestation, adulteration, has also been implemented

and accomplished for pomegranate fruit. Most of the imaging techniques focuses on the evaluation of external parameters ranging from fruit colour, size, and appearance. It is recommended that future research in imaging techniques should focus on improving its data acquisition speed and reducing the large data size and focus on detecting diseases and pest in pomegranate fruit. Findings from this review shows that very little have been achieved in investigating the feasibility of HSI and MSI for pomegranate quality analysis. Future research must explore the potential of this technique for a holistic quality analysis assessment of pomegranate fruits. The non-destructive techniques reviewed in this paper shows the capability, benefits, application and the evaluation of pomegranate fruit quality attributes.

SECTION II

Chapter 4: Early bruises detection on pomegranate (*Punica granatum* L.), using hyperspectral imaging coupled with artificial neutral network algorithm

Chapter 5: Pomegranate bruise severity detection using Vis-NIR and SWIR hyperspectral imaging technique

Chapter 6: Non-destructive maturity quality assessment of pomegranate fruit by VNIR/SWIR hyperspectral imaging

---

CHAPTER 4

Early bruises detection on pomegranate (*Punica granatum L.*), using hyperspectral imaging coupled with artificial neutral network algorithm

Abstract

Bruise damage is one of the many causes of fruit quality reduction and postharvest losses that often occurred during fruit pre-harvest and post- harvest handling operations. The detection of fruit bruise, especially for early detection, has in recent times, received increased global attentions. In this study, vis-NIR hyperspectral imaging technique coupled with artificial neural network was used to detect surface bruise of pomegranate. A total of 60 pomegranate fruit (cv. Wonderful) sample were grouped into three different after bruised time regime (immediate, 7 days, and 14 days) groups of 30 samples each. Two hyperspectral imaging setups: visible and near infrared (400 to 1000 nm) and short wavelength infrared (1000 to 2500 nm), were utilized to obtained spectral and spatial data of samples of the different groups. After comparing different pre-treatment methods, standard normal variate (SNV) transformation method with the best performance was selected for exported spectral data pre-processing. After spectral pre-processing, the average spectrum of the whole fruit surface (WF) and region of interest (ROI) of each sample served as input to a two-layer feed-forward artificial neural network (ANN) machine learning algorithm for classification model development. The results showed bruising accuracies to range from 80% - 90% on the same day of bruise. Overall bruise accuracy was 86.7% for bruised sample and 90% of sound samples. Model was able to recognize bruise immediately with an accuracy of 90% immediately, 100% after 7 days of bruise damage and 100% accuracy after 14 days of bruise impact. Model recognition accuracy increased with the increase in days of bruise occurrence. It can be concluded that vis-NIR hyperspectral imaging has certain feasibility in the early bruise detection of fruits. This study demonstrated the potential of using hyperspectral imaging technology in sensing and classification of early bruise on pomegranate fruit.

4.1. Introduction

Bruise damage is the most common type of mechanical damage that affects fresh horticultural produce. It reduces quality to the consumer and decreases the income to the growers alike [239, 332, 333]. Bruise damage is usually as a result of fruits being subjected to high impact and vibration [239, 262, 332]. Bruise damage occurs when the bruised fruit outer tissue fails without rupturing after being induced to excessive mechanical stress [239, 332, 334]. Some of these tissue failure of the skin of fresh produce results from the effect of large external force on fruit surface and occurs during impact, compression or vibration against a hard surface or on against fruit leading to cell breakage [36, 239].

Several factors have been attributed to the cause of fruit bruise damage, some of these includes genetic (species/genotype), seasonality, climate change and environmental conditions, farming/orchard practices; and the effect of fruit properties [36, 261], the major contributing factor have been linked to the amount of mechanical energy applied and absorbed by produce during its preharvest and postharvest handling chain [261, 262, 335].

Pomegranate (*Punica granatum L.*) is a notoriously ancient deciduous fruit of Middle Eastern origin with over 500 different cultivars grown in different parts of the world including South Africa [169, 264, 336]. Pomegranate fruit is mostly consumed as fresh arils but can also be savored in its processed form such as juice, dried arils, jams, etc. Pomegranate fruit industry have received boost in revenue and production due to the ever-increasing demand which have been linked to its nutritional and health benefits [3, 4, 337, 338]. Some of the health benefit associated with its consumption include; prevention of inflammatory diseases, induction of anti-proliferative, and enhances antimetastatic side effects in human [169].

Studies show pomegranate fruit to be very susceptible to bruise damage [332], and most bruises tend to occur during transportation back and forth orchard and packhouse during postharvest handling of the fruit [261, 262]. It has also been suggested the most bruise damage do take place during harvest in the farm, fruit unloading at the packhouses and vibrations during conveyance on the processing line [261]. Opara et el. [261] reported a significant correlation between bruised fruits and decay/insect damage. This indicates that bruised fruit are prone to insect attack as bruising makes the affected spot on the fruit rind soft and susceptible to insect attack. Several other studies has shown the detrimental effect of bruise on the physical and biochemical quality of pomegranate fruit [339, 340].

The economic losses in the fruit and vegetable industry related to bruising are considerable [239, 341]. Bruise damage to pomegranate fruit, considerably reduces the market value and causes huge economic loss [261, 262], as these fruits do not meet export quality and are devalued at marketplace (Figure 4.1).

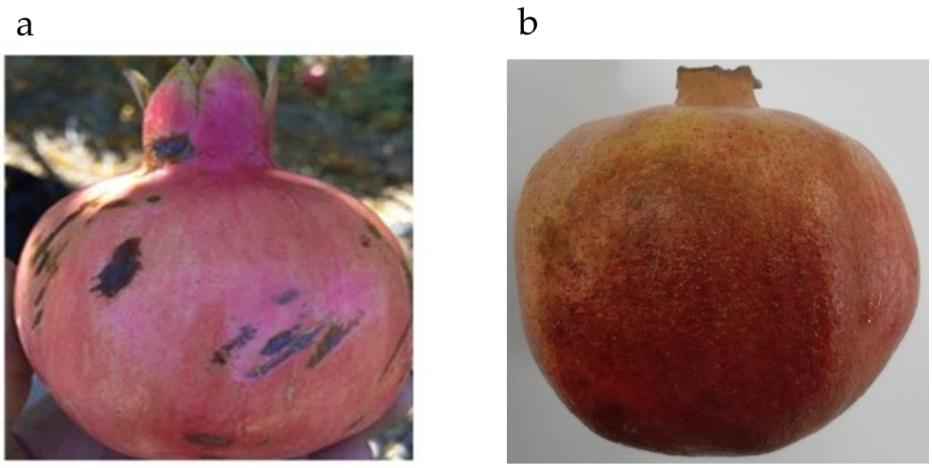

Figure 4.1. Pomegranate fruit manifesting bruise damage conditions (a) physical injury on the rind causing peel discoloration; (b) peel browning as the result of bruised damaged

Pomegranate fruit possess very hard and thick rind/peel, different from other fruit with soft tissues and surface like apple, pear, etc. [21]. Early detection of bruises on pomegranate fruit is difficult due to the tough and leathery skin or rind [332]. Hence, detection is only visible long after the impact [326]. Now in industry, bruises are identified through manual line inspection by expert sorters who are trained to visually remove bruised fruit during line operation. The ever-increasing demand to meet growing consumer market for fresh pomegranate fruit has rendered this approach for bruise detection ineffective. Manually picking up suspected bruised fruit is laborious, time consuming and very subjective and no longer sustainable. Therefore, researchers are finding alternative technology to under such task more efficiently and guarantee rapid and non-destructive detection of early bruise damage.
Research findings have reported pomegranate fruit to respond physiologically to bruise damage [339]. Some of the changes associated with bruise damage include increased peel electrolyte leakage (PEL), higher browning score and increased polyphenol oxidase (PPO) enzyme activity. The incident of high respiration rate after undergoing bruise damage has also been reported [339]. Physico-chemical changes such as the changes in total soluble solids (TSS), titratable acidity (TA), Brix-to-acid ratio (TSS: TA) and Brim A have also been observed after fruit are exposed to bruising [339]. There have been numerous studies evaluated such quality attributes nondestructively using spectroscopic analysis [11, 295, 324]. However, spectroscopic assessment by a spectrophotometer has a drawback as compared to an imaging approach, this is because it measures a relatively small area of the sample of interest. With the development of optical sensors, research has witnessed the emergence of the hyperspectral imaging system.

Hyperspectral imaging (HSI) system is a dynamic technology that is now being used for non-destructive inspection in the agricultural, biosecurity and food domain. HSI is a non-invasive/ nondestructive technique that merges spectroscopy and imaging into one system [48, 342, 343]. It is developed by creating images from more than one spectral component of the electromagnetic wavelength from the same region of an object and at the same scale [54]. Extracted data (hypercubes) from HSI systems are 3-dimensional (3D) structures and they consist of two spatial and one spectral dimension [48, 328] which provides more reliable diagnostic data than traditional machine vision or spectroscopy techniques in analyzing the characteristics of objects.
HSI combines with machine learning algorithms for data analysis and model development [112, 344]. Particularly for object image identification and recognition in the postharvest industry, several deep learning methods have been explored for fruit quality analysis [114, 345, 346]. For most applications, the Convolutional neural networks (CNN) is preferred in most state-of-the-art computer vision tasks over traditional deep learning algorithms such as Multilayer Perceptron (MLP), Linear Regression (LR), Random Forest, Support Vector Machine, etc. [114, 344, 347]. One challenge of CNN is its

tendency to take long to train model due to complexity of input data and often requiring high computation power resources [347, 348]. The MLP on the other hand, has shown to provide excellent results in some classification problems[145, 235, 346]. The MLP method employed in this study, is an ANN based system, that consist of simple processing units called neurons. They work on the relationship between a set of inputs and outputs by updating internal interconnections called weights using the back-propagation algorithm. Some of its advantages includes ability to work with nonlinear data, robustness, trainability and generalization of data, lower test time [346, 349]. Typical, an MLP network is composed of a set of source nodes as input layer, one or more hidden layers of computation nodes, and an output layer of nodes [350]. Non-destructive technique have found application in different fruit defects, bruise and disease detection studies [19, 142]. Particularly for bruise detection, several studies have been investigated, Examples includes apples [89, 101, 185], strawberries [177, 351], blueberries [147, 352], peaches [205], kiwifruit [199], pears [206, 208], jujube [194], cucumbers [353], and so forth. Studies on time of bruise could provide vital information that allows bruised fruits to be sorted and graded more effectively. It could also be crucial in monitoring the development of bruise damage as it makes damage fruits prone to infections [130, 185]. For example, Ferrari et al. [185], developed PLS-DA models for discriminating time of bruise incidence on 'Pink Lady' apple fruit dataset, input data were considered in three classes i.e., recent bruises (day1), day 3, and day 6 after bruising. The authors achieved classification results of 91.33%, 91.27% and 98.44% for day 1, day 3 and day 6 after bruising respectively. Thereby proving the efficacy of HSI in distinguishing bruise time and development. Another author in a different study also distinguished apple fruit time of bruise occurrence [354]. Results showed the model achieved higher accuracy when classifying older bruise (3days after) than first day (1h) after bruise. The study demonstrated hyperspectral imaging system developed in the spectral region of 400 and 1000 nm was effective in the early detection of bruises on 'McIntosh' apples.

These studies all recommended HSI as a promising tool for non-destructive application for bruise damage diagnosis. However, pomegranate possesses a different challenge for bruise detection due to its thick peel. To the best of our knowledge, no study has attempted to investigate early bruise detection on pomegranate fruit using hyperspectral imaging. Therefore, the aim of this research is to investigate the potential of a hyperspectral imaging system to be employed for early detection of bruise damage on pomegranate fruit and to verify the ability of the system to discriminate recent from old bruises. To carry out this study, we explore three specific objectives: (1) To develop classification model to distinguish bruised and healthy (unbruised) fruit, (2) To investigate the effect of spectral range on classification model accuracy and (3) To identify the effect of full image data (WF) and region of interest (ROI) of exported spectral data on model classification accuracy.

4.2. Materials and Methods

4.2.1. Fruit procurement and sample preparation

In this study, pomegranate fruit (cv. Wonderful) of commercial harvest maturity was procured from Sonlia pack-house in the Western Cape region, South Africa. Sample pomegranates of average weight of 280 ± 45g were individually sorted, washed and stored at 7.0 ± 1°C and 90 ± 2% RH, which is the recommended storage condition for optimum storage of pomegranate fruit [11]. A total of 60 pomegranate fruit without visible surface defects were selected from the prepared samples. The fruit samples used were of average TSS values of 16.36± 1.05 °Brix, and TSS/TA of 10.08± 2.13%.

4.2.2. Bruise simulation

Samples were split into two groups of 30 samples, Group A representing dropping induced bruising level, 60 cm, and Group B, unbruised. Simulated drop impact bruise was carried out according to Hussein et al. [339]. Samples from Group A were dropped from 60 cm height and allowed to fall on ceramics surface once before being caught (Figure 4.2). Bruise damage was created on the middle (sideways) around the equatorial region of the fruit. Considering that samples were fruit of the same average size. Impact energy (Ei, mJ) absorbed by the dropped fruit for each drop height was calculated using equation 4.1:

$$Ei = mgh \tag{4.1}$$

Where m is the mass of each individual pomegranate fruit, g is the gravitational constant, and h is the drop height. The calculated average impact energy was 680 mJ.

Figure 4.2. Bruise simulation set up. picture of pomegranate fruit sample under drop impact bruise from 60 cm height (a) fresh unbruised fruit sample (b) fruit placed at 60 cm drop height (c) bruised fruit sample after fruit dropped under free fall due to gravity.

4.2.3. Hyperspectral image acquisition system

To investigate the effect of spectral range on classification model accuracy, samples were scanned using two different hyperspectral imaging cameras: HySpex VNIR-1800 camera and HySpex SWIR-384 camera (NEO; Norsk Electro Optikk, Norway). Both sets of cameras are installed together, and

imaging of sample is carried out simultaneously at the Central Analytical Facility (CAF) Vibrational Spectroscopy Unit at Stellenbosch University (Figure 4.3a).

Prior to undergoing imaging of the samples, the system was set up as follows. The distance between sample and camera was set to 20.5 cm; the grey standard was fixed at 68 mm from above the spectral ranges from 400 to 1000 nm and 950 to 2500 nm for the VNIR and SWIR cameras, respectively. The SWIR camera has 384 spatial pixels and 288 spectral wavebands with a spectral interval of 6 nm. The VNIR camera has 1800 spatial pixels and 186 wavebands with a 3.26 nm spectral interval. The cameras were mounted above a translation stage which has a speed regulation system. A 30 cm focal length lens with a field view of 9.470 cm (SWIR) and 9.733 cm (VNIR) were used. Reflectivity reference data were obtained for each fruit. Hence, each image was obtained as a three-dimensional image block (x, y, λ), including 1800 × y pixels on the space dimension (x, y), and 128 bands at 3.26-nm intervals within a range of 400 to 1000 nm on the spectral dimension (λ). The camera specifications for both equipment is elaborated and compared in (Table 4.1).

Sample imaging was carried out on 1st day, 7th day and 14th day after simulated bruising to evaluate the ability of the hyperspectral imaging to discriminate the different days after bruising. After imaging on the different days, samples were returned to the cold room and stored at 7.0 ± 1 °C and 90 ± 2% RH.

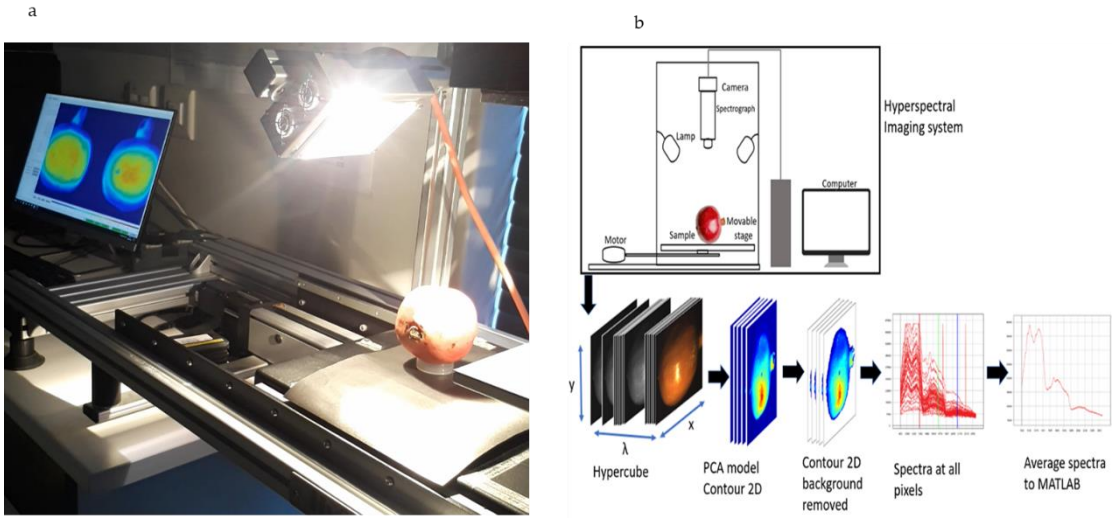

Figure 4.3. Pomegranate fruit sample under scanning using a hyperspectral imaging system (a) Set up of image acquisition from two line scanning hyperspectral imaging cameras combined; HySpex VNIR-1800 camera and the HySpex SWIR-384 camera (NEO; Norsk Electro Optikk, Norway) (b) Schematic of hyperspectral imaging system: consisting of a CCD camera, a Spectrograph with a standard C-mount zoom lens, a halogen lighting unit, a white nylon fabric tent, and a PC supported with image acquisition software.

Table 4.1. Summary of hyperspectral imaging system, comparison of SWIR and VNIR camera specifications

Main specifications	**SWIR**	**VNIR**
Spectral range	930 – 2500 nm	400 – 1000 nm
Spatial pixels	384	1800
Spectral channels	288	186
Spectral sampling	5.45 nm	3.26 nm
FOV*	16°	17°
Pixel FOV across/along*	0.73/0.73 mrad	0.16/0.32 mrad
Bit resolution	16 bit	16 bit
Noise floor	150 e-	2.4 e-
Dynamic range	7500	20000
Peak SNR (at full resolution)	>1100	>255
Max speed (at full resolution)	400 fps	260 fps
Power consumption	30 W	30 W
Dimensions (l-w-h)	38 – 12 – 17.5 cm	39 – 9.9 – 15 cm
Weight	5.7 kg	5.0 kg
Camera interface	CameraLink	CameraLink

Samples were placed with the top end facing the hyperspectral imaging system to ensure that the bruise impacted surface is captured. The acquisition time of one scan of the fruit surface for VNIR and SWIR cameras was less than one minute. The whole hyperspectral imaging set-up was controlled by PC supported with HySpex software for spectral image acquisition, binning, and camera and motor control.

4.2.4. Hyperspectral image calibration

Raw acquired hyperspectral images are usually impacted by uneven intensity distribution of the light source and dark current in the charge coupled device (CCD) detector, to minimize this effect, image correction was performed using known true spectral information. Eqn. (2) provides the formula for the image correction.

$$\rho_{xy}(\lambda) = \rho_{ref}(\lambda)\frac{R_{xy}(\lambda)-R_{dark}(\lambda)}{R_{ref}(\lambda)-R_{dark}(\lambda)} \qquad (4.2)$$

where $\rho_{ref}(\lambda)$ is the reflectivity of the 50% grey calibration plate (Zenith Polymer® Reflectance standard; SphereOptics GmbH, Germany); $R_{xy}(\lambda)$ is the original uncorrected hyperspectral image; $R_{ref}(\lambda)$ the image of the calibration board and $R_{dark}(\lambda)$ is the completed black image collected after turning off the light source and $\rho_{xy}(\lambda)$ the spectra of the corrected image.

The system operation and image acquisition were carried out using 'Breeze' software (version 2021.1.5, Umeå, Prediktera, Sweden) installed on a computer running the Windows 10 operating system. The acquired images were corrected with a 50% grey reference (Zenith Polymer® Reflectance standard; Sphere Optics GmbH, Germany) and a dark reference. The corrected images were imported into Breeze software version 2021.1.5 (Prediktera, Umeå, Sweden) and converted to absorbance. The Breeze version 2021.1.5 and Evince version 2.7.13 software (Prediktera, Umeå, Sweden) were used to extract spectral information, select effective wavelengths, minimize irrelevant information including noise and background signal caused by random interference. Subsequent hyperspectral data processing was implemented on the Image Processing Toolbox™ Hyperspectral Imaging Library in MATLAB® (The MathWorks, Inc., Natick, Massachusetts, United States).

4.2.5. Explorative analysis using PCA

The original hyperspectral image of the pomegranate fruit obtained from the hyperspectral cameras (Figure 4.3a). It follows the steps of; reflectance calibration, data reduction and noise/stage background removal (Figure 4.3b). PCA analysis is one of the most efficient methods for dimensional reduction in hyperspectral image analysis [182]. It enables contextualizing the obtained data by finding the dominant spectral data from the captured image (Figure 4.4).

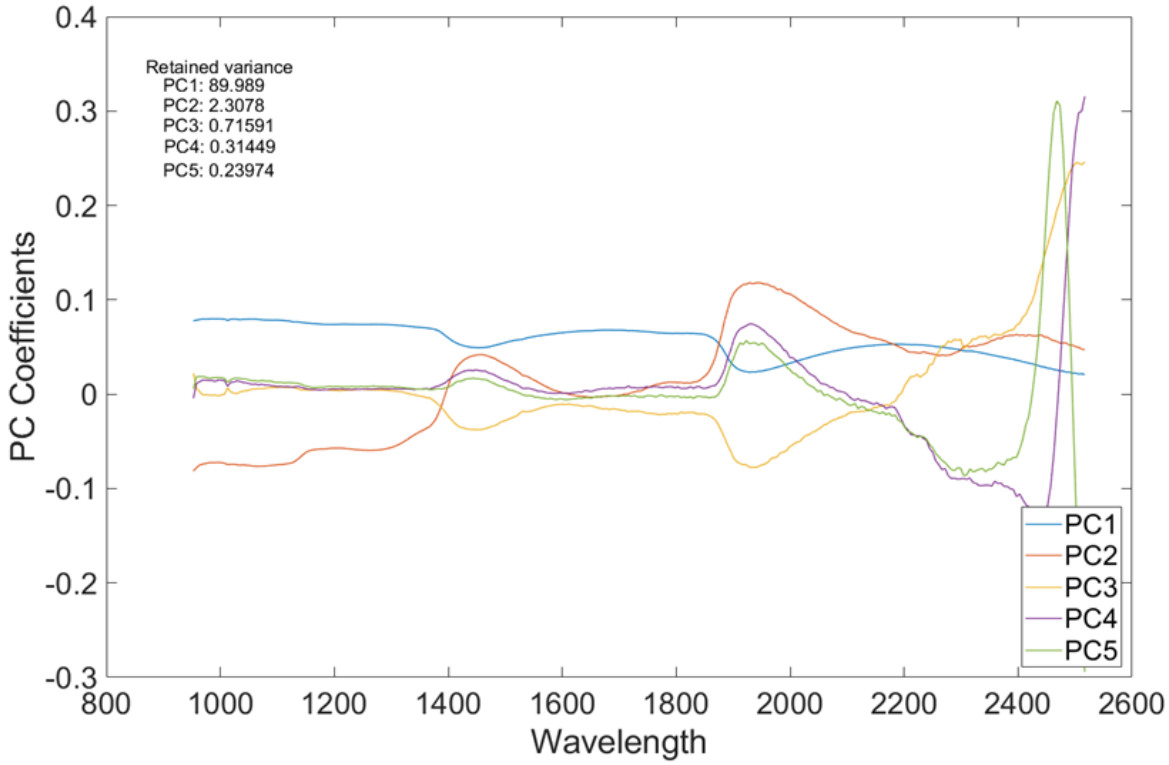

Figure 4.4 A plot of principal component analysis (PCA) coefficients vs wavelength of the SWIR HS image.

4.2.6. Selection of effective wavelength images

To perform optimal wavelengths selection, we propose a novel method, the noise-whitened Harsanyi–Farrand–Chang (NWHFC) method. The NWHFC is a virtual dimensionality (VD) approach developed from the Neyman–Pearson detection theory-based thresholding methods [355, 356]. The NWHFC is an improvement on the Harsanyi–Farrand–Chang (HFC) method, with an inclusion of noise estimation that decorrelates noise with signal sources for improved signal detection [355, 356]. For each sample, the number of spectrally distinct endmembers were estimated using the noise-whitened Harsanyi–Farrand–Chang (NWHFC) and the corresponding bands were identified using PCA method (Figure 4.5 and 4.6) for dimensionality reduction.

Figure 4.5, top row, displays the first five spectral bands of the original data of unbruised fruit. Variability is not significant both between bands and spatially on the fruit surface. Figure 4.5, bottom row, shows the same fruit seen with the identified five informative bands. Clearly, differentiations comes both spatially and spectrally with the informative bands. The same informative bands used on a fruit that was bruised by dropping from 60 cm height is shown in Figure 4.6. The accentuation of the bruise mark in the bottom raw (viewed with the informative bands) is apparent. The residences of the five effective bands are shown as vertical dashed line on the class mean spectra of the two cameras.

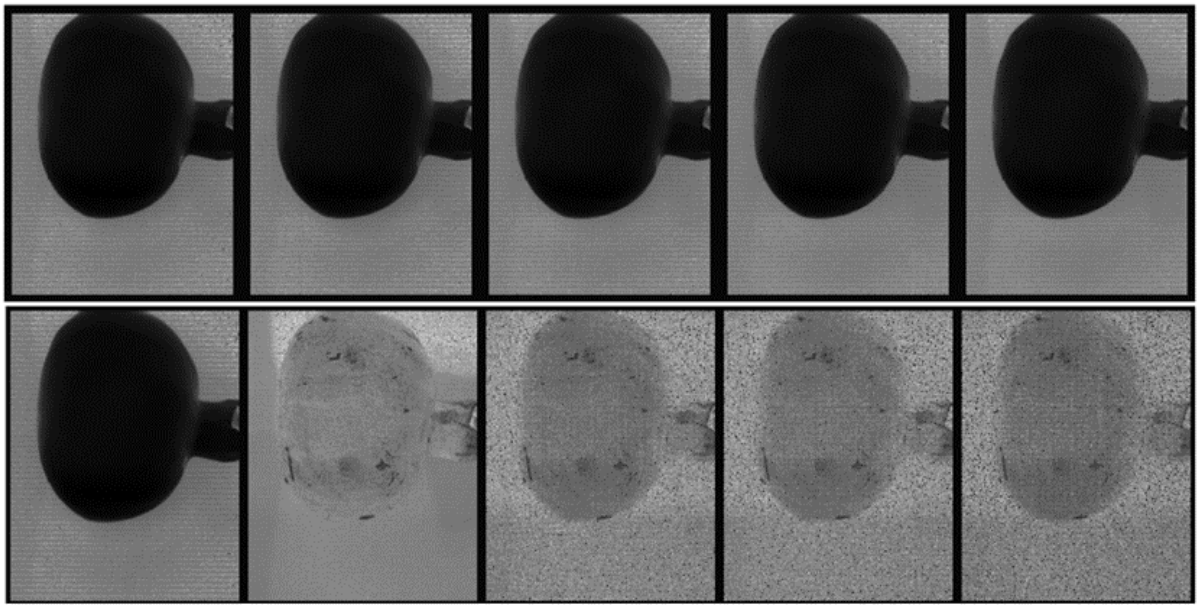

Figure 4.5 Display of the first 5 spectral bands in the input data cube (top row) and the five most informative bands (bottom row) of a typical pomegranate fruit without bruise

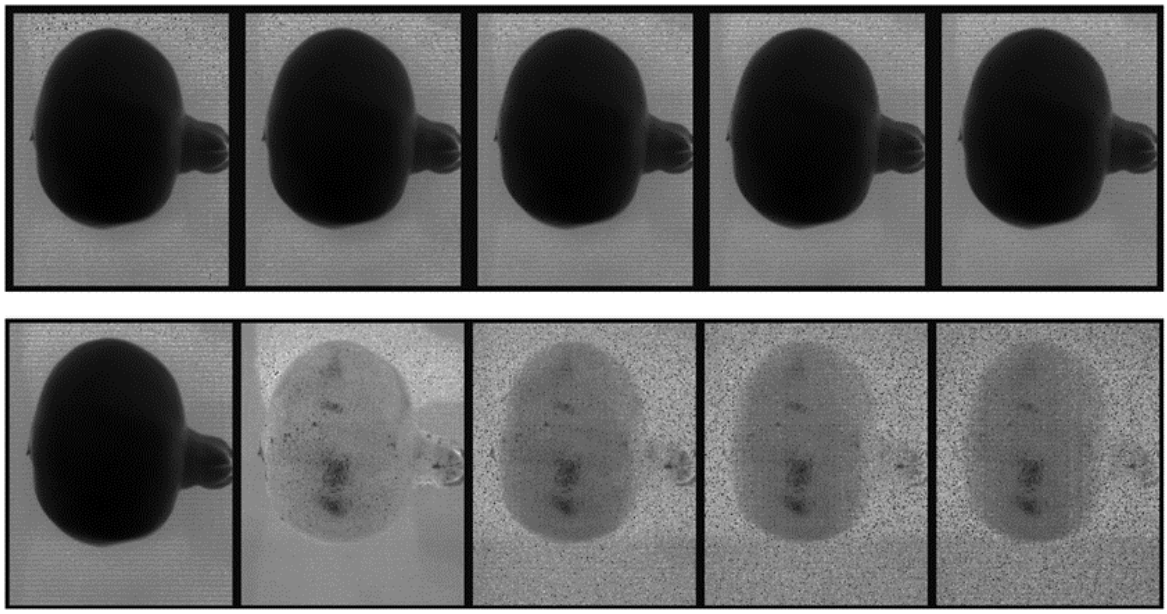

Figure 4.6 Display of the first 5 spectral bands in the input data cube (top row) and the five most informative bands (bottom row) of a typical unbruised pomegranate fruit.

For each fruit, ROI and whole fruit surface (WFS), averaged reflectance values at the five effective wavelengths were obtained and used as training data for the classification model development. Selecting out the informative bands and disregarding the redundant bands considerably decreases the data size for the subsequent classification model development. A more compact classification model was obtained by the data dimensionality reduction as described.

Some differences are observed between pomegranate fruit bottom and its surface as the fruit is not flat, this usually results in slight variations on the measured sample spectra. The magnitude of this variation depends on the individual sample involved. Internal chemical composition of some samples may result in greater variation. However, to eliminate this fluctuation, the standard normal variable (SNV) transformation was applied for spectral preprocessing. The SNV reduces disturbance in spectral data by correcting spectra with the mean and standard deviation of each spectrum [103]. After the explorative PCA analysis, the average spectra of each sample were extracted and saved separately for classification model development.

4.2.7. Data processing and analysis

Supervised classification models based on a two-layer feed-forward artificial neural network (ANN), with sigmoid hidden and softmax output neurons was used to classify inputs into two target (for bruise detection) and three target (bruise severity) categories. The ANN learning system attempts to imitate the neurological processing of human beings in its computational technique [50, 357]. It simulates human intuition in its decision-making system and classifying permutations. Its ability to learn and

make a generalize decision on the behavior of any complex and nonlinear process makes it stand out as a powerful modeling tool [50, 358]. The network splits data into training set (70%), validation (15%) and test set (15%). Reflectance data for each selected wavelength was used as out input data to the neural network for training, validation and test data set of the classification model. The input data is designated as the variable (X), while the target/class is the variables (Y). Target class (Y) must correspond in rows as the input variables (X). To achieve this, a dummy binary-coded matrix of equal rows as the X was created. In this study, for the case of bruise detection, 2-column response matrix Y was introduced in which samples belonging to the first class (bruised) were described by the dependent vector [1 0] while the (No bruise) class were represented by the vector [0 1]. In the case of a combined days after bruise, a 3-column matrix was generated with the first class immediate after bruise described by [1 0 0], day 7 after bruise [0 1 0], and day 14 after bruise [0 0 1], respectively. Classification was accomplished by using the machine learning and deep learning functions in MATLAB. Classification performances were evaluated based on its overall classification accuracy for training set, test set and validation set as well as class error. A good model should possess high classification accuracy and low-class error. A model with a 100% classification accuracy means that the model made no classification error.

4.3. Results and discussions

4.3.1. Spectral Analysis

In this study, to investigate the effect of spectral extracted from the entire fruit surface (WFS) and that of a specified region of interest (ROI) on model classification accuracy, spectral data from the two different portions of the imaged fruit sample were utilised for classification model development. The spectral profiles for both the ROI and the entire fruit surface for the two different cameras (spectral range) are shown in Figure 4.7a -4.7d.

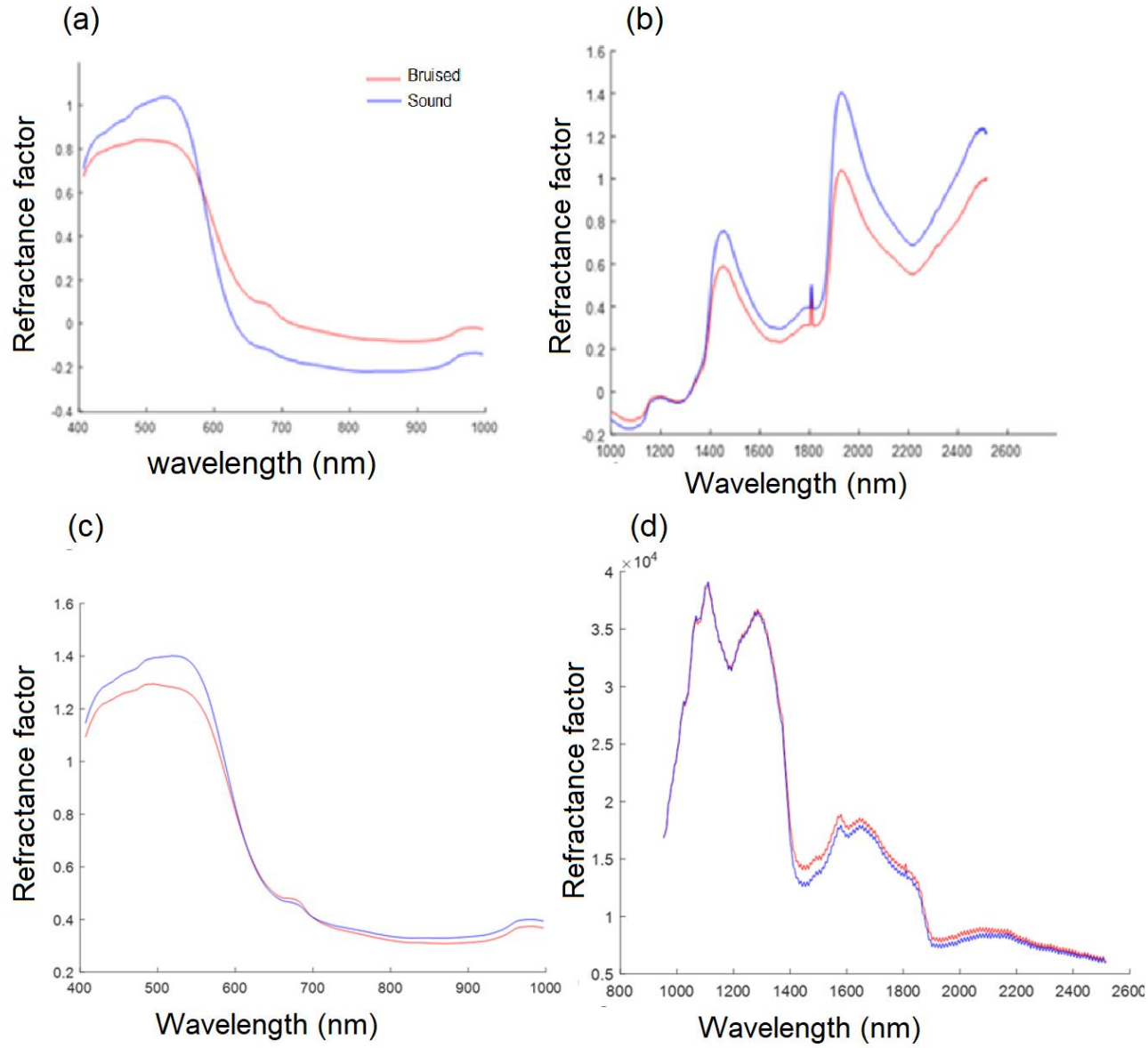

Figure 4.7. Representative reflectance spectra of ROIs data (a) VNIR and (b) SWIR wavelength regions and whole fruit surface (c) VNIR and (d) SWIR, for bruised and sound samples of pomegranate fruit.

The spectral of the ROI (Figure 4.7a and 4.7b), showed a distinctive difference between bruise and sound sample as compared to that of the entire fruit surface (Figure 4.7c and 4.7d). This indicates that spectral was more informative of the precise region of the fruit as compared to spectral of the entire fruit surface. Though, a slight difference between bruised and sound sample is still noticed on this spectral profile of the extracted whole fruit data.

Also, the average spectra of ROIs as well as full fruit surface representing bruises at different stages (unbruised, immediately (day1), 7days, and 14 days) were illustrated (Figure 4.8) for ROI and (Figure 4.9) for whole fruit surface (WFS). The reflectance from bruised surface was consistently lower than that from the normal tissue over the entire spectral region. This observation has been made by several researchers [101, 147, 354]. This decrease of reflectance of bruised tissue can be attributed to the fact that there is an outflow of water from the surface of the sample that have been bruised [101, 182].

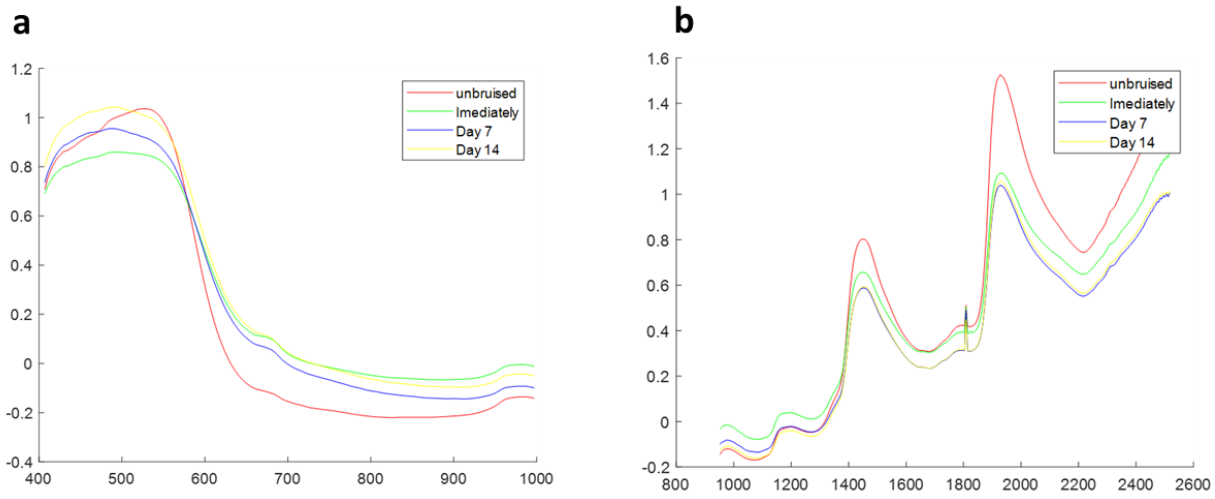

Figure 4.8. The average spectra of ROIs representing bruises at different stages; unbruised, (immediately(day1), 7days, and 14 days) data (a) VNIR and (b) SWIR wavelength.

Reflectance spectral for bruised samples for the different days after bruise regime as well as unbruised samples is also shown in Figure 4.8a (VNIR spectral range) and Figure 4.8b (SWIR spectral range). for ROI, and that of the whole fruit surface spectral range (WF) Figure 4.9a (VNIR spectral range) and 4.9b (VNIR spectral range). It can be observed that the lower spectral was observed for the samples immediately after bruise damage (red). Since early bruise detection is our main concern, the figure illustrates the system can detect bruises at this stage, proving it could detect even for later period as well.

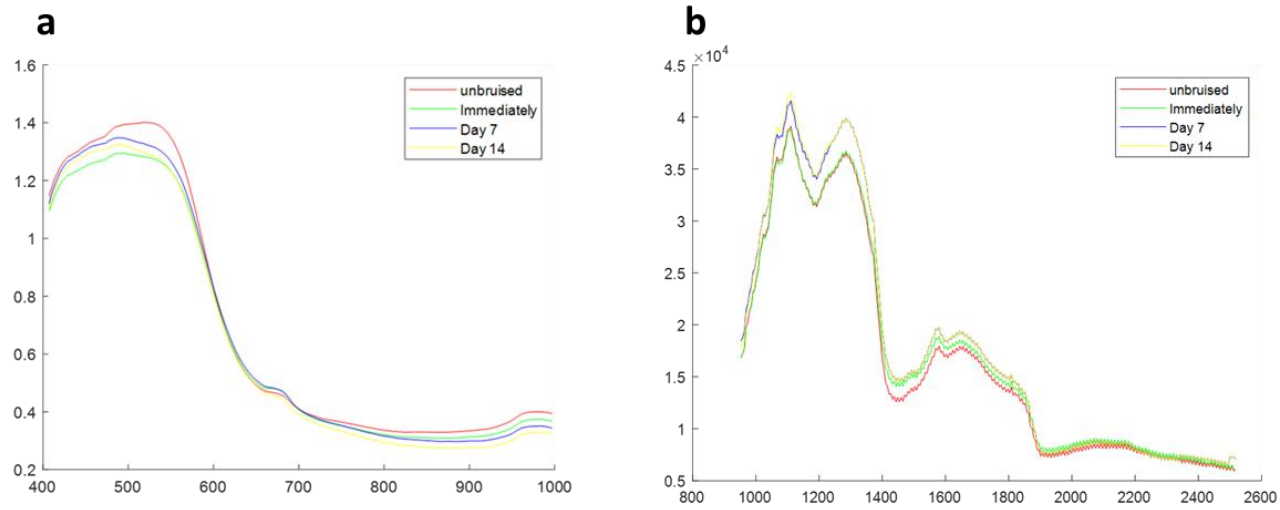

Figure 4.9. The average spectra of entire fruit surface (WFS) representing bruises at different stages unbruised, (immediately(day1), 7days, and 14 days) data (a) VNIR and (b) SWIR wavelength

It is obvious that the spectral signature difference between the bruised and sound samples immediately after bruise is of key importance. Spectral curve shows the highest difference in reflectance between the bruised and unbruised tissue in the SWIR wavelength region (Figure 4.9b), as compared to the visible region (Figure 4.8a). Similar trend was observed in apple bruise detection [354] as well as blueberry bruise detection [147]. Both authors reported that this difference in these wavelengths is caused by the outflow of water from the bruised tissues in the first period after damage.

4.3.2. Optimal classification model performance for VNIR camera

Table 4.1 summarizes the classification accuracies for the different spectral ranges, days of bruise occurrence and the fruit area surface considered. For the VNIR spectral range, the model showed good classification accuracy ranging from 83.3% – 90% on the first day of impact bruise (Figure 4.9). The ANN classifier recognized sound fruit 90% better than the bruised samples 86.7% for the ROI and 83.3% for the WF pixel (Figure 4.9a and 4.9b). The recognition accuracy increased as bruise stayed beyond the first day (Appendix A1). For day 7 and day 14 after bruise, under the ROI pixel, model made 100% accuracy for sound samples and only wrongly classified 1 sample of the bruised sample. For the WF surface, accuracy was 96.7% for sound samples and 90% for bruised samples for day 7 and 100% for day 14 after bruise damage. Similar trend was observed in the study on apple [95]. The authors reported recognition to increase from 1 min after bruise (87.04%) to an accuracy of 98.15% after day 4 of bruising. Fu and Wang, [206] reported an increase in recognition accuracy from 86.67% immediately after bruise to 96.67% 3 days after bruising. Zhu & Li [95] employed PLS-DA algorithm for rapid detection of apple bruises and reported bruise development resulting increased recognition accuracy from 86.11% immediately to 97.22% after 4days of bruising.

The results from the ROI were slightly higher than those when the whole fruit (WF) surface was used. Under WF as input data, model yielded an accuracy of 96.7% for sound samples and 90% for bruised samples. Similar trend is reported for Golden Delicious apple [185]. The authors applied the whole signal and recognition rate was 64.23% and when an interval of 10 was considered, accuracy increased to 92.2%. Higher classification accuracy was obtained for the early detection of bruises on 'McIntosh' apples for older bruises as compared to recent ones [354].

4.3.3. Optimal classification model performance for SWIR camera

The summary of classification model performance for the SWIR spectral range is given in Table 4.2. On the first day of bruise damage, under the region of interest, model accuracy ranged from 83.3-86.7% and 80-83.3% for the WF. The confusion matrix (Figure 4.10a and 4.10b) illustrates how model correctly or incorrectly classified bruised and sound sample on immediately after impact bruise damage. Under the ROI input data, Of the total samples 30 sound samples, model recognized 26 as sound, and wrongly group 4 samples as bruised (Figure 4.10a), yielding an accuracy of 86.7%, a lower recognition rate was observed for the bruised samples (83.3%) as model correctly classified 25 of the 30 samples as bruised and 5 as sound sample. For the WF surface, recognition accuracy was 80% for bruised sample and 83.3% for sound samples (Figure 4.10b). The model performance of the SWIR spectral range was slightly lower than that of the VNIR input spectral. when spectral data from the entire fruit surface (WF) was considered. The model had correctly classified sound and bruised samples at 90% and 83.3% respectively under the VNIR spectral range, while for the SWIR spectral data, recognition accuracy for both sound and bruised samples were 83.3% and 80% respectively (Figure 4.10b).

For the model after 7^{th} days after bruising, accuracies ranged from 93.3% to 100% for both spectral ranges under consideration which is an improvement compared to that of day 1 (Table 4.3). For both spectral ranges, data from the ROI showed 100% accuracy for sound samples, for bruised samples, accuracy was 96.7% for VNIR spectral range and 93.3% for SWIR spectral range when the ROI was considered. The results were slightly lower when the entire fruit surface was used. Under WF as input data, the model yielded an accuracy of 96.7% for sound samples and 90% for bruised samples for VNIR data and 93.3% accuracy for both sound and bruised samples for SWIR data. A full confusion table is presented in Appendix A1 and A2.

The trend shows that model classified samples better as bruise developed, also VNIR spectral data

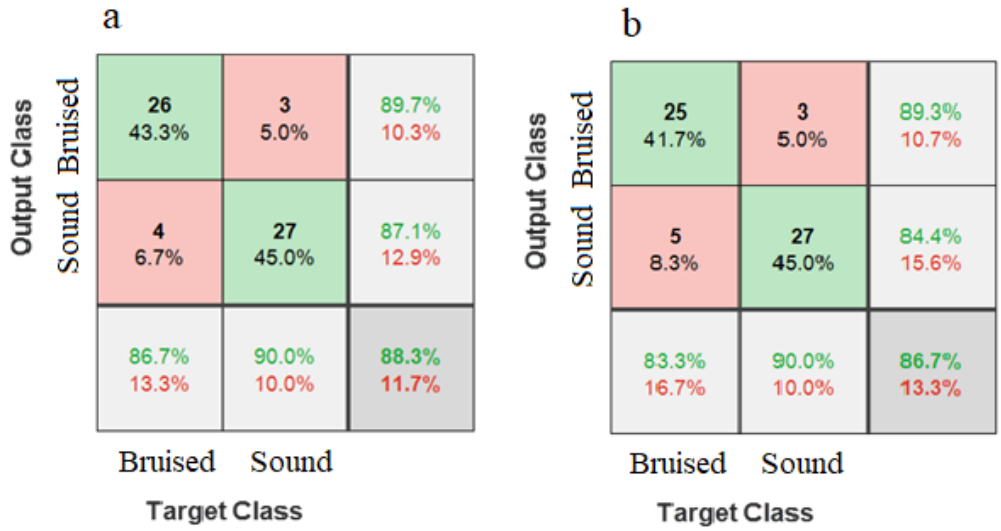

Figure 4.10. Confusion matrix for the independent test set on the VNIR spectral data immediately after bruise damage. ROI (4.10a), WF (4.10b). The x axis refers to the true categories, and the y axis refers to the classifier outputs. The integers in the matrix show a number of samples. The color encodes the percentage of a class of blocks (x) classified into a predicted class (y).

Table 4.3 presents the overall performance accuracy of the classification model for the different days of bruise detection on pomegranate fruit. It shows clearly that the highest recognition accuracy achieved immediately after bruising is 88.3%, the average increased to 98.3% a week after bruise damage, after 14 days of bruising, model achieved a 100% accuracy.

Baranowski et al. [133] also reported better model accuracies for the VNIR input data (90%) than the SWIR input (85%) in their study on apple. Model consistently showed slightly better recognition accuracy for sound fruit classification over bruised samples. This trend is observed in a similar study on strawberry [351]. The authors obtained the highest classification accuracy of 99.9% for healthy samples and 86.1% for bruised samples.

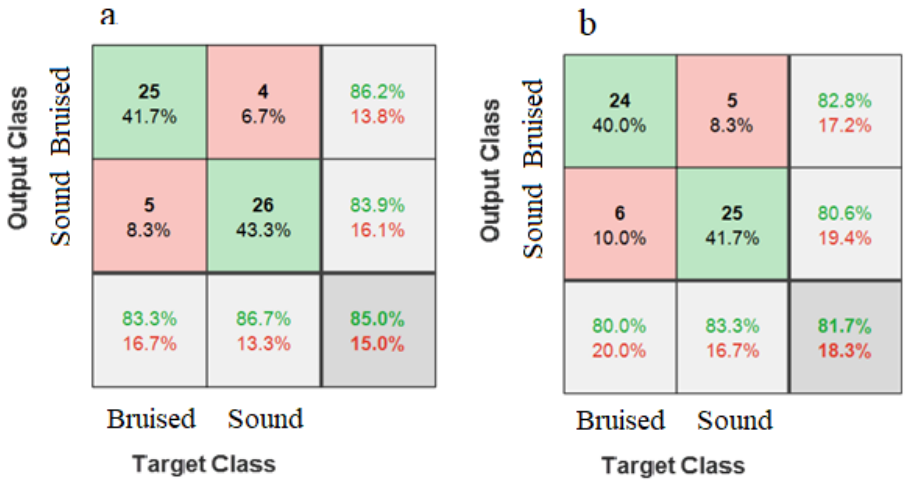

Figure 4.11. The confusion matrix obtained of the classification performance for SWIR spectral data immediately after bruise damage. ROI (4.11a), WF (4.11b); The x axis refers to the true categories, and the y axis refers to the classifier outputs. The integers in the matrix show several samples. The color encodes the percentage of a class of blocks (x) classified into a predicted class (y).

4.3.4. Classification model performance for combined data for bruise detection

Table 4.4 presents the results for the combined data of the bruised samples on the different days after bruising. Figure 4.12 illustrates the confusion matrix of the classification based on the ANN model. For both VNIR and SWIR spectral ranges, the highest accuracy achieved was 86.7% and 83.3% respectively for the 14th day after bruising. Bruise recognition on the first day was poor 53.3% for SWIR and 60% for VNIR, of the 30 samples bruised on first day, model classified 16 samples accurately, misplaced 12 samples as bruised on the 7th day and 2 wrongly classified as bruised on the 14th day (Figure 4.12b).

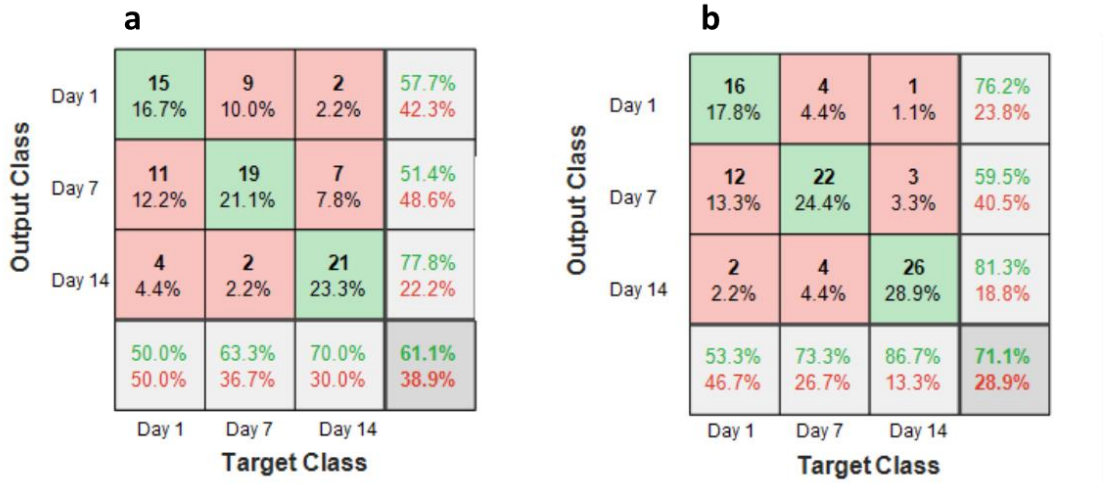

Figure 4.12. Summary of confusion matrices from test data illustrating model performance for the combined days after bruise for the 50 by 50 region of interest for both SWIR and VNIR input data (a) SWIR classification performance (b) VNIR classification performance.

Table 4.2: Classification result of test data set of ANN model for distinguishing sound (NB –not bruised) and bruised (BR) tissues based on VNIR and SWIR reflected for the extracted (ROI) and the image of whole fruit surface of fruit samples

Day 1		SWIR				VNIR			
		Sample number	Correctly classified	Misclassified	Accuracy (%)	Sample number	Correctly classified	Misclassified	Accuracy (%)
ROI	Sound	30	26	4	86.7	30	27	3	90
	Bruised	30	25	5	83.3	30	26	4	86.7
WF	Sound	30	25	5	83.3	30	27	3	90
	Bruised	30	24	6	80	30	25	5	83.3
DAY 7									
		SWIR				VNIR			
		Sample number	Correctly classified	Misclassified	Accuracy	Sample number	Correctly classified	Misclassified	Accuracy
ROI	Sound	30	30	0	100	30	30	0	100
	Bruised	30	28	2	93.3	30	29	1	96.7
WF	Sound	30	28	2	93.3	30	29	1	96.7
	Bruised	30	28	2	93.3	30	27	3	90
DAY 14									
		SWIR				VNIR			

		Sample number	Correctly classified	Misclassified	Accuracy	Sample number	Correctly classified	Misclassified	Accuracy
ROI	Sound	30	30	0	100	30	30	0	100
	Bruised	30	29	1	96.7	30	30	0	100
WF	Sound	30	30	0	100	30	30	0	100
	Bruised	30	28	2	93.3	30	30	0	100

Table 4.3. Overall performance of the test data of classification model for the different days of bruise detection on pomegranate fruit using the ANN algorithm

Bruise days	Wavelength	Accuracy (%)	
		ROI	WF
Immediately (Day1)	SWIR	85	81.7
	VNIR	88.3	86.7
1 week after (Day7)	SWIR	96.7	93.3
	VNIR	98.3	93.3
2 Weeks after (Day14)	SWIR	98.3	96.7
	VNIR	100	100

Table 4.4. Combined performance of the classification model for the different days of bruise detection on pomegranate fruit using the ROI data

Days of bruising	Combined model classification performance			
	Wavelength	Sample number	Accuracy (%)	Class error (%)
Day 1	SWIR	30	50	50
	VNIR	30	53.3	46.7
Day 7	SWIR	30	73.3	26.7
	VNIR	30	73.3	26.7
Day 14	SWIR	30	76.7	23.3
	VNIR	30	86.7	13.3

Figure 4.10 shows a plot of overall classification accuracies against the different days of bruise development (immediate, 7days and 14 days). As can be observed, detection on day one was 88.3% for ROI and 86.7% for the WF input under the VNIR spectral range. Though slightly lower, the SWIR spectral range also obtained relatively similar accuracy, with model yielding 85% for the ROI and 81.7% for the WF.

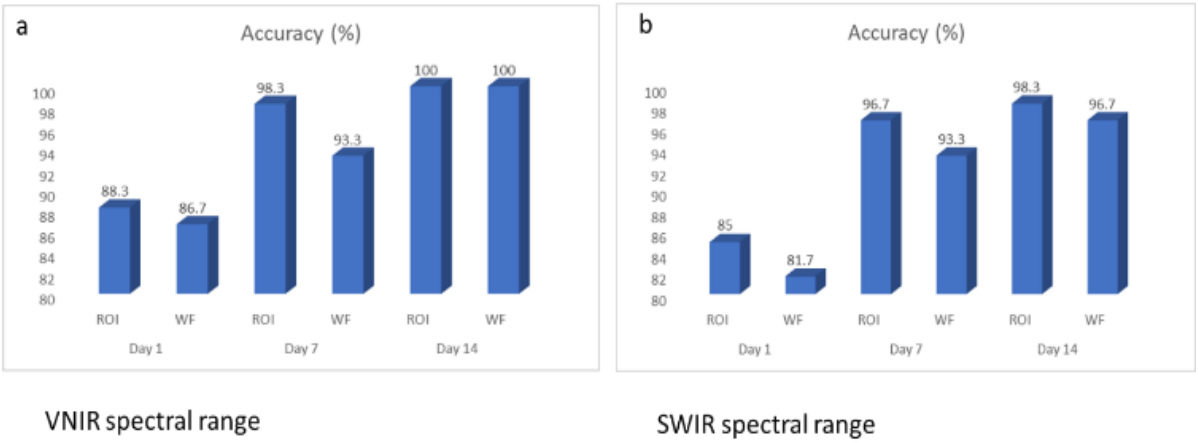

Figure 4.13. Chart showing different recognition accuracies for the model developed for the different days after bruise, for (a) VNIR spectral range, (b) SWIR spectral range.

This result gradually increased as we moved from day 7 up to day 14, indicating as bruise developed, model was able to accurately detect bruise presence. This finding has been reported on other application for different fruits [99, 206]. The difference studies show initial high accuracy for early detection, thereby indicating the hyperspectral imaging system can be utilized as non-destructive testing technique.

4.4 Conclusions

The results confirm hyperspectral imaging technique combined with machine learning methods (ANN) to be an effective technique for early bruise detection. Both image surfaces considered showed bruise can be detected in early stage of bruising with an accuracy of 88.3%. The overall highest classification accuracy achieved was 100% during the 7th and 14th day after bruising. The model accuracy increases with the increase in days of bruise occurrence. Overall accuracy on first day of bruise occurrence was 90%. Both methods of data extraction are good enough to detect the early bruise damage which is invisible to the naked eye. This study presents a feasibility in the early bruise detection of pomegranate fruit using the hyperspectral imaging technique. Although this paper focused on pomegranate bruise development inspection, the techniques employed for data extraction and manipulation presented in this study are easily adaptable and can be suitable to other food applications.

Accuracy of prediction of classification can be improved by increasing the number samples. In this study 30 samples were scanned per class (no bruise, dropped from 60 cm or dropped from 100 cm). Hence, a total of 90 samples were scanned. This amount is in the range most previous studies have reported. Lab scale HS imaging system is costly and time-consuming and doing

such experiment in replicates is a challenge. To augment this bottleneck, this research implemented data dimensionality reduction by using effective wavelength selection technique.

CHAPTER 5

Vis-NIR and SWIR hyperspectral imaging method to detect bruises in pomegranate fruit

Abstract

Fresh pomegranate fruit is susceptible to bruising, a common type of mechanical damage during harvest and at all stages of postharvest handling. Accurate and early detection of such damages in pomegranate fruit plays an important role in fruit grading. This study investigated the detection of bruises in fresh pomegranate fruit using hyperspectral imaging technique. A total of 90 sample of pomegranate fruit were divided into three groups of 30 samples, each representing purposefully induced pre-scanning bruise by dropping samples from 100 cm and 60 cm height on a metal surface. The control has no pre-scanning bruise (no drop). Two hyperspectral imaging setups were examined: visible and near infrared (400 to 1000 nm) and short wavelength infrared (1000 to 2500 nm). Region of interest (ROI) averaged reflectance spectra was implemented to reduce the image data. For all hypercubes a principal components analysis (PCA) based back-ground removal were done prior to segmenting the region of interest (ROI) using the Evince® multi-variate analysis software 2.4.0. For each sample, the number of spectrally distinct features were estimated using the noise-whitened Harsanyi–Farrand–Chang (NWHFC) method implemented in MATLAB, and the corresponding bands were identified using PCA method. A two-layer feed-forward artificial neural network (ANN) is used for classification. The accuracy of bruise severity classification ranged from 80 to 96.7%. When samples from both bruise severity (Bruise damage induced from a 100cm and 60 cm drop heights respectively) cases were merged, class recognition accuracy were 88.9% and 74.4% for the SWIR and Vis-NIR, respectively. This study implemented the method of selecting out informative bands and disregarding the redundant ones to decrease the data dimensionality. This study demonstrated the potential of using hyperspectral imaging technology in sensing and classification of bruise severity in pomegranate fruit.

5.1. Introduction

Pomegranate (*Punica granatum L.*) is undeniably one of the most ancient deciduous fruit in the world [4, 169, 264]. With its origin traceable to the Middle East, it has expanded and is now been grown across the world, even meeting commercial export in South Africa [270, 338]. Pomegranate fruit can be consumed as fresh arils or in its processed form such as juice, dried arils, jams, etc. In the past decades, the demand for pomegranate fruit has been increasing due to its nutritional and health benefits [2, 3, 264]. It has been recounted to be highly effective for preventing inflammatory diseases and induces anti-proliferative and antimetastatic side effects in human [169].

Bruise is the most common type of postharvest mechanical injury affecting pomegranate fruit [261, 262]. Bruise reduces fruit quality and causes considerable post-harvest losses and decreases the income [239, 333, 335]. Bruise usually results when the fruit is subjected to high impact and vibration [34, 261, 333]. Bruise damage normally manifest when the outer tissue of the fruit fails without rupturing due to excessive mechanical stress [239, 334, 335]. Studies show that most bruises occur during harvest and transportation to the packhouse and during handling in the packaging processing line. Studies has shown the detrimental effect of bruise on the physical and biochemical quality of pomegranate fruit [335, 340]. The economic losses in the fruit and vegetable industry due to bruising is substantial [34, 341]. In the pomegranate industry, bruise damage reduces the market value considerably and causes a huge economic loss [261, 262], as bruised fruits do not meet export quality and are devalued at marketplace.

Unlike other fruit with soft tissues and thin rind/peel such as apples and pear, early detection of bruises on pomegranate fruit is difficult due to the tough and leathery skin of this fruit [332]. Bruise on pomegranate fruit is only visible long after the impact [326]. Typically, in the industry, bruises are identified through visual inspection by trained panels or line operators and removed manually. This approach for bruise diagnosis is laborious, time consuming and subjective. Therefore, there is a need for alternative technology for a rapid and non-destructive detection of early bruise damage. Study shows that pomegranate fruit responds physiologically and in some physico-chemical changes when they undergo bruises. This is indicative in the changes in total soluble solids (TSS), titratable acidity (TA), Brix-to-acid ratio (TSS:TA) and BrimA when exposed to bruising [326]. Spectroscopic analysis is gaining widespread research attention because of its ability to extract this huge chemical information content for predicting and analysis of this samples [342].

There have been different imaging and feature extraction approaches for fruit bruise detection and measurement [359–362]. The shortcoming with most of these approaches is the need for wider spectral range [342]. Spectroscopic assessment for fruit quality gained attention in research as viable nondestructive technique for quality attributes and grading [11, 290, 363]. Other imaging techniques

that have been applied for bruise detection in recent times include X-ray [326], Thermal imaging (TI) [362], Magnetic resonance imaging (MRI) [364], Fluorescence imaging (FI)[183, 365] as well as hyperspectral imaging [366, 367].

Hyperspectral imaging (HSI) has emerged as a powerful non-destructive inspection technique in the agricultural, biosecurity diagnostic and food domain recently. HSI is a non-invasive/ nondestructive technique that integrates spectroscopy as well imaging to form one system [343]. It is developed by creating images from more than one spectral component of the electromagnetic wavelength from the same region of an object and at the same scale[54]. The data extracted (hypercubes) from HSI systems are 3-dimensional (3D) structures that consist of two spatial and one spectral dimension[48, 328]. This non-destructive approach has been proposed for detections of different fruit defects [19, 142]. It has been employed for disease detection [39, 166], common defects [14, 202, 368, 369], physical damage [102], and in particular for bruise detection [99, 100, 182, 186]. Some of the specific fruits that have been investigated for bruise damage includes; apples [101, 185, 205], strawberries [177, 351], blueberries [147, 352], peaches [205], kiwifruit [199], pears [206, 208], jujube [194], cucumbers [353], and so forth. These studies reported successes in accurate classification of bruise severity suggesting the potential of implementing the technique. However, there has been no known study reported on bruise detection on pomegranate fruit. It is expected that for the different fruit texture, peel type and morphology, and the different causative factors to bruises on fruit, it is still difficult to decide exactly the most suited hyperspectral system to deploy for detection of bruises on pomegranate fruit. This study seeks to explore this novelty to detect and classify bruise and level of bruise severity on pomegranate fruit.

5.2. Materials and methods

5.2.1. Fruit procurement and sample preparation

In this study, pomegranate fruit (cv. Wonderful) was procured from Sonlia pack-house in the Western Cape region, South Africa. Sample pomegranates were individually washed and stored at 7.0 ± 1°C and 90 ± 2% RH, which is the recommended storage condition for optimum storage of pomegranate fruit [11]. The reference bruising tests, and the subsequent hyperspectral scanning were taken for harvest mature pomegranates. The fruit samples used were of average TSS values of 16.36± 1.05 °Brix, and TSS/TA of 10.08± 2.13%.

5.2.2. The reference bruised fruit samples

Bruise damages were created on the middle (equatorial) region of the fruit by dropping fruit from a predefined height onto a steel surface with side of the fruit perpendicular to the metal surface. This

experiment follows the previously developed method by Hussein et al. [335] (Figure 4.2). Each pomegranate fruit was dropped once from a given height to the metal surface and caught by hand after the first rebound to avoid multiple impacts. Following impact tests, fruit were incubated at ambient condition (19 – 22 °C, 60 ± 5 % RH) for an hour prior to image acquisition. A total of 90 pomegranates were used for this study. Samples were sub-divided into three groups of 30 samples, each representing dropping induced bruising level: 100 cm, 60 cm, and no drop (not bruised) (Figure 4.2). Assuming the fall was nearly free, impact energies applied on the fruit surface were calculated according to impact force from falling object. The calculated average impact energy was approximately 760 ± 0.5 mJ and 680 ± 0.8 mJ for the falling from 100 cm and 60 cm heights, respectively.

All data analysis and pre-processing of hyperspectral data is as detailed in chapter 4 materials and methods.

5.3. Results and discussions

5.3.1. Principal component analysis (PCA)

One of the very effective ways for dimensional reduction in hyperspectral image analysis is the PCA method [103]. It enables contextualizing the obtained data by finding the dominant spectral data from the captured image. It follows the steps of; reflectance calibration, data reduction and noise/stage background removal (Figure 4.2).

Figure 5.1 depicts the averaged spectral of all the samples scanned with the VNIR (Figure 5.1(a)) and SWIR (Figure 5.1 (b)) cameras squeezed out using the Evince software (version 2.7.10, Prediktera, Sweden). Evince extracted the spatial (horizontal and vertical), and spectral profiles from the image display. Each sample fruit exhibited a unique spectral signature based on the sample's composition, surface structure, viewing geometry, etc. The assumption is that bruising can create its own signature by affecting the surface structure and composition. However, the overall shape (locations of wavelength bands where highs and lows) is similar across the electromagnetic spectrum for all samples in both cameras. Hence, the classification parameter this study used to identify bruise se-verity and presence/absence of a bruise was based on reflectance values at bands than the overall shape of the spectra.

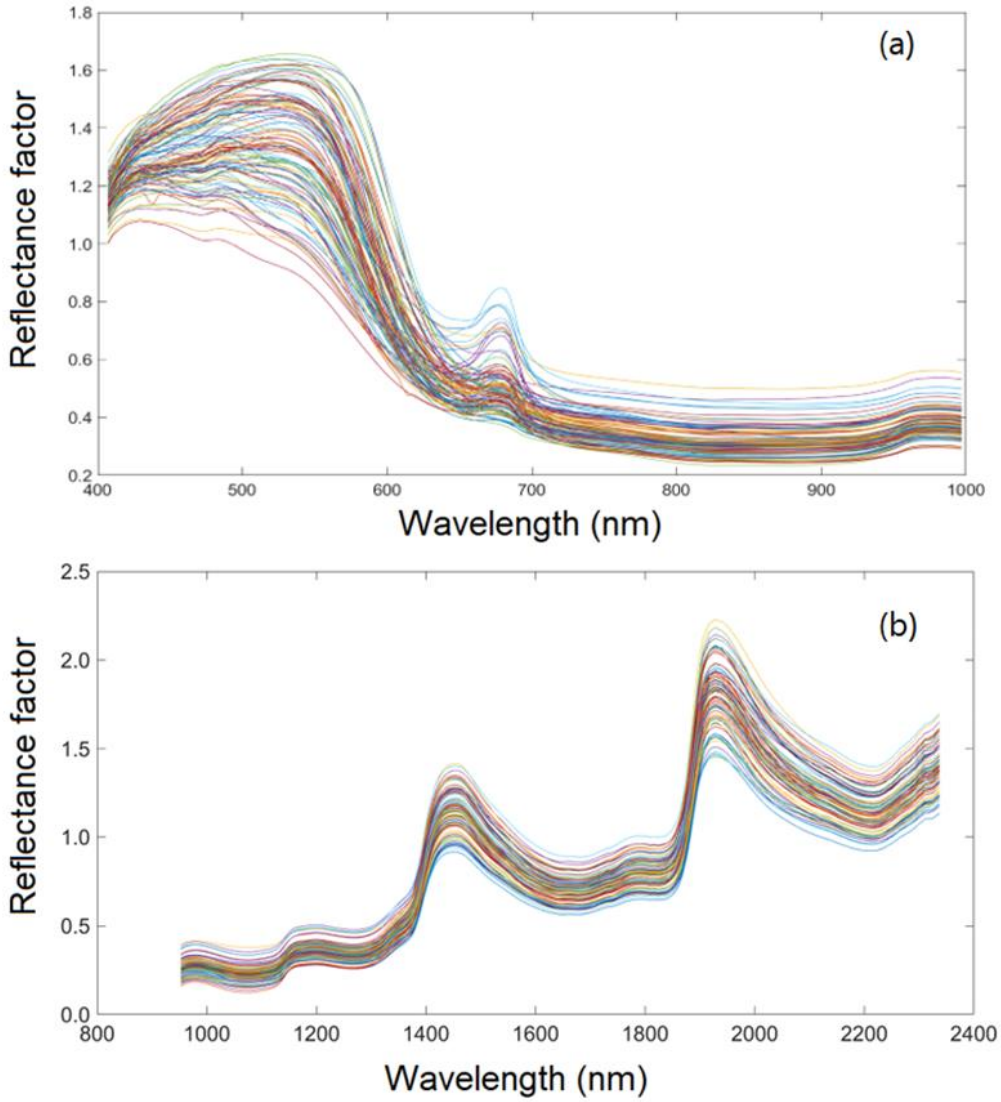

Figure 5.1. Spectral characteristic curves of the SWIRL data. average spectra of the hyperspectral images of all samples.

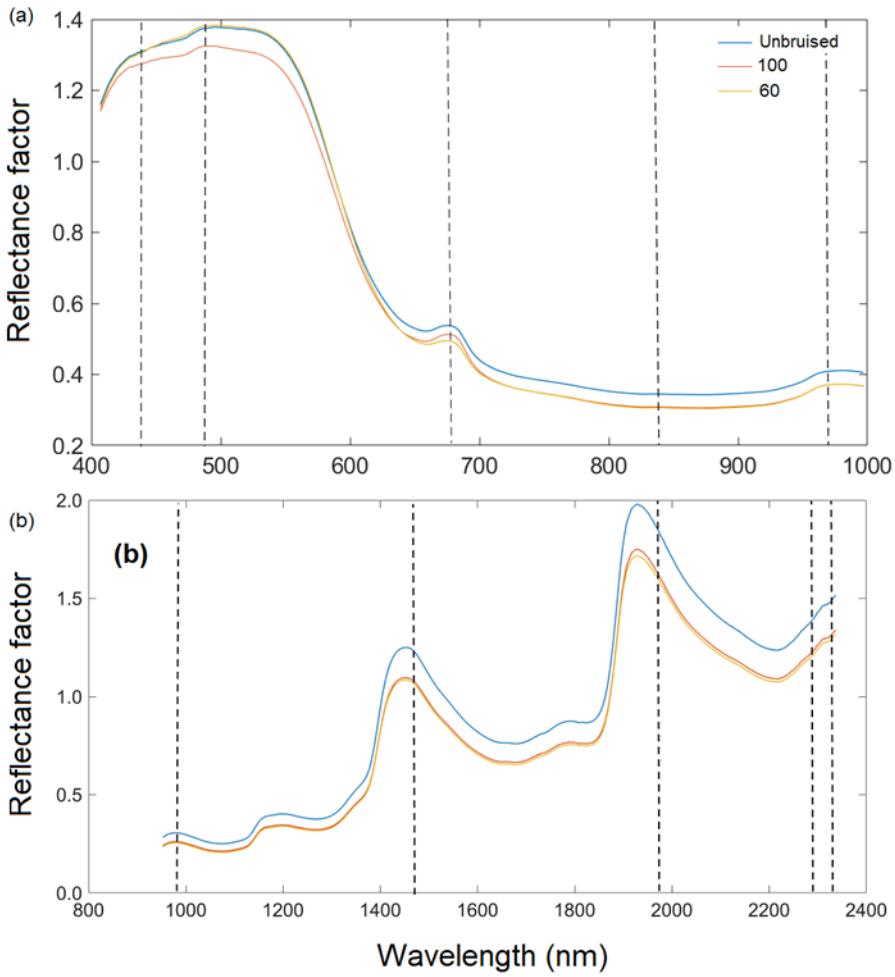

Figure 5.2. Class mean spectral of the three bruise severity classes of the VNIR (a) and SWIR (b) camera. The vertical dashed lines identified the most informative bands selected by the effective wavelength selection technique.

5.3.2. Classification model development for bruise fruit detection

The test set results for bruise detection classification accuracy of the VNIR and SWIR data are summarized on Table 5.1. The results for classification were grouped into three groups or levels of severity, group 1 comprised fruit bruised at 60 cm and unbruised fruit, group 2 was made up of samples bruised at 100 cm and unbruised samples and finally group 3 which combined the two-bruised fruit samples (60 cm vs 100 cm). For bruise severity classification training, each ROI averaged reflectance values at the five wavelengths (1 × 5), presented to the classification model, is accompanied by a (1 × 3) target matrix where each column indicates a category with a one in either element 1, 2, or 3, defining the desired network output (no bruising, bruised at 60 cm and 100 cm). On the other hand, the bruise classification problem, which is a binary (two-class) problem distinguishing between bruised and unbruised samples, is accompanied by a (1 × 2) target matrix where each column indicates a category with a one in either element 1 or 2. The ANN pattern recognition algorithm divides the data randomly into training (70%), testing (15%) and validation (15%) sets during model development.

The effect of the structure of the artificial neural network (number of hidden neurons and random division of sample into training, testing and validation sets) on the performance of the classification was evaluated using the test set model performance provided by the confusion matrices. Confusion matrix is a very popular measure used while solving classification problems and it is used in this paper to report the classification performances. For the bruise severity classification which has three classes, the confusion matrix is a 3 x 3 and the bruise classification, which is binary, has a 2 x 2 confusion matrix.

5.3.2.1. Classification performance for SWIR camera

The ANN model accurately discriminated between bruised fruit from unbruised ones (Table 5.1). The confusion matrix showing the performance of the model in classifying bruised and unbruised pomegranate fruit is shown in Figure 5.3a for severity SI and Figure 5.4a for severity SII for the SWIR camera. For the first severity stage SI (60 cm drop height), the model showed an average recognition accuracy of bruised samples and unbruised samples to be 76.7% and 90% respectively. The last column of the matrix indicates the ratio of the number of correctly classified samples to the number of all the total samples classified (Figure 5.3a). In the first column, for a total of 30 bruised samples, 23 were correctly classified as bruised while 7 were misclassified as unbruised. In the second column, out of the 30 unbruised samples, 27 were correctly recognized as unbruised while only 3 samples were misclassified. This yielded an overall classification accuracy of 83.3% and a classification error of 16.7%. Similar accuracy was obtained by [95]. The authors investigated bruises on apple using HSI. The classification model was trained using Adaboost algorithm coupled with Savitzky–Golay and MSC preprocessing, model yielded an accuracy of 98.61%. The performance of the second severity group is presented (Figure 5.4a). The classification accuracy for this severity level (SII) improved as compared to the severity level I (SI). The average recognition accuracy improved from 83.3% (Figure 5.3a) to 93.3% (Figure 5.4a). The same accuracy was maintained for the unbruised samples, but a higher accuracy was obtained as 29 of the samples bruised under 100 cm drop height were rightly classified. For the third category, SIII, comprising of samples bruised at 60 cm height (30) and those bruised at 100 cm height (30) from both SI and SII respectively were combined, model showed an average classification accuracy of 80% (Figure 5.5a). model performance showed high false positive and true negative of 8 out of 30 samples for 60 cm drop bruised samples and 4 out of 30 samples for 100 cm drop bruised samples. This shows model accurately classified SII (86.7%) data as compared to SI data (73.3%).

5.3.2.2. Classification performance for VNIR camera

The results for the model recognition accuracy are listed in Table 5.2. Different model accuracy for all three cases study is shown (Figure 5.3b, Figure 5.4b and 5.5b). As can be seen from the results, for bruise severity category one (SI), the VNIR model slightly outperformed the SWIR model, achieving an accuracy of 83.3% and 96.7% for bruised and unbruised samples (Figure 5.3b). The confusion matrix shows that for 30 samples bruised from a drop height of 60 cm, 25 were rightly recognized while 5 were wrongly classified. The second column indicates that only 1 of the 30 unbruised samples was wrongly classified. This resulted in an average classification of 90% and class error of 10%.

For the case of severity category two (SII), the model showed similar performance to the SWIR, achieving an equal average accuracy of 93.3%. Unlike the SWIR, the model misclassified 3 samples of 100cm dropped bruise samples out a total of 30 samples and correctly classified 27, achieving a 90% accuracy and class error of 10% (Figure 5.4b). The study on kiwifruit when applying VNIR-HSI system for bruise detection resulted similar low classification error of 14.5% [107]. For the VNIR camera, it can be observed that the unbruised samples were always better recognized compared to the bruised data, irrespective of the bruise severity.

Similar trend was observed in several studies on bruising and detection of other defects on pome fruits [99][369]. The result indicate that model was able to achieved higher accuracies as the severity heightened, this was contrary to findings by [103]. The authors reported lower identification accuracy for severely bruised samples. Both cameras performed equally as they both obtained an average accuracy of 93.3%. The confusion matrix for model performance for a combined data is presented in (Figure 5.5). model showed higher recognition accuracy for SII samples (93.3%) as compared to SI (90%). The VNIR data set performed slightly better than the SWIR when both bruised samples were grouped together. The average classification accuracy for the VNIR was 91.7% while that of the SWIR was 80%. The result indicates that the model was able to recognize the different bruise severity when they are modelled against each other. Some of the reasons for model misclassification might be as a result of light scattering effect during image data acquisition[103]. The shiny nature of pomegranate fruit could have an impact of how light penetrates the fruit during imaging.

For the third category, SIII, comprising of samples bruised at 60cm height (30) and those bruised at 100cm height (30) using the VNIR camera (Figure 5.5b). The model showed 90% accuracy in classifying samples bruised at 60cm drop height and 93.3% classification for samples bruised from a 100cm drop height. The overall accuracy of this discrimination between the two-bruise severity was 91.7%. This means the model could identify bruised samples from unbruised samples as well as detect the different bruise severities when grouped together.

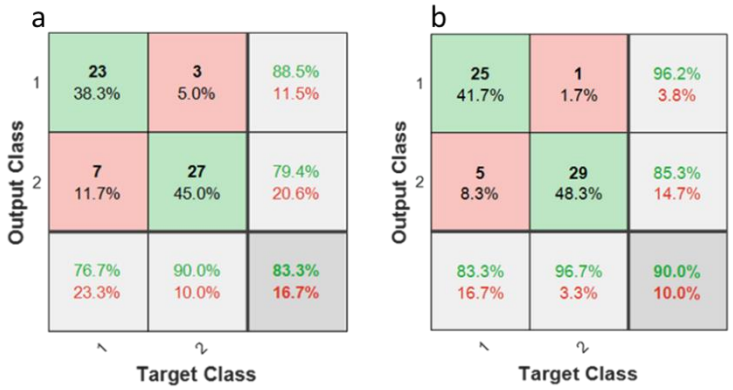

Figure 5.3. The confusion matrix of the classification performance of the first severity SI case study, where samples bruised from a 60 cm drop height (1) and unbruised sample (2) for SWIR (a), and VNIR (b)

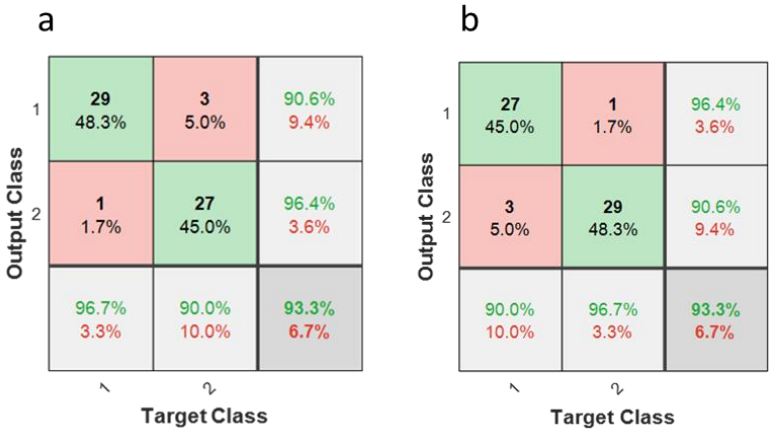

Figure 5.4. The confusion matrix of the classification performance of the second severity SII case study, where samples bruised from a 100 cm drop height (1) and unbruised sample (2) for SWIR (a), and VNIR (b)

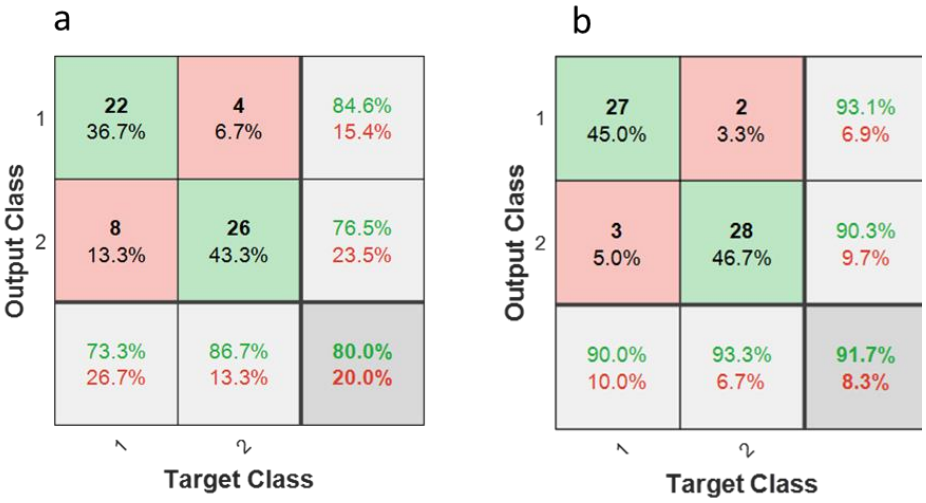

Figure 5.5. The confusion matrix of the classification performance of the third category (SIII) case study, where samples bruised from a 60cm drop height (1) and 100cm drop height sample (2) for SWIR (a), and VNIR (b)

5.3.3. Classification model development for combined data for bruise detection

Table 6.2 gives the combined classification performance of the ANN model for bruise detection of pomegranate fruit. Figure 5.4 illustrates the confusion matrix of the classification based on the ANN model. The columns of the matrix refer to the true categories, and the rows refer to the classifier outputs. For instance, for the SWIR (Figure 5.6a), of the 30 sample fruits in the first block (60 cm drop), 25 were correctly classified as “60 cm drop” 2 were classified as “100 cm drop” and 1 was classified as “No drop”. Of the 30 “100 cm drop”, 4 were wrongly classified as “60 cm drop,” 25 were correctly classified, and 1 was wrongly classified as “No drop.” Of the 30 “No drop”, all the 30 were correctly classified. The bottom row and the extreme-right column of the confusion matrix summarizes the performance of the classification model. Accordingly, the overall accuracy of the ANN model in classifying the SWIR data was 88.9% (classification error of 11.1%) and for the VNIR data the classification accuracy was 74.4% (classification error of 25.6%) (Figure 5.6b). This result agrees with the study on blackspot by [370], where they concluded that SWIR achieved better results than VNIR data (98.56% against 95.46%). The results of sound samples classified as sound (true positives) (90% and 100%), were better than results for bruised samples classified as bruised (83.3%, 70%). This is the case for most reported study. [371], reported 93% for non-bruised apples correctly classified and 86% accuracy for bruised samples.

Applying Adaboost algorithm for visual detection of bruises in apple, Zhang and Li [95] observed out of the 54 samples of intact apples, 52 was correctly classified and only 2 was wrongly classified yielding an accuracy of 96.3%, while for the bruised samples, 87.04% was achieved.

For jujube bruise detection, Zeng et al. [194] achieved almost 100% accuracy for healthy sample detection, in the NIR region, the authors attributed the lower accuracy for bruised samples to (browning coloration) of the bruised jujube samples which is similar to the healthy ones and made classification difficult.

Classification accuracies can also be impacted by the state of the sample, at the time of image acquisition. [372], compared static and online application of multispectral data. The authors found classification accuracies to be higher for the static data (91.5%) as compared to the online (samples in motion on a translation stage) (87.3%).

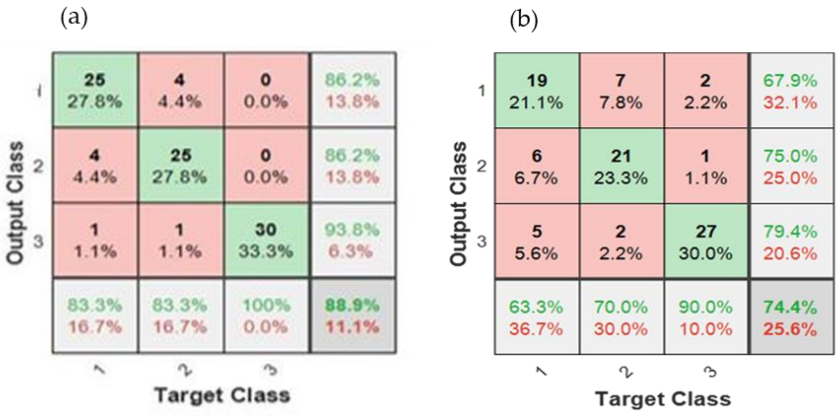

Figure 5.6. Summary of confusion matrices obtained for the combined ANN model for both SWIR and VNIR input data (a) SWIR classification performance (b) VNIR classification performance.

Table 5.1. Summary of results for the different bruise severity of pomegranate fruit.

Type	Spectra range	Test set			
		Sample number	Correct class	Incorrect Class	Accuracy (%)
Sound (Unbruised)	SWIR	30	27	3	90
	VNIR	30	29	1	96.7
Bruised at 60cm	SWIR	30	23	7	76.7
	VNIR	30	25	5	83.3
Bruised at 100cm	SWIR	30	29	1	96.7
	VNIR	30	27	3	90
Combined 60cm and 100cm	SWIR	30	22	8	73.3
	VNIR	30	27	3	90

Table 5.2. Combined performance of the classification model for bruise severity detection on pomegranate fruit.

Drop distance (cm)	Combined test set result for ANN model classification			
	Wavelength	Sample number	Accuracy (%)	Class error (%)
SI	SWIR	30	83.3	16.7
	VNIR	30	90	10
SII	SWIR	30	93.3	6.7
	VNIR	30	93.3	6.7
SI and SII	SWIR	30	80	20
	VNIR	30	91.7	8.3

5.4. Conclusions

This study investigates the detection and classification of bruises on pomegranate fruit surface using hyperspectral imaging system. The use of VNIR and SWIR cameras were explored. The result of the classification accuracy metric indicated that both cameras were able to accurately recognize bruised and unbruised pomegranate fruit samples. Both SWIR and VNIR data yielded highly accurate classification results ranging from 80% - 96.7%. The overall average classification accuracy achieved was 93.3% for model to distinguish fruits dropped at 100cm and 90% for fruit dropped at 60 cm height for the VNIR camera. Model performance was slightly lowered when both severity cases were combined, and model was able to accomplish a recognition accuracy of 80% and 91.7% for both SWIR and VNIR camera respectively. The model accuracy increases with the increase in bruise severity (93.3%). This study laid a foundation for further development of an in-line inspection system using hyperspectral imaging technique for bruise detection on pomegranate fruits.

While gathering satisfactory datasets is very important, HS imaging tasks are still costly and time-consuming. Usually, HS image data sets are not enough for training artificial neural networks for classification model development. Using the raw HS image, as is, can easily create a high dimensional data that can significantly cause overfitting. To augment this bottleneck, this paper implemented data dimensionality reduction by selecting out informative bands and disregarding the redundant ones. The study developed a more compact classification model by the data dimensionality reduction method.

CHAPTER 6

Non-destructive assay of internal quality of pomegranate fruit by Vis-NIR hyperspectral imaging

Abstract

The demand for high-quality pomegranate fruit is increasing globally, as the fruit has several health benefits. Alternative ways to assess fruit quality attributes that are fast, accurate and non-destructive are being implemented to meet strict quality control for safety and consumers' satisfaction. This paper evaluated the potential and feasibility of hyperspectral imaging technique for measuring quality attributes of pomegranate fruit. Hyperspectral image scanning was done by using visible and near infrared (Vis-NIR) (400 to 1000 nm) camera. After scanning, samples were crushed to extract the juice and total soluble solids (TSS), titratable acidity (TA), pH and color components (L*, a*, b*) were measured using conventional techniques. The possibility was investigated to determine whether key fruit attributes, namely, total soluble solids (TSS); titratable acidity (TA), TSS/TA could be determined on intact pomegranate fruit using hyperspectral imaging technique with artificial neural network prediction model. The study implemented effective band method to reduce the data dimensionality and data augmentation technique to increase the training data set. A two-layer feed-forward network with sigmoid hidden neurons and linear output neurons was used to fit the reflectance values at the effective wavelength to quality attributes (TSS:TA ratio and TA). Three different network training algorithms: Levenberg-Marquardt backpropagation (LMBA) algorithm (LMBA), Bayesian regularization algorithms (BRA) and Scaled conjugate gradient algorithm (SCGA) were compared. The optimum model achieved a prediction correlation coefficient (R^2) and root mean square error of prediction (RMSEP) for TA of 0.852 and 0.024, respectively. TSS:TA ratio prediction has R^2 of 0.861 and MSE of 0.665. These results have established that hyperspectral imaging technique combined with artificial neural network regression algorithm provide very useful approach that allows rapid screening of pomegranate maturity quality parameters.

6.1. Introduction

Pomegranate (*Punica granatum L.)*, an ancient deciduous fruit of Middle Eastern origin is an emerging crop in South Africa [1, 169]. Pomegranate is gaining global acceptance as consumers are utilizing the fruit both as fresh and in processed form such as juice and jams [246, 264, 373]. In the past several decades, the demand for pomegranate fruit has been increasing due to its nutritional and health benefits [2, 3, 264]. This global awareness has resulted in considerable increase in commercial farming of pomegranate fruit [5, 374]. Fruit inspection and sorting is the core towards achieving pack of uniform produce as regards to quality specifications, size, colour, etc. [6]. Therefore, together with the recent attention for food quality and safety, technologies for estimating the quality of fresh pomegranate fruit are being sought [7, 44].

At present, pomegranate fruit is sorted manually or automatically based on its physical appearance. However, it is the aril part that is edible and determines the eating satisfaction. In addition, since pomegranate is a non-climacteric fruit, it is essential to harvest it at optimum ripening stage (assessed by juice TSS, TA and TSS:TA ratio) to retain good quality in the postharvest [375]. Currently, many objective criteria for judging maturity of pomegranate have been used, for example, firmness, total soluble solids, pH, titratable acidity, and others [2, 376]. However, standard methods for these quality measurements are mostly destructive, slow, and prone to operational error as it involves human visual inspection.

Some of the existing standard destructive methods used for quality control include high performance liquid chromatography (HPLC), gas chromatography–mass spectrometry (GC-MS), spectrometric, colorimetric and microbiological methods [12, 377, 378]. The agribusiness industry is now shifting attention towards objective, fast, real-time and non-chemical detection technology, for quality assessment [15, 19, 57, 142]. Recently, non-destructive techniques like multispectral and hyperspectral imaging techniques are being utilized to assess the different quality concerns of pomegranate fruit [11, 290, 297, 379]. Many excellent reviews have been written in the last five years on the most frequently used non-destructive quality assessment techniques [19, 57, 142].

Hyperspectral imaging has emerged as a powerful non-destructive inspection tool in the agricultural, biosecurity diagnostic and food quality monitoring and control domain recently [48, 380]. This technique is based on a two-dimensional (2-D) spatial matrix of vectors, each of which represents a spectrum ranging from VIS to NIR to form a three-dimensional (3-D) image dataset, known as hypercube [380]. This technology integrates spectroscopy and

imaging to acquire both spectral and spatial information simultaneously. This combined features makes it a powerful tool for fruit\food quality assessment and defect detection, maturity indexing and physicochemical attributes in horticultural products [9, 13, 14].

Hyperspectral images with their spatial and spectral dimensions are usually large sets of information. To this end, data storage and analysis capabilities are frequent limitations of using hyperspectral data. Hence, image data size and dimensionality reduction process are very important in preparing HS images for model development. By implementing dimensionality reduction, redundant information can be eliminated. This process considerably simplifies the subsequent processes of classification model development. PLS, PCA and ANN methods frequently used to perform dimensionality reduction [170, 381]. In this context, several dimensionality reduction methods have been proposed [382, 383]. Li et al. [14] applied PCA based dimensionality reduction technique for bruise detection on oranges. The authors selected most discriminant wavelengths in the range 400–1,000 nm and achieved better detection accuracy at six wavelengths (630, 691, 769, 786, 810 and 875 nm). Similarly, Wang et al. [232] applied the same technique for sour skin damage detection on onions.

Artificial neural network (ANN) has gained wide acceptance as a machine learning tool for its predictive and classification ability [25, 50]. ANN is a type of supervised learning network, built from the principle of the human neuron system [357]. This algorithm is a computational based technique, usually when fed an input data, it tries to simulates the human intuition in making decisions and drawing conclusions, input data can be complex, noisy, irrelevant, and partial [25, 357]. One key highlight of the ANN is its adaptability in learning, yields good generalization and is very noise tolerance [50]. It has been utilized for several in diagnostic application for fruit quality [25, 144, 357], and provides more robust algorithms and higher accuracy than unsupervised methods [50].

Number of samples for training is crucial for artificial neural network-based classification problems [235]. Insufficient training samples have been a significant bottleneck for supervised HSI classification. This problem considerably hinders the practical application of HS image-based systems. Using insufficient training sets can significantly cause overfitting [235], while collecting sufficient HS image datasets remains costly and time-consuming [236]. Wambugu et al. [234] summarized and discussed several training sample generation methods including data augmentation: transformation-based (translation, flipping, rotation), mixture-based, or the addition of noise and synthetic data generation (synthesizer network using generative adversarial networks (GANs)). Augmentation implements realistic

transformation to increase the diversity of the training set. Zhang et al. [237] implemented additional images generation technique by image rotation, image gamma correction, scale transformation and noise injection in fruit category identification problem. HS image data augmentation technique is usually applied in classification problems than fruit internal quality prediction models.

Specifically for pomegranate fruit, Khodabakhshian et al. [18] develop a prototype multispectral imaging system for online quality assessment. The authors developed prediction models based on the four effective wavelengths (700, 800, 900, and 1000 nm). Multiple linear regression (MLR) was applied, and the model yielded good prediction accuracy for TSS (R^2 = 0.97, RMSEP=0.22), TA (R^2=0.92, RMSEP=0.26) and pH (R^2=0.94, RMSEP=0.038). In a similar study to estimate maturity of pomegranate fruit, Munera et al. [212] combined spectral and color data obtained from pomegranate fruit cv. 'Mollar de Elche' and developed prediction models for physicochemical properties such as total soluble solids, titratable acidity, maturity index, BrimA, internal colour, total phenolic compounds content and antioxidant activity. However, model performance for these parameters showed poor results with R^2p ranging between 0.45 – 0.85 for intact fruit using spectral data as input data. The authors demonstrated that hyperspectral imaging has better and greater potential to monitor some physicochemical properties and maturity of the intact fruit compared to color image data. Both studies highlighted the potential of HSI to non-destructively predict fruit maturity attributes.

In this study, the capability and potentiality of HS imaging technique coupled with artificial neural network model to quantify TSS/TA and TA non-destructively on intact pomegranate fruit is explored. Key fruit attributes, namely, total soluble solids (TSS); titratable acidity (TA), TSS/TA were determined on intact pomegranate fruit using hyperspectral imaging technique with artificial neural network prediction model. The study aimed to implement effective band selection method to reduce the data dimensionality and data augmentation technique to increase the training data set. A two-layer feed-forward network with sigmoid hidden neurons and linear output neurons will be explored to fit the reflectance values at the effective wavelength to quality attributes (TSS:TA ratio and TA).

6.2. Materials and methods

6.2.1. Fruit procurement and sample preparation

This research was performed during the 2021 season with commercially mature pomegranate fruit (cv. Wonderful). Fruit maturity and storage condition is as already indicated in the previous chapter. A total of 100 fruit were procured from Sonlia pack-house (33°34′851″S,

19°00′360″E) and transported to Postharvest Technology and Research Laboratory, Stellenbosch University. Upon arrival, fruit without any physical defect and with good appearance were sorted and placed under cold storage at 7 ºC before experiment was performed. Pomegranate fruit samples from three (3) maturity stages according to Mphahlele et al., [284], were selected for this study, and grouped into unripe (100 DAFB), mid-ripe (121 DAFB) and full-ripe stage (141 DAFB).

6.2.2. Hyperspectral image data acquisition

Hyperspectral images were acquired for 97 samples of pomegranate fruits using a prototype hyperspectral imaging system and performed at the Central Analytical Facility (CAF) Vibrational Spectroscopy Unit of Stellenbosch University. The Vis-NIR hyperspectral imaging cameras, HySpex VNIR-1800 was used to acquire hyperspectral image data of pomegranate fruit. In the VNIR camera, images are acquired at wavelengths ranging from 400 to 1000 nm with a waveband of 186 and spectral resolution of 3.26 nm. Figure 1 illustrates the hyperspectral image acquisition system and the formation of three-dimensional hyperspectral data (hypercube). The VNIR has spatial pixels (x) of 1800 which corresponds to the number of photodetectors along the spatial dimension of the detector array of the camera. The second spatial dimension (y) is the number of pixels in the scanning direction and is physically bounded by the size of the scene and the speed of the translation stage. A 30 cm focal length lens with field view of 9.733 cm were used. Reflectivity reference data were obtained for each fruit. Hence, each image was obtained as a three-dimensional image block (x, y, λ), including 1800 × y pixels on the space dimension (x, y), and 186 bands at 3.26-nm intervals within a range of 400 to 1000 nm on the spectral dimension (λ). The camera was mounted above a translation stage which has a speed regulation system (Figure 6.2).

6.2.3. Reference measurement

Destructive measurements: total soluble solids (TSS), titratable acidity (TA), pH and colour attributes (L*, a*, b*) ware taken for each pomegranate fruit. For individual fruit sample, rind colour components were measured using a calibrated colour Chroma Meter (CR-400 Minolta Corp, Osaka, Japan). Colour parameters which includes Chroma (C*) and Hue angle (h°) was derived from the colour components L*, a*and b* as described by Pathare et al. [32]. Individual fruit were manually peeled and the extracted arils were juiced using a Liquafresh juice extractor. The juice was filtered through a 1 mm sieve and immediately used to measure the TSS, pH and TA. Total soluble solids (TSS) content was measured using digital hand-held refractometer (Palette, PR-32α, Atago, Tokyo, Japan) and results were expressed in percentage. The pH values were determined at room temperature using a calibrated pH meter (Crison, Model 00924, Barcelona, Spain). Titratable acidity (TA) was measured by diluting 2 mL of supernatant in 70 mL of distilled water and titrating with 0.1M NaOH using a Metrohm 862 compact titrosampler (Herisua, Switzerland) results were expressed in percentage of citric acid. TSS/TA was also calculated [11]. These measurements were performed in three repetition per individual fruit and average was calculated expressed as mean ± SD.

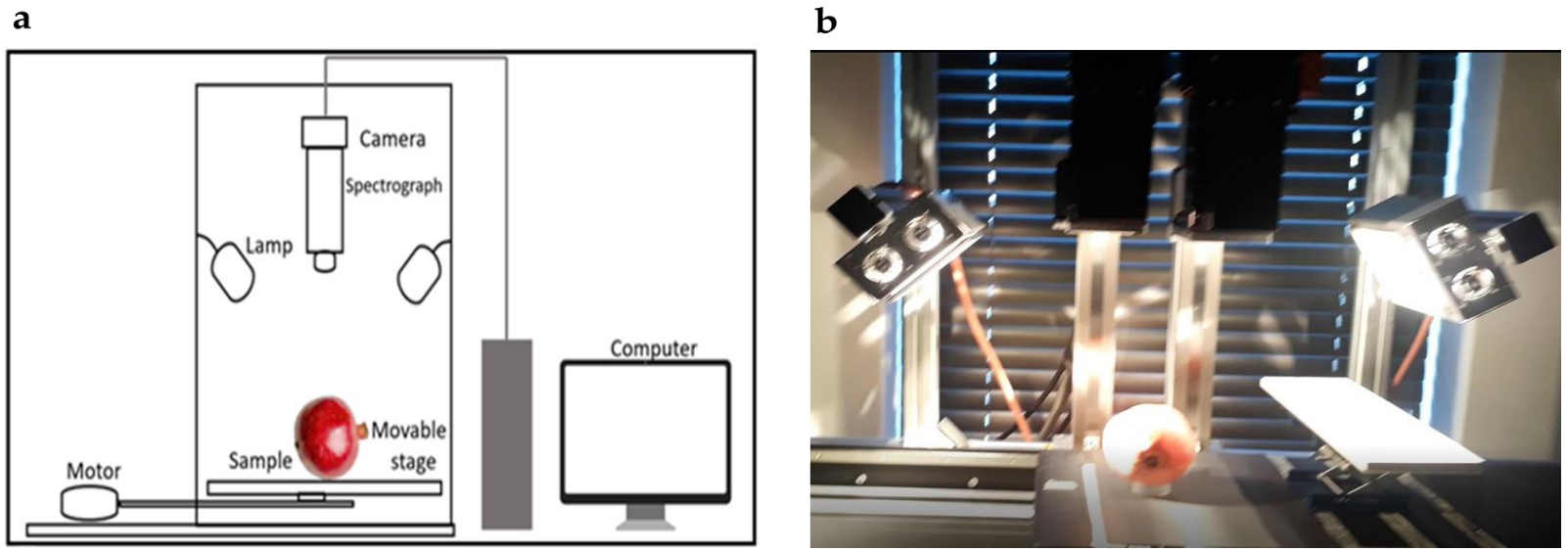

Figure 6.1: Schematic of the hyperspectral imaging system (a) and its picture (b). Hyperspectral image data acquisition was obtained at the CAF Centre, Department of Food Science building, Stellenbosch University. A line scanning hyperspectral camera is placed above a moving translation stage, and lighting is being provided by two dimmable halogen lamps.

6.2.4. Hyperspectral image calibration

To minimize the impact of the uneven intensity distribution of the light source and dark current in the charge coupled device (CCD) detector on the hyperspectral images, image correction was performed using known true spectral information. Eqn. (4.1) provides the formula for the image correction.

6.2.5. Spectral profile extraction

The original hyperspectral images (hypercubes) (Figure 6.2(a)) were imported into Evince software (version 2.7.10, Prediktera, Sweden). At this stage, a single hypercube is about 6GB in size. Spatial cropping of the HS image (Figure 6.2(b)) reduced the data size to 2 GB. Evince further used for PCA exploration of the HS image (Figure 6.2(c)) and PCA based segmentation of the fruit (Figure 6.2 (d)) and compile the file to transfer to MATLAB. At this stage the file size is considerably reduced (≈0.5GB) and fast and easy processing possible.

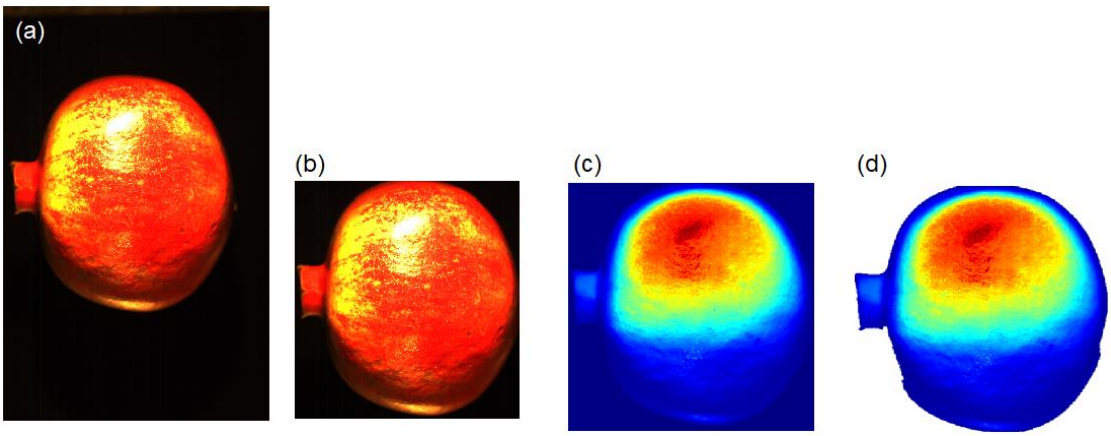

Figure 6.2: A typical explorative PCA analysis. Segmentation of the pomegranate fruit on the hyperspectral image.

6.2.6. Data analysis

Hyperspectral data processing was implemented using the hyperspectral imaging library in MATLAB® (The MathWorks, Inc., Natick, Massachusetts, United States). The HS image processing workflow is summarized in Figure 6.3.

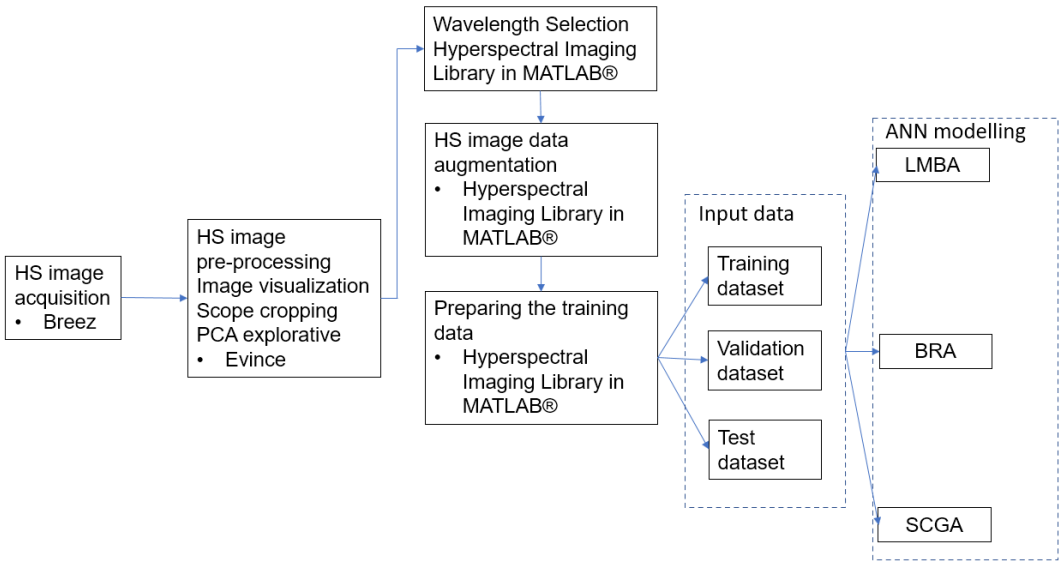

Figure 6.3: The overall workflow for developing HS imaging bases artificial neural network fruit quality predictor model.

6.2.6.1. Effective wavelength selection

Effective wavelength selection was carried out as discussed in chapter 4 and chapter 5.

6.2.6.2. Data augmentation

For data augmentation, a manual procedure was implemented to take segments form the HS images of each fruit with size about 50 × 50 pixels were excised (Figure 6.4) with the help of. The number of segmented hypercubes taken from each fruit original HS image was according to its TSS class as summarized in Table 6.1. This way each HS image provided additional augmented sample HS image for training. For each segment, average reflectance value corresponding to the selected most informative bands were computed and compiled as model inputs with the corresponding values of fruit quality as target output. After data augmentation, the number of samples within one TSS group is shown in Table 6.1.

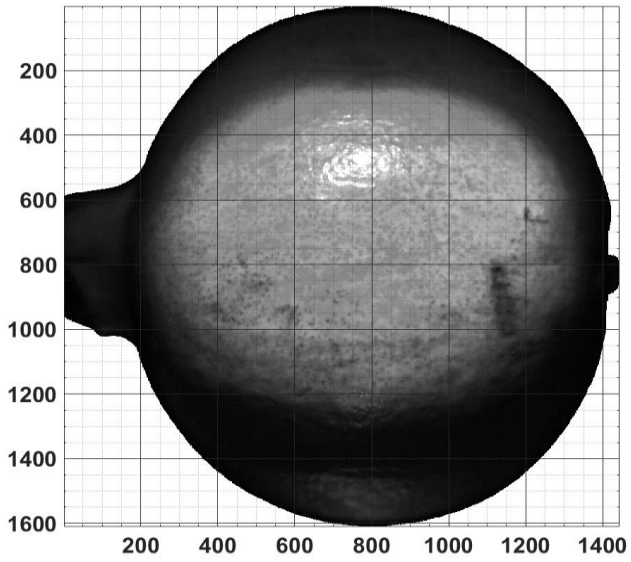

Figure 6.4: Data augmentation for generating additional hypercube for training. This augmentation procedure generated 12 hypercubes from a single HS image.

Table 6.*2* The mean °Brix, and STDV denotes the standard deviation of samples in each group

TSS	Mean	STDV
10.98 to 15.9	14.86	0.69
16.0 to 16.9	16.13	0.27
17.0 to 17.85	16.96	0.21

6.2.6.3. Predictive ANN model development

A two-layer feed-forward network with sigmoid hidden neurons and linear output neurons (Figure 6.5) was used to fit the reflectance values from the effective wavelength to fruit quality data (TSS:TA ratio and TA). This type of ANN is suited for multi-dimensional mapping problems given arbitrarily consistent data and enough neurons in its hidden layer [40]. Three different network training algorithms: Levenberg-Marquardt backpropagation (LMBA) algorithm (LMBA), Bayesian regularization algorithms (BRA) and Scaled conjugate gradient algorithm (SCGA) were compared. The fitting process train the neural network on the set of ROI averaged reflectance values to produce an associated set of target fruit quality indices. Once the neural network has fit the data, if forms a generalization of the input-output relationship and can be used to generate outputs for inputs it was not trained on. Hence, a trained and ready model takes reflectance values at the selected bands of a sample as input and predict its quality (total soluble solids (TSS:TA ratio) and titratable acidity (TA)).

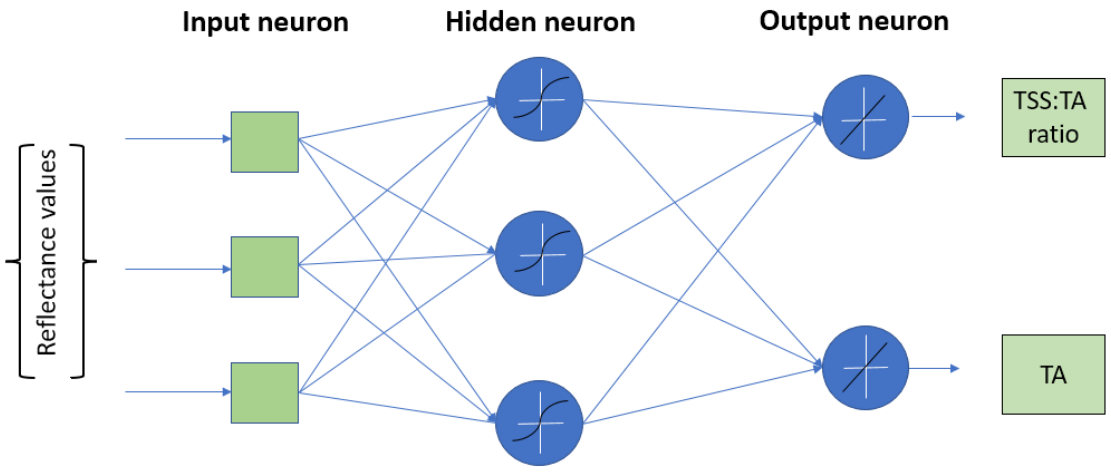

Figure 6.5: Data augmentation for generating additional hypercube for training. This augmentation procedure generated 12 hypercubes from a single HS image.

The input data (reflectance values at the three informative bands of 1430 samples) is randomly divided into 70% training, 15% validation and 15% testing. So, the 3-3-2 neural network topology was taken as the optimum topology. A topology with the smaller number of hidden neurons and with good performance is the one we are looking for. A model with too many neurons memorizes each exemplar pair (noise and all) rather than generalizing from the data in the same way as a polynomial of high degree memorizes each data points [384]. After training, the model validation is carried out and it is used to measure network generalization, it brings the training measure to a halt when generalization stops improving. The test performance does not impact on the training and thus provides an independent measure of network performance during and after training [385].

Prediction performance of the model is measured in correlation analysis between model predictions and target values (regression R^2) and using the mean squared error (MSE). A good model should have an R^2 value close to 1 to show a close relationship between outputs and target and lower MSE values. MSE should be close to zero which mean no error exit between outputs and targets and a small difference between the MSE for training and test result.

6.3. Results and discussion

6.3.1. Fruit quality

The statistical values (mean, standard deviation (SD) and range) for reference data for selected maturity parameters of intact pomegranate fruit are presented in Table 6.2. Results show that the reference measurement values were quite varied and covered a large range of the mean data. Studies categorise pomegranate fruit maturity under three groups, depending on days after

full bloom [284], typically, fruit harvested between 82 - 100 DAFB are grouped as unripe, then those between 110 - 140 DAFB are considered mid-ripe, while fruit harvested between 141-165 DAFB are said to be fully ripe [269, 284]. The TSS/TA ratio as well as BrimA index have been established as a reliable maturity index for pomegranate fruit [273, 289, 391, 392]. The TSS/TA ratio often defines the taste of pomegranate fruit during development [212]. Typical TSS/TA values of pomegranate "Wonderful" fruit for unripe maturity stage range between 7.8 ± 2.6 and 10.2± 2.2, and increase as the fruit moves to mid-ripe stage, this values range from 10.7 ± 2.7 to 16.8± 3.6, fully ripe maturity stages are reported to have TSS/TA vary from 12.2 ± 3.5 to (16.6 ± 2.8 depending on the growing location [284].

Table 6.2 shows the mean, standard deviation, minimum and maximum value of results obtained from the reference data for the different quality parameters of "Wonderful" pomegranate fruit samples selected for this study. It shows TSS/TA values to range between 4.792 to 15.67 for the different maturity stages, this results is similar to those reported by Mphahlele et al., [284]. The fruit maturity was estimated using similar range of data.

6.3.2. Spectral characteristics

The full and averaged reflectance spectral profile for intact pomegranate fruit (cv. Wonderful) are presented in Figure 6.6. The spectral signature follows similar trends for all the fruit (Figure 6a), the average spectral (Figure 6b) shows a high reflectance within the wavelength of 400 – 600 nm, and then lowers. The PCA loading for effective wavelength selection is shown in Figure 6.7. For PCA analysis, loading shows only 4 PC were selected and utilized for further analysis. The reason for PCA analysis was to reduce the dimensionality of the dataset, while retaining most of the variability.

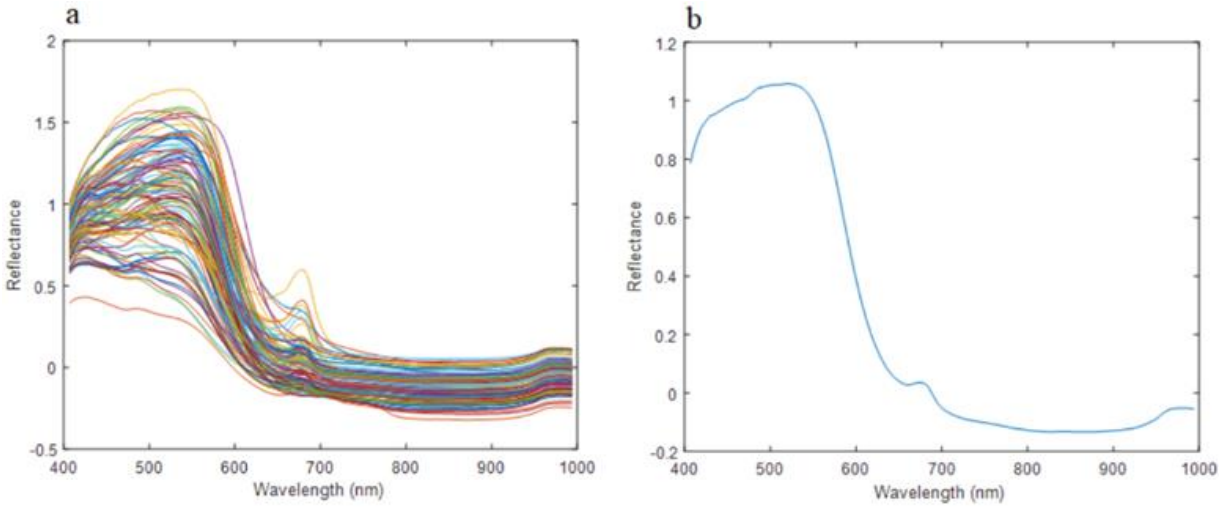

Figure 6.6: Full and averaged reflectance spectral profile for intact pomegranate fruit (cv. Wonderful) for the Vis-NIR spectral range.

The principal component analysis conducted on the selected optimal wavelengths showed that the first four components explained 98.73% (PC1–86.06%, PC2 – 9.76%, PC3 – 2.23% and PC4–0.70%) (Figure 6.7).

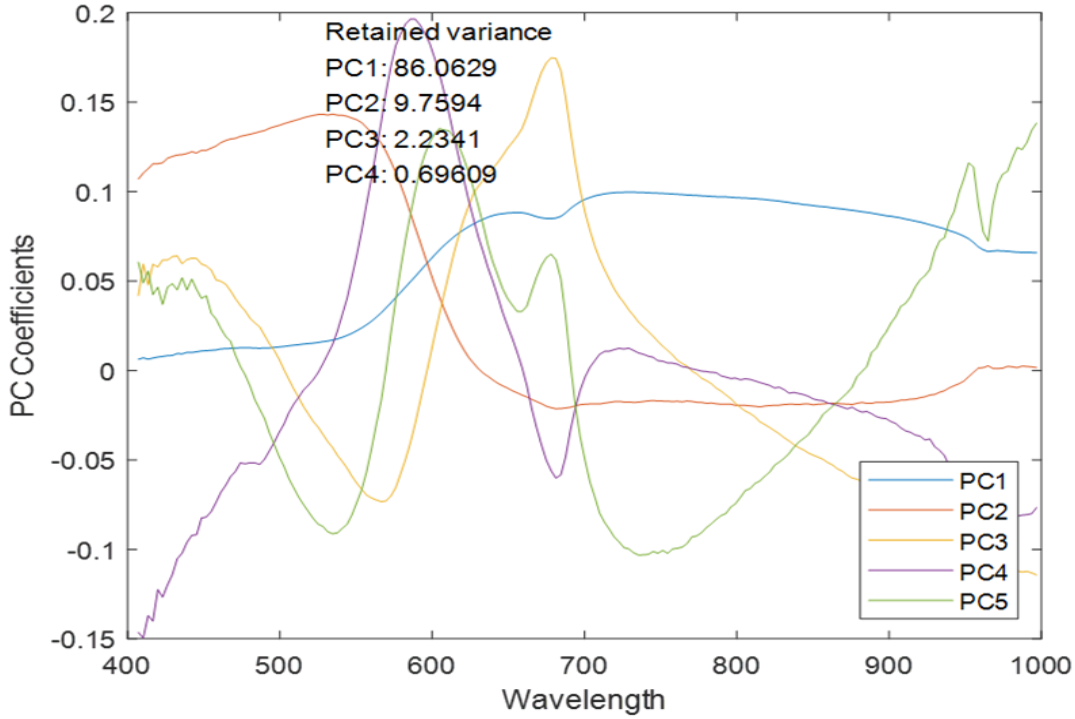

Figure 6.7: Loading score for PCA analysis for in the spectral range of 400 – 1000 nm.

The effective wavelength can be selected using the pixel purity index (PPI) method implemented on original hyperspectral data cube by using the noise-whitened Harsanyi–Farrand–Chang (NWHFC) method implemented in MATLAB. Figure 6.4 shows different phase of the spectral data analysis of the original RGB image data to the PCA data.

Figure 6.8 illustrates the selected most effective wavelength achieved using the pixel purity index (PPI) method. It shows the most effective or optimal wavelengths for predicting quality attributes of pomegranate fruits. This means the reflectance at 407, 639, and 917 nm contain the peak chemical information for regression model development.

Table 6.2. Mean, standard deviation (SD) and range of values for reference data for selected ripeness parameters of intact pomegranate fruit.

Parameters		Reference values		
	Mean	SD	Min	Max
C*	42.69	4.65	32	51.66
TA	1.67	0.33	1.08	2.57
TSS	16.36	1.05	10.95	17.85
TSS/TA	10.09	2.13	4.79	15.67
Hue	40.23	10.25	22.42	67.34
pH	2.99	0.13	2.68	3.355
a*	32.55	6.99	14.62	45.46
b*	26.52	4.79	13.61	36.74
L*	50.60	5.63	38.06	65.55

6.3.3. Model development using all three mapping algorithms

The development of models using LMBA, BRA and SCGBA algorithms was done for each quality parameter while evaluating different pre-processing methods; whereby, the latter were selected based on high R^2 values, and low MSE values. The best performing models for quality parameters are presented in Table 6.3.

6.3.3.1. Model performance for TA analysis

The total acidity of pomegranate fruit was adequately mapped with its spectral data, model statistics using achieved best performance using the BR algorithm (R^2 = 0.851, MSE = 0.428) for training and (R^2 = 0.700, MSE = 0.4283) for test model. Figure 6.8a shows the scatter plot for model performance of TA. The overall average R^2 of 0.696 was obtained.

Table 6.3. Summary of network training and test model performance for ripeness quality attributes of pomegranate fruit

Quality parameter	Algorithm	Training set		Test set	
		R^2	MSE	R^2	MSE
TSS	LMBA	0.421	0.428	0.422	0.398
TA	BRA	0.852	0.024	0.699	0.134
TSS/TA	SCGA	0.861	0.665	0.847	0.528
pH	LMBA	0.828	1.296	0.850	1.187
a*	LMBA	0.933	3.962	0.712	3.870
b*	BRA	0.950	3.926	0.885	3.870
C	LMBA	0.830	9.139	0.739	9.465
L*	LMBA	0.919	2.456	0.869	2.316
hue	SCGA	0.843	35.084	0.824	32.806

LMBA, Levenberg-Marquardt backpropagation algorithm; BRA, Bayesian regularization algorithms; SCG, Scaled conjugate gradient backpropagation algorithm; L*, lightness; a*, redness; C*, Chroma; h*, hue angle; TSS, total soluble solid; TA, titratable acidity; pH, Potential hydrogen, TSS/TA, total soluble solid/ total acid; R^2; Coefficient of determination; MSE, mean square error.

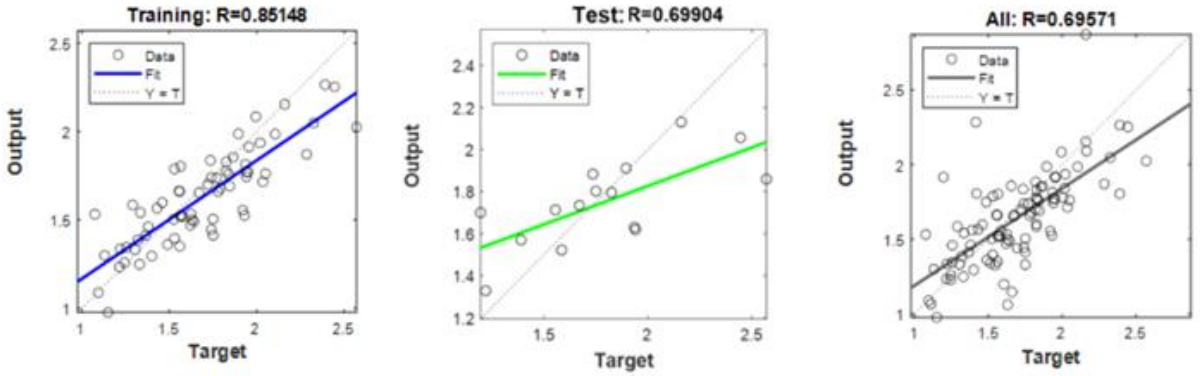

Figure 6.8: Measured (target) against predicted (output) for TA for training (a), test (b) and overall (c) sets using selected spectral data.

6.3.3.2. Model performance for TSS/TA analysis

The results show model obtaining for TSS/TA ratio a regression coefficient R^2 = 0.86, MSE= 0.428) for the training set and test model (R^2 = 0.847, MSE = 0.4283). Model achieved better results for TSS/TA compared to the model by Munera et al. [212]. The author reported

prediction R^2 of 0.78 and RMSE of 0.72. Figure 6.9 shows the scatter plot for the TSS/TA fitting model.

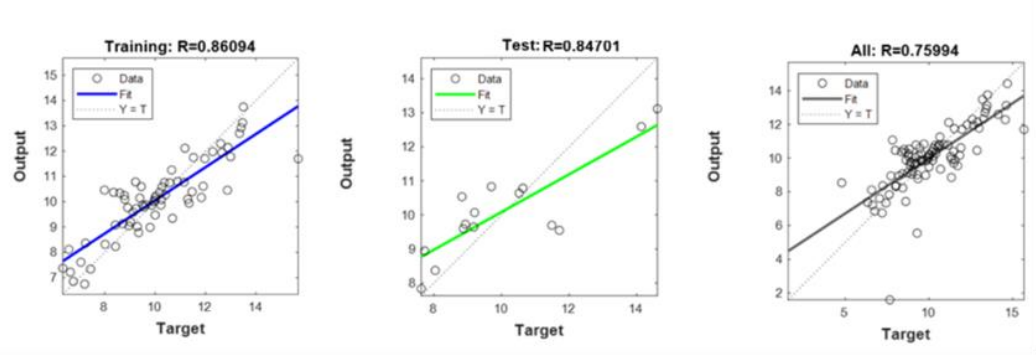

Figure 6.9. Measured (target) against predicted (output) for TSS/TA for training (a), test (b) and overall (c) sets using selected spectral data.

6.3.3.3. Model performance for pH analysis

The pH is another important index for quality and maturity estimation for pomegranate fruit, pH values often range between 2.8 – 3.4 depending on cultivar and maturity stage [269, 284]. It indicates the acidic/sour taste of the fruit, reference data shows pH to range between 2.68 – 3.355, across the three different maturity stages. The highest R^2 value and the lowest MSE for the prediction of pH was achieved to be 0.828 and 0.4283 respectively, this was obtained using the LMB algorithm. The R^2 for test set was 0.8495. Similar results was obtained for pH in a study pomegranate using PLS model [23], the author achieved R^2 values of 0.85 and RMSEP value of 0.064, respectively. The scatter plot for the output vs target is presented in Figure 6.10.

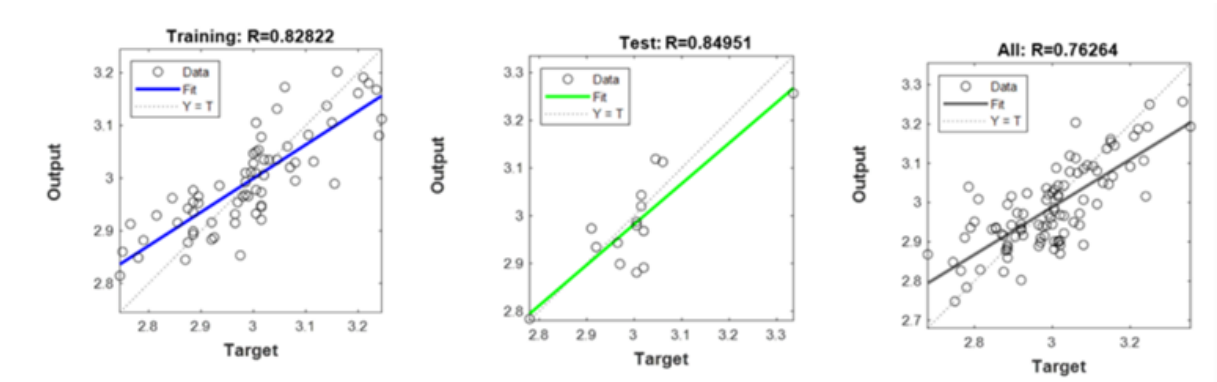

Figure 6.10. Measured (target) against predicted (output) for pH for training (a), test (b) and overall (c) sets using optimum wavelength selected spectral data.

6.3.3.4. Model performance for color analysis

For colour parameters, model development using the Levenberg-Marquardt backpropagation algorithm yielded good prediction models with R^2 = 0.9331 training set for redness (a*), 0.421,

hue showed R^2 = 0.843 for training and 0.824 for test model. Similar result was obtained for Lightness (L) and Chroma (C*) with R^2 for the training set 0.919 and 0.830 respectively.

The statistical data for model development showed that both LMB algorithm yielded reasonably accurate training and test models as compared to the other two algorithm. Of the 9 selected quality attributes assessed, 4 achieved better correlation coefficient with a* (redness) achieving the high R^2 value of 0.933. Similar results were achieved by Model for color performed better than those plum [89], the authors achieved for redness a* an R^2 value of 0.81 and for b* R^2= 0.86.

Summary of the measured (target) against predicted (output) sets for all color parameter is presented in Figure 6.11. The parameters are arranged in redness a* (6.1I), Chroma (6.11II), hue (6.11III), and Lightness L (6.11IV).

6.3.4 Classification according to maturity stage

Tables 6.4 shows the training, test and overall set results of the models to discriminate the maturity stage using spectral data of the intact pomegranate fruit. The overall result shows model to achieve an accuracy of 84.4% and class error of 15.6%. the highest accuracy was obtained for the ripe classification with a 96.7% accuracy. In the test set, both unripe and ripe fruit obtained 100% accuracy. This is similar to result obtained by Munera et al., [212], the authors achieved 100% for immature fruit, 95% for half ripe and 90% for ripe fruit. The confusion matrices of illustrating classification model performance for the different fruit maturity categories are presented on Figure 6.12.

Table 6.4. Summary of classification result for maturity stage discrimination using the spectral data of the intact pomegranate fruit

TSS/TA		Training set		Test set		Overall set	
Class	Range	Class error (%)	Accuracy (%)	Class error (%)	Accuracy (%)	Class error (%)	Accuracy (%)
Unripe	4.79 - 9.0	17.4	82.6	0	100	16.7	83.3
Semi-ripe	9.1 – 11.5	25	75	33.3	66.7	26.7	73.3
Ripe	11.6 – 15.67	16.1	83.9	0	100	3.3	96.7

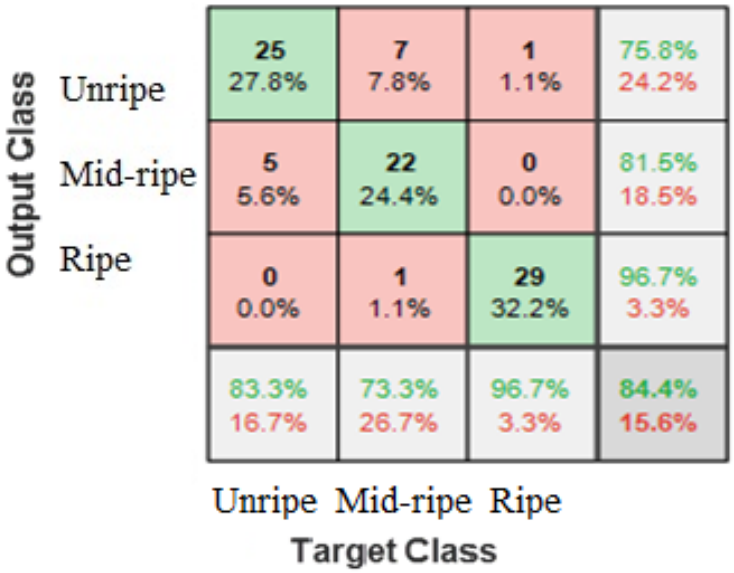

Figure 6.11. Confusion matric showing classification model performance for maturity discrimination of pomegranate fruit into different maturity stages using TSS/TA data.

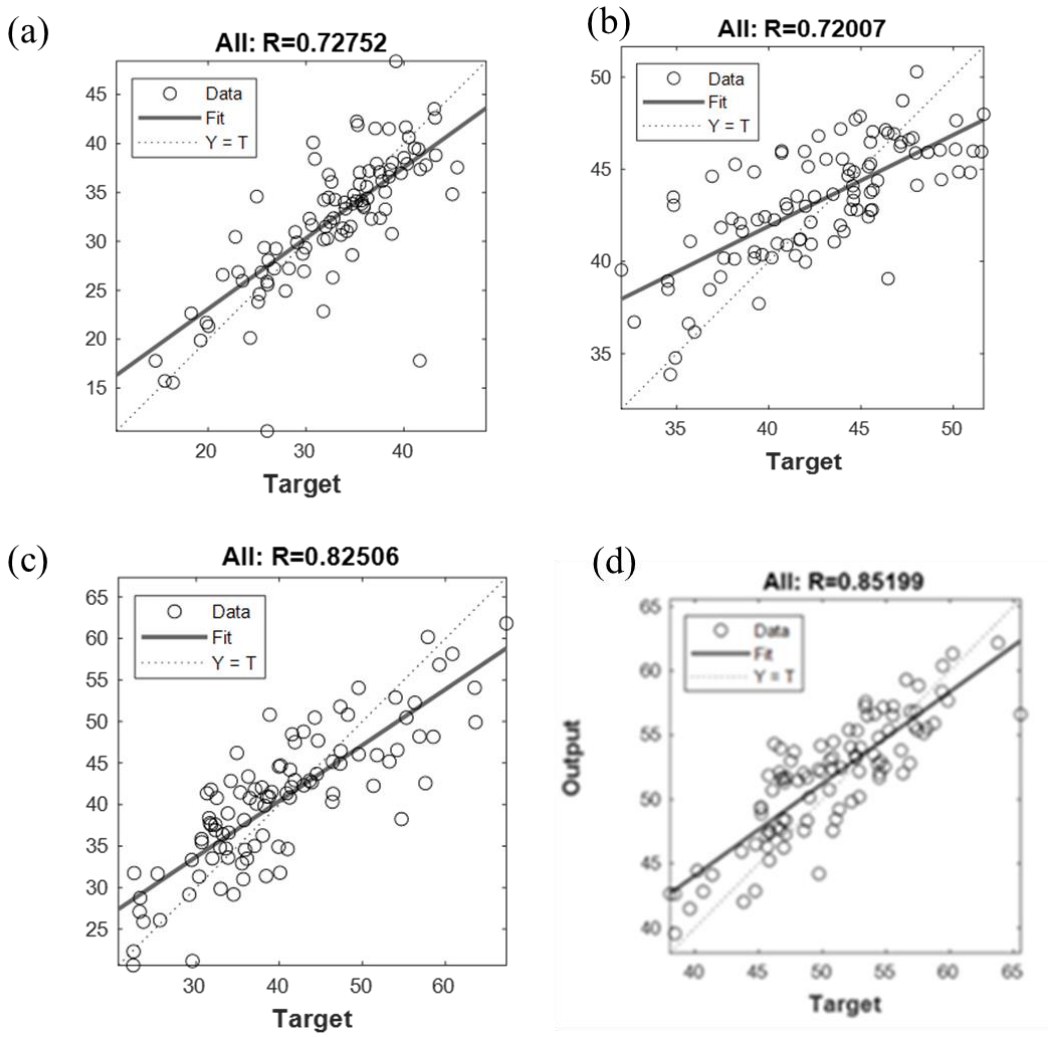

Figure 6.12. Measured (target) against predicted (output) for the combined training and test sets on optimum model performance of redness a* (6.12a), Chroma C* (6.12b), hue (6.12c), and lightness L (6.12d).

6.4. Conclusion

This study developed regression model based on Vis-NIR hyperspectral imaging data using neural fitting algorithms. Three different algorithms were utilized with all sowing varying degree of accuracy. All model showed good correlation between the VNIR spectral extracted from a 50x50 region of interest on the fruit surface and the quality attribute considered except for the TSS prediction. Neural network was effectively applied in optimally selecting three wavelengths (407, 639, and 917 nm), using pixel purity index (PPI) values of each variable (wavelength). Models developed using Vis-NIS spectral data presented good model accuracies, the R^2 values for colour attributes were very high ranging from 0.824 to 0.951. This research demonstrates the feasibility of hyperspectral reflectance imaging technique to predict maturity quality attributes of pomegranate fruit.

Future study in this area of research should expand more by including the prediction model to incorporate pomegranate fruit cultivars differences and other internal quality attributes such as total phenolics content, total anthocyanin content, vitamin C, etc. The HSI system can also potentially be further developed as a low-cost multi-spectral imaging system using the key wavelengths identified from the calibration models, this may lead to improved and better calibration models especially for TSS and other related attributes. These findings can be employed by the pomegranate processing industry to develop a grading/sorting system to rapidly evaluate several organoleptic and physicochemical attributes of pomegranate fruit.

SECTION III

Chapter 7: General discussion & conclusions

References, Appendices

CHAPTER 7

General discussion and conclusions

7.1. Introduction

Pomegranate (*Punica granatum L.*) fruit has seen tremendous growth in commercial exports within South Africa over the past decade. Over 1000 hectares have been commercially planted within South Africa reaching a total of over 8000 tons of exported pomegranate fruits. Considering that pomegranate cultivar Wonderful is the most widely grown and consumed cultivar on a global scale, it accounts for a total production of 56% of pomegranates grown within South Africa. One of the major challenges the pomegranate industry faces in its quest for waste reduction and higher economic returns is through efficient quality and freshness monitoring and analysis tool in the postharvest handling chain.

The rising global safety concerns for fruit and vegetables that meet the desire of local and international consumer has necessitated the advancement of research into non-invasive/non-destructive quality analysis, however, in the fruit and vegetable industries, quality inspections are mainly manual and mechanical, laborious, time-consuming, costly, and subjective.

Hyperspectral imaging (HSI) has emerged as a powerful non-destructive inspection technique in the agricultural, biosecurity diagnostic and food domain recently. HSI is a non-invasive/ non-destructive technique that integrates spectroscopy as well imaging to form one system [343]. It is developed by creating images from more than one spectral component of the electromagnetic wavelength from the same region of an object and at the same scale [253]. The data extracted (hypercubes) from HSI systems are 3-dimensional (3D) structures that consist of two spatial and one spectral dimension [48, 328]. This combined feature makes it a powerful tool for fruit\food quality assessment and defect detection, maturity indexing and physicochemical attributes in horticultural products.

Hyperspectral technique is however limited by several factors, which includes the speed of image acquisition and image data processing. To overcome this problem, studies in recent years have been focused on determining a few most effective wavebands by using hyperspectral imaging, then implementing it in a multispectral imaging configuration (MSI). Different

machine learning algorithms have been developed to also improve on the analysis of hyperspectral imaging data and model performance in recent times [16].

Therefore, the main objective of this study was to assess the application of hyperspectral/multispectral imaging for predicting the major quality attributes in fresh pomegranate fruit as well detect the presence of bruise or internal defect using artificial neural networks (ANNs).

Section I: Review of literature which includes a summary of hyperspectral imaging technique application for diagnostic fruit disease and defects detection as well review non-destructive efforts towards application for pomegranate fruit evaluation.

Section II: Application of hyperspectral imaging technique to monitor early bruise detection and development and bruise severity on pomegranate fruit as well the assay of internal quality of intact pomegranate fruit.

7.2. General discussion

7.2.1. Application of hyperspectral imaging technique for early bruises detection on pomegranate (*Punica granatum L.*), coupled with artificial neural network algorithm

Pomegranate fruit possess very hard and thick rind/peel, different from other fruit with soft tissues and surface like apple, pear, etc. [21]. Making the possibility of visible early indication on the fruit surface very difficult [339]. Manually picking up suspected bruised fruit is laborious, time consuming and very subjective and no longer sustainable. Therefore, prompting researchers into looking at alternative techniques for bruise detection.

Studies have shown that hyperspectral imaging (HSI) is a dynamic technology that is now being used for non-destructive inspection in the agricultural, biosecurity and food domain. HSI is a non-invasive/ non-destructive technique that merges spectroscopy and imaging into one system, such combination of spectral and spatial data can be harnessed to extract deeper information on the fruit [388]. Its feasibility have been explored for several studies and all yielding accurate results [101, 185]. No study has yet been conducted testing its potential on pomegranate fruit, hence this study has investigated the potential of a hyperspectral imaging system to be employed for early detection of bruise damage on pomegranate fruit. The results confirm hyperspectral imaging technique combined with machine learning methods (ANN) to be an effective technique for early bruise detection. Both image surfaces considered showed bruise can be detected in early stage of bruising with an accuracy of 88.3%. The overall highest classification accuracy achieved was 100% during the 7th and 14th day after bruising.

Although this paper focused on pomegranate bruise development inspection, the techniques employed for data extraction and manipulation presented in this study are easily adaptable and can be suitable to other food applications.

7.2.2. Application of hyperspectral imaging technique for pomegranate bruise severity detection using Vis-NIR and SWIR hyperspectral imaging data

This study has demonstrated the potential of hyperspectral imaging integrated with artificial neural network in distinguishing different bruising degrees on pomegranate fruit. Effective wavelength selection for optimum model performance by selecting the number of spectrally distinct features were estimated using the noise-whitened Harsanyi–Farrand–Chang (NWHFC) method implemented in MATLAB, and the corresponding bands were identified using PCA method. The results have shown that both spectral ranges of the two different cameras explored were efficient in classifying the bruise and to their different severity with accuracy of detection ranging from 80% - 96.7%. The overall average classification accuracy achieved was 93.3% for model to distinguish fruits dropped at 100cm and 90% for fruit dropped at 60cm height for the VNIR camera. Model performance was slightly lowered when both severity cases were combined, and model was able to accomplish a recognition accuracy of 80% and 91.7% for both SWIR and VNIR camera respectively. The model accuracy increases with the increase in bruise severity (93.3%). This study laid a foundation for further development of an in-line inspection system using hyperspectral imaging technique for bruise detection on pomegranate fruits.

7.2.3. Application of hyperspectral imaging technique for non-destructive assay of internal quality of pomegranate fruit and maturity classification

Consumers preference for fresh horticultural products is often biased towards the external aspects of the quality as related to size, appearance and colour characteristics [32]. Repeated consumption of the said fresh produce is most determined by consumer satisfaction based on sensory characteristics such as soluble solids content (SSC), titratable acidity (TA), soluble solids to acid (SSC/TA) ratio [389, 390]. The study conducted in chapter 6 evaluated the maturity quality attributes of intact pomegranate fruit. All model using the VNIR data showed good correlation between the VNIR spectral extracted from a 50x50 region of interest on the fruit surface and the quality attribute considered. Less model accuracy was observed for the TSS prediction with both hyperspectral imaging system. The NWHFC method was applied in

optimally selecting three wavelengths (407, 639, and 917 nm), in the VNIR spectral range. Models developed using the SWIR spectral data showed very poor regression model, while those developed using the Vis-NIS spectral data presented good model accuracies, the R^2 values for colour attributes were very high ranging from 0.824 to 0.951. Spectral data was qualitatively analysed to discriminate different fruit maturity, model obtained the highest accuracy for ripe with a classification accuracy of 96.7%, while unripe fruit was classified correctly 83.3% accuracy and mid-ripe 73.3%. This research demonstrates the feasibility of hyperspectral reflectance imaging technique to predict selected maturity attributes of pomegranate fruit.

7.3. General conclusion and recommendations

In conclusion, this thesis made a significant contribution to the potential application of hyperspectral imaging technique for postharvest diagnostic testing method for pomegranate fruit. It summarized various application of HSI as a diagnostic tool for food inspection and biosecurity over the past decade (2012 - 2022). The combined feature of imaging and spectroscopy enables the collection of massive spectral information for every pixel which provides the chemical constituents of samples and a chance to refine the data and perform critical analysis adequately. It is expected that future research studies could utilize the three effective wavebands of 407, 639 and 917nm in the VNIR wavelength range to develop and implement fast and efficient multispectral online bruise detection system for pomegranate fruit. In this study, we have utilized limited sample size, and halogen light source and ANN classifier for model development, future studies can also explore larger sample size, investigate the effect of different lighting source, preprocessing methods, and classifiers for a more robust qualitative and quantitative study. Overall classification accuracy ranged between 81.7 – 88.3% for early detection of bruise damage, and between 83.3% - 93.3% for distinguishing bruise severity of pomegranate fruit. This technique employed in the present study can be utilized for other horticultural fruits and vegetables. Factors such as fruit geometry and presence of husk, calyx and seasonality were not considered in the model development reported in the thesis. It is, therefore, recommended that for successful commercial online application, future studies need to consider such factors as increased sample size, additional cultivars, growing locations, and seasonality.

References

[1] M. Karimi, R. Sadeghi, and J. Kokini, “Pomegranate as a promising opportunity in medicine and nanotechnology,” *Trends in Food Science and Technology*, vol. 69, pp. 59–73, 2017.

[2] O. A. Fawole, and U. L. Opara, “Developmental changes in maturity indices of pomegranate fruit: A descriptive review.,” *Scientia Horticulturae*. vol. 159, pp. 152–161, 2013.

[3] E. P. Lansky, and R. A. Newman, “Punica granatum (pomegranate) and its potential for prevention and treatment of inflammation and cancer.,” *Journal of Ethnopharmacology*, vol. 109, no. 2, pp. 177–206, 2007.

[4] L. U. Opara, M. R. Al-Ani, and Y. S. Al-Shuaibi, “Physico-chemical properties, vitamin c content, and antimicrobial properties of pomegranate fruit (Punica granatum L.).,” *Food and Bioprocess Technology*, vol. 2, no. 3, pp. 315–321, 2009.

[5] D. Holland, K. Hatib, and I. Bar-ya, “Pomegranate: Botany, Horticulture, Breeding.,” John Wiley & Sons, Inc. vol. 35, pp. 127–192, 2009.

[6] G. ElMasry, M. Kamruzzaman,, D. W. Sun, and P. Allen, “Principles and applications of hyperspectral imaging in quality evaluation of agro-food products: A review.,” *Critical Reviews in Food Science and Nutrition*, vol. 52, no. 11, pp. 999–1023, 2012.

[7] L. S. Magwaza, and U. L. Opara, “Investigating non-destructive quantification and characterization of pomegranate fruit internal structure using X-ray computed tomography.,” *Postharvest Biology and Technology*. vol. 95, pp. 1–6, 2014.

[8] O. A. Fawole, “Maturity indexing, pharmacological properties and postharvest performance of pomegranate fruit grown in South Africa. Doctorate Thesis, Stellenbosch University, December 2013.

[9] S. Cubero, N. Aleixos, E. Moltó, J. Gómez-Sanchis, and J. Blasco, “Advances in machine vision applications for automatic inspection and quality evaluation of fruits and vegetables,” *Food and Bioprocess Technology*, vol. 4, no. 4, pp. 487–504, 2011.

[10] A. Baiano, “Applications of hyperspectral imaging for quality assessment of liquid based and semi-liquid food products: A review.,” *Journal of Food Engineering*, vol. 214, pp. 10–15, 2017.

[11] E. Arendse, O. A. Fawole, L. S. Magwaza, H. Nieuwoudt, and U. L. Opara, “Fourier transform near infrared diffuse reflectance spectroscopy and two spectral acquisition modes for evaluation of external and internal quality of intact pomegranate fruit.” *Postharvest Biology and Technology*. vol. 138, pp. 91–98, 2018.

[12] J. Nicolaï, B.M., Beullens, K., Bobelyn, E., Peirs, A., Saeys, W., Theron, K.I. and Lammertyn, “Nondestructive measurement of fruit and vegetable quality by means of NIR spectroscopy: A Review.” *Postharvest Biology and Technology*. vol. 46, no. 2, pp. 99–118., 2007.

[13] I. Chandrasekaran, S. S. Panigrahi, L. Ravikanth, and C. B. Singh, “Potential of near-infrared (NIR) spectroscopy and hyperspectral imaging for quality and safety assessment of fruits: an overview,” *Food Analytical Methods*. vol. 12, no. 11, pp. 2438–2458, 2019.

[14] J. Li, X. Rao, and Y. Ying, “Detection of common defects on oranges using hyperspectral reflectance imaging,” *Computers and Electronics in Agriculture*, vol. 78, no. 1, pp. 38–48, 2011.

[15] G. Özdoğan, X. Lin, and D. W. Sun, “Rapid and noninvasive sensory analyses of food products by hyperspectral imaging: Recent application developments,” *Trends in Food Science and Technology*, vol. 111, pp. 151–165, 2021.

[16] W. Hu, Y. Huang, L. Wei, F. Zhang, and H. Li, “Deep convolutional neural networks for hyperspectral image classification,” *Journal of Sensors*, vol. 2015, pp. 258619, 2015.

[17] P. Rajkumar, N. Wang, G. EImasry, G. S. V. Raghavan, and Y. Gariepy, “Studies on banana fruit quality and maturity stages using hyperspectral imaging,” *Journal of Food Engineering*. vol. 108, no. 1, pp. 194–200, 2012.

[18] R. Khodabakhshian, B. Emadi, M. Khojastehpour, M. R. Golzarian, and A. Sazgarnia, “Development of a multispectral imaging system for online quality assessment of pomegranate fruit,” *International Journal of Food Properties*, vol. 20, no. 1, pp. 107–118, 2017.

[19] E. Arendse, H. Nieuwoudt, L. S., Magwaza, J. F. I. Nturambirwe, O. A., Fawole, U. L. Opara, “Recent advancements on vibrational spectroscopic techniques for the detection

of authenticity and adulteration in horticultural products with a specific focus on oils, juices and powders," *Food and Bioprocess Technology*, 2020. Available: https://doi.org/10.1007/s11947-020-02505-x.

[20] A. Baiano, C. Terracone, G. Peri, and R. Romaniello, "Application of hyperspectral imaging for prediction of physico-chemical and sensory characteristics of table grapes," *Computers and Electronics in Agriculture*, vol. 87, pp. 142–151, 2012.

[21] E. Arendse, O. A. Fawole, L. S. Magwaza, and U. L. Opara, "Non-destructive prediction of internal and external quality attributes of fruit with thick rind: A review.," *Journal of Food Engineering*, vol. 217, pp. 11–23, 2018.

[22] E. Arendse, O. A. Fawole, L. S. Magwaza, and U. L. Opara, "Non-destructive characterization and volume estimation of pomegranate fruit external and internal morphological fractions using X-ray computed tomography" *Journal of Food Engineering*, vol. 186, pp. 42–49, 2016.

[23] R. Khodabakhshian, B. Emadi, M. Khojastehpour, R. Golzarian, and A. Sazgarnia, "Non-destructive evaluation of maturity and quality parameters of pomegranate fruit by visible/near infrared spectroscopy" *International Journal of Food Properties*, vol. 00, no. 00, pp. 1–14, 2016. Available: http://dx.doi.org/10.1080/10942912.2015.1126725.

[24] E. Arendse, O. A. Fawole, L. S. Magwaza, H. H. Nieuwoudt, and U. L. Opara, "Development of calibration models for the evaluation of pomegranate aril quality by Fourier-transform near infrared spectroscopy combined with chemometrics" *Biosystems Engineering*, vol. 159, pp. 22–32, 2017.

[25] L. Pan, Q. Zhang, W. Zhang, Y. Sun, P. Hu, and K. Tu, "Detection of cold injury in peaches by hyperspectral reflectance imaging and artificial neural network.," *Food Chemistry*, vol. 192, pp. 134–141, 2016.

[26] N. T. Vetrekar, R. S. Gad, I. Fernandes, J. S. Parab, A. R. Desai, J. D. Pawar, G. M. Naik, and S. Umapathy, "Non-invasive hyperspectral imaging approach for fruit quality control application and classification: case study of apple, chikoo, guava fruits" *The Journal of Food Science and Technology*, vol. 52, pp. 6978–6989, 2015.

[27] C. Zhang, C. Guo, F. Liu, W. Kong, Y. He, and B. Lou, "Hyperspectral imaging

analysis for ripeness evaluation of strawberry with support vector machine.," *Journal of Food Engineering*, vol. 179, pp. 11–18, 2016.

[28] Y. Y. Pu, Y. Z. Feng, and D. W. Sun, "Recent progress of hyperspectral imaging on quality and safety inspection of fruits and vegetables: A review.," Comprehensive Reviews in Food Science and Food Safety. vol. 14, no. 2, pp. 176–188, 2015.

[29] B. Nicolaï, B. D. Ketelaere, A. Dizon, et al., "Non-destructive evaluation: detection of external and internal attributes frequently associated with quality and damage. In: Postharvest Handling: A Systems Approach (edited by W.J. Florkowiski, R.L. Shewfelt, B. Brueckner & S.E. Prussia).," Academic Press, Elsevier, Amsterdam. pp. 421– 442, 2009.

[30] S. A. Wadood, G. Boli, Z. Xiaowen, I. Hussain, and W. Yimin, "Recent development in the application of analytical techniques for the traceability and authenticity of food of plant origin," *Microchemical Journal*, vol. 152, p. 104295, 2020.

[31] F. Mendoza, R. Lu, D. Ariana, H. Cen, and B. Bailey, "Integrated spectral and image analysis of hyperspectral scattering data for prediction of apple fruit firmness and soluble solids content," *Postharvest Biology and Technology*, vol. 62, no. 2, pp. 149–160, 2011.

[32] P. B. Pathare, U. L. Opara, and F. A.-J. Al-Said, "Colour measurement and analysis in fresh and processed foods: a review," *Food and Bioprocess Technology*. vol. 6, no. 1, pp. 36–60, 2013.

[33] L. Chen, and U. L. Opara, "Texture measurement approaches in fresh and processed foods - A review.," *Food Research International*. vol. 51, no. 2, pp. 823–835, 2013.

[34] U. L. Opara, and P. B. Pathare, "Bruise damage measurement and analysis of fresh horticultural produce-A review," *Postharvest Biology and Technology*. vol. 91, pp. 9–24, 2014.

[35] V. Van linden, D. N. Sila, T. Duvetter, J. De Baerdemaeker, and M. Hendrickx, "Effect of mechanical impact-bruising on polygalacturonase and pectinmethylesterase activity and pectic cell wall components in tomato fruit," *Postharvest Biology and Technology*. vol. 47, no. 1, pp. 98–106, 2008.

[36] Z. Hussein,, O. A. Fawole, and U. L. Opara, "Preharvest factors influencing bruise

damage of fresh fruits – a review.," *Scientia Horticulturae*. vol. 229, no. October 2017, pp. 45–58, 2018.

[37] M. K. Tripathi, and D. D. Maktedar, "A role of computer vision in fruits and vegetables among various horticulture products of agriculture fields: A survey.," *Information Processing in Agriculture*. vol. 7, no. 2, pp. 183–203, 2020.

[38] L. Pan, W. Zhang, N. Zhu, S. Mao, and K. Tu, "Early detection and classification of pathogenic fungal disease in post-harvest strawberry fruit by electronic nose and gas chromatography – mass spectrometry," Food Research International, vol. 62, pp. 162–168, 2014.

[39] A. Siedliska, P. Baranowski, M. Zubik, and W. Mazurek, "Detection of fungal infections in strawberry fruit by VNIR / SWIR hyperspectral imaging," *Postharvest Biology and Technology*. vol. 139, no. September 2017, pp. 115–126, 2018.

[40] S. Cui, P. Ling, H. Zhu and H. M. Keener, "Plant pest detection using an artificial nose system: A review," Sensors, pp. 1–18, 2018.

[41] N. Ekramirad, A. A. Adedeji, and R. Alimardani, "A review of non-destructive methods for detection of insect infestation in fruits and vegetables" Innovations in Food Research, vol. 2, pp. 6–12, 2016.

[42] H. S. El-Mesery,, H. Mao, and A. E.-F. Abomohra, "Applications of Non-destructive Technologies for Agricultural and Food Products Quality Inspection.," *Sensors*. vol. 19, pp. 845–867, 2019.

[43] C. N. Berger, S. V. Sodha, R. K. Shaw, P. M. Griffin, D. Pink, H. Paul and G. Frankel, "Fresh fruit and vegetables as vehicles for the transmission of human pathogens," *Environmental Microbiology,* vol. 12, no. 9, pp. 2385–2397, 2010.

[44] Y. Z. Feng, and D. W. Sun, "Application of hyperspectral imaging in food safety inspection and control: a review," *Critical Reviews in Food Science and Nutrition*, vol. 52, no. 11, pp. 1039–1058, 2012.

[45] T. King, M. Cole, J. M. Farber, G. Eisenbrand, D. Zabaras, E. M. Fox, and J. P. Hill, "Trends in food science & technology food safety for food security safety," *Trends in Food Science and Technology,* vol. 68, pp. 160–175, 2017.

[46] D. W. Sun, "Hyperspectral imaging for food quality analysis and control.," In: Elsevier

2010.

[47] S. Srivastava, and S. Sadistap, “Non-destructive sensing methods for quality assessment of on-tree fruits : a review,” *Journal of Food Measurement and Characterization*, vol. 12, no. 1, pp. 497–526, 2018.

[48] A. A. Gowen, C. P. O’Donnell, P. J. Cullen, G. Downey, and J. M. Frias, “Hyperspectral imaging - an emerging process analytical tool for food quality and safety control,” *Trends in Food Science and Technology*, vol. 18, no. 12, pp. 590–598, 2007.

[49] H. Lu, Y. Huang, and R. Lu, “Innovative hyperspectral imaging-based techniques for quality evaluation of fruits and vegetables: a review,” *Applied Sciences*. vol. 2017, no. 7, p. 189, 2017.

[50] J. F. I. Nturambirwe, and U. L. Opara, “Machine learning applications to non-destructive defect detection in horticultural products,” *Biosystems Engineering*. vol. 189, pp. 60–83, 2020.

[51] H. Wang, J. Peng, C. Xie, Y. Bao, and Y. He, “Fruit quality evaluation using spectroscopy technology: A review.,” *Sensors*, vol. 15, no. 5, pp. 11889–11927, 2015.

[52] D. Wu, and D. W. Sun, “Advanced applications of hyperspectral imaging technology for food quality and safety analysis and assessment: A review - Part I: Fundamentals,” *Innovative Food Science and Emerging Technologies*, vol. 19, pp. 1–14, 2013.

[53] Z. Xiong, D. Sun, X. Zeng, and A. Xie, “Recent developments of hyperspectral imaging systems and their applications in detecting quality attributes of red meats: A review,” J*ournal of Food Engineering*. vol. 132, pp. 1–13, 2014.

[54] W. Su, and D. Sun, “Fourier transform infrared and Raman and hyperspectral imaging techniques for quality determinations of powdery foods: a review,” *Comprehensive Reviews in Food Science and Food Safety*, vol. 17, pp. 104–122, 2018.

[55] T. H. Johansen, K. Mollersen, S. Ortega, H. Fabelo, M. G. Callico, and G. Fred, “Recent advances in hyperspectral imaging for melanoma detection,” *WIREs Comput Stat*. no. March 2019, pp. 1–17, 2020.

[56] R. J. Murphy, S. Schneider, and S. T. Monteiro, “Consistency of measurements of wavelength position from hyperspectral imagery: use of the ferric iron crystal field

absorption at ~ 900 nm as an indicator of mineralogy.," *IEEE Transactions on Geoscience and Remote Sensing*, vol. 52, no. 5, pp. 2843–2857, 2014.

[57] B. Lu, P. D. Dao, J. Liu, Y. He, and J. Shang, "Recent advances of hyperspectral imaging technology and applications in agriculture," *Remote Sensing*, vol. 12, no. 16, pp. 1–44, 2020.

[58] O. Rozenstein, A. Devir, and A. Karnieli, "In-field absolute calibration of ground and airborne VIS-NIR-SWIR hyperspectral point spectrometers," *Remote Sensing*, vol. 6, no. 2, pp. 1158–1170, 2014.

[59] M. Doneus, G. Verhoeven, C. Atzberger, M. Wess, and M. Ru, "New ways to extract archaeological information from hyperspectral pixels," *Journal of Archaeological Science*, vol. 52, pp. 84–96, 2014.

[60] A. Guyot, M. Lennon, N. Thomas, G. Simon, T. Petit, T. Lorho, S. Cassen, and L. Hubert-Moy, "Airborne hyperspectral imaging for submerged archaeological mapping in shallow water environments.," Remote Sens. vol. 11, p. 2237, 2019.

[61] M. R. Almeida, D. N. Correa, J. J. Zacca, L. P. L. Logrado, and R. J. Poppi, "Detection of explosives on the surface of banknotes by Raman hyperspectral imaging and independent component analysis," *Analytica Chimica Acta*, vol. 860, pp. 15–22, 2015.

[62] H. Yao, and D. Lewis, Spectral preprocessing, and calibration techniques., 2010.

[63] H. Photonics, and A. R. Reserved, "Hyperspectral Imaging for Advanced Machine Vision © 2018.," p. 2018.

[64] P. Vithu, and J. A. Moses, "Machine vision system for food grain quality evaluation: a review.," *Trends in Food Science and Technology*, vol. 56, pp. 13–20, 2016.

[65] C. Pandey, P. K. Sethy, P. Biswas, S. K. Behera, and M. R. Khan, "Quality *Evaluation of Pomegranate Fruit using Image Processing Techniques*," *International Conference on Communication and Signal Processing*, August, 2020.

[66] X. Liming, and Z. Yanchao, "Automated strawberry grading system based on image processing," *Computers and Electronics in Agriculture*, vol. 71, no. 1, pp. 32–39, 2010.

[67] F. López-García, G. Andreu-García, J. Blasco, N. Aleixos, and J. M. Valiente,

"Automatic detection of skin defects in citrus fruits using a multivariate image analysis approach," *Computers and Electronics in Agriculture*, vol. 71, no. 2, pp. 189–197, 2010.

[68] H. Huang, L. Liu, and M. O. Ngadi, "Recent developments in hyperspectral imaging for assessment of food quality and safety," *Sensors*, vol. 14, no. 4, pp. 7248–7276, 2014.

[69] B. Zhang, D. Dai, J. Huang, J. Zhou, Q. Gui, and F. Dai, "Influence of physical and biological variability and solution methods in fruit and vegetable quality nondestructive inspection by using imaging and near-infrared spectroscopy techniques: A review," *Critical Reviews in Food Science and Nutrition*. vol. 58, no. 12, pp. 2099–2118, 2018.

[70] D. F. Barbin, G. Elmasry, D. W. Sun, and P. Allen, "Predicting quality and sensory attributes of pork using near-infrared hyperspectral imaging," *Analytica Chimica Acta*. vol. 719, pp. 30–42, 2012.

[71] B.-H. Zhang, J.-B. Li, L. Zheng, W-Q. Huang, S.-X. Fan, C.-J. Zhao, and Q.-D. Meng, "Development of a hyperspectral imaging system for the early detection of apple rottenness caused by Penicillium," *Journal of Food Process Engineering*, vol. 38, no. 5, pp. 499–509, 2015.

[72] D. Pietro Cavallo, M. Cefola, B. Pace, A. F. Logrieco, and G. Attolico, "Non-destructive and contactless quality evaluation of table grapes by a computer vision system.," *Computers and Electronics in Agriculture*, vol. 156, no. June 2018, pp. 558–564, 2019.

[73] E. R. Arboleda, C. L. T. de Jesus, and L. M. S. Tia, "Pineapple maturity classifier using image processing and fuzzy logic," *IAES International Journal of Artificial Intelligence*. vol. 10, no. 4, pp. 830–838, 2021.

[74] L. Angel, S. Lizcano, and J. Viola, "Assessing the state of maturation of the pineapple in its perolera variety using computer vision techniques," *2015 20th Symposium on Signal Processing, Images and Computer Vision, STSIVA 2015 - Conference Proceedings*. no. November 2018, p. 2015.

[75] H. A. Badrul, J. I. Asnor, S. Rosnah, and Z. W. W. H. Wan, "Ripeness level

classification for pineapple," *Journal of Theoretical and Applied Information Technology*. vol. 57, no. 3, pp. 587–593, 2013.

[76] S. Mohammad, K. H. Ghazali, N. C. Zan, S. S. M. Radzi, and R. A. Karim, "Classification of fresh N36 pineapple crop using image processing technique," *Advanced Materials Research*. vol. 418–420, pp. 1739–1743, 2012.

[77] Y. Gurubelli, M. Ramanathan, and P. Ponnusamy, "Fractional fuzzy 2DLDA approach for pomegranate fruit grade classification," *Computers and Electronics in Agriculture*. vol. 162, no. March, pp. 95–105, 2019.

[78] M. Fashi, L. Naderloo, and H. Javadikia, "The relationship between the appearance of pomegranate fruit and color and size of arils based on image processing," *Postharvest Biology and Technology*, vol. 154, no. April, pp. 52–57, 2019.

[79] N. A. Syazwan, M. S. B. S. Rizam, and M. T. Nooritawati, "Categorization of watermelon maturity level based on rind features," *Procedia Engineering*, vol. 41, no. Iris, pp. 1398–1404, 2012.

[80] H. K. Noh, and R. Lu, "Hyperspectral laser-induced fluorescence imaging for assessing apple fruit quality," *Postharvest Biology and Technology*, vol. 43, no. 2007, pp. 193–201, 2007.

[81] I. Vermaak, A. Viljoen, and S. W. Lindström, "Hyperspectral imaging in the quality control of herbal medicines – The case of neurotoxic Japanese star anise," *Journal of Pharmaceutical and Biomedical Analysis*, vol. 75, pp. 207–213, 2013.

[82] G. ElMasry, and D. W. Sun, "Principles of hyperspectral imaging technology," *Hyperspectral Imaging for Food Quality Analysis and Control*, pp. 3–43, 2010.

[83] Y. Karimi, N. Maftoonazad, H. S. Ramaswamy, S. O. Prasher, and M. Marcotte, "Application of hyperspectral technique for color classification avocados subjected to different treatments," *Food and Bioprocess Technology*, vol. 5, no. 1, pp. 252–264, 2012.

[84] H. Cen, R. Lu, D. P. Ariana, and F. Mendoza, "Hyperspectral imaging-based classification and wavebands selection for internal defect detection of pickling cucumbers," *Food and Bioprocess Technology*, vol. 7, pp. 1689–1700, 2014.

[85] M. Vidal, and J. M. Amigo, "Pre-processing of hyperspectral images. Essential steps

before image analysis," *Chemometrics and Intelligent Laboratory Systems*, vol. 117, pp. 138–148, 2012.

[86] J. Colling, "Launch of new hyperspectral imaging unit at Stellenbosch University.," pp. 1–3, 2018.

[87] B. Diezma, L. Lleó, J. M. Roger, A. Herrero-Langreo, L. Lunadei, and M. Ruiz-Altisent, "Examination of the quality of spinach leaves using hyperspectral imaging," *Postharvest Biology and Technology*. vol. 85, pp. 8–17, 2013.

[88] P. N. Schaare, and D. G. Fraser, "Comparison of reflectance, interactance and transmission modes of visible-near infrared spectroscopy for measuring internal properties of kiwifruit (Actinidia chinensis)," *Postharvest Biology and Technology*, vol. 20, no. 2, pp. 175–184, 2000.

[89] B. Li, M. Cobo-Medina, J. Lecourt, N. B. Harrison, R. J. Harrison, and J. V. Cross, "Application of hyperspectral imaging for nondestructive measurement of plum quality attributes," *Postharvest Biology and Technology*, vol. 141, pp. 8–15, 2018.

[90] M. Amigo, H. Babamoradi, and S. Elcoroaristizabal, "Analytica Chimica Acta Hyperspectral image analysis . A tutorial.," vol. 896, pp. 34–51, 2015.

[91] L. S. Magwaza, U. L. Opara, H. Nieuwoudt, P. J. R. Cronje, and W. Saeys, "NIR spectroscopy applications for internal and external quality analysis of citrus fruit — A review," *Food Bioprocess Technology*, pp. 425–444, 2012.

[92] N. K. Mahanti, R. Pandiselvam, A. Kothakota, P. S. Ishwarya, S. K. Chakraborty, M. Kumar and D. Cozzolino, "Emerging non-destructive imaging techniques for fruit damage detection: Image processing and analysis," *Trends in Food Science and Technology*, vol. 120, no. December 2021, pp. 418–438, 2022.

[93] L. Xu, P. T. Shi, Z. H. Ye, S. M. Yan, and X. P. Yu, "Rapid analysis of adulterations in Chinese lotus root powder (LRP) by near-infrared (NIR) spectroscopy coupled with chemometric class modeling techniques," *Food Chemistry*, vol. 141, no. 3, pp. 2434–2439, 2013.

[94] L. Ravikanth, D. S. Jayas, N. D. G. White, and P. G. Fields, "Extraction of spectral information from hyperspectral data and application of hyperspectral imaging for food and agricultural products," *Food and Bioprocess Technology*, pp. 1–33, 2017.

[95] M. Zhang, and G. Li, “Visual detection of apple bruises using AdaBoost algorithm and hyperspectral imaging,” *International Journal of Food Properties*, vol. 21, no. 1, pp. 1598–1607, 2018.

[96] H. Xu,, J. Ren,, J. Lin, S. Mao, Z. Xu, Z. Chen, J. Zhao, Y. Wu, N. Xu, and P. Wang, “The impact of high-quality data on the assessment results of visible / near-infrared hyperspectral imaging and development direction in the food fields: A review,” *Journal of Food Measurement and Characterization*, no. s11694, 2023. Avaliable: https://doi.org/10.1007/s11694-023-01822-x.

[97] A. Iqbal,, D. Sun, and P. Allen, “An overview on principle , techniques and application of hyperspectral imaging with special reference to ham quality evaluation and control.,” *Food Control*. vol. 46, pp. 242–254, 2014.

[98] G. K. Naganathan, L. M. Grimes, J. Subbiah, C. R. Calkins, A. Samal, and G. E. Meyer, “Visible/near-infrared hyperspectral imaging for beef tenderness prediction,” *Computers and Electronics in Agriculture*, vol. 64, no. 2, pp. 225–233, 2008.

[99] W. Che,, L. Sun,, Q. Zhang, W. Tan, D. Ye, D. Zhang, and Y. Liu, “Pixel based bruise region extraction of apple using Vis-NIR hyperspectral imaging,” *Computers and Electronics in Agriculture*, vol. 146, no. February, pp. 12–21, 2018.

[100] Y. Fang, F. Yang, Z. Zhou, L. Lin, and X. Li, “Hyperspectral wavelength selection and integration for bruise detection of korla pears,” *Journal of Spectroscopy*, vol. 2019, p. 6715247, 2019.

[101] A. Siedliska, P. Baranowski, and W. Mazurek, “Classification models of bruise and cultivar detection on the basis of hyperspectral imaging data.,” *Computers and Electronics in Agriculture*. vol. 106, pp. 66–74, 2014.

[102] W. Lee, M. S. Kim, H. Lee, S. R. Delwiche, H. Bae, D.-Y. Kim, B-K. Cho, “Hyperspectral near-infrared imaging for the detection of physical damages of pear,” *Journal of Food Engineering*. vol. 130, pp. 1–7, 2014.

[103] W. Tan, L. Sun,, F. Yang, et al., “Study on bruising degree classification of apples using hyperspectral imaging and GS-SVM.,” *Optik*. vol. 154, pp. 581–592, 2018.

[104] J. F. I. Nturambirwe, W. J. Perold, and U. L. Opara, “Classification learning of latent bruise damage to apples using shortwave infrared hyperspectral imaging,” *Sensors*,

vol. 21, no. 4990, p. 2021.

[105] I. Orina, M. Manley, and P. J. Williams, “Non-destructive techniques for the detection of fungal infection in cereal grains,” *Food Research International*, vol. 100, no. July, pp. 74–86, 2017.

[106] D. F. Barbin, G. Elmasry, D. W. Sun, P. Allen, and N. Morsy, “Non-destructive assessment of microbial contamination in porcine meat using NIR hyperspectral imaging,” *Innovative Food Science and Emerging Technologies*, vol. 17, pp. 180–191, 2013.

[107] Q. Lü, and M. Tang, “Detection of hidden bruise on kiwi fruit using hyperspectral imaging and parallelepiped classification,” *Procedia Environmental Sciences*, vol. 12, pp. 1172–1179, 2012.

[108] J. Xiong, R. Lin, R. Bu, Z. Liu, Z. Yang, and L. Yu, “A micro-damage detection method of litchi fruit using hyperspectral imaging technology,” *Sensors (Switzerland)*, vol. 18, no. 3, p. 2018.

[109] K. Sendin, M. Manley, and P. J. Williams, “Classification of white maize defects with multispectral imaging,” *Food Chemistry*, vol. 243, no. September 2017, pp. 311–318, 2018.

[110] K. Sendin, M. Manley, V. Baeten, J. A. F. Pierna, and P. J. Williams, “Near infrared hyperspectral imaging for white maize classification according to grading regulations,” *Food Analytical Methods*, vol. 12, no. 2019, pp. 1612–1624, 2019.

[111] J. C. Keresztes, M. Goodarzi, and W. Saeys, “Real-time pixel based early apple bruise detection using short wave infrared hyperspectral imaging in combination with calibration and glare correction techniques,” *Food Control*, vol. 66, pp. 215–226, 2016.

[112] W. Hu, Y. Huang, L. Wei, F. Zhang, and H. Li, “Deep convolutional neural networks for hyperspectral image classification,” *Journal of Sensors*, vol. 2015, no. 258619, p. 2015.

[113] A. Krizhevsky, I. Sutskever, and G. E. Hinton, “ImageNet classification with deep convolutional neural networks, *Unpublished manuscript*, 2010.

[114] Z. Wang, M. Hu, and G. Zhai, “Application of deep learning architectures for accurate

and rapid detection of internal mechanical damage of blueberry using hyperspectral transmittance data," *Sensors (Switzerland)*, vol. 18, no. 4, pp. 1–14, 2018.

[115] U. B. Gewali, S. T. Monteiro, and E. Saber, "Machine learning based hyperspectral image analysis: A survey," 2018. Available: arXiv:1802.08701V2.

[116] Y. Chen, X. Zhao, S. Member, X. Jia, and S. Member, "Spectral – spatial classification of hyperspectral data based on deep belief network," IEEE *Journal Of Selected Topics in Applied Earth Observations and Remote Sensing*, vol. 8, no. 6, pp. 2381–2392, 2015.

[117] D. Omanović, C. Santinelli, S. Marcinek, and M. Gonnelli, "ASFit - An all-inclusive tool for analysis of UV–Vis spectra of colored dissolved organic matter (CDOM)," *Computers and Geosciences*, vol. 133, pp. 104334, 2019. Available: https://doi.org/10.1016/j.cageo.2019.104334

[118] S. R. Brogi, C. Balestra, R. Casotti, G. Cossarini, Y. Galletti, M. Gonnelli, S. Vestri, and C. Santinelli, "Time resolved data unveils the complex DOM dynamics in a Mediterranean river," *Science of the Total Environment*, vol. 733, pp. 139212, 2020. Available: https://doi.org/10.1016/j.scitotenv.2020.139212.

[119] M. Danner, "The EnMAP managed vegetation scientific processor towards an automatic retrieval of canopy structure and leaf biochemical properties from hyperspectral images, Dissertation zur Erlangung des Doktorgrades an der Fakultät für Geowissenschaften der Ludwig-Maximilians-Universität München, 2019.

[120] T. Hank, K. Berger, M. Wocher, M. Danner, and W. Mauser, "Introducing the Potential of the Enmap-Box for Agricultural Applications Using Desis and Prisma Data.," International Geoscience and Remote Sensing Symposium (IGARSS). no. 3, pp. 467–470, 2021.

[121] K. Richter, T. Hank, C. Atzberger, M. Locherer, and W. Mauser, "Regularization strategies for agricultural monitoring: the enmap vegetation analyzer (AVA) Dept. of Geography, Ludwig-Maximilians University Munich, Luisenstr. 37, 80333 Munich, Germany; Institute of Surveying, Remote Sensing and Land Informati.," pp. 6613–6616, 2012.

[122] N. Liu, P. A. Townsend, M. R. Naber, P. C. Bethke, W. B. Hills, and Y. Wang,

"Hyperspectral imagery to monitor crop nutrient status within and across growing seasons," *Remote Sensing of Environment*, vol. 255, no. August 2020, p. 112303, 2021.

[123] E. Greenberg,, D. R. Thompson,, D. Jensen, Townsend, N. Queally, A. Chlus, C. G. Fichot, J. P. Harringmeyer, and M. Simard, "An improved scheme for correcting remote spectral surface reflectance simultaneously for terrestrial BRDF and water-surface sunglint in coastal environments," *Journal of Geophysical Research: Biogeosciences*, vol. 127, no. 3, pp. 1–21, 2022.

[124] H. Zhu, B. Chu, Y. Fan, X. Tao, W. Yin, and Y. He, "Hyperspectral imaging for predicting the internal quality of kiwifruits based on variable selection algorithms and chemometric models," *Scientific Reports*, vol. 7, no. 1, pp. 1–13, 2017.

[125] V. V. Rozanov, T. Dinter, A. V. Rozanov, A. Wolanin, A. Bracher, and J. P. Burrows, "Radiative transfer modeling through terrestrial atmosphere and ocean accounting for inelastic processes: Software package SCIATRAN," *Journal of Quantitative Spectroscopy and Radiative Transfer*. vol. 194, pp. 65–85, 2017.

[126] L. Zhao, S. Chen, Y. Xue, and T. Cui, "Study of atmospheric carbon dioxide retrieval method based on normalized sensitivity," *Remote Sensing*, vol. 14, no. 5, p. 1106, 2022.

[127] HiPic, "High performance image control and processing software," 2015. Available: http://www.imagelab.at/en_home.

[128] A. J. Mathews, "Object-based spatiotemporal analysis of vine canopy vigor using an inexpensive unmanned aerial vehicle remote sensing system," *Journal of Applied Remote Sensing*, vol. 8, no. 1, p. 085199, 2014.

[129] S. S. Panda,, G. Hoogenboom, and J. O. Paz, "Remote sensing and geospatial technological applications for site-specific management of fruit and nut crops: A review," *Remote Sensing*, vol. 2, no. 8, pp. 1973–1997, 2010.

[130] P. Baranowski, W. Mazurek, and J. Pastuszka-Woźniak, "Supervised classification of bruised apples with respect to the time after bruising on the basis of hyperspectral imaging data," *Postharvest Biology and Technology*, vol. 86, pp. 249–258, 2013.

[131] M. Hu, Q. Dong, and B. Liu, "Classification and characterization of blueberry

mechanical damage with time evolution using reflectance, transmittance and interactance imaging spectroscopy," *Computers and Electronics in Agriculture*, vol. 122, pp. 19–28, 2016.

[132] I. H. Witten, E. Frank, L. Trigg, M. Halll, G. Holmes, and S. J. Cunningham, "Weka: practical machine learning tools and techniques with java implementations," *SIGMOD Record*, vol. 31, no. 1, pp. 76–77, 2002.

[133] P. Baranowski, W. Mazurek, J. Wozniak, and U. Majewska, "Detection of early bruises in apples using hyperspectral data and thermal imaging," *Journal of Food Engineering*, vol. 110, no. 3, pp. 345–355, 2012.

[134] S. Munera, C. Besada, J. Blasco, S. Cubero, A. Salvador, P. Talens, and N. Aleixos, "Astringency assessment of persimmon by hyperspectral imaging," *Postharvest Biol. Technol.*, vol. 125, pp. 35–41, 2017.

[135] S. Munera, J. M. Amigo, J. Blasco, S. Cubero, P. Talens, and N. Aleixos, "Ripeness monitoring of two cultivars of nectarine using VIS-NIR hyperspectral reflectance imaging," *Journal of Food Engineering*, vol. 214, pp. 29–39, 2017.

[136] Y. Shao, Y. Wang, G. Xuan, Z. Gao, Z. Hu, C. Gao, and K. Wang, "Assessment of strawberry ripeness using hyperspectral imaging," *Analytical Letters*, vol. 54, no. 10, pp. 1547-1560, 2020. Available: https://doi.org/10.1080/00032719.2020.1812622.

[137] D. M. Musingarabwi, H. H. Nieuwoudt, P. R. Young, H. A. Eyéghè-bickong, and M. A. Vivier, "A rapid qualitative and quantitative evaluation of grape berries at various stages of development using Fourier-transform infrared spectroscopy and multivariate data analysis," *Food Chemistry*, vol. 190, pp. 253–262, 2016.

[138] G. Alves, D. Oliveira, F. De Castilhos, C. M. Claire, and S. Bureau, "Comparison of NIR and MIR spectroscopic methods for determination of individual sugars, organic acids and carotenoids in passion fruit," *Food Research International*, vol. 60, pp. 154–162, 2014.

[139] OPUS release notes, "What is new in OPUS 7. 2," January 2013.

[140] SIMCA Application note, "How to turn process data into information, 10 June 2020.

[141] A. Iqbal, D. Sun, and P. Allen, "Prediction of moisture, color and pH in cooked, pre-sliced turkey hams by NIR hyperspectral imaging system," *Journal of Food*

Engineering, vol. 117, no. 1, pp. 42–51, 2013.

[142] E. E. Okere, E. Arendse, H. Nieuwoudt, O. A. Fawole, W. J. Perold, and U. L. Opara, "Non-invasive methods for predicting the quality of processed horticultural food products , with emphasis on dried powders , juices and oils : A review," *Foods*, p. 3061, 2021.

[143] P. C. Williams, "Implementation of near-infrared technology. In: Williams, P.C. and Norris, K., Eds., Near-Infrared Technology in the Agricultural and Food Industries.," 2nd Edition, *American Association of Cereal Chemists*, St. Paul. pp. 145–169, 2001.

[144] R. A. Kumar, V. S. Rajpurohit, and V. B. Nargund, "A neural network assisted machine vision system for sorting pomegranate fruits," *Proceedings of the 2017 2nd IEEE International Conference on Electrical, Computer and Communication Technologies, ICECCT 2017*. p. 2017.

[145] D. Lorente, N. Aleixos, J. Gómez-Sanchis, S. Cubero, and J. Blasco, "Selection of optimal wavelength features for decay detection in citrus fruit using the roc curve and neural networks," *Food and Bioprocess Technology*, vol. 6, no. 2, pp. 530–541, 2013.

[146] D. Lorente, J. Blasco, A. J. Serrano, E. Soria-Olivas, N. Aleixos, and J. Gómez-Sanchis, "Comparison of ROC feature selection method for the detection of decay in citrus fruit using hyperspectral images," *Food Bioprocess Technology*, vol. 6, pp. 3613–3619, 2013.

[147] S. Fan, C. Li, W. Huang, and L. Chen, "Data fusion of two hyperspectral imaging systems with complementary spectral sensing ranges for blueberry bruising detection," *Sensors (Switzerland)*, vol. 18, no. 12, p. 2018.

[148] D. R. Amancio, C. H. Comin, D. Casanova, G. Travieso, O. M. Bruno, F. A. Rodrigues, L. d. Costa, "A systematic comparison of supervised classifiers," *PLoS ONE*, vol. 9, no. 4, p. e94137, 2014.

[149] N. V. Rivera, J. Go´mez-Sanchis, J. Chanona-Pe´rez, J. J. Carrasco, M. Milla´n-Giraldo, D. Lorente, S. Cubero, J. Blasco, "Early detection of mechanical damage in mango using NIR hyperspectral images and machine learning," *Biosystems. Engineering*, vol. 122, pp. 91–98, 2014.

[150] E. Bonah, X. Huang, J. H. Aheto, and R. Osae, "Application of electronic nose as a

non-invasive technique for odor fingerprinting and detection of bacterial foodborne pathogens: a review," *Journal of Food Science and Technology*, vol. 57, no. 6, pp. 1977–1990, 2020.

[151] S. Khanal, K. Kushal, J. P. Fulton, S. Shearer, and E. Ozkan, "Remote sensing in agriculture — accomplishments , limitations , and opportunities," *Remote Sensing*, vol. 12, p. 3783, 2020.

[152] A. Wendel, J. Underwood, and K. Walsh, "Maturity estimation of mangoes using hyperspectral imaging from a ground based mobile platform," *Computers and Electronics in Agriculture*, vol. 155, no. August, pp. 298–313, 2018.

[153] L. A. Suarez, A. Robson, J. McPhee, J. O'Halloran, and C. van Sprang, "Accuracy of carrot yield forecasting using proximal hyperspectral and satellite multispectral data," *Precision Agriculture*, vol. 21, no. 6, pp. 1304–1326, 2020.

[154] F. Vanegas, D. Bratanov, J. Weiss, K. Powell, and F. Gonzalez, "Multi and hyperspectral UAV remote sensing: Grapevine phylloxera detection in vineyards," *IEEE Aerospace Conference Proceedings*, vol. 2018-March, no. October, pp. 1–9, 2018.

[155] J. Abdulridha, O. Batuman, and Y. Ampatzidis, "UAV-based remote sensing technique to detect citrus canker disease utilizing hyperspectral imaging and machine learning," *Remote Sensing*, vol. 11, no. 11, p. 1373, 2019.

[156] H. Ma, K. Zhao, X. Jin, J. Ji, Z. Qiu, and S. Gao, "Spectral difference analysis and identification of different maturity blueberry fruit based on hyperspectral imaging using spectral index," *International Journal of Agricultural and Biological Engineering*, vol. 12, no. 3, pp. 134–140, 2019.

[157] H. Al-Saddik, J. C. Simon, and F. Cointault, "Development of spectral disease indices for 'flavescence dorée' grapevine disease identification," *Sensors (Switzerland)*, vol. 17, no. 12, p. 2772, 2017.

[158] M. Alhammadi, "Using QuickBird satellite images to study salinity effect on date palm field," pp. 1–6, 2010. Available: https://geosp.net/wp-content/uploads/2012/11/Mohamed-Alhammadi1.pdf.

[159] J. Franke, and G. Menz, "Multi-temporal wheat disease detection by multi-spectral

remote sensing," *Precision Agriculture*, vol. 8, no. 3, pp. 161–172, 2007.

[160] K. Usha, and B. Singh, "Potential applications of remote sensing in horticulture-A review," *Scientia Horticulturae*, vol. 153, pp. 71–83, 2013.

[161] W. Guo, F. Zhao, and J. Dong, "Nondestructive measurement of soluble solids content of kiwifruits using near-infrared hyperspectral imaging," *Food Analytical Methods*, vol. 9, no. 1, pp. 38–47, 2016.

[162] S. Fan, W. Huang, Z. Guo, B. Zhang, and C. Zhao, "Prediction of soluble solids content and firmness of pears using hyperspectral reflectance imaging," *Food Analytical Methods*, vol. 8, no. 8, pp. 1936–1946, 2015.

[163] W. Hu, D. W. Sun, and J. Blasco, "Rapid monitoring 1-MCP-induced modulation of sugars accumulation in ripening 'Hayward' kiwifruit by Vis/NIR hyperspectral imaging," *Postharvest Biology and Technology*, vol. 125, pp. 168–180, 2017.

[164] M. Zhang, Y. Jiang, C. Li, and F. Yang, "Fully convolutional networks for blueberry bruising and calyx segmentation using hyperspectral transmittance imaging," *Biosystems Engineering*, vol. 192, pp. 159–175, 2020.

[165] H. Jiang, C. Zhang, Y. He, X. Chen, F. Liu, and Y. Liu, "Wavelength selection for detection of slight bruises on pears based on hyperspectral imaging," *Applied Sciences (Switzerland)*, vol. 6, no. 12, p. 2016.

[166] J. Li, W. Huang, X. Tian, C. Wang, S. Fan, and C. Zhao, "Fast detection and visualization of early decay in citrus using Vis-NIR hyperspectral imaging," *Computers and Electronics in Agriculture*, vol. 127, pp. 582–592, 2016.

[167] J. Gómez-Sanchis, J. Blasco, E. Soria-Olivas, D. Lorente, P. Escandell-Montero, J. M. Martínez-Martínez, M. Martínez-Sobera, and N. Aleixos., "Hyperspectral LCTF-based system for classification of decay in mandarins caused by Penicillium digitatum and Penicillium italicum using the most relevant bands and non-linear classifiers," *Postharvest Biology and Technology*, vol. 82, pp. 76–86, 2013.

[168] T. Guo, X. Ahlawat, A. Zare, and T. Liu, "Evaluation of postharvest senescence in Broccoli via hyperspectral imaging," p. 2020. Available: https://doi.org/10.1101/2020.12.16.423030.

[169] S. Pareek, D. Valero, and M. Serrano, "Postharvest biology and technology of

pomegranate," *Journal of the Science of Food and Agriculture*, vol. 95, no. 12, pp. 2360–2379, 2015.

[170] U. Siripatrawan, Y. Makino, Y. Kawagoe, and S. Oshita, "Rapid detection of Escherichia coli contamination in packaged fresh spinach using hyperspectral imaging," *Talanta*, vol. 85, no. 1, pp. 276–281, 2011.

[171] L. Palou, J. Usall, J. A. Muñoz, J. L. Smilanick, and I. Viñas, "Hot water, sodium carbonate, and sodium bicarbonate for the control of postharvest green and blue molds of clementine mandarins," *Postharvest Biology and Technology*, vol. 24, no. 1, pp. 93–96, 2002.

[172] J. Li, W. Luo, Z. Wang, and S. Fan, "Early detection of decay on apples using hyperspectral reflectance imaging combining both principal component analysis and improved watershed segmentation method," *Postharvest Biology and Technology*, vol. 149, no. December 2018, pp. 235–246, 2019.

[173] A. Folch-Fortuny, J. M. Prats-Montalbán, S. Cubero, J. Blasco, and A. Ferrer, "VIS/NIR hyperspectral imaging and N-way PLS-DA models for detection of decay lesions in citrus fruits," *Chemometrics and Intelligent Laboratory Systems*, vol. 156, pp. 241–248, 2016.

[174] D. M. Bulanon, T. F. Burks, D. G. Kim, and M. A. Ritenour, "Citrus black spot detection using hyperspectral image analysis," *Agricultural Engineering International: CIGR Journal*, vol. 15, no. 3, pp. 171–180, 2013.

[175] N. P. Niphadkar, T. F. Burks, J. W. Qin, and M. A. Ritenour, "Estimation of citrus canker lesion size using hyperspectral reflectance imaging," *International Journal of Agricultural and Biological Engineering*, vol. 6, no. 3, pp. 41–51, 2013.

[176] Q. Liu, D. Zhou, S. Tu, H. Xiao, B. Zhang, Y. Sun, L. Pan, and K. Tu, "Quantitative visualization of fungal contamination in peach fruit using hyperspectral imaging," *Food Analytical Methods*, vol. 13, no. 6, pp. 1262–1270, 2020.

[177] Q. Liu, K. Sun, J. Peng, M. Xing, L. Pan, and K. Tu, "Identification of bruise and fungi contamination in strawberries using hyperspectral imaging technology and multivariate analysis," *Food Analytical Methods*, vol. 11, no. 5, pp. 1518–1527, 2018.

[178] Q. Gu, L. Sheng, T. Zhang, Y. Lu, Z. Zhang, K. Zheng, H. Hu, and H. Zhou, "Early

detection of tomato spotted wilt virus infection in tobacco using the hyperspectral imaging technique and machine learning algorithms," *Computers and Electronics in Agriculture*, vol. 167, p. 105066, 2019. Available: https://doi.org/10.1016/j.compag.2019.105066.

[179] C. Xie, Y. Shao, X. Li, and Y. He, "Detection of early blight and late blight diseases on tomato leaves using hyperspectral imaging.," *Nature Publishing Group*, vol. 5, p. 16564, 2015.

[180] N. Nguyen-Do-Trong, J. C. Dusabumuremyi, and W. Saeys, "Cross-polarized VNIR hyperspectral reflectance imaging for non-destructive quality evaluation of dried banana slices, drying process monitoring and control," *Journal of Food Engineering*, vol. 238, no. May, pp. 85–94, 2018.

[181] C. Xie, B. Chu, and Y. He, "Prediction of banana color and firmness using a novel wavelengths selection method of hyperspectral imaging," *Food Chemistry*, vol. 245, no. March 2017, pp. 132–140, 2018.

[182] W. Tan, L. Sun, F. Yang, W. Che, D. Ye, D. Zhang, and B. Zou, "The feasibility of early detection and grading of apple bruises using hyperspectral imaging," *Journal of Chemometrics*, vol. 32, no. 10, pp. 1–14, 2018.

[183] M.-T. C. Yi-Chich Chiu, Xing-Liang Chou, Tony E. Grift, "Automated detection of mechanically induced bruise areas in golden delicious apply using flourescence umagery," *Transactions of the ASABE*. vol. 58, no. 2, pp. 215–225, 2015.

[184] X. Luo, T. Takahashi, K. Kyo, and S. Zhang, "Wavelength selection in vis/NIR spectra for detection of bruises on apples by ROC analysis," *Journal of Food Engineering*, vol. 109, no. 3, pp. 457–466, 2012.

[185] C. Ferrari, G. Foca, R. Calvini, and A. Ulrici, "Fast exploration and classification of large hyperspectral image datasets for early bruise detection on apples," *Chemometrics and Intelligent Laboratory Systems*, vol. 146, pp. 108–119, 2015.

[186] X. Zhu, and G. Li, "Rapid detection and visualization of slight bruise on apples using hyperspectral imaging," *International Journal of Food Properties*, vol. 22, no. 1, pp. 1709–1719, 2019.

[187] M. H. Hu, Q. L. Dong, B. L. Liu, U. L. Opara, and L. Chen, "Estimating blueberry

mechanical properties based on random frog selected hyperspectral data," *Postharvest Biology and Technology*, vol. 106, pp. 1–10, 2015.

[188] G. A. Leiva-Valenzuela, R. Lu, and J. M. Aguilera, "Prediction of firmness and soluble solids content of blueberries using hyperspectral reflectance imaging," *Journal of Food Engineering*, vol. 115, no. 1, pp. 91–98, 2013.

[189] D. Chun-Wang, Y. Yang, Z. Jian-qiang, Z. Hong-kai, and L. Fei, "Detection of thrips defect on green-peel citrus using hyperspectral imaging technology combining PCA and B-spline lighting correction method," *Journal of Integrative Agriculture*, vol. 13, no. 10, pp. 2229–2235, 2014.

[190] T. H. Siregar, U. Ahmad, S. Sutrisno, and A. Maddu, "Mechanical damage detection of Indonesia local citrus based on fluorescence imaging," *IOP Conference Series: Earth and Environmental Science*, vol. 147, no. 1, p. 2018. Available: https//doi.org/10.1088/1755-1315/147/1/012006.

[191] R. Lu, and D. P. Ariana, "Detection of fruit fly infestation in pickling cucumbers using a hyperspectral reflectance/transmittance imaging system," *Postharvest Biology and Technology*, vol. 81, pp. 44–50, 2013.

[192] H. Cen, R. Lu, Q. Zhu, and F. Mendoza, "Nondestructive detection of chilling injury in cucumber fruit using hyperspectral imaging with feature selection and supervised classification," *Postharvest Biology and Technology*, vol. 111, pp. 352–361, 2016.

[193] J. Nogales-Bueno, J. M. Hernández-Hierro, F. J. Rodríguez-Pulido, and F. J. Heredia, "Determination of technological maturity of grapes and total phenolic compounds of grape skins in red and white cultivars during ripening by near infrared hyperspectral image: A preliminary approach," *Food Chemistry*, vol. 152, pp. 586–591, 2014.

[194] L. Feng, S. Zhu, L. Zhou, Y. Zhao, Y. Bao, C. Zhang, and Y. He, "Detection of subtle bruises on winter jujube using hyperspectral imaging with pixel-wise deep learning method.," *IEEE Access*, vol. 7, pp. 64494–64505, 2019.

[195] K. Yu, Y. Zhao, X. Li, Y. Shao, F. Zhu, and Y. He, "Identification of crack features in fresh jujube using Vis/NIR hyperspectral imaging combined with image processing.," *Computers and Electronics in Agriculture*. vol. 103, pp. 1–10, 2014.

[196] L. Wu, J. He, G. Liu, S. Wang, and X. He, "Detection of common defects on jujube

using Vis-NIR and NIR hyperspectral imaging," *Postharvest Biology and Technology*, vol. 112, pp. 134–142, 2016.

[197] H. Lu,, X. Yu,, L. Zhou, and Y. He, "Selection of spectral resolution and scanning speed for detecting green jujubes chilling injury based on hyperspectral reflectance imaging," *Applied Sciences (Switzerland)*, vol. 8, no. 4, p. 2018.

[198] A. Benelli, C. Cevoli, A. Fabbri, and L. Ragni, "Ripeness evaluation of kiwifruit by hyperspectral imaging," *Biosystems Engineering*, no. p. 2021. Avaliable: https://doi.org/10.1016/j.biosystemseng.2021.08.009.

[199] Q. Lü, M. J. Tang, J. R. Cai, J. W. Zhao, and S. Vittayapadung, "Vis/NIR hyperspectral imaging for detection of hidden bruises on kiwifruits," *Czech Journal of Food Sciences*, vol. 29, no. 6, pp. 595–602, 2011.

[200] S. Teerachaichayut, and H. T. Ho, "Non-destructive prediction of total soluble solids , titratable acidity and maturity index of limes by near infrared hyperspectral imaging," *Postharvest Biology and Technology*, vol. 133, no. July, pp. 20–25, 2017.

[201] K. Q. Yu, Y. R. Zhao, Z. Y. Liu, X. L. Li, F. Liu, and Y. He, "Application of visible and near-infrared hyperspectral imaging for detection of defective features in loquat," *Food and Bioprocess Technology*, vol. 7, no. 11, pp. 3077–3087, 2014.

[202] S. Munera, J. Gómez-Sanchís, N. Aleixos, J. Vila-Frances, G. Colelli, S. Cubero, E. Soler, and J. Blasco, "Discrimination of common defects in loquat fruit cv. 'Algerie' using hyperspectral imaging and machine learning techniques," *Postharvest Biology and Technology*, vol. 171, p. 111356, 2021.

[203] R. P. Haff, S. Saranwong, W. Thanapase, A. Janhiran, S. Kasemsumran, and S. Kawano, "Automatic image analysis and spot classification for detection of fruit fly infestation in hyperspectral images of mangoes," *Postharvest Biology and Technology*, vol. 86, pp. 23–28, 2013.

[204] P. Rungpichayapichet, M. Nagle, P. Yuwanbun, P. Khuwijitjaru, B. Mahayothee, and J. Müller, "Prediction mapping of physicochemical properties in mango by hyperspectral imaging," *Biosystems Engineering*, vol. 159, no. 2011, pp. 109–120, 2017.

[205] J. Li,, L. Chen, and W. Huang, "Detection of early bruises on peaches (Amygdalus

persica L.) using hyperspectral imaging coupled with improved watershed segmentation algorithm," *Postharvest Biology and Technology*, vol. 135, no. July 2017, pp. 104–113, 2018.

[206] X. Fu, and M. Wang, "Detection of early bruises on pears using fluorescence hyperspectral imaging technique," *Food Analytical Methods*, vol. 15, no. 1, pp. 115–123, 2022.

[207] X. Yu, H. Lu, and D. Wu, "Development of deep learning method for predicting firmness and soluble solid content of postharvest Korla fragrant pear using Vis/NIR hyperspectral reflectance imaging," *Postharvest Biology and Technology*, vol. 141, no. November 2017, pp. 39–49, 2018.

[208] H. Q. Dang, I. Kim, B. K. Cho, and M. S. Kim, "Detection of bruise damage of pear using hyperspectral imagery," *International Conference on Control, Automation and Systems*, pp. 1258–1260, 2012.

[209] R. Khodabakhshian, and B. Emadi, "Application of Vis/SNIR hyperspectral imaging in ripeness classification of pear," *International Journal of Food Properties*, vol. 20, no. 3, pp. S3149–S3163, 2018.

[210] X. Wei,, F. Liu,, Z. Qiu,, Y. Shao, and Y. He, "Ripeness classification of astringent persimmon using hyperspectral imaging technique," *Food and Bioprocess Technology*, vol. 7, no. 5, pp. 1371–1380, 2014.

[211] S. Munera, A. Rodríguez-Ortega, N. Aleixos, S. Cubero, J. Gómez-Sanchis, and J. Blasco, "Detection of invisible damages in 'rojo brillante' persimmon fruit at different stages using hyperspectral imaging and chemometrics,." *Foods*. vol. 10, no. 9, p. 2170, 2021.

[212] S. Munera, F. Hernández, N. Aleixos, S. Cubero, and J. Blasco, "Maturity monitoring of intact fruit and arils of pomegranate cv. ' Mollar de Elche ' using machine vision and chemometrics," *Postharvest Biology and Technology*, vol. 156, no. April, p. 110936, 2019.

[213] M. Fashi, L. Naderloo, and H. Javadikia, "Pomegranate grading based on pH using image processing and artificial intelligence," *Journal of Food Measurement and Characterization*. no. 0123456789, p. 2020.

[214] B. Li, M. Cobo-Medina, J. Lecourt, N. B. Harrison, R. J. Harrison, and J. V. Cross, "Application of hyperspectral imaging for nondestructive measurement of plum quality attributes," *Postharvest Biology and Technology*, vol. 141, no. March, pp. 8–15, 2018.

[215] N. Goel, and P. Sehgal, "Fuzzy classification of pre-harvest tomatoes for ripeness estimation - An approach based on automatic rule learning using decision tree," *Applied Soft Computing*, vol. 36, pp. 45–56, 2015.

[216] B. K. Cho, M. S. Kim, I. S. Baek, D. Y. Kim, W.-H. Lee, J. Kim, H. Bae, Y.-S. Kim, "Detection of cuticle defects on cherry tomatoes using hyperspectral fluorescence imagery," *Postharvest Biology and Technology*, vol. 76, pp. 40–49, 2013.

[217] A. Rahman, E. Park, H. Bae, and B.-K. Cho, "Hyperspectral imaging technique to evaluate the firmness and the sweetness index of tomatoes," *Agricultural Science Korean Journal of Agricultural Science*, vol. 45, no. 4, pp. 823–837, 2018.

[218] J. V. Roy, J. C. Keresztes, N. Wouters, B. De Ketelaere, and W. Saeys, "Measuring colour of vine tomatoes using hyperspectral imaging," *Postharvest Biology and Technology*, vol. 129, pp. 79–89, 2017.

[219] Q. Zhu, C. He, R. Lu, F. Mendoza, and H. Cen, "Ripeness evaluation of 'Sun Bright' tomato using optical absorption and scattering properties," *Postharvest Biology and Technology*, vol. 103, pp. 27–34, 2015.

[220] S. Shrestha, L. C. Deleuran, and R. Gislum, "Classification of different tomato seed cultivars by multispectral visible-near infrared spectroscopy and chemometrics," *Journal of Spectral Imaging*, vol. 5, pp. 1255, 2016. Available: https//doi/10.1255/jsi.2016.a1.

[221] S. Shrestha, L. C. Deleuran, M. H. Olesen, and R. Gislum, "Use of multispectral imaging in varietal identification of tomato," *Sensors (Switzerland)*, vol. 15, no. 2, pp. 4496–4512, 2015.

[222] Z. L. Xiong, C, Liu, C, Pan W, Ma F, Xiong C, Qi L, Chen F, Lu X, Yang J, "Non-destructive determination of total polyphenols content and classification of storage periods of Iron Buddha tea using multispectral imaging system," *Food Chemistry*, vol. 176, pp. 130–136., 2015.

[223] N. Shetty, M. H. Olesen, R. Gislum, L. C. Deleuran, and B. Boelt, “Use of partial least squares discriminant analysis on visible-near infrared multispectral image data to examine germination ability and germ length in spinach seeds,” *Journal of Chemometrics*, vol. 26, no. 8–9, pp. 462–466, 2012.

[224] S. Lohumi, H. Bae, Y.-W. Seo, D.-Y. Kim, S. Lohumi, E. Park, and B.-K. Cho,” Development of non-destructive sorting technique for viability of watermelon seed by using hyperspectral image processing,” *Journal of the Korean Society for Nondestructive Testing*, vol. 36, no. 1, pp. 35–44, 2016. Available: http://dx.doi.org/10.7779/JKSNT.2016.36.1.35.

[225] Y. Guo, H. Ding, J. Xu, and H. Xu, “Clustering analysis based on hyperspectral DN values of waste oil,” *Remote Sensing for Land & Resources*, vol. 26, pp. 37–41, 2014. Available: https://www.gtzyyg.com/EN/10.6046/gtzyyg.2014.01.

[226] O. J. Martinez-Gila, D. Cano-Marchal, P. Gámez-Garcia, and J. Gómez, “Hyperspectral imaging for determination of some quality parameters for olive oil,” *In: Proceedings of the 18th International Conference on Automation and Computing (ICAC), Loughborough, UK*. pp. 7–8, 2012.

[227] V. Lakshmi, and A. Pradesh, “Some adultered foods in market and linked especially by children,” *International Journal of Science and Innovative Technology*, vol. 1, no. 2, pp. 106–113, 2012.

[228] I. Orrillo, J. P. Cruz-Tirado, A. Cardenas, M. Oruna, A. Carnero, D. F. Barbin, and R. Siche, “Hyperspectral imaging as a powerful tool for identification of papaya seeds in black pepper,” *Food Control*, vol. 101, pp. 45–52, 2019.

[229] M. Sandasi, W. Chen, I. Vermaak, and A. Viljoen, “Non-destructive quality assessment of herbal tea blends using hyperspectral imaging,” *Phytochemistry Letters*, vol. 24, pp. 94–101, 2018.

[230] H. Eksi-Kocak, O. Mentes-Yilmaz, and I. H. Boyaci, “Detection of green pea adulteration in pistachio nut granules by using Raman hyperspectral imaging,” *European Food Research and Technology*, vol. 242, no. 2, pp. 271–277, 2016.

[231] A. A. Adedeji, N. Ekramirad, A. Rady, and A. Hamidisepehr, “Non-destructive technologies for detecting insect infestation in fruits and vegetables under postharvest

conditions: A critical review," *Foods.* vol. 9, pp. 1–28, 2020.

[232] W. Wang, C. Li, E. W. Tollner, R. D. Gitaitis, and G. C. Rains, "Shortwave infrared hyperspectral imaging for detecting sour skin (Burkholderia cepacia)-infected onions," *Journal of Food Engineering*, vol. 109, no. 1, pp. 38–48, 2012.

[233] Z. Zhong, J. Li, Z. Luo, and M. Chapman, "Spectral-spatial residual network for hyperspectral image classification: A 3-D deep learning framework," *IEEE Transactions on Geoscience and Remote Sensing*, vol. 56, no. 2, pp. 847–858, 2018.

[234] N. Wambugu, Y. Chen, Z. Xiao, K. Tan, M. Wei, X. Liu, and J. Li, "Hyperspectral image classification on insufficient-sample and feature learning using deep neural networks: A review," *International Journal of Applied Earth Observation and Geoinformation*, vol. 105, p. 102603, 2021.

[235] M. Castelluccio, G. Poggi, C. Sansone, and L. Verdoliva, "Land use classification in remote sensing images by convolutional neural networks," pp. 1–11, 2015. Available: http://arxiv.org/abs/1508.00092.

[236] V. Mnih,, K. Kavukcuoglu,, D. Silver, et al., "Human-level control through deep reinforcement learning.," *Nature*. vol. 518, no. 7540, pp. 529–533, 2015.

[237] Y. D. Zhang, Z. Dong, X. Chen, W. Jia, S. Du, K. Muhammad, and S. Wang, "Image based fruit category classification by 13-layer deep convolutional neural network and data augmentation.," *Multimedia Tools and Applications*. vol. 78, no. 3, pp. 3613–3632, 2019.

[238] J. J. Bird, C. M. Barnes, L. J. Manso,, A. Ekárt, and D. R. Faria, "Fruit quality and defect image classification with conditional GAN data augmentation," *Scientia Horticulturae*, vol. 293, no. April 2021, p. 2022.

[239] U. L. Opara, and P. B. Pathare, "Bruise damage measurement and analysis of fresh horticultural produce — A review," *Postharvest Biology and Technology*, vol. 91, pp. 9–24, 2014.

[240] R. Spielmanns, J. Spielmanns, L. Damerow, and M. M. Blanke, "Non-destructive determination of surface features of pomegranate fruit," vol. 1137, pp. 247–250, 2016.

[241] A. Khoshroo, A. Keyhani, S. Rafiee, R. A. Zoroofi, and Z. Zamani, "Pomegranate quality evaluation using machine vision," *Acta Horticulturae*, vol. 818, pp. 347–352,

2009.

[242] L. Czieczor, C. Bentkamp, L. Damerow, and M. Blanke, “Non-invasive determination of the quality of pomegranate fruit,” *Postharvest Biology and Technology*, vol. 136, no. October 2017, pp. 74–79, 2018.

[243] I. Matityahu, P. Marciano, D. Holland, R. Ben-Arie, and R. Amir, “Differential effects of regular and controlled atmosphere storage on the quality of three cultivars of pomegranate (Punica granatum L.),” *Postharvest Biology and Technology*, vol. 115, pp. 132–141, 2016.

[244] A. Khoshroo, A. Keyhani, R. A. Zoroofi, S. Rafiee, Z. Zamani, and M. R. Alsharif, “Classification of pomegranate fruit using texture analysis of MR images,” *Agricultural Engineering International: CIGR Journal*. vol. 11, no. 1182, p. 2009.

[245] E. E. Okere, “Non-invasive measurement of quality attributes of processed pomegranate products,” Masters thesis, Stellenbosch University, 2020.

[246] K. Dhinesh, and D. Ramasamy, “Pomegranate processing and value addition: review.,” *Journal of Food Processing & Technology*, vol. 07, no. 03, p. 2016.

[247] E. A. Akuru, C. T. Mpendulo, C. E. Oyeagu, and C. W. T. Nantapo, “Pomegranate (Punica granatum L.) peel powder meal supplementation in broilers: effect on growth performance, digestibility, carcase and organ weights, serum and some meat antioxidant enzyme biomarkers,” *Italian Journal of Animal Science*, vol. 20, no. 1, pp. 119–131, 2021.

[248] E. A. Akuru, C. E. Oyeagu, T. C. Mpendulo, F. Rautenbach, and O. O. Oguntibeju, “Effect of pomegranate (Punica granatum L) peel powder meal dietary supplementation on antioxidant status and quality of breast meat in broilers,” *Heliyon*, vol. 6, no. 12, p. e05709, 2020. Available: https://doi.org/10.1016/j.heliyon.2020.e05709.

[249] T. P. Magangana, N. P. Makunga, C. la Grange, M. A. Stander,, O. A. Fawole, and U. L. Opara, “Blanching pre-treatment promotes high yields, bioactive compounds, antioxidants, enzyme inactivation and antibacterial activity of ‘wonderful’ pomegranate peel extracts at three different harvest maturities,” *Antioxidants*, vol. 10, no. 7, p. 1119, 2021.

[250] T. P. Magangana, N. P. Makunga, O. A. Fawole, M. A. Stander, and U. L. Opara, "Antioxidant, antimicrobial, and metabolomic characterization of blanched pomegranate peel extracts: effect of cultivar," *Molecules*, vol. 27, no. 9, pp. 1–24, 2022.

[251] L. Zhang, and M. J. McCarthy, "Assessment of pomegranate postharvest quality using nuclear magnetic resonance," *Postharvest Biology and Technology*, vol. 77, pp. 59–66, 2013.

[252] A. R. Kumar, V. S. Rajpurohit, and K. Y. Bidari, "Multi class grading, and quality assessment of pomegranate fruits based on physical and visual parameters multi class grading and quality assessment of pomegranate fruits based on physical and visual," *International Journal of Fruit Science*, vol. 19, no. 4, pp. 372–396, 2019.

[253] W. H. Su, and D. W. Sun, "Fourier transform infrared and Raman and hyperspectral imaging techniques for quality determinations of powdery foods: a review," *Comprehensive Reviews in Food Science and Food Safety*. vol. 17, no. 1, pp. 104–122, 2018.

[254] W. H. Su, H. J. He, and D. W. Sun, "Non-Destructive and rapid evaluation of staple foods quality by using spectroscopic techniques: A review," *Critical Reviews in Food Science and Nutrition*, vol. 57, no. 5, pp. 1039–1051, 2017.

[255] O. P. Zhen, N. Hashim, and B. Maringgal, "Quality evaluation of mango using non-destructive approaches: A review," *Journal of Agricultural and Food Engineering*, vol. 1, no. 0003, pp. 2716-6236, 2020. Available: http://doi.org/10.37865/jafe.2020.0003.

[256] T. Sun, K. Huang, H. Xu, and Y. Ying, "Research advances in nondestructive determination of internal quality in watermelon / melon: A review," *Journal of Food Engineering*, vol. 100, no. 4, pp. 569–577, 2010.

[257] N. P. Seeram, Y. Zhang, J. D. Reed, C. G. Krueger, and J. Vaya, "Pomegranates. In: Ancient Roots to Modern Medicine", *Medicinal and Aromatic Plants — Industrial Profiles*, vol. 43, 2006. Available: https//doi.org/ 10.1017/CBO9781107415324.004.

[258] J. A. Teixeira da Silva, T. S. Rana, D. Narzary, N. Verma, D. T. Meshram, and S. A. Ranade, "Pomegranate biology and biotechnology: A review," *Scientia Horticulturae*.

vol. 160, pp. 85–107, 2013.

[259] S. Fukuda, “Emotion and Innovation,” *Springer Link*. vol. 2, pp. 11–21, 2013.

[260] D. M. Barrett, J. C. Beaulieu, and R. Shewfelt, “Color, flavor, texture, and nutritional quality of fresh-cut fruits and vegetables: Desirable levels, instrumental and sensory measurement, and the effects of processing,” *Critical Reviews in Food Science and Nutrition*. vol. 50, no. 5, pp. 369–389, 2010.

[261] I. K. Opara, O. A. Fawole, C. Kelly, and U. L. Opara, “Quantification of on-farm pomegranate fruit postharvest losses and waste, and implications on sustainability indicators: South African case study,” *Sustainability (Switzerland)*, vol. 13, no. 9, pp. 1–20, 2021.

[262] I. K. Opara, O. A. Fawole, and U. L. Opara, “Postharvest losses of pomegranate fruit at the packhouse and implications for sustainability indicators,” *Sustainability (Switzerland)*, vol. 13, no. 9, p. 2021.

[263] A. J. Zele, B. Feigl, P. Adhikari, M. L. Maynard, and D. Cao, “Melanopsin photoreception contributes to human visual detection, temporal and colour processing,” *Scientific Reports*, vol. 8, no. 1, pp. 1–10, 2018.

[264] F. A. Al-Said, L. U. Opara, and R. A. Al-Yahyai, “Physico-chemical and textural quality attributes of pomegranate cultivars (Punica granatum L.) grown in the Sultanate of Oman,” *Journal of Food Engineering*, vol. 90, no. 1, pp. 129–134, 2009.

[265] N. Ekrami-Rad, J. Khazaei, and M. H. Khoshtaghaza, “Selected mechanical properties of pomegranate peel and fruit,” *International Journal of Food Properties*, vol. 14, no. 3, pp. 570–582, 2011.

[266] M. A. Rao, and J. F. Steffe, “Viscoelastic properties of foods.,” *New York, USA: Elsevier Applied Science.* p. 1992.

[267] I. H. L. Cavalcante, L. F. Cavalcante, J. M. de Sousa Miranda, and A. B. G. Martins, “Physical and chemical characteristics of tropical and non-conventional fruits,” *Food Industrial Processes - Methods and Equipment*, 2012. Available: https//doi.org/10.5772/30871.

[268] O. A. Fawole, and U. L. Opara, “Changes in physical properties, chemical and elemental composition and antioxidant capacity of pomegranate (cv. Ruby) fruit at five

maturity stages," *Scientia Horticulturae*, vol. 150, pp. 37–46, 2013.

[269] O. A. Fawole, and U. L. Opara, "Effects of maturity status on biochemical content, polyphenol composition and antioxidant capacity of pomegranate fruit arils (cv. 'Bhagwa')," *South African Journal of Botany*, vol. 85, pp. 23–31, 2013.

[270] A. O. Adetoro,, U. L. Opara, and O. A. Fawole, "Effect of hot-air and freeze-drying on the quality attributes of dried pomegranate (Punica granatum L.) arils during long-term cold storage of whole fruit," *Agriculture (Switzerland)*. vol. 10, no. 11, pp. 1–16, 2020.

[271] T. Kaseke, U. L. Opara, and O. A. Fawole, "Effect of microwave pretreatment of seeds on the quality and antioxidant capacity of pomegranate seed oil," *Foods*, vol. 9, no. 9, p. 2020.

[272] T. Kaseke, O. A. Fawole, L. Mokwena, and U. L. Opara, "Effect of cultivar and blanching of pomegranate seeds on physicochemical properties, nutritional qualities and antioxidant capacity of extracted oil," *Journal of Food Measurement and Characterization*, vol. 15, no. 1, pp. 93–106, 2021.

[273] M. Viuda-Martos, J. Fernández-Lóaez, and J. A. Pérez-álvarez, "Pomegranate and its many functional components as related to human health: A review," *Comprehensive Reviews in Food Science and Food Safety*, vol. 9, no. 6, pp. 635–654, 2010.

[274] A. Parashar, S. K. Gupta, and A. Kumar, "Studies on separation techniques of pomegranate seeds and their effect on quality of Anardana," *African Journal of Biochemistry Research*, vol. 3, no. 10, pp. 340–343, 2009.

[275] V. More, B. Kapse, A. Kadam, and L. Pimpalpalle, "Studies on drying of pomegranate arils for preparation of Anardana,"*International Journal of Chemical Studies*, vol. 5, no. 3, pp. 724–728, 2017.

[276] A. O. Adetoro, U. L. Opara, and O. A. Fawole, "Effect of blanching on enzyme inactivation, physicochemical attributes and antioxidant capacity of hot-air dried pomegranate (Punica granatum l.) arils (cv. wonderful)," *Processes*, vol. 9, no. 1, pp. 1–18, 2021.

[277] P. Bakshi, B. Bhushan, V. K. Wali, M. Bakshi, A. Sharma, and D. J. Bhat, "Standardization of drying method and organoleptic evaluation of wild pomegranate (Anardana) seeds," *World Journal of Agricultural Sciences*, vol. 9, no. 5, pp. 397 -

400, 2013. Available: https//doi.org/ 10.5829/idosi.wjas.2013.9.5.1750.

[278] D. Singh, M. Chaudhary, M. L. Meena, L. Wangchu, and H. Dayal, "Drying of pomegranate seeds (Anardana) under different conditions," *Acta Horticulturae*, no. 890, pp. 433–439, 2015. Available: https//doi.org/10.17660/ActaHortic.2011.890.59.

[279] A. Khoddami, Y. B. C. Man, and T. H. Roberts, "Physico-chemical properties and fatty acid profile of seed oils from pomegranate (Punica granatum L.) extracted by cold pressing," *European Journal of Lipid Science and Technology*, vol. 116, no. 5, pp. 553–562, 2014.

[280] C. Venkata, S. Prakash, and I. Prakash, "Bioactive chemical constituents from pomegranate (Punica granatum) juice, seed and peel-A review," *Journal of Research in Chemistry and Environment*, vol. 1, no. 1, pp. 1–181, 2011.

[281] T. Kaseke, U. L. Opara, and O. A. Fawole, "Novel seeds pretreatment techniques: effect on oil quality and antioxidant properties: a review," *Journal of Food Science and Technology*, 2021. Available: https://doi.org/10.1007/s13197-021-04981-1.

[282] A. Paul, and M. Radhakrishnan, "Pomegranate seed oil in food industry: Extraction, characterization, and applications," *Trends in Food Science and Technology*, vol. 105, no. September, pp. 273–283, 2020.

[283] R. R. Mphahlele, "Impacts of preharvest and postharvest handling and processing on bioactive compounds and functional properties of pomegranate fruit fractions and by-products," Doctorate thesis, Stellenbosch University, 2016.

[284] R. R. Mphahlele, O. J. Caleb, O. A. Fawole, and U. L. Opara, "Effects of different maturity stages and growing locations on changes in chemical, biochemical and aroma volatile composition of 'Wonderful' pomegranate juice," *Journal of the Science of Food and Agriculture*, vol. 96, no. 3, pp. 1002–1009, 2016.

[285] R. R. Mphahlele, O. A. Fawole, L. M. Mokwena, and U. L. Opara, "Effect of extraction method on chemical, volatile composition and antioxidant properties of pomegranate juice," *South African Journal of Botany*, vol. 103, pp. 135–144, 2016.

[286] A. M. Mouazen,, B. Nicolaï, and L. A. Terry, "The use of Vis / NIRS and chemometric analysis to predict fruit defects and postharvest behaviour of ' Nules Clementine ' mandarin fruit," *Food Chemistry*. vol. 163, pp. 267–274, 2014.

[287] J. B. M. Nicolaï, I. Bulens, J. De Baerdemaker, B. De Ketelaere, M. L. A. T. M. Hertog, P. Verboven, and K. Lammertyn, "Non-Destructive evaluation: detection of external and internal attributes frequently associated with quality and damage," Postharvest Handling (Third Edition) A Systems Approach. pp. 363–385, 2014.

[288] R. Khodabakhshian, B. Emadi, M. Khojastehpour, M. R. Golzarian, and A. Sazgarnia, "Quick quality evaluation of pomegranate arils using NIR spectroscopy. *Iranian Research Organisation for Food Science and Technology*, vol. 2, pp. 103–114, 2015.

[289] E. Arendse, O. A. Fawole, L. S. Magwaza, H. Nieuwoudt, and U. L. Opara, "Evaluation of biochemical markers associated with the development of husk scald and the use of diffuse reflectance NIR spectroscopy to predict husk scald in pomegranate fruit," *Scientia Horticulturae*, vol. 232, pp. 240–249, 2018.

[290] B. Jamshidi, E. Mohajerani, H. Farazmand, A. Mahmoudi, and A. Hemmati, "Pattern recognition-based optical technique for non-destructive detection of Ectomyelois ceratoniae infestation in pomegranates during hidden activity of the larvae," *Spectrochimica Acta - Part A: Molecular and Biomolecular Spectroscopy*, vol. 206, pp. 552–557, 2019.

[291] R. Khodabakhshian, "Feasibility of using Raman spectroscopy for detection of tannin changes in pomegranate fruits during maturity," *Scientia Horticulturae*, vol. 257, no. July, p. 108670, 2019.

[292] E. Arendse, O. A. Fawole, L. S. Magwaza, H. Nieuwoudt, and U. L. Opara, "Comparing the analytical performance of near and mid infrared spectrometers for evaluating pomegranate juice quality," *Food Science and Technology,* vol. 91, pp. 180–190, 2018.

[293] H. Vardin, A. Tay, B. Ozen, and L. Mauer, "Authentication of pomegranate juice concentrate using FTIR spectroscopy and chemometrics," *Food Chemistry*, vol. 108, no. 2, pp. 742–748, 2008.

[294] R. Boggia, M. C. Casolino, V. Hysenaj, P. Oliveri, and P. Zunin, "A screening method based on UV-Visible spectroscopy and multivariate analysis to assess addition of filler juices and water to pomegranate juices," *Food Chemistry*, vol. 140, no. 4, pp. 735–741, 2013.

[295] E. E. Okere, H. Nieuwoudt, W. J. Perold, and U. L. Opara, “Non-destructive evaluation of the quality characteristics of pomegranate kernel oil by fourier transform near-infrared and mid-infrared spectroscopy,” *Frontiers in Plant Science*, vol. 13, 2022. Available: https://doi.org/10.3389/fpls.2022.867555.

[296] O. Uncu, A. Napiórkowska, T. K. Szajna, and B. Ozen, “Evaluation of three spectroscopic techniques in determination of adulteration of cold pressed pomegranate seed oils,” *Microchemical Journal*, vol. 158, p. 105128, 2020. Available: https://doi.org/10.1016/j.microc.2020.105128.

[297] V. Adiani, S. Gupta, R. Ambolikar, and P. S. Variyar, “Development of rapid method to assess microbial quality of minimally processed pomegranate arils using FTIR.,” *Sensors and Actuators, B: Chemical*, vol. 260, pp. 800–807, 2018.

[298] D. Yang, and Y. Ying, “Applications of Raman spectroscopy in agricultural products and food analysis: A review,” *Applied Spectroscopy Reviews*, vol. 46, no. 7, pp. 539–560, 2011.

[299] C. V. Raman, and K. S. Krishnan, “A new type of secondary radiation,” *Nature*, 1928.

[300] Y. Xu, P. Zhong, A. Jiang, X. Shen, X. Li, Z. Xu, Y. Shen, Y. Sun, and H. Lei, “Raman spectroscopy coupled with chemometrics for food authentication: A review.,” *Trends in Analytical Chemistry*, vol. 131, p. 2020.

[301] A. M. Nikbakht, T. T. Hashjin, R. Malekfar, and B. Gobadian, “Nondestructive determination of tomato fruit quality parameters using Raman spectroscopy,” *Journal of Agricultural Science and Technology*, vol. 13, pp. 517 – 526, 2011.

[302] R. Khodabakhshian, and M. H. Abbaspour-Fard, “Pattern recognition-based Raman spectroscopy for non-destructive detection of pomegranates during maturity,” *Spectrochimica Acta - Part A: Molecular and Biomolecular Spectroscopy*, vol. 231, pp. 118 - 127, 2020. Available: https://doi.org/10.1016/j.saa.2020.118127.

[303] A. Bhargava, and A. Bansal, “Fruits and vegetables quality evaluation using computer vision : A review,” *Journal of King Saud University - Computer and Information Sciences*, vol. 33, no. 3, pp. 243–257, 2021.

[304] D. P. Penumuru,, S. Muthuswamy, and P. Karumbu, “Identification and classification of materials using machine vision and machine learning in the context of industry 4.0,”

Journal of Intelligent Manufacturing, vol. 31, no. 5, pp. 1229–1241, 2020.

[305] J. Blasco, S. Cubero-García, S. Alegre-Sosa, J. Gómez-Sanchís, V. López-Rubira, and E. Moltó, "Automatic inspection of the pomegranate (Punica granatum L.) arils quality by means of computer vision," *Spanish Journal of Agricultural Research*, vol. 6, no. 1, pp. 12–16, 2008.

[306] J. Blasco, S. Cubero, J. Gómez-Sanchís, P. Mira, and E. Moltó, "Development of a machine for the automatic sorting of pomegranate (Punica granatum) arils based on computer vision," *Journal of Food Engineering*, vol. 90, no. 1, pp. 27–34, 2009.

[307] S. Srivastava, and S. Sadistap, "Data processing approaches and strategies for non-destructive fruits quality inspection and authentication: a review," *Journal of Food Measurement and Characterization*, vol. 12, no. 4, pp. 2758–2794, 2018.

[308] C. Akin, M. Kirci, E. O. Gunes, and Y. Cakir, "Detection of the pomegranate fruits on tree using image processing," 2012 *1st International Conference on Agro-Geoinformatics, Agro-Geoinformatics 2012*, vol. 2, pp. 632–636, 2012.

[309] A. Bakhshipour, A. Jafari, and S. M. Hosseini, "Recognition of pomegranate on tree and stereoscopic locating of the fruit," *American-Eurasian Journal of Agricultural & Environmental Sciences*, vol. 12, no. 10, pp. 1288–1294, 2012.

[310] S. K. Behera, A. Pattnaik, A. K. Rath, N. K. Barpanda, and P. K. Sethy, "Yield estimation of pomegranate using image processing techniques," *International Journal of Innovative Technology and Exploring Engineering*, vol. 8, no. 6, pp. 798–803, 2019.

[311] F. Salmanizadeh, S. M. Nassiri, A. Jafari, and M. H. Bagheri, "Volume estimation of two local pomegranate fruit (Punica granatum L.) cultivars and their components using non-destructive X-ray computed tomography technique.," *International Journal of Food Properties*. vol. 18, no. 2, pp. 439–455, 2015.

[312] L. Zhang, and M. J. McCarthy, "Black heart characterization and detection in pomegranate using NMR relaxometry and MR imaging," *Postharvest Biology and Technology*. vol. 67, pp. 96–101, 2012.

[313] B. Nouri, S. S. Mohtasebi, and S. Rafiee, "Quality detection of pomegranate fruit infected with fungal disease," *International Journal of Food Properties*, vol. 23, no. 1, pp. 9–21, 2020.

[314] A. Sanaeifar, S. S. Mohtasebi, M. Ghasemi-varnamkhasti, and M. M. Shafie, "Evaluation of an electronic nose system for characterization of pomegranate varieties," *AgricEngInt: CIGR Journal*. vol. 18, no. 3, pp. 317–323, 2016.

[315] G. Payel, and C. Sunil, "Quality analysis of pomegranate by non-destructive soft x-ray method," *Journal of Food Processing & Technology*, vol. 05, no. 06, p. 2014.

[316] J. F. I. Nturambirwe, "Advances in spectral techniques for fruit quality evaluation: case of ULF-NMR and NIRS," Doctorate thesis, Stellenbosch University, 2017.

[317] J. Stepisnik, "Spectroscopy: NMR down to Earth," *Nature*. vol. 439, no. 7078, pp. 799–801, 2006.

[318] K. Eberle, "Evaluation of near infrared and nuclear magnetic resonance spectroscopy for rapid quality control of South African extra virgin olive oils," Doctorate thesis, Stellenbosch University, 2005.

[319] L. Schoeman, P. Williams, A. du Plessis, and M. Manley, "X-ray micro-computed tomography (μCT) for non-destructive characterisation of food microstructure," *Trends in Food Science and Technology*, vol. 47, pp. 10–24, 2016.

[320] A. du Plessis,, C. Broeckhoven,, A. Guelpa, and S. G. le Roux, "Laboratory x-ray micro-computed tomography: A user guideline for biological samples.," *GigaScience*. vol. 6, no. 6, pp. 1–11, 2017.

[321] E. Arendse, O. A. Fawole, and U. L. Opara, "Discrimination of pomegranate fruit quality by instrumental and sensory measurements during storage at three temperature regimes," *Journal of Food Processing and Preservation*, pp. 1745–4549, 2014.

[322] A. Léonard, S. Blacher, C. Nimmol, and S. Devahastin, "Effect of far-infrared radiation assisted drying on microstructure of banana slices: An illustrative use of X-ray microtomography in microstructural evaluation of a food product," *Journal of Food Engineering*, vol. 85, no. 1, pp. 154–162, 2008.

[323] E. Arendse, O. A. Fawole, L. S. Magwaza, and U. L. Opara, "Estimation of the density of pomegranate fruit and their fractions using X-ray computed tomography calibrated with polymeric materials," *Biosystems Engineering*, vol. 148, pp. 148–156, 2016.

[324] E. Arendse, O. A. Fawole, L. S. Magwaza, and U. L. Opara, "Non-destructive estimation of pomegranate juice content of intact fruit using X-ray computed

tomography," *Acta Hortic*, pp. 1201, https://doi.org/10.17660/ActaHortic.2018.1201.40. 2018.

[325] E. Arendse, O. A. Fawole, L. S. Magwaza, and U. L. Opara, "Non-destructive characterization and volume estimation of pomegranate fruit external and internal morphological fractions using X-ray computed tomography," *Journal of Food Engineering*, vol. 186, pp. 42–49, 2016.

[326] Z. Hussein, "Bruise damage susceptibility of pomegranates. Doctorate thesis, Stellenbosch University, 2019.

[327] M. Kamruzzaman, D. Barbin, G. Elmasry, D. W. Sun, and P. Allen, "Potential of hyperspectral imaging and pattern recognition for categorization and authentication of red meat," *Innovative Food Science and Emerging Technologies*, vol. 16, pp. 316–325, 2012.

[328] A. A. Gowen, Y. Feng, E. Gaston, and V. Valdramidis, "Recent applications of hyperspectral imaging in microbiology," *Talanta*, vol. 137, pp. 43–54, 2015.

[329] W. H. Su, and D. W. Sun, "Potential of hyperspectral imaging for visual authentication of sliced organic potatoes from potato and sweet potato tubers and rapid grading of the tubers according to moisture proportion," *Computers and Electronics in Agriculture*, vol. 125, pp. 113–124, 2016.

[330] W. Su, and D. Sun, "Multispectral imaging for plant food quality analysis and visualization," *Comprehensive Reviews in Food Science and Food Safety*, vol. 17, pp. 220–239, 2018.

[331] F. W. Hong, and K. S. Chia, "A review on recent near infrared spectroscopic measurement setups and their challenges," *Measurement: Journal of the International Measurement Confederation*, vol. 171, no. November 2020, p. 108732, 2021.

[332] Z. Hussein, O. A. Fawole, and U. L. Opara, "Bruise damage susceptibility of pomegranates (Punica granatum, L.) and impact on fruit physiological response during short term storage," *Scientia Horticulturae*. vol. 246, no. June 2018, pp. 664–674, 2019.

[333] M. M. Shafie, A. Rajabipour, and H. Mobli, "Determination of bruise incidence of pomegranate fruit under drop case," *International Journal of Fruit Science*, vol. 17,

no. 3, pp. 296–309, 2017. Available: https://doi.org/10.1080/15538362.2017.1295416.

[334] E. Ahmadi, H. Barikloo, and B. Soliemani, “The effect of fruit properties on the apricot bruises susceptibility,” *Journal of Food Measurement and Characterization*, vol. 8, no. 1, pp. 46–53, 2014.

[335] Z. Hussein, O. A. Fawole, and U. L. Opara, “Bruise damage susceptibility of pomegranates (Punica granatum, L.) and impact on fruit physiological response during short term storage,” *Scientia Horticulturae*, vol. 246, pp. 664–674, 2019.

[336] I. Kahramanoglu, and S. Usanmaz, Pomegranate production and marketing,” *CRC Press Taylor & Francis Group, 2016.* Available: http://www.copyright.com/.

[337] O. A. Fawole, and U. L. Opara, “Fruit growth dynamics, respiration rate and physico-textural properties during pomegranate development and ripening,” *Scientia Horticulturae*, vol. 157, pp. 90–98, 2013.

[338] POMASA, “The economic contribution of South Africa’s pomegranate industry,” *Division for Macro & Resource Economics of the Western Cape Department of Agriculture (WCDoA) in collaboration with the Pomegranate Producers Association of South Africa (POMASA)*, March, pp. 1–29, 2021.

[339] Z. Hussein,, O. A. Fawole, and U. L. Opara, “Determination of physical, biochemical and microstructural changes in impact-bruise damaged pomegranate fruit.,” *Journal of Food Measurement and Characterization*. vol. 13, no. 3, pp. 2177–2189, 2019.

[340] M. M. Shafie, A. Rajabipour, S. Castro-García, F. Jiménez-Jiménez, and H. Mobli, “Effect of fruit properties on pomegranate bruising,” *International Journal of Food Properties*, vol. 18, no. 8, pp. 1837–1846, 2015. Available: https://doi.org/10.1080/10942912.2014.948188.

[341] M. Van Zeebroeck, V. Van linden, H. Ramon, J. De Baerdemaeker, B. M. Nicolaï, and E. Tijskens, “Impact damage of apples during transport and handling,” *Postharvest Biology and Technology*, vol. 45, no. 2, pp. 157–167, 2007.

[342] J. Xing, and J. De Baerdemaeker, “Bruise detection on ‘ Jonagold ’ apples using hyperspectral imaging,” *Postharvest Biology and Technology*, vol. 37, pp. 152–162, 2005.

[343] D. Wu, and D. W. Sun, “Advanced applications of hyperspectral imaging technology

for food quality and safety analysis and assessment: A review - Part I: Fundamentals," *Innovative Food Science and Emerging Technologies*, vol. 19, pp. 1–14, 2013.

[344] S. Fan, J. Li, Y. Zhang, X. Tian, Q. Wang, X. He, C. Zhang, and W. Huang, "On line detection of defective apples using computer vision system combined with deep learning methods," *Journal of Food Engineering*, vol. 286, no. November 2019, p. 110102, 2020.

[345] K. Sethi, A. Gupta, G. Gupta, and V. Jaiswal, "Comparison of machine learning algorithms on different datasets," *26th IEEE Signal Processing and Communications Applications Conference, SIU 2018*. no. April, pp. 1–4, 2018.

[346] S. R. Shah, M. A. Mohd Z., I. M. Yassin, A. H. Hasliza, and A. Zabidi, "Non-destructive classification of watermelon ripeness using Mel-frequency cepstrum coefficients and multilayer perceptrons," *Proceedings of the International Joint Conference on Neural Networks*. p. 2010. Available: https//doi.org/ 10.1109/IJCNN.2010.5596573.

[347] A. Ramcharan, K. Baranowski, P. McCloskey, B. Ahmed, J. Legg, and D. P. Hughes, "Deep learning for image-based cassava disease detection," *Frontiers in Plant Science*, vol. 8, no. October, pp. 1–7, 2017.

[348] A. Botalb, M. Moinuddin, U. M. Al-Saggaf, and S. S. A. Ali, "Contrasting convolutional neural network (CNN) with multi-layer perceptron (MLP) for big data analysis," *International Conference on Intelligent and Advanced System, ICIAS 2018*. pp. 3–7, 2018.

[349] X. He, and Y. Chen, "Modifications of the multi-layer perceptron for hyperspectral image classification," *Remote Sensing*, vol. 13, no. 17, p. 2021.

[350] M. M. A. Mia, S. K. Biswas, M. C. Urmi, and A. Siddique, "An algorithm for training multilayer perceptron (mlp) for image reconstruction using neural network without overfitting," *International Journal Of Scientific and Technology Research*, vol. 4, no. 02, pp. 271–275, 2015.

[351] M. Nagata, J. G. Tallada, and T. Kobayashi, "Bruise detection using NIR hyperspectral imaging for strawberry," *Environmental Control in Biology*, vol. 44, no. 02, pp. 12–26, 2006.

[352] Y. Jiang, C. Li, and F. Takeda, “Nondestructive detection and quantification of blueberry bruising using near-infrared (NIR) hyperspectral reflectance imaging,” *Scientific Reports*, vol. 6, pp. 1–14, 2016.

[353] D. P. Ariana, R. Lu, and D. E. Guyer, “Near-infrared hyperspectral reflectance imaging for detection of bruises on pickling cucumbers,” *Computers and Electronics in Agriculture*, vol. 53, no. 1, pp. 60–70, 2006.

[354] G. ElMasry, N. Wang, C. Vigneault, J. Qiao, and A. ElSayed, “Early detection of apple bruises on different background colors using hyperspectral imaging,”*Food Science and Technology*, vol. 41, no. 2, pp. 337–345, 2008.

[355] C. I. Chang, and Q. Du, “Estimation of number of spectrally distinct signal sources in hyperspectral imagery,” *IEEE Transactions on Geoscience and Remote Sensing*. vol. 42, no. 3, pp. 608–619, 2004.

[356] D. Mishra, J. Wang, S. T. Wang, Q. Cao, H. Hurbon, W. Akers, and M. Y. Berezin, “Selection of hyperspectral endmember extraction algorithm for tumor delineation in animal models.,” *In: Optical Molecular Probes, Imaging and Drug Delivery*, 2021. Available: https://doi.org/10.1364/OMP.2021.OF2E.2.

[357] S. Youssefi, Z. Emam-Djomeh, and S. M. Mousavi, “Comparison of artificial neural network (ANN) and response surface methodology (RSM) in the prediction of quality parameters of spray-dried pomegranate juice,” *Drying Technology*, vol. 27, no. 7, pp. 910–917, 2009.

[358] M. Jamshidi, “Tools for intelligent control: fuzzy controllers, neural networks and genetic algorithms,” *Philosophical Transactions of the Royal Society A: Mathematical, Physical & Engineering Sciences*, vol. 361, pp. 1781–1808, 2003.

[359] Z. Du, X. Zeng, X. Li, X. Ding, J. Cao, and W. Jiang, “Recent advances in imaging techniques for bruise detection in fruits and vegetables,” *Trends in Food Science and Technology*, vol. 99, no. March, pp. 133–141, 2020.

[360] G. Kim, G. H. Kim, J. Park, D. Y. Kim, and B. K. Cho, “Application of infrared lock-in thermography for the quantitative evaluation of bruises on pears,” *Infrared Physics and Technology*, vol. 63, pp. 133–139, 2014.

[361] H. R. A. M. A. Shahin, E. W. Tollner, R. W. McClendon, “Apple classification based

on surface bruises using image processing and neural networks," *Transactions of the ASAE*. vol. 45, no. 5, pp. 1619–1627, 2002.

[362] X. Zeng, Y. Miao, S. Ubaid, X. Gao, and S. Zhuang., "Detection and classification of bruises of pears based on thermal images," *Postharvest Biology and Technology*, vol. 161, no. August 2019, p. 111090, 2020.

[363] R. Khodabakhshian, B. Emadi, M. Khojastehpour, M. R. Golzarian, and A. Sazgarnia, "Non-destructive evaluation of maturity and quality parameters of pomegranate fruit by visible/near infrared spectroscopy," *International Journal of Food Properties*. vol. 20, no. 1, pp. 41–52, 2017.

[364] M. S. Razavi, A. Asghari, M. Azadbakh, and H. A. Shamsabadi, "Analyzing the pear bruised volume after static loading by Magnetic Resonance Imaging (MRI)," *Scientia Horticulturae*, vol. 229, no. November 2017, pp. 33–39, 2018.

[365] C. D. Everard, M. S. Kim, and H. Lee, "Assessment of a handheld fluorescence imaging device as an aid for detection of food residues on processing surfaces," *Food Control*, vol. 59, pp. 243–249, 2016.

[366] Q. Zhu, J. Guan, M. Huang, R. Lu, and F. Mendoza, "Predicting bruise susceptibility of 'Golden Delicious' apples using hyperspectral scattering technique," *Postharvest Biology and Technology*, vol. 114, pp. 86–94, 2016.

[367] R. Dian, S. Li, L. Fang, and Q. Wei, "Multispectral and hyperspectral image fusion with spatial-spectral sparse representation," *Information Fusion*, vol. 49, no. December 2017, pp. 262–270, 2019.

[368] J. Li, X. Rao, F. Wang, W. Wu, and Y. Ying, "Automatic detection of common surface defects on oranges using combined lighting transform and image ratio methods.," *Postharvest Biology and Technology*, vol. 82, pp. 59–69, 2013.

[369] B. Zhang,, J. Li,, S. Fan, W. Huang, C. Zhao, C. Liu, and D. Huang, "Hyperspectral imaging combined with multivariate analysis and band math for detection of common defects on peaches (Prunus persica)," *Computers and Electronics in Agriculture*, vol. 114, pp. 14–24, 2015.

[370] A. López-Maestresalas, J. C. Keresztes, M. Goodarzi, S. Arazuri, C. Jarén, and W. Saeys, "Non-destructive detection of blackspot in potatoes by Vis-NIR and SWIR

hyperspectral imaging," *Food Control*, vol. 70, pp. 229–241, 2016.

[371] J. Xing, C. Bravo, P. T. Jancsók, H. Ramon, and J. De Baerdemaeker, "Detecting bruises on 'Golden Delicious' apples using hyperspectral imaging with multiple wavebands," *Biosystems Engineering*, vol. 90, no. 1, pp. 27–36, 2005.

[372] W. Huang, J. Li, Q. Wang, and L. Chen, "Development of a multispectral imaging system for online detection of bruises on apples," *Journal of Food Engineering*, vol. 146, pp. 62–71, 2015.

[373] R. Chandra, D. K. Babu, V. T. Jadhav, and J. A. Teixeira da Silva, "Origin, history and domestication of pomegranate," *Fruit, Vegetable and Cereal Science and Biotechnology*. vol. 4, no. October 2016, pp. 1–6, 2010.

[374] U. L. Opara, J. Atukuri, and O. A. Fawole, "Application of physical and chemical postharvest treatments to enhance storage and shelf life of pomegranate fruit-A review," *Scientia Horticulturae*, vol. 197, pp. 41–49, 2015.

[375] O. A. Fawole, "Maturity indexing, pharmacological properties and postharvest performance of pomegranate fruit grown in South Africa. Doctorate thesis, Stellenbosch University, 2013.

[376] F. Boussaa, F. Zaouay, F. Burlo-Carbonell, N. Nuncio-Jáuregui, M. Gmati, B. E. Arbi, P. Melgarejo, F. Hernandez, and M. Mars, "Combined effects of cropping system and harvest date determine quality and nutritional value of pomegranate fruits (Punica granatum L. cv. Gabsi)," *Scientia Horticulturae*, vol. 249, no. August 2018, pp. 419–431, 2019.

[377] M. Alfouzan,, B. Al-Otaibi,, K. Issa, and S. A. Alshebeili, "Near infra red (NIR)-based classification of orange juice," *2017 International Conference on Electrical and Computing Technologies and Applications, ICECTA 2017*. vol. 2018-January, no. November 2017, pp. 1–5, 2018.

[378] B. Gaspardo, S. Del Zotto, E. Torelli, S.R. Cividino, G. Firrao, G. Della Riccia, and B. Stefanon, "A rapid method for detection of fumonisins B_1 and B_2 in corn meal using Fourier transform near infrared (FT-NIR) spectroscopy implemented with integrating sphere," *Food Chemistry*, vol. 135, no. 3, pp. 1608–1612, 2012.

[379] A. Ambaw, E. Arendse,, A. Du Plessis, and U. L. Opara, "Analysis of the 3D

microstructure of pomegranate peel tissue using X-ray micro-CT.," *Acta Horticulturae*. vol. 1201, pp. 197–204, 2018.

[380] M. Manley, "Near-infrared spectroscopy and hyperspectral imaging: Non-destructive analysis of biological materials," *Chemical Society Reviews*, vol. 43, no. 24, pp. 8200–8214, 2014.

[381] M. Sun, D. Zhang,, L. Liu, and Z. Wang, "How to predict the sugariness and hardness of melons: A near-infrared hyperspectral imaging method," *Food Chemistry*, vol. 218, pp. 413–421, 2017.

[382] E. Martel,, R. Lazcano,, J. López, D. Madronal, R. Salvador, S. Lopez, E. Juarez, R. Guerra, C. Sanz, and R. Sarmiento, "Implementation of the principal component analysis onto high-performance computer facilities for hyperspectral dimensionality reduction: Results and comparisons," *Remote Sensing*, vol. 10, no. 6, p. 2018.

[383] I. T. Jollife, and J. Cadima, "Principal component analysis: A review and recent developments," *Philosophical Transactions of the Royal Society a: Mathematical, Physical and Engineering Sciences*, vol. 374, no. 2065, p. 2016. Available: http://dx.doi.org/10.1098/rsta.2015.0202.

[384] H. Malmgren, "Revision of an artificial neural network enabling industrial sorting, April, 2019.

[385] MATLAB, "Neural Net Fitting," Retrieved from https://www.mathworks.com/help/deeplearning/ref/neuralnetfitting-app.html.

[386] J. J. Martínez, P. Melgarejo, F. Hernández, D. M. Salazar, and R. Martínez, "Seed characterisation of five new pomegranate (Punica granatum L.) varieties," *Scientia Horticulturae*, vol. 110, no. 3, pp. 241–246, 2006.

[387] N. Hasnaoui, M. Mars, S. Ghaffari, M. Trifi, P. Melgarejo, and F. Hernandez, "Seed and juice characterization of pomegranate fruits grown in Tunisia: Comparison between sour and sweet cultivars revealed interesting properties for prospective industrial applications," *Industrial Crops and Products*, vol. 33, no. 2, pp. 374–381, 2011.

[388] A. A. Gowen,, C. P. O'Donnell,, M. Taghizadeh,, P. J. Cullen,, J. M. Frias, and G. Downey, "Hyperspectral imaging combined with principal component analysis for

bruise damage detection on white mushrooms [Agaricus bisporus)," *Journal of Chemometrics*, vol. 22, no. 3–4, pp. 259–267, 2008.

[389] L. S. Magwaza, and U. L. Opara, "Analytical methods for determination of sugars and sweetness of horticultural products-A review," *Scientia Horticulturae*, vol. 184, pp. 179–192, 2015.

[390] L. Chen, and U. L. Opara, "Approaches to analysis and modeling texture in fresh and processed foods – A review," *Journal of Food Engineering*, vol. 119, no. 3, pp. 497–507, 2013.

Appendix

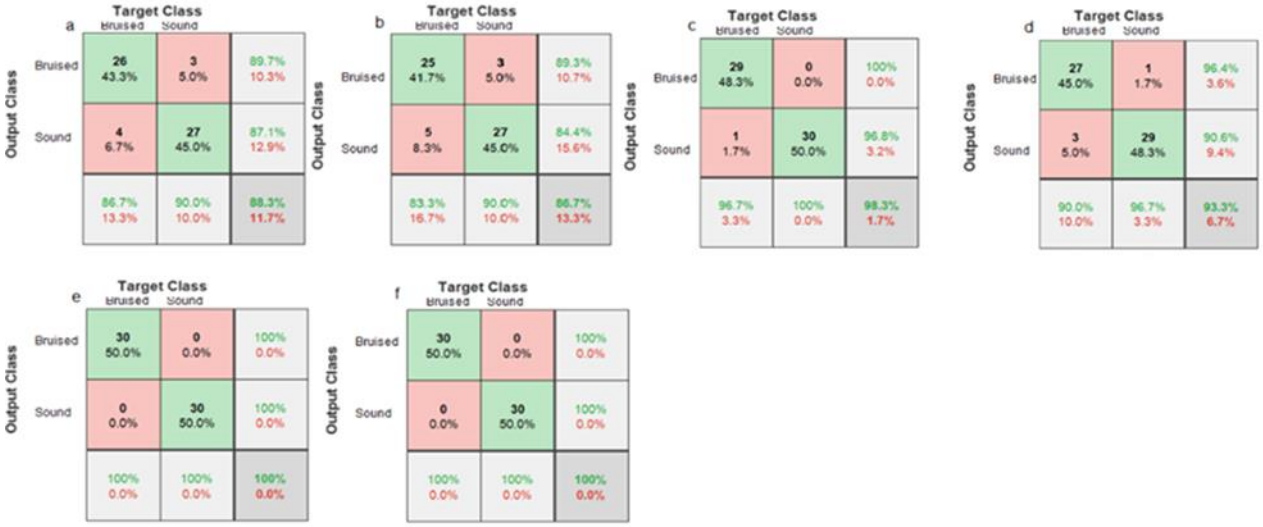

Figure A1. The confusion matrix obtained of the classification performance for VNIR spectral data during the different bruise development, Day 1 ROI (a), WF (b); Day 7 ROI (c), WF (d); Day 14 ROI (e), WF (f). The x axis refers to the true categories, and the y axis refers to the classifier outputs. The integers in the matrix show number of samples. The color en-codes the percentage of a class of blocks (x) classified into a predicted class (y).

Figure A2. The confusion matrix obtained of the classification performance for SWIR spectral data during the different bruise development, Day 1 ROI (a), WF (b); Day 7 ROI (c), WF (d); Day 14 ROI (e), WF (f). The x axis refers to the true categories, and the y axis refers to the classifier outputs. The integers in the matrix show number of samples. The color en-codes the percentage of a class of blocks (x) classified into a predicted class (y).

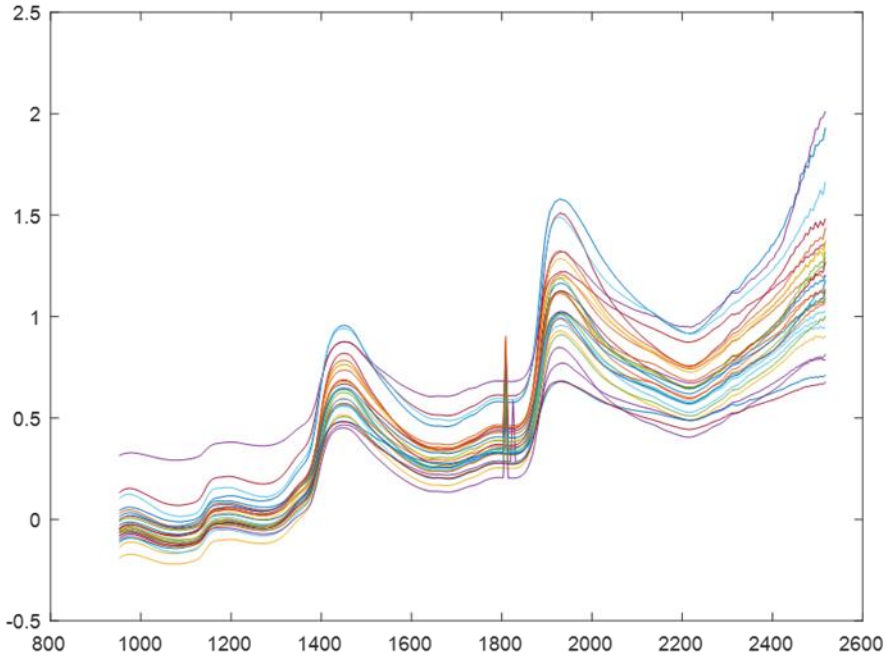

Figure A3. Full spectral profile of bruised pomegranate fruit on day 1 after bruise damage

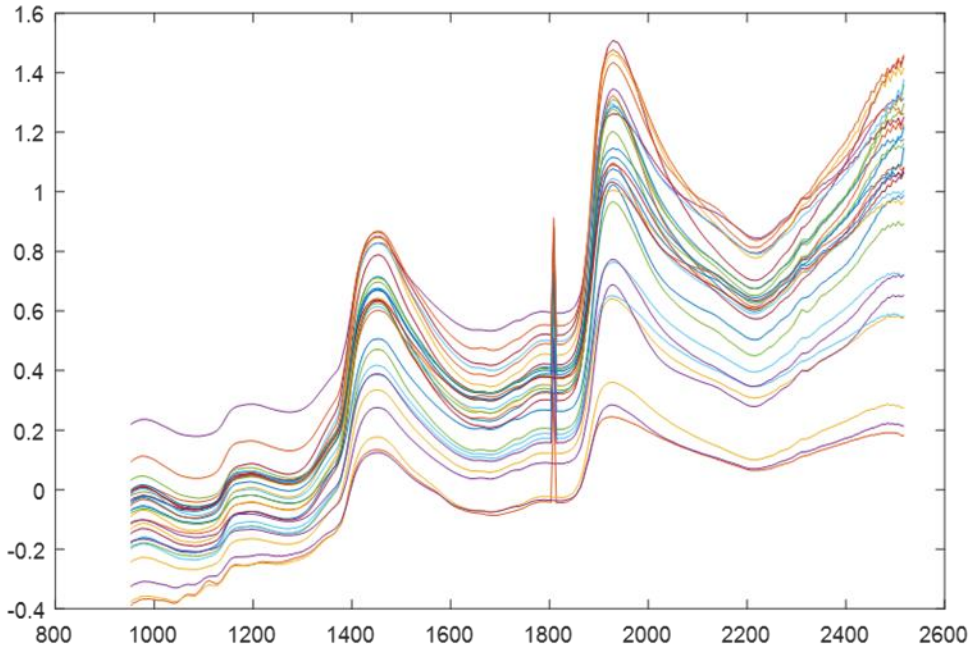

Figure A4. Full spectral profile of bruised pomegranate fruit on day 7 after bruise damage

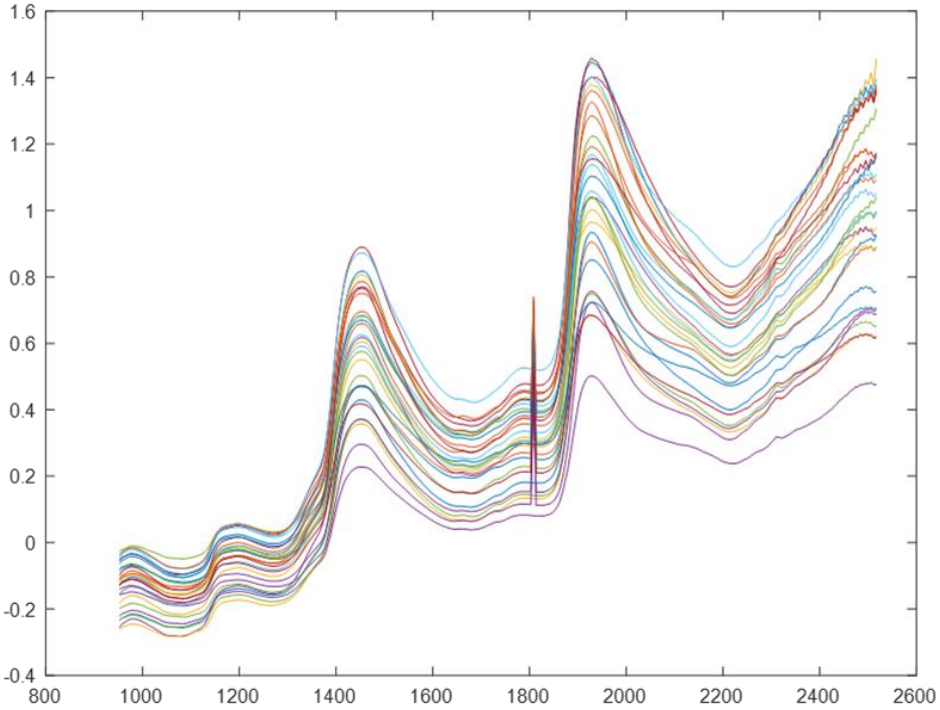

Figure A5. Full spectral profile of bruised pomegranate fruit on day 14 after bruise damage